# *An Ultrasonic System for Intravascular Measurement and Visualisation of Anatomical Structures and Blood Flow*

***Ahmad A. Kardan***

*A Thesis submitted for the Degree of Doctor of Philosophy of the University of London and the Diploma of Membership of Imperial College*

*July 1991*

*Electrical Engineering Department*
*Imperial College of Science, Technology and Medicine*
*University of London*

# *Abstract*

In this work the design and construction of a special purpose A-mode ultrasonic imaging system for intravascular diagnostic application has been investigated. This system contains the instrumentation and data acquisition parts of an intravascular imaging system for utilisation in conjunction with a especially designed software. This system can be employed to work along with the percutaneous transluminal treatment techniques (balloon and laser angioplasty, atherectomy etc).

The system designed contains the complete electronic hardware using commercially available components and a especially designed *Miniature Ring Array Transducer*.

From the early 1970s the interesting technique of balloon angioplasty opened a new era in the examination of vascular structures having small diameters. A major technical key to the wider use and improved clinical efficiency of angioplasty, and the fundamental motivation for intravascular ultrasound technique is the relatively poor information on vascular diseases provided by conventional angiography. In fact, the two-dimensional images (shadow gram projections of contrast-opacified vessels) may often provide a deficient or misleading representation of the actual three-dimensional vasculature.

Therefore, this project was conducted to produce a simple commercially available hardware and a *Miniature Ring Array Transducer* to provide a system for data acquisition during intravascular

examination. This system provides a tool for detailed visualization of anatomical structures and percentage of stenosis in the intima. By means of especially written software, the three dimensional model of arterial sections can be reconstructed. This work is divided into four separate areas, which constitute the main components of this thesis.

First a general study on medical imaging systems with detailed concentration on the ultrasound techniques has been carried out. This was done to provide a basic knowledge of different types of imaging systems and to create the necessary motivation for the continuation of this work.

In the second part of this project, the construction of ring array transducers has been investigated. The final goal of research was to make a catheter mounted ultrasound ring array transducer with overall diameter of 2 mm.

The design and construction of the electronic circuity and the necessary interface for data acquisition and its transportation to a micro-VAX computer, has been the third phase of this research.

Finally, at the forth stage, the capability of this system with more emphasis on the 3D reconstruction of arterial structures has been investigated. Also, some effort was put into examining the feasibility of the system for intravascular blood flow measurement.

From the point of view of hardware and transducer design, this system can be extended to have a higher frequency transducer for intravascular tissue characterization and to develop a faster hardware system for real time image reconstruction.

*In Memory of martyrs*

***Hossein Saleh Ghaffari** and **Mahmoud Rezaeei***

*Dedicated to all unknown martyrs who did not hesitate to give all in defence of their honour and beliefs.*

## Acknowledgements

*I would like to express my gratitude to professor R.I. Kitney for his encouragements during the course of this project. I am also grateful to all members of Biomedical Systems Group and particularly Dr K. Straughan and my fellow students for their help and companion during my course of studies.*

*There are other individuals who have guided me through the duration of this work, especially worthy of mention are my parents to whose care and effort I owe all my successes in life. I should also mention my brothers* ***Abbas Kardan*** *and* ***Ghasem Rahravan*** *and my sisters, whom I have constantly thought of and remembered while not being with them. I am greatly indebted to my dear brother* ***Hossein Ghadiri*** *and my sister in low* ***Zahra Zeinalian*** *who have continuously assisted me in the duration of my studies.*

*I am also indebted to all my dear friends who have encouraged and supported me in any possible way. In particular I would wish to thank martyr* ***Hossein Saleh Ghaffari****, my brother in law* ***Mahmoud Zeinalian****, and my dear friend* ***Hossein Pedram*** *who encouraged me from the beginning in achieving this goal. I am grateful to my generous friend* ***Farzad Yazdi*** *for his candid support and appeasement at difficult moments which has continued throughout this work. In this manner I would wish to express my heartily appreciation to* ***Hamid Tavakoli*** *for his sincere sympathy and brotherly company. I would also wish to thank Mrs. Pourhonar for her care and Ahmad Sabbaghi for his friendship during my studies.*

*Remembering long term association with all friends in this college, in particular Mohamad Movahedi, Yazdan Keyhanian, Atta Badi, Amir Zarrati, Saeed Sanei, Hossein Jelveh, Weysel Omer, Harold Wilson, Paul Rubenstein, and Anil Bharath I would like to thank theme all.*

*To find a word of appreciation is always difficult and perhaps impossible if a very especial person is in mind. I did try in every possible way to think of some words and phrases to go a little way in expressing my heartily gratitude to my dear wife Akram Zeinalian. However, words cannot describe her constant encouragement and companionship without which none of this would have been possible. In reality she has been a more than equal partner in all aspects of my life which includes this work. In view of her sincere dedication to the family, expressing my truthful affection to her is the least possible note of thanks.*

*In a similar manner I would like to thank my dear children* ***Ali, Zeinab*** *and* ***Kosar*** *whose tolerance of my often very difficult times I shall never forget. I shall always remember your patience and the suffering that you have endured during this delicate period of your childhood.*

# CONTENTS

# CONTENTS

**CHAPTER FIVE : 3D VISUALISATION OF VASCULAR STRUCTURES :**



**CHAPTER SIX : TRANSVERSE DOPPLER FLOW MEASUREMENT :**



**Chapter Seven : CONCLUSIONS AND SUGGESTIONS FOR FURTHER RESEARCH :**

## *Introduction*

This thesis begins with Chapter One discussing the different types of imaging modalities in biomedical systems. A comprehensive study of the instrumentation aspects of plain x-ray, Computerised Tomography, Emission Imaging, Magnetic Resonance Imaging and Ultrasound will be presented to provide the basic background knowledge for the interested researchers in biomedical imaging.

Chapter Two concentrates on the physical aspects of ultrasound and its important role in medical applications. All properties of ultrasound as a mechanical wave will be discussed including propagation, reflection, refraction, scattering, absorption, diffraction and attenuation. What is discussed will create a strong platform for those interested in the construction of ultrasound transducers. At the end, a review of biological tissues and their acoustic properties is presented. The biological construction of vessels will be outlined and a brief discussion of the causes of Arteriosclerosis is discussed.

Chapter Three begins by reviewing the construction of a general purpose circular transducer. Next the different building blocks of various types of array transducers are presented. These are linear array, phased array and annular array. We then review catheter mounted transducers with two different classes of applications, imaging and non-imaging. Then the construction of a miniature array transducer is studied in detail and its acoustical and electrical properties are outlined.

In Chapter Four the complete A-mode ultrasound system for intravascular imaging developed for this project is presented. The topics discussed will include ultrasonic transceiver, filtering stage, control logic unit, multiplexing circuit, Analogue to Digital converter, FIFO memory unit and control unit for memory buffer. At the end the technical specification of the complete system will

be presented.

Chapter Five will present the results obtained using the designed miniature ring array transducer in three dimensional reconstruction. These results will include experiments from perspex phantoms and arterial specimens. Arteriosclerosis is simulated using "blu-tac" and a perspex phantom with the resulting images displayed. The results show that the current system would benefit from research into more sophisticated tissue characterisation algorithms.

In Chapter Six I employ a single element transducer having the same size as the elements of the miniature ring array transducer for flow measurements. In this section, I obtain results that are based on the theory of transverse Doppler effect. My aim in carrying out these experiments is to test the capability of the miniature ring array transducer in transverse Doppler flow measurements. Enhancing the theory of transverse Doppler is beyond the scope of this thesis.

Finally Chapter Seven is a comprehensive discussion of our conclusions during the course of this work. I will present my suggestions for those researchers who may be interested in carrying out this work further in future.

## *Statement of Originality*

The following aspects of this work are believed to be original

1) The design, construction and evaluation of a *Miniature Ring Array Transducer* (MRAT) with an overall diameter of 2 mm consisting of 12 elements.

2) The development of fluid injected brass-loaded wax as a backing material for miniature transducers.

3) Use of surgical dressing spray as a matching layer of the transducer elements having a strong biological compatibility with human tissues and also as an electrically insulating material.

4) The design and implementation of dedicated modular ultrasonic system with interface for connection to a micro-VAX computer system.

5) Utilisation of A-mode ultrasound for three dimensional reconstruction of arterial structures.

6) The evaluation of the MRAT technology as a diagnostic tool for intravscular imaging.

7) Simulation of Arteriosclerosis disease using a narrowed phantom and obstructing material inside a perspex phantom and its successful imaging using the miniature ring array transducer developed.

8) Validation of the theory of transverse Doppler effect using the miniature ring array transducer.

*Chapter One*

# *Biomedical Imaging Systems*

## 1-1 : INTRODUCTION :

In this chapter the four most important techniques in biomedical imaging are discussed. The general view of each technique with more details of hardware and instrumentation will be discussed to make a starting platform for the second chapter with more emphasis on ultrasound imaging techniques. At the end of this chapter the cost, portability, reliability, and safety of each system is analysed to find out why in recent years ultrasound imaging has opened a new horizon in biomedical imaging.

## 1-2 : X-RAY ANGIOGRAPHY :

X-ray imaging has been employed in medical applications for more than half a century. The components which are common to both the conventional film cineangiography system and the digital angiography system could be categorized as an X-ray tube which

is capable of rapid short-duration pulsing, a scatter reduction grid, an image intensifier, coupling optics and a camera. Fig (1-1) shows the configuration of an X-ray system. The difference between cineangiograpgy and digital angiography is in their use of the different types of camera. Cineangiography system uses a fast frame rate cine camer, whereas the digital angiography employs a video camera.

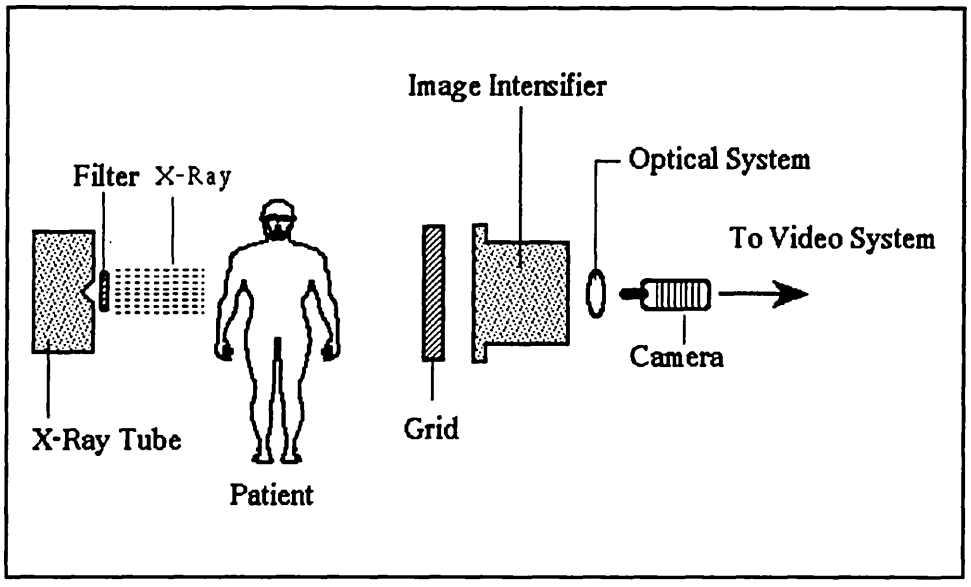


*Fig(1-1) : Cineangiography Imaging System.*

**1-2-1 : X-RAY TUBE :**

Fig (1-2) shows the structure of an x-ray tube. This device is a high voltage vacuum diode. The emitted electrons from a heated filament are accelerated by a high voltage field and subsequently strike the anode. The result of this impact is decleration of electrons and subsequent release of less than 1% of energy in the form of x-rays. Therefore more than 99% of energy is converted to unwanted heat and it is therefore necessary to use a heavy metal such as tungsten or one of its alloys to make the anode.

The anode is also bevelled to spread the heat over a larger surface area.

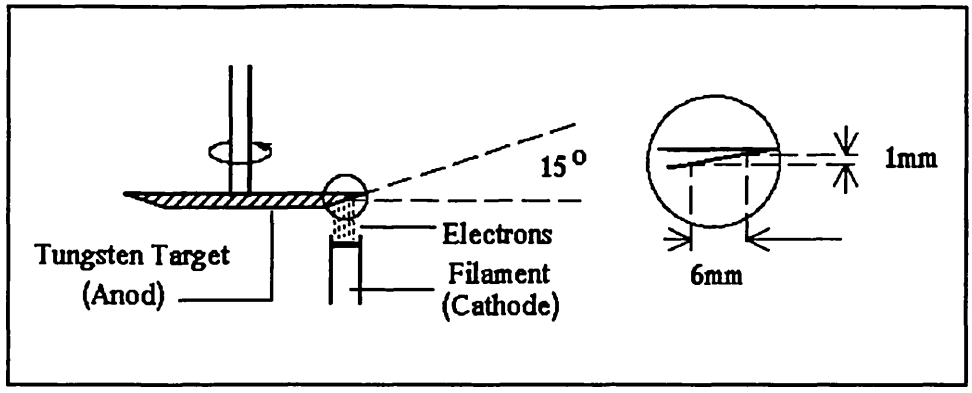


*Fig (1-2) : Internal design of X-Ray tube.The bevelling edge of the rotating anode provides a small effective focal spot size.*

In addition it is made cylindrically symmetric, in order to be able to rotate at a high speed of 3000 to 10000 RPM to allow heat to be spread over a larger area.

### 1-2-2 : SCATTER REDUCTION GRID :

Absorption and scattering are two important factors which affect the x-ray imaging technique. In fact only those x-rays which are unaffected by either absorption or scattering can pass through the patient's body. If we name this part of x-rays as primary radiation, the image information is provided by spatial modulation of the x-rays absorbtion which is carried by primary radiation. The x-rays which are scattered by the patient's body are reflected in different angles and those which are detected make a source of image noise and as a consequence degrade the signal to noise ratio (SNR). By means of a scatter reduction grid fixed between the patient and the detector it is possible to improve SNR. The sectional view of an x-ray scatter reduction grid is shown in Fig (1-3).

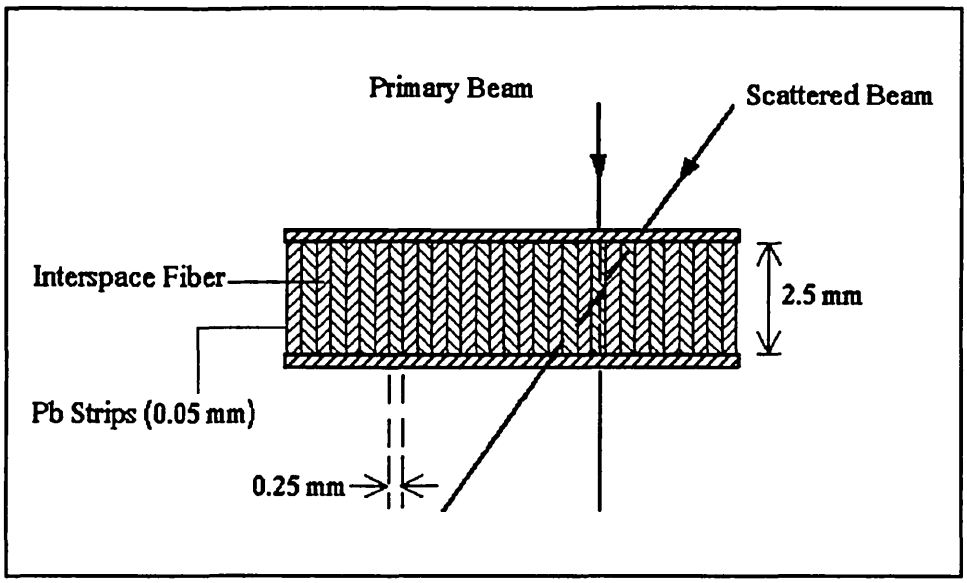


*Fig (1-3) : A cross-sectional view of an x-ray scatter reduction grid.*

Scatter reduction grid consists of many narrow lead strips laminated between wider strips of low-density fibre or aluminium. The scatter reduction grid absorbs a large fraction of the scattered x-rays within the lead strips and typically,

50 to 60 percent of the primary radiation passes through such a grid. After passing through the scatter reduction grid, the ratio of primary to scattered radiation is enhanced by a factor of five or more and consequently an improvement in signal-to-noise ratio is achieved.

## 1-2-3 : IMAGE INTENSIFIER :

An Image Intensifier performs two main functions. Its first task is to detect the x-ray radiation, and it also converts the energy carried by x-rays to bright photons with high energy. These photons can be later viewed by video or conventional film cameras.

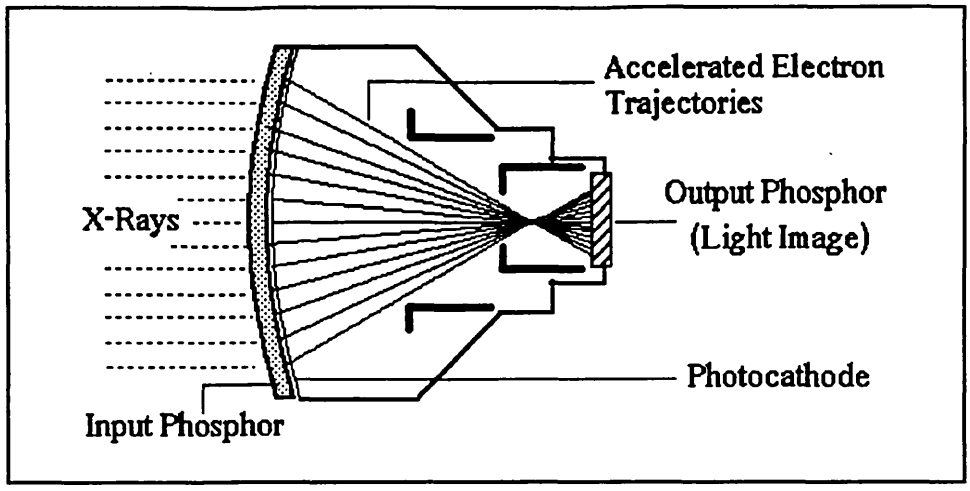


*Fig (1-4) : A cross-sectional view of an image intensifier.*

As can be seen in Fig (1-4), this device has two surfaces as input and output covered with absorbing materials. The input surface is usually covered by cesiumiodide and converts x-rays to light beams. Then these light beams strike a thin metal photo-cathode and cause electrons to be liberated. Such electrons are accelerated and focused onto the output phosphor surface and produce a bright magnified optical image which is proportional to the absorbed x-ray distribution at the input surface.

## 1-2-4 : OPTICAL SYSTEM :

To couple the image formed at the output of the image intensifier to either a cine film or a video camera a two-element lens system is used to regulate the amount of light. The size of the optical image formed at the camera is changed by changing the focal length of the lenses. Fig (1-5) shows the configuration of the optical system.

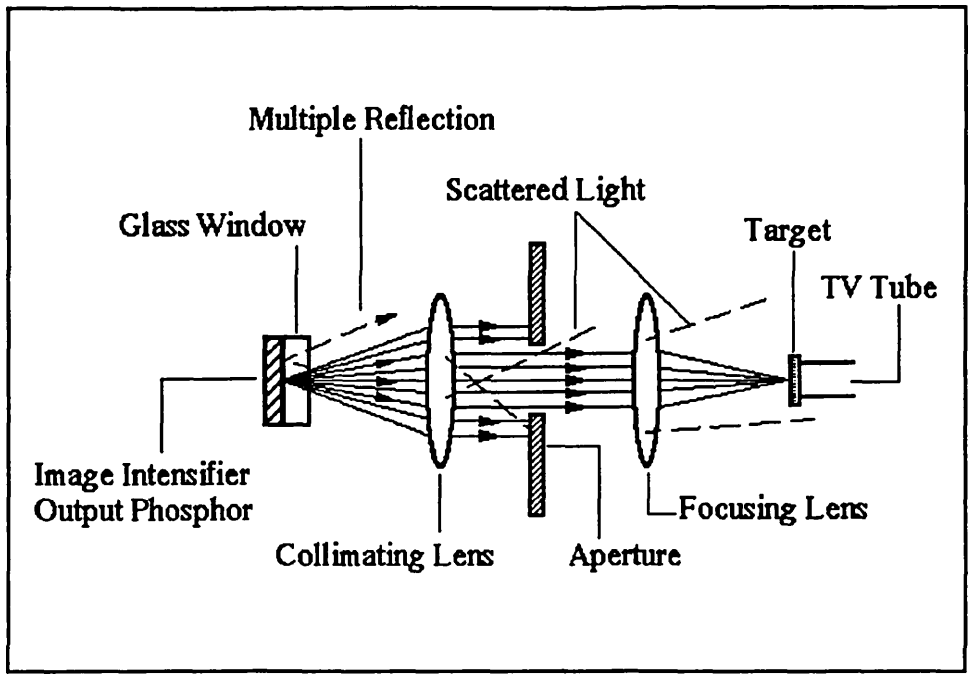


*Fig (1-5) : Optical Coupling between Image Intensifier and the video camera.*

**1-2-5 : NOISE :**

In both, cineangiography and digital angiography some limitations exist in image quality which are related to the physical aspects of x-ray image formation, but independent of imaging equipment. To form a useful image, many x-ray photons must be detected. Due to the detection process which exhibits a statistical variation across the detector surface, a random spatial modulation of the x-ray intensity results . This randomly distributed variation is called quantum noise. The level (standard deviation) of this random modulation $\sigma$ is related to the number of detected photons $N$. This relation is expressed by the Equation (1-1).

$$\sigma = \sqrt{N} \qquad (1-1)$$

On the other hand, the differential absorption of the x-ray beam by a patient located between the x-ray beam and detector results in a non-random modulation of x-ray intensity across the detector surface. The number of incident x-ray photons $N_0$ on a uniform absorber is related to the number of them $N$ which pass through the absorber according to the Equation (1-2).

$$N = N_0 . e^{-\mu \rho x} \qquad (1-2)$$

where $\rho$ is the density and and $x$ is the thickness of the absorbing material respectively. $\mu$ which is called the mass attenuation coefficient is the characteristic of the atomic number of the absorber. In the case of a nonuniform absorber such as a human body spatial variation in $\rho$ and $x$ causes differential absorption which results in modulation of the x-ray intensity across the detector. In fact this modulation carries the image information.

Therefore, to have a visible image,it is necessary that the non-random modulation can compete with the random or quantum noise in the image . Unfortunately, sometimes the random noise fluctuations are quite intense relative to the non-random image information, and thus they mask the desired information.

The Equation (1-1) shows that noise increases with $N$, the number of detected photons. But we must be aware that absolute noise level is not displayed in an image and what we can see is a noise level relative to image contrast. the image contrast could be expressed as:

$$\Delta N = N_i - N_o \qquad (1\text{-}3)$$

that is;

$$\Delta N = N.\,(Diffrential\ Absorption) \qquad (1\text{-}4)$$

where $N_i$ and $N_o$ are the numbers of detected x-rays inside and outside the patient's body. Now if we divide Equation (1-1) by Equation (1-4) we can see that relative to image contrast $\Delta N$, the random noise $\sigma$ is decreased as the number of detected x-rays are increased.

$$\frac{\sigma}{\Delta N} = \frac{\sqrt{N}}{N.\,(Diffrential\ Absorrption)} \qquad (1\text{-}5)$$

Equation (1-5) is the inverse of signal to noise ratio. Therefore;

$$SNR = \sqrt{N}.\,(Diffrential\ Absorption) \qquad (1\text{-}6)$$

or;

$$SNR = \sqrt{nA}.\,(Differential\ Absorption) \qquad (1\text{-}7)$$

where $n$ is the number of x-ray photons per unit area and $A$ is the projected area of the

patient's body. From Equation (1-5) we can see that larger objects have a higher SNR and are more readily detected. Therefore in the case of thinner, less dense and narrow structures, for having reasonable differential absorption (visible image) we have to increase the x-ray intensity. This is particularly true in angiography where both the differential absorption and spatial extent is decreased simultaneously as vessels become smaller.

## 1-3 : EMISSION IMAGING :

Nuclear Medicine Imaging, Emission Imaging or Radionuclide Imaging, all refer to studies which involve injection of a radioactive isotope that emits gamma rays. Gamma rays are the result of interaction in the nucleus of the isotope in transition from a high level state of energy a lower one. The photons emitted from radioisotope materials are very similar to light photons. So they are tiny visible particles with a very high amount of energy ( several Kilo electron volts). In comparison to x-rays there is no physical difference between them. The gamma rays differ from x-rays in their origin of generation. They result from nuclear reactions whereas x-rays are produced by acceleration of electrons. For different parts of body, gamma rays with different level of energy are required, and they are achieved by different techniques. For example in cardiology radioisotopes decay in one of the following ways.

**a** : *electron emission*,

**b** : *positron emission*,

**c** : *isometric transition*, and

**d** : *K-electron capture*.

In practice these forms of decay are categorised by *single photon emission* and *positron emission.* The term of single photon is used to characterise radio nuclides whose photons arise from electron capture, electron emission, or isometric transition. Although the single photon isotopes emit photons in a few different energy levels, only one energy level is normally used for detection.

In positron emission, isotopes such as Carbon 11, Nitrogen 13, Oxygen 15, Potassium 38, Gallium 68 and Rubidium 82 undergo a transition in which a nuclear proton changes into a neutron with the emission of a positive electron (positron). This positron immediately combines with a nearby electron and in accordance with to the Einstein formula $\mathbf{E = m.C^2}$, 1.022 Mev of energy is produced. Thus energy is divided equally between two photons which fly away from one another at an angle of 180°.

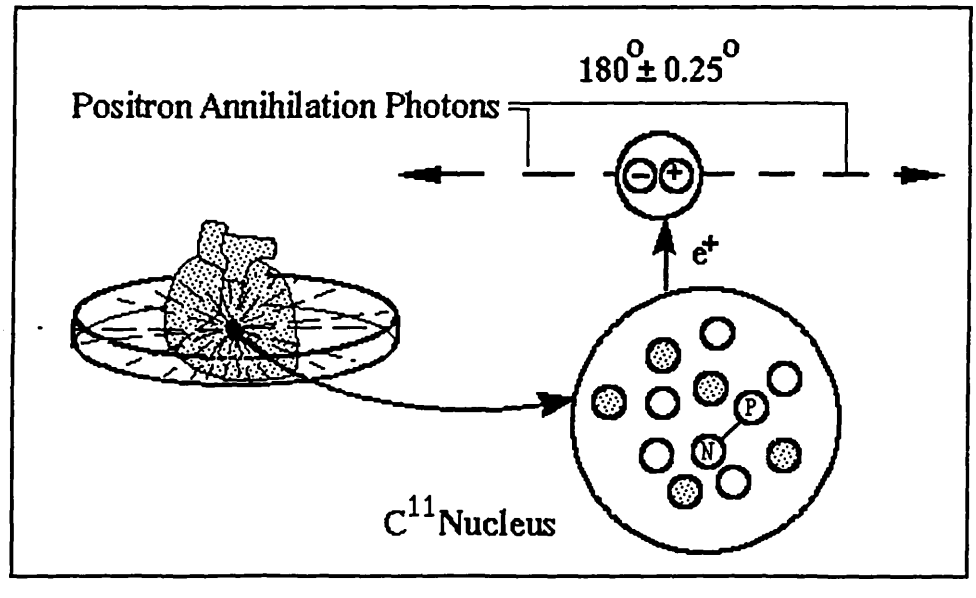


*Fig (1-6) : Positron emmitting from a carbon-11 nucleus. During the radioactiv transformation,a proton becomes a neutron with the release of a positron and a neutrino.*

Fig (1-6) shows that after a proton changes to a neutron due to the radioactive transformation, a positron $e^+$ and a neutronio $\nu$ will release. This positron at some distance from the nucleus annihilates with an electron $e^-$ and two high-energy photons will result. More details on types of radionuclide decay is provided in Evan's text (1955)[47] and Budinger et al(1984)[20].

### 1-3-1 : ATTENUATION :

In radionuclide imaging there are three sources of attenuation which cause only one of every 10000 photons to be detected.

1 : *Scattering*; Photons are scattered by interacting with tissue atoms which are located between the source of radionuclide radiation and the detector. Scattering leads to image degradation.

2 : *Absorption*; A considerable amount of photons are absorbed by tissue before they can reach the detector. In practice scattering and absorption together cause 50 to 80 percent loss of the original photons, depending on how deep the radiation source is located in the body, and the energy of the photons.

3 : *Direction of Emission*; Some photons are emitted in a direction other than that toward which the detector is looking. Because of this problem only one photon in about 10000 original photons is detectable.

## 1-3-2 : INSTRUMENTATION :

Taking into consideration the characteristics and limitations mentioned above, the detectors and instruments used to create an image in a radionuclide imaging system are described in the following sections.

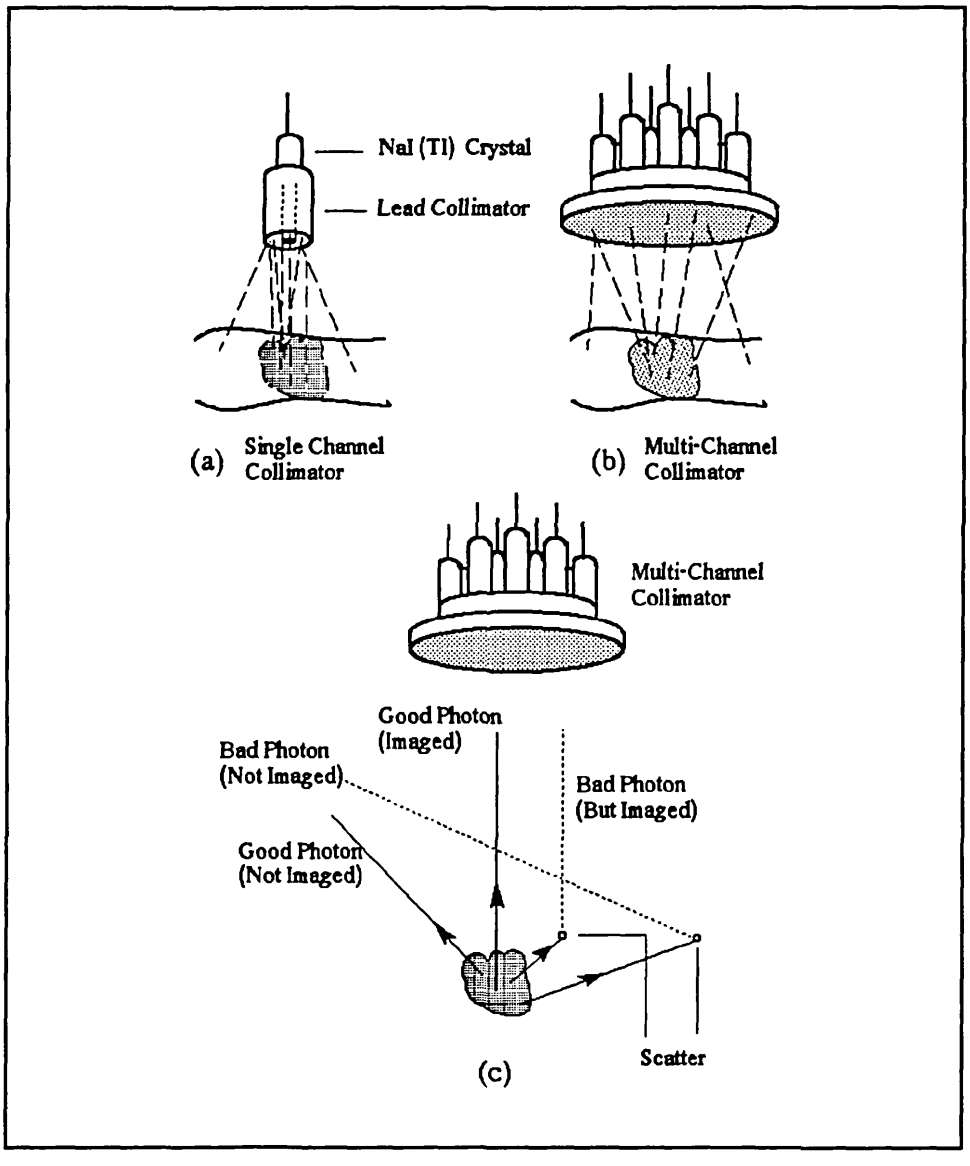


*Fig (1-7) : Single channel and multi-channel collimator.*

### 1-3-2-A : LEAD COLLIMATOR :

In order to solve, or at least to ease the problem of scattering, a lead collimator is used. The collimator acts as a type of lens for photon detection and excludes most of the scattered photons. The schematic illustration of a single channel lead collimator is shown in Fig (1-7-a). By putting a number of collimators together a multi-channel collimator is created, which is illustrated in Fig (1-7-b). As Fig (1-7-c) shows although lead collimator rejects most of the scattered photons, some of them after scattering, change their directions and will be detected.

### 1-3-2-B : ANGER CAMERA :

The Anger camera is the essential part of radionuclide system for detecting the high energy photons and producing an electrical current proportional to their intensity. As Fig (1-8-a) shows the Anger camera consists of a set of photomultiplier tubes which are covered by a layer of NaI(TI) crystal. The operation of each photomultiplier tube is illustrated in Fig (1-8-b).

The photons which are emitted through the collimator in collision with the atoms in the thick crystal of the camera lose their energy by scattering, photoelectric interaction or both. Thus, these interactions cause the crystal to produce light (Scintillate).

The number of light photons produced by the crystal is proportional to the total photon energy absorbed by it. The crystal, by means of a light pipe, is optically coupled to the photomultiplier tube. Each photo tube takes light as its input and produces a pulse in its output proportional to the absorbed energy. The detected pulses have a spectrum of

amplitudes. Then the electronic circuitry sets an energy window which detects only the photo peak. After acceptance of one pulse in accordance with its amplitude, the x, y position of the event is passed to the memory of computer and used to form an image.

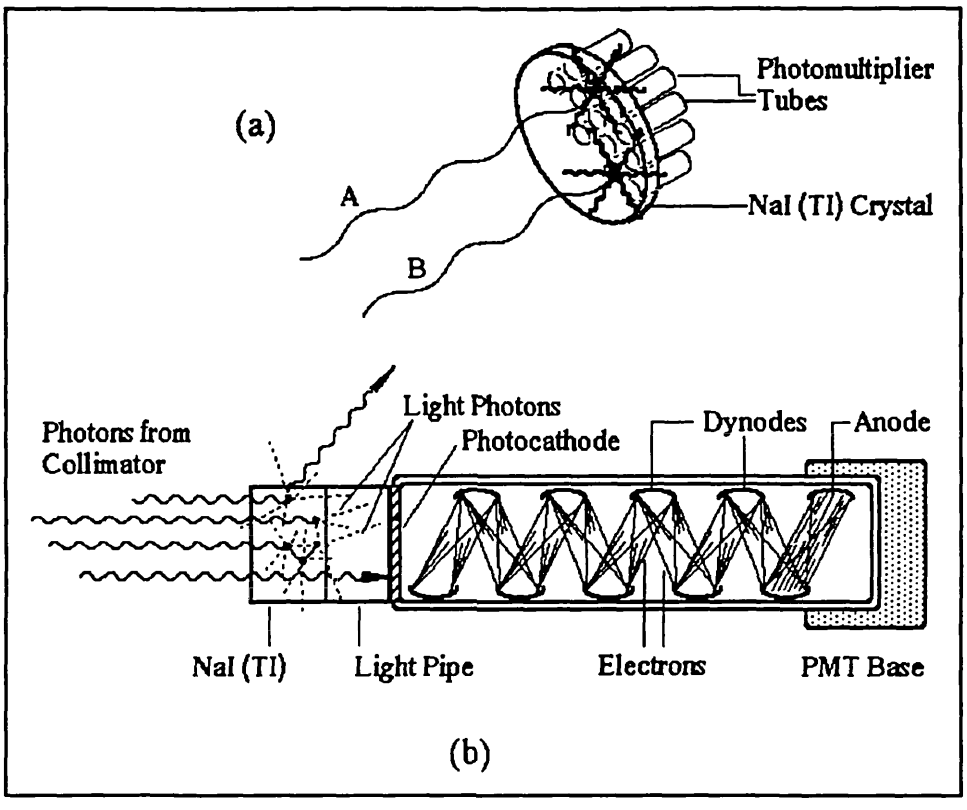


*Fig (1-8) : (a) Basic consept of the Anger Camera. (b) The basic photon detector composed of a NaI(TI) or other scintillator crystal and optically coupled to a phototube.*

## 1-3-2-C : DETECTION TECHNIQUES :

In the case of single photon radionuclide imaging, the simplest form of producing an image is longitudinal emission. The image produced by this technique is the superposition of out-of-focus planes with the in-focus planes. Fig (1-9-a) shows the simplest mode in

which a patient is rotated in front of the camera, Budinger (1980)[19]. Fig (1-9-b and c)show other modes of trans-axial emission computed tomography. In the rotating camera system the anger camera can rotate 360 degree on a suitable mechanical frame.

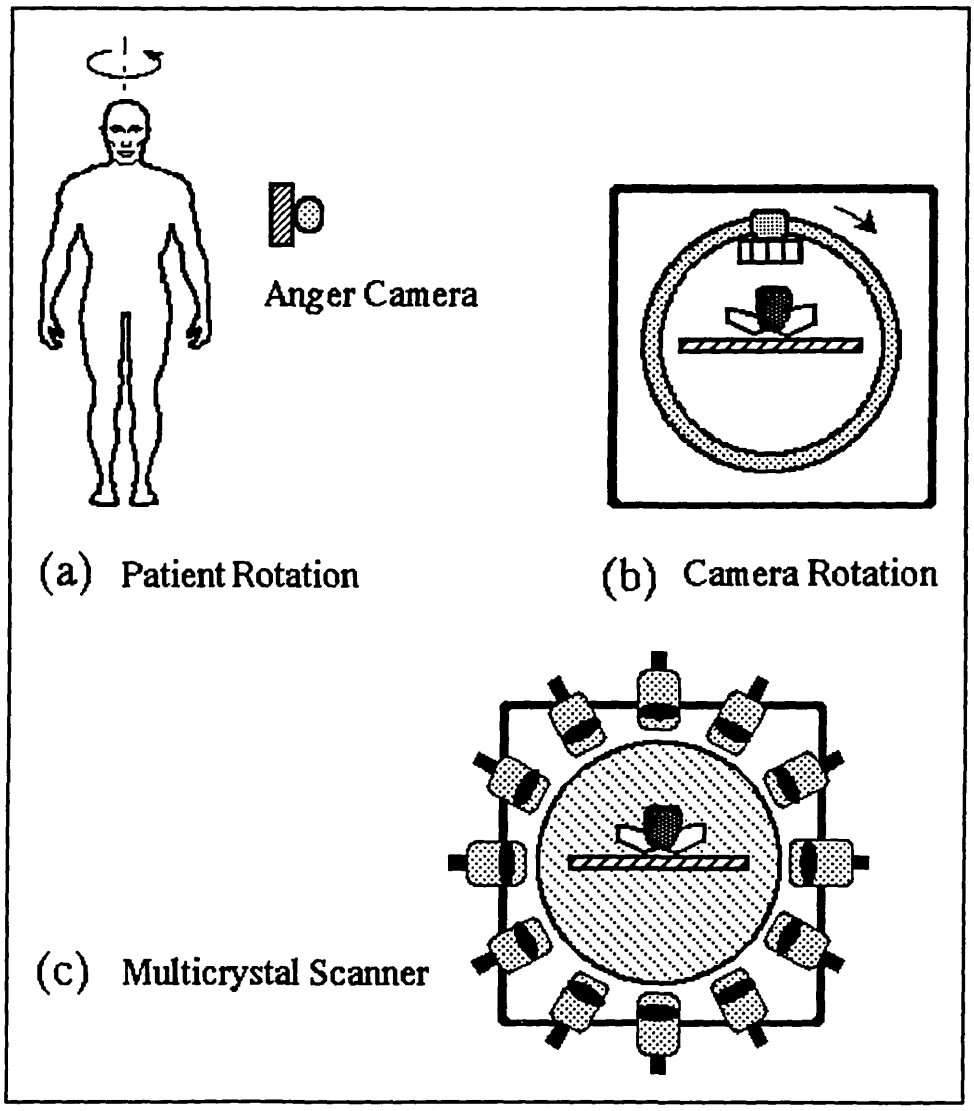


*Fig (1-9) : Different Types of techniques which are applied to transaxial emmision Computed Tomography. (a) Patient Rotation, (b) Camera Rotation, and (c) Multicrystal Scanner.*

The collected data during the rotation of camera is used to reconstruct an image. In the case of positron tomography, after the collision process is taken place, two high-energy photons depart from each other at 180 degree. This fact is the basis for an electronic collimator. Due to the high speed of the photons (speed of light), they arrive at the detectors at the same time. Thus, as Fig (1-10) illustrates, by monitoring the two detectors which have received signals within a very short time interval, it is possible to determine the line along which the source must reside.

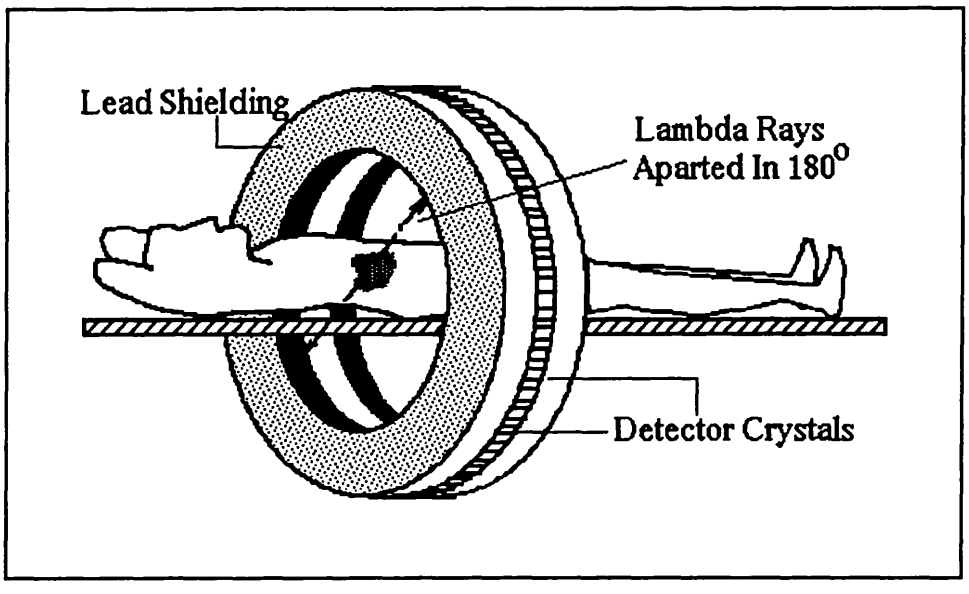


*Fig (1-10) : A modern positron emission tomographic device with closely packed detectors. Each detector contains its own scintillation crystals and photomultiplier tube.*

By having 500000 detections of such events a computer reconstruction of the image is possible . Fig (1-11-a) shows the longitudinal Positron Emission Tomography (PET) system, which consists of two gamma cameras oriented in parallel.

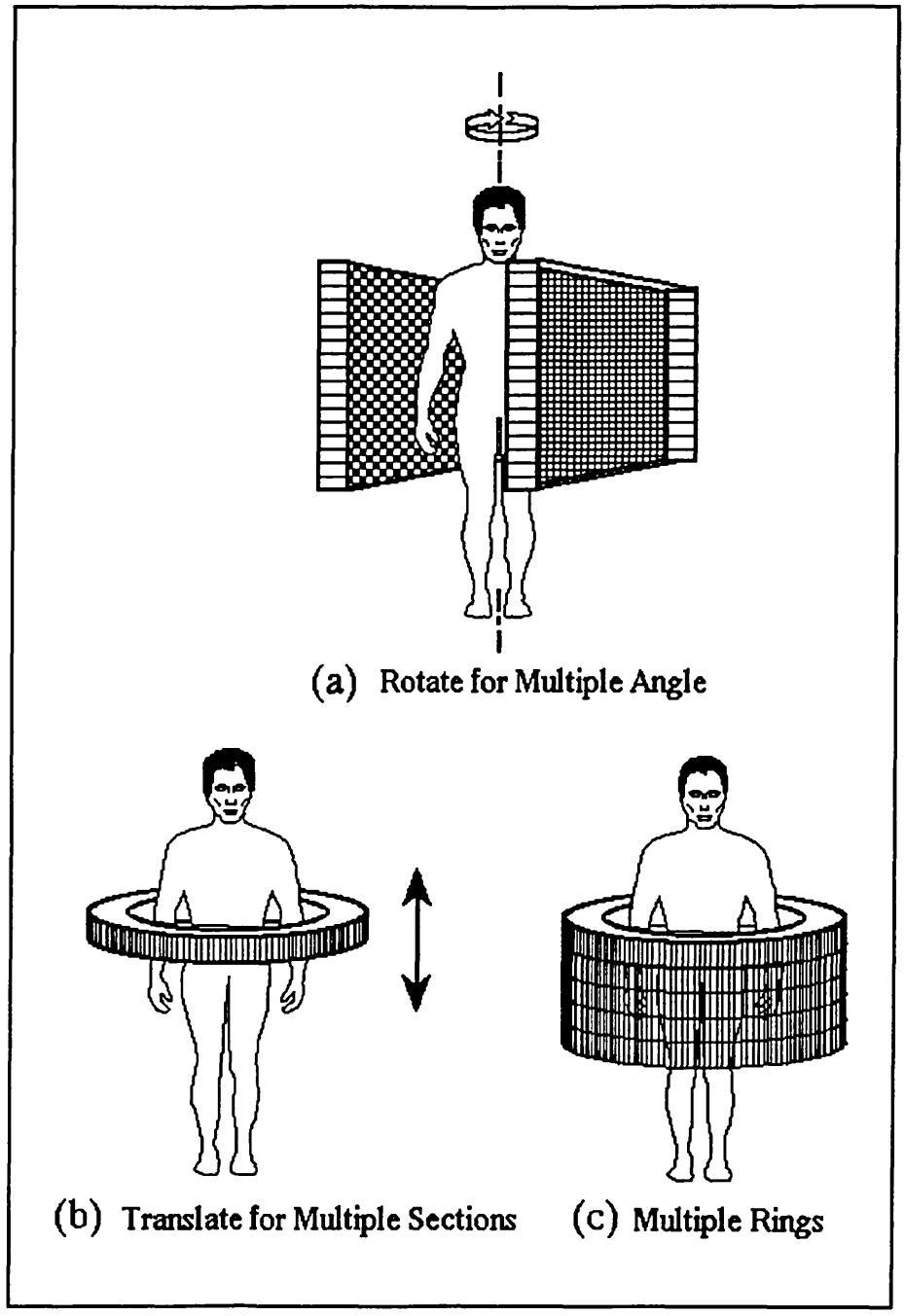


*Fig (1-11) : Different types of positron emission tomographic devices. (a) Plannar detector, (b) Single ring array detector, and (c) multiple-ring array detector.*

Since it is difficult to have quantitative data in longitudinal PET, multi-detector configurations have been developed. In these systems the acquisition of one or more trans-axial images is possible and there is no need for patient to be rotated as illustrated in Fig (1-11-b and c). For more details refer to Budinger et al. (1979)[21].

## 1-4 : COMPUTED TOMOGRAPHY :

Computed Tomographic (CT) imaging is a method for creating a sectional image of the body by means of mathematical calculations over a series of projections provided from a part of an object. In this technique the penetrating radiation source is x-ray. In comparison to the other sources of energy, x-rays achieve more speed, higher resolution and better contrast. In fact the principle of computed tomography or CT scanning is based on the Radon theory that by having a series of one dimensional projections of an object from many angles of view, it is possible to reconstruct a two-dimensional image of it.

Radon (1917)[138] first derived the equations which describe the reconstruction of an object from its projections. Later Cormak (1980)[32] applied this technique to phantoms and Hounsfield (1980)[72] developed the first clinically useable CT scanner.
It is evident that CT's success is mostly due to its better contrast sensitivity. On the other hand because of some limitations in computer technology, there are some restrictions on speed and resolution of CT scanners.

### 1-4-1 : BASIC PHYSICS OF CT SCANNING :

Radon's equation which is the foundation of computed tomography, describes the

reconstruction of an object from its projections. In order to perform this task, it is required to obtain the projections along all possible lines within the cross sectional plane of the object.

It is obvious that different tissues have different elemental compositions and , therefore, would cause different attenuations for the x-ray radiation. The amount of attenuation for a very small thickness of a homogeneous medium $\delta I$, is proportional to the initial number of x-ray photons $I_0$, linear attenuation coefficient $\mu$, and the thickness x. Therefore;

$$\delta I = -\mu . I_0 . \delta x \qquad (1-8)$$

For a thick medium which in the case of biomedical examinations is the human body, attenuation takes an exponential form expressed by, Herman (1980)[70];

$$I = I_0 . e^{-\mu x} \qquad (1-9)$$

or rearranged in another form;

$$\ln(\frac{I}{I_0}) = \mu . x \qquad (1-10)$$

If we consider the actual medium, (the human body), it is a combination of different tissues that have different attenuation coefficients. If we assume that these coefficients are constant across a very small thickness of tissue, on a straight line throughout the body, we can rewrite Equation (1-10) as;

$$\ln\left(\frac{I}{I_0}\right) = \int \mu(E,x)\,dx \qquad (1\text{-}11)$$

Equation (1-11) shows that the logarithm of the ratios of the intensities is equal to the summation of all small distances ***dx***'s multiplied by the corresponding linear attenuation coefficients $\mu$'s. The term $\mu(E,X)$ indicates that the attenuation coefficient $\mu$, is a function of distance, because of different layers of tissues, and the x-ray energy, ***E***.

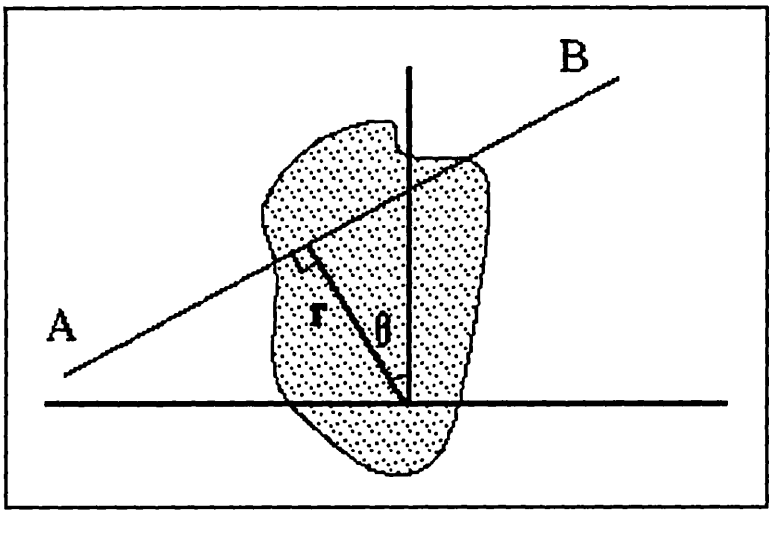


*Fig (1-12) : The geometry of a single x-ray beam through a section of an object.*

Now let us consider the geometry of a single x-ray through a section of the object as shown in Fig (1-12). The line between point ***A*** and point ***B*** could be completely specified by the angle $\Theta$ and the distance ***r*** along a perpendicular line through an origin. Then it is possible to find out all lines of projection and apply Equation (1-8) to each of them.

The final stage is a mathematical calculation of Radon's equation to reconstruct the two dimensional image of the object.

## 1-4-2 : INSTRUMENTATION :

The source of energy in a CT scanner is an x-ray generator which was discussed in section 1-2. Thus in this section we only describe the data acquisition techniques.

The simplest scanning geometry for making projection measurements along various lines consists of a single " pencil" x-ray beam which traverses a desired slice to be examined at a particular angle of view. As Fig (1-13 ) shows each line of projection is placed between the source and detector, and by rotation of the x-ray source we can capture different lines of projection.

The x-ray detector records the intensity of transmitted x-ray during translation of the x-ray tube and detector as shown in the picture. This set of measurements is reflected to the profile. Each point in the profile represents the transmitted x-ray intensity for one line of transmission.

This process is repeated for multiple angles of view and a separate profile is obtained for each angle. Thus the objective of computer reconstruction is to convert or transform a series of profiles into a CT image.

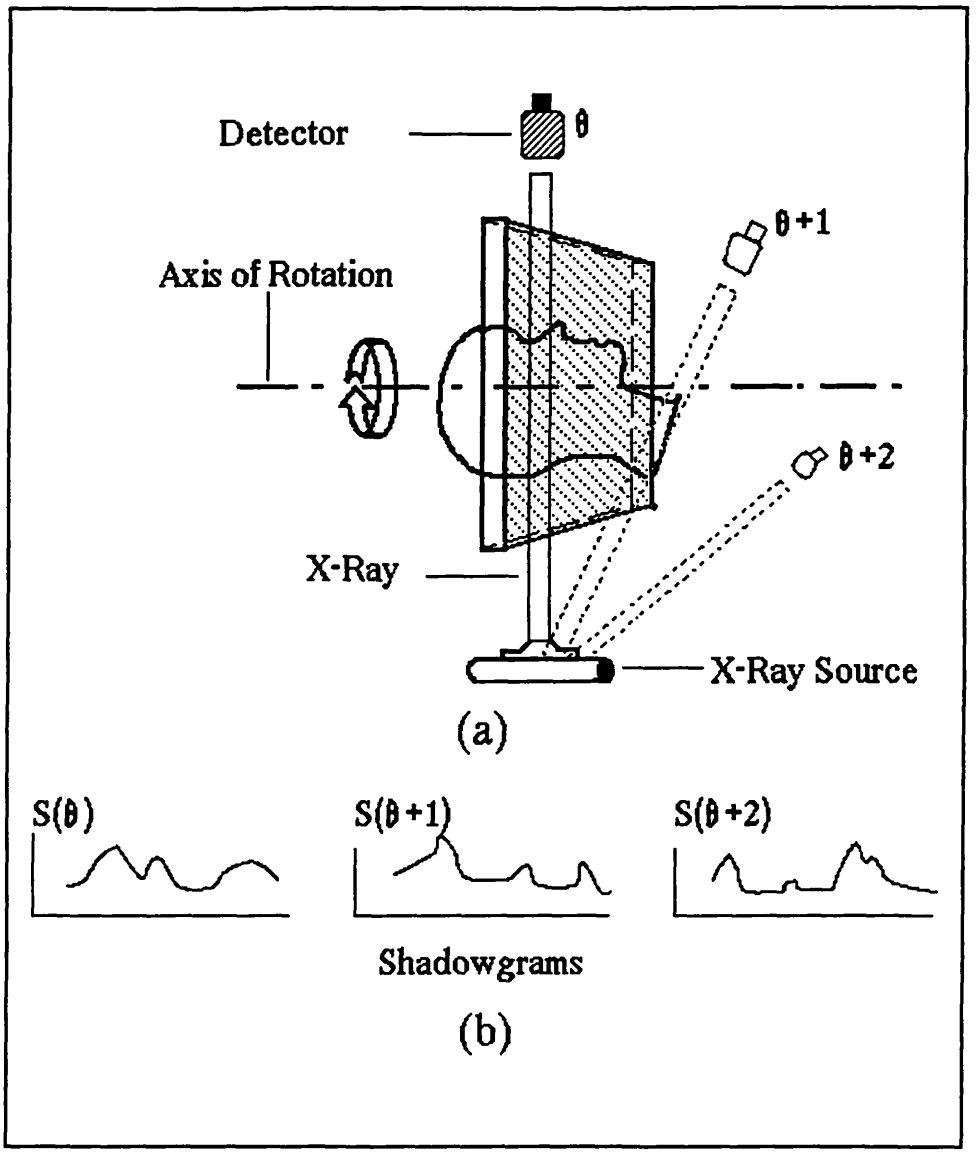


*Fig (1-13) : (a) The scanning geometry used by first generation of CT scanners. (b) The shadowgrams captured in the angles θ, θ+1, and θ+2 respectively.*

Fig (1-14) shows three different approaches used for data acquisition. In the original scanner shown in Fig (1-14-a), a pencil x-ray beam would traverses to the slice of body to be examined at a particular angle of view. An x-ray detector would record the

transmitted x-ray intensity during translation of the x-ray to produce the profile. Fig (1-14-b and c) show two modern scanners which have the benefit of multiple x-ray beam detectors.

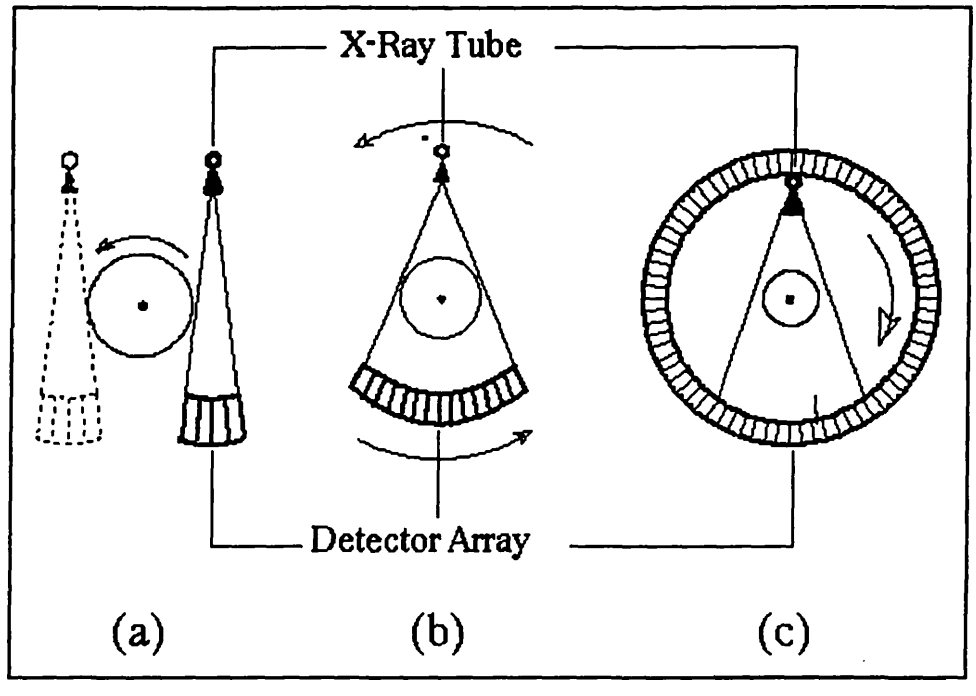


***Fig (1-14) : Fan beam Scanning configuration in the modern CT scanners. (a) Translate-rotate, (b) rotate-rotate, and (c) rotate-stationary types.***

In this approach x-ray beams are arranged as a fan in combination with multi-element detector arrays. Due to the large collection angle of the fan (30 to 40 degree or more), up to several hundred times more photons per second are detected. Thus, scanning speed is reduced from 300 s in early scanners to 1-6 seconds in modern fan systems,Body and Parker (1983)[14].

### 1-4-3 : LIMITATION IN CT SCANNING :

In addition to the limitations already mentioned for plain x-ray angiography, there are some important limitations specific to CT scanning.

In commercially available CT scanners the number of individual rays sampled within a fan varies up to 750 and the number of fan projections may be 1000 or more. Therefore, up to 750000 measurements are recorded in a single scan. As each projection effectively forms one pixel of the final image, the image matrix will be less than 850 x 850 pixel. In commercial CT scanners, the resolution varies from 256x256 to 512x512. This lack of high resolution image is the price which is paid for speed. Of course some geometrical limitations such as the number of detector elements, their dimensions, x-ray width and collimator configuration also contributes to the degree of obtained resolution. For a more detailed discussion on the principles and physical concepts of computed tomography refer to articles by T.H. Newton (1981)[122] and G. Herman (1983)[69].

## 1-5 : MAGNETIC RESONANCE IMAGING :

Magnetic Resonance Imaging (MRI), also called as Nuclear Magnetic Resonance Imaging (NMR), is a new technique in medical imaging which is based on the interaction of atomic nuclei with externally applied magnetic and Radio Frequency (RF) fields, Bloch et al (1946)[12] and Purecell et al (1946)[137]. In effect it is a spatial encoding of the nuclear magnetic resonance signal, Lauterbur (1973)[94]. The MRI signal is a low energy electro-magnetic radiation. This radiation is due to energetic transitions of nuclei in response to a radio frequency (RF) pulse in the presence of a static magnetic field, Bloch et al (1946)[12]. Nowadays, by utilizing spin echo pulse sequences and two dimensional

fourier transformation, high-quality images of the heart have been generated, Lanzer et al (1984)[92].

High magnetic resonance enables MRI to identify a variety of tissue characteristics, cardiac abnormalities, and even quantitative flow evaluation Wesbey et al (1984)[169], and Stark et al (1984)[154]. This technique is completely noninvasive and requires no exposure to ionizing radiation. There have been no report of having harmful effects either from the imposed low energy RF pulses or from the static and time-varying magnetic fields.

### 1-5-1 : BASIC PHYSICS OF MRI :

As mentioned previously, nuclear magnetic resonance is the result of interaction of atomic nuclei with applied magnetic and RF fields. Since hydrogen is an abundant element in living organisms, the proton (the hydrogen nuclei) could be the most easily imaged constituent of the body, and therefore proton MRI is the most practical imaging technique in MRI systems.

Protons have an intrinsic angular moment called spin. The proton's spinning charge generates a magnetic field and a magnetic moment. The magnetic moments of the hydrogen nuclei, in the absence of an external magnetic field, are in random orientations as illustrated in Fig (1-15-a).

If an external magnetic field of $\mathbf{B_0}$ is applied, individual nuclei align themselves either in parallel or anti-parallel to the direction of this field. The energy level of these two states are different, and those in the direction of the same external field have lower energy. Protons can switch between different states of energy by absorbing or emitting

the required electromagnetic energy in the form of photon. Of course it is impossible to consider the behaviour of one photon in any measurement. Hence, what is measured in an MRI experiment is the action of all protons within a sample.

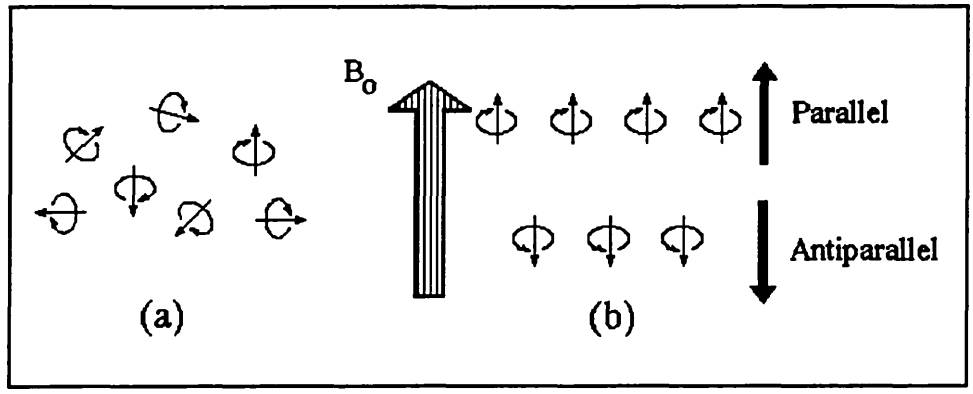


*Fig (1-15) : Schmatic representation of hydrogen nuclei (protons) aligniing in a static external magnetic field. (a) Hydrogen nuclei in the absence of magnetic field. (b) After an external magnetic field of $B_0$ is applied.*

Thus if we intentionally switch the protons to a higher state, we can measure the intensity of an electromagnetic signal which is proportional to several parameters including the tissue structure. Let us assume that the direction of the external static field lies along the $z$ axis. If somehow the macroscopic magnetization vector (the net vector sum of the individual magnetic moments) is moved away from the $z$ axis, it will precess (rotate about) the $z$ axis with the angular frequency of $\omega_l$ (Larmor frequency), in such a manner that,

$$\omega_1 = \gamma \cdot B_0 \qquad (1\text{-}12)$$

where $B_0$ is the magnetic field and $\gamma$ is the gyro-metric ratio.

To perturb the magnetization vector away from the z axis, an RF pulse of energy must be introduced at the Larmor frequency. This pulse will tip the magnetization vector and the degree of tipping is determined by magnitude and duration of this RF pulse. A 90° pulse, is an RF pulse which cause the magnetization vector to be tipped by 90° such that it lies totally in the x-y plane.

Following the 90° pulse, an RF energy will be emitted by the precessing nuclei with a frequency equal to the Larmor frequency. The intensity of this emission is proportional to the magnetization component in the x-y plane. This component which is called *transverse magnetization* decays exponentially. Therefore, the signal intensity also decays in the same manner. The decay of the *transverse magnetization*, $M_T$ is expressed as :

$$M_T(t) = M_T(0) \cdot e^{\frac{-t}{T_2}} \qquad (1\text{-}13)$$

where $T_2$ the *transverse time*, is typically from 20 to 400 msec. Obviously after a 90° pulse, the component of magnetization vector along the z axis starts to restore itself. This is due to the absence of the RF pulse, that photons begin to realign with the main field. The *longitudinal magnetization*, $M_L$ has an exponential growth and is described as;

$$M_L(t) = M_0 \cdot (1-e^{\frac{-t}{T_1}}) \qquad (1\text{-}14)$$

In Equation (1-14), $M_0$ is the *longitudinal magnetization* after complete equilibrium and $T_1$ is called the *longitudinal relaxation time* and reflects realignment of the photons with the magnetic field. $T_1$ varies from 200 msec to 3 sec for different types of tissues. Fig (1-16-a) shows the transverse and longitudinal magnetic resonance relaxation. Fig (1-16-b) shows the differences in intensities for different tissues.

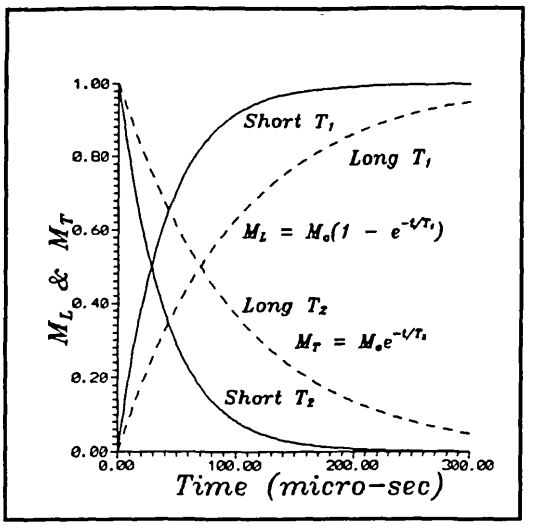


*Fig (1-16a) : Transverse and longitudinal magnetic resonance relaxation times.*

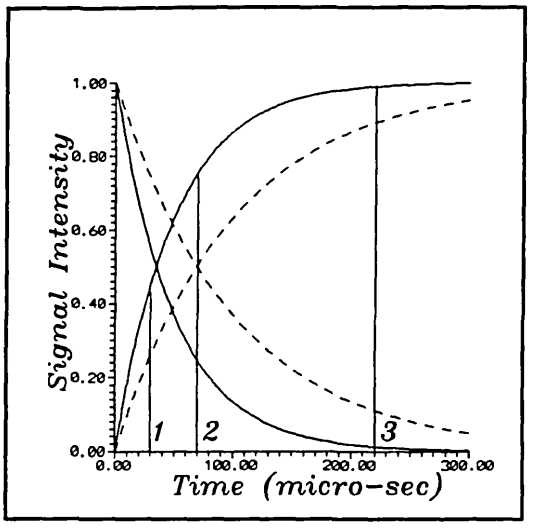


*Fig (1-16b): Signal intensity versus time for two tissues,one with a relatively long (dashed line) and one with a relatively short (solid line) $T_1$ or $T_2$ values.*

It is clear that at times 1 and 3 minimal differences in intensity between the tissues is seen, while measurement of signal intensity at time 2 yields a large difference in intensity.

Considering what has so far been discussed, to reconstruct an image with good contrast it is necessary to concentrate on the variability of the MRI signal image intensity among tissues with different structures. Therefore a complex interplay between some important factors is inevitable. These factors include;

**a** : *local proton density,*

**b** : *relaxation times $T_1$ and $T_2$,* and

**c** : *specific sequence of RF pulses.*

On the basis of the interdependence of sampling times, tissue relaxation parameters, and image contrast, several RF pulse sequences have been developed. Readers who are interested for mor information can refer to Crooks (1981)[33] and Wesbey et al (1984)[169].

The detected signal in MRI system is composed of multiple frequencies which is possible to identify them. The identification of these frequencies lead to the estimation of both position and relative intensity information.

### 1-5-2 : INSTRUMENTATION :

It could be a misconception if we refer to an MRI system as a large magnet. Although the magnet is an important part of the MRI system but it is not the only component which determines the performance or overall price of the system. The original components of the MRI systems could be classified as the magnet, the gradient system, the RF generator, a computer and the mass storage device.

Fig (1-17) shows the associated components in a modern MRI system. The magnet in the MRI system is a large super conductive magnet with a hole in its centre. This hole is large enough to contain a human body. The magnetic field is along the axis of the magnet's hole.

To provide the necessary superconductivity and to reduce the electrical power consumption, the electrical windings of the magnet are cooled by liquid helium at approximately 4° K. It is possible to get a magnetic field of about 0.25 T by resistive magnets, however much larger magnetic fields can be achieved with superconductive magnets.

Another important component in the performance of an MRI system is the gradient system. It comprises of the $x$ ,$y$ and $z$ magnetic field gradient coils which are located inside the bore of the magnet. The gradient System provides the spatial information, and its coils must be energized by high quality power amplifiers capable of compensating eddy current (the rapid change in magnetic field induces a current in the windings of a magnet, called eddy current.). The proper control and compensation of eddy current by means of the gradient power amplifiers, yields high quality images.

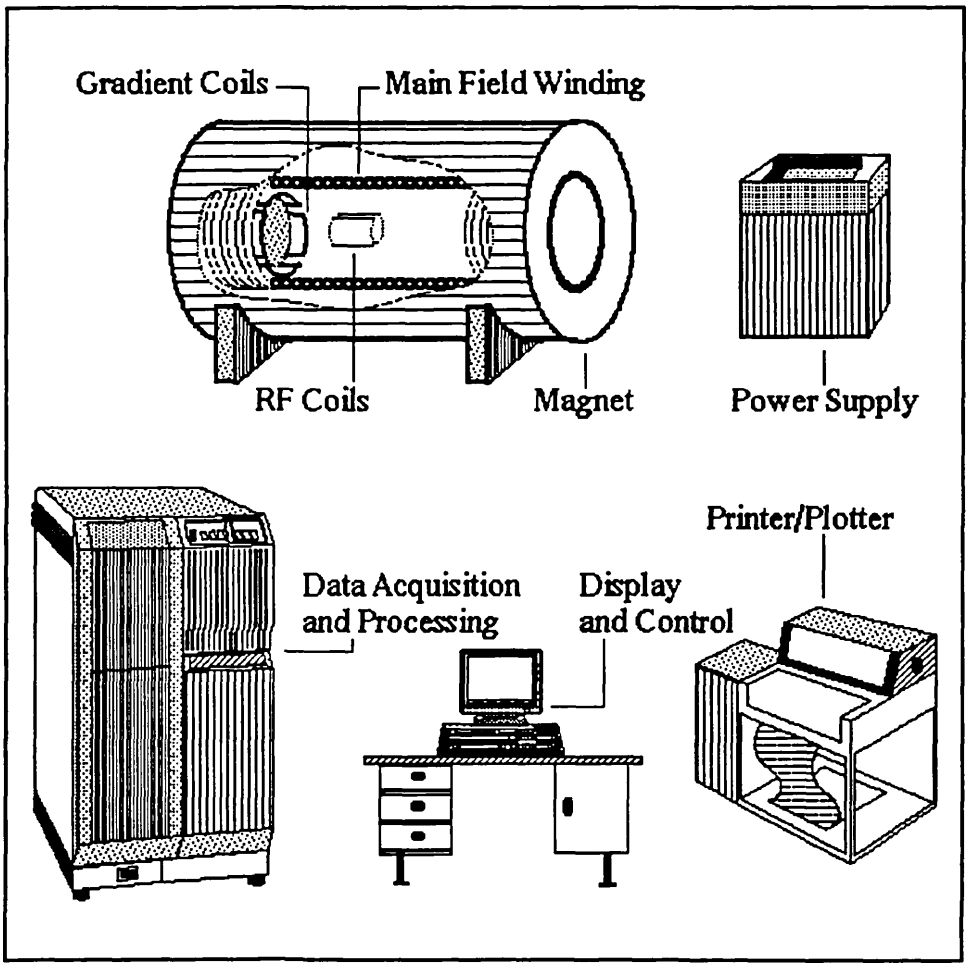


*Fig (1-17) : The main components of a modern MRI System.*

The transmission and reception of the RF energy is accomplished by a high quality short wave transceiver. To transmit the RF signal, a looped RF antenna is placed around the patient as shown in Fig (1-17).

The system's computer also has an essential role, by performing several important tasks. Since in an MRI system there are no moving parts, the gradient fields and RF pulses must be controlled by the computer. This control means having the precise timing and accurate measurements on the amplitude of the RF pulses. This computer also controls the data acquisition process. To generate an image of good quality it is necessary to acquire up to 20 slices simultaneously. These slices are later used to reconstruct a 3D image, often by employing array processors. Since it is necessary to store a large number of images per one patient, the necessity of a mass storage must be considered.

## 1-6 : ULTRASOUND or ECHO-IMAGING :

Since this chapter is a review of various of imaging techniques, it would be suitable to conclude our discussion with an introduction to echo-imaging.

Nearly seventy years ago sonar was developed by Langvin. Twenty years later Pulse-echo techniques were established. Throughout the years, A-mode and B-mode ultrasound imaging has been developed. In comparison to the other imaging techniques, ultrasound offers a relatively inexpensive instrumentation, handy and portable equipment with perfect quantitative and qualitative measurement techniques. In the following sections first a brief discussion on ultrasound wave, its generation and its features will be offered. At the end of this section different types of ultrasound imaging techniques will be discussed.

## 1-6-1 : ULTRASOUND WAVE :

In echo or ultrasound imaging techniques the ultrasound wave is introduced into the body and its propagation throughout the tissues is examined. The interaction of ultrasound with the tissue is mainly one of reflection. The reflected ultrasound waves propagate out of the body and are converted to electrical signals. These signals contain information about the different layers of tissues or any abnormality inside the body. As it will be discussed later these electrical signals are converted into diagnostic signals or images.

Ultrasound in medicine is a cyclic disturbance that passes through the tissues with a frequency of more than 1-20 MHz. The lower frequencies provide good penetration ability but less resolution while the higher frequencies provide better resolution with less penetration ability. Ultrasound is a longitudinal wave and its compression and rarefaction happens in the direction of wave propagation. The speed of ultrasound wave propagation through a medium depends upon its compressibility and density.

The relation between speed of ultrasound wave $v$, density of medium and its compressibility is expressed as :

$$v = \frac{1}{\rho x} \qquad (1\text{-}15)$$

or ;

$$v = \frac{k}{\rho} \qquad (1\text{-}16)$$

where $\rho$ is the density, $x$ is the compressibility and $k$ is the elastic modulus of the medium.

On the other hand the periodic travelling distance of ultrasound propagation $\lambda$, relatess to its frequency $f$, and the velocity of the ultrasound wave $v$. This means that;

$$v = f.\lambda \qquad (1\text{-}17)$$

Knowing the exact speed of ultrasound is extremely important for perfect performance of pulse-echo imaging instrumentation, focusing of real-time scanners, quantitative measurements, and interpretation of doppler effects.

## 1-6-2 : ULTRASOUND SOURCE :

The periodic sequence of compression and rarefaction of a longitudinal ultrasonic wave is shown in Fig (1-18).

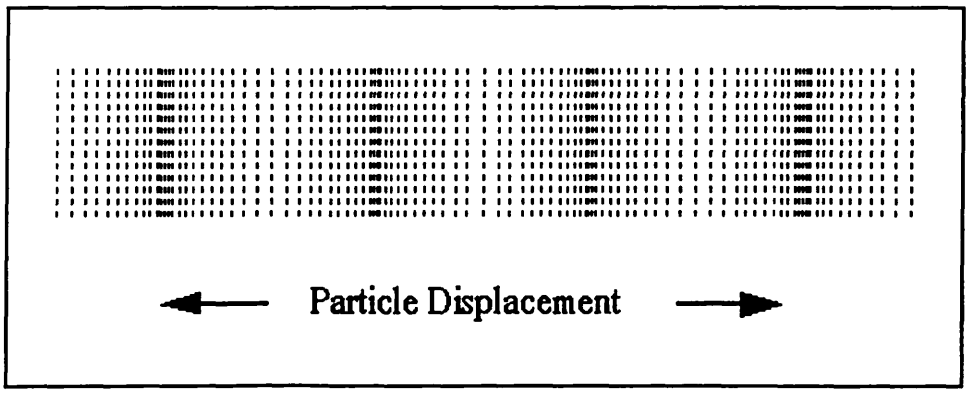


*Fig (1-18) : In a longitudinal wave the displacement of particles is parallel to the direction of propagation.*

For generation of such a wave, it is possible to move a piston moving forwards and backwards. Since the ultrasound wave vibrates at a high frequency, the moving piston must be capable of oscillation at a very high frequency. The ultimate choice is a wafer of piezoelectric material such as lead zirconate titanate (PZT) or polymer piezoelectric films known as (PVDF).

Piezoelectricity is a property of ferroelectric materials. These materials consist of microscopic ovoid structures which are highly polarized. If an electric field is applied to them, the microscopic ovals orient along the electric field and the thickness of the piezoelectric material increases. When the electric field is removed the wafer of piezoelectric returns to its original shape and reduces its thickness as illustrated in Fig (1-19).

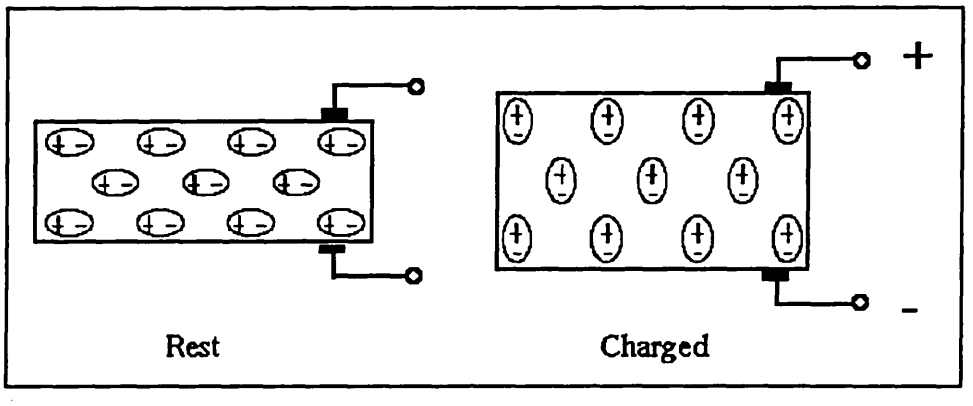


*Fig (1-19) : Representation of a piezoelectric material at rest, (a), and when a voltage is placed across it, (b).*

## 1-6-3 : REFLECTION :

As the ultrasound wave propagates through the tissue, its intensity decreases. The change in intensity is the result of diffraction, reflection, scattering, refraction and absorption.

In chapter 2 we will discuss these effects in more detail. However, a brief discussion of reflection is necessary before describing different types of ultrasound imaging techniques.

The reflection of sound wave is identical to the optical reflection of light. When the propagating ultrasound encounters the boundary (interface) between two tissues, a portion of the wave is reflected at the interface, while the remainder continues its propagation. Except of the normal incident beam, the transmitted portion of the ultrasound beam does not continue in a straight line, and is refracted at the angle of $\theta$, as illustrated in Fig (1-20).

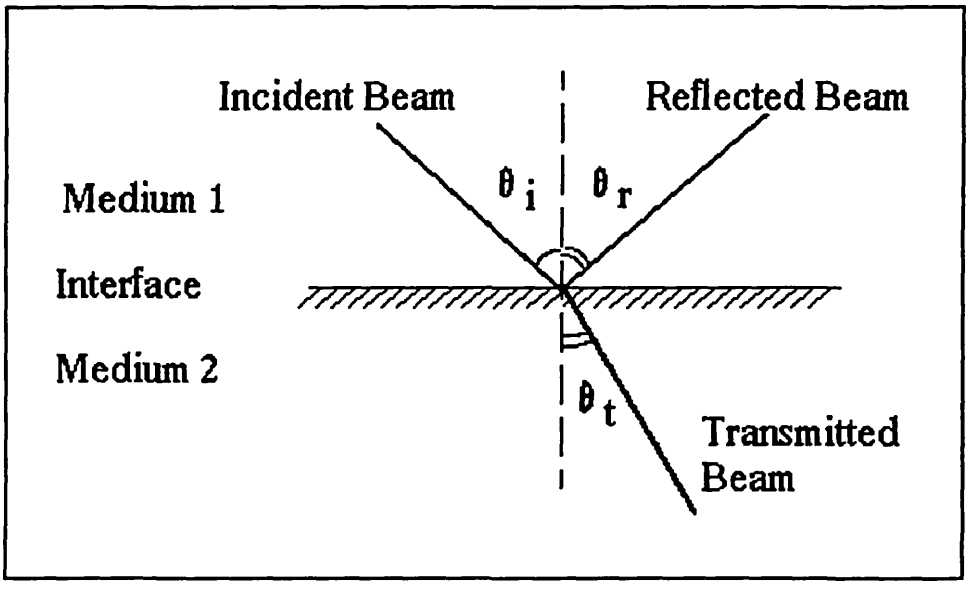


*Fig (1-20) : Interaction of an ultrasound beam at the specular interface of two media.*

The amount of energy which is reflected or transmitted in the interface of two tissues is dependent on the acoustic impedance of the tissue $Z$, defined as;

$$Z = \rho . v \qquad (1-18)$$

where $\rho$ is the density of tissue and $v$ is the speed of sound in tissue.

In order to achieve a good reflector it is necessary to have an approximately planar interface with relatively larger size in comparison to the wavelength. The roughness of surface also should be very small compared to a wavelength.

Having satisfied the above conditions, the reflection coefficient is expressed by Equation (1-19).

$$R = \left[\frac{Z_1 - Z_2}{Z_1 + Z_2}\right]^2 \qquad (1\text{-}19)$$

where $Z_1$ and $Z_2$ are the acoustic impedances of either side of the boundary. It is clear from Equation (1-19) that as the difference between the acoustic impedances of the tissues becomes larger the reflection coefficient becomes greater. For example this would be the case in the interface between bone and muscle.

In most of the ultrasound imaging techniques the incident beam is propagated normal to the interface surface. Thus the reflected beam is returned along the same path as the transmitted beam and hence it could be detected by the same transducer as shown in Fig (1-21).In such a case the remainder of wave continues to propagated along its previous path.

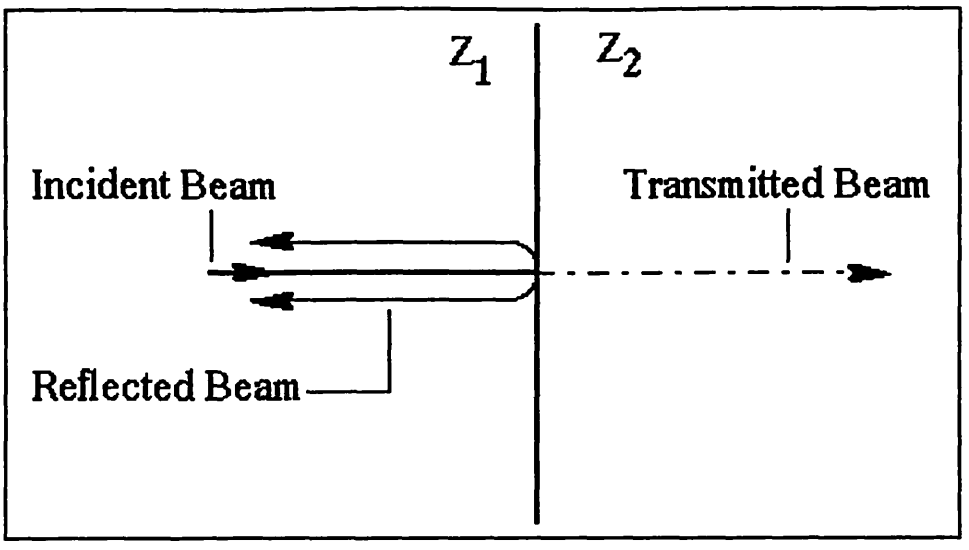


*Fig (1-21) : Interaction of a specular reflector with a normal incident beam.*

**1-6-4 : ECHO RANGING :**

The basic principle underlying diagnostic pulse-echo ultrasound is the measurement of the time necessary for sound to travel from the transducer to the target and be reflected back to it. Thus the mathematical expression for the echo ranging principle is defined as;

$$T = \frac{2D}{v} \qquad (1\text{-}20)$$

where $D$ is the distance between the ultrasound source and the target, $v$ is the speed of the ultrasound wave in the medium and $T$ is the time for a complete travel from transducer to the target (Transmission), and back to the transducer (Reflection).

Considering that the speed of sound in tissue is about 1540 m/s, and the normally small distance between the transducer and the point of examination, the times involved are very short and typically measured in hundreds of microseconds. This fact causes a bit more complexity of instrumentation but has no effect on the basic principle of echo ranging. Therefore, the process of ultrasound echo ranging could be classified as:

**a :** *Generation of an ultrasound pulse*

**b :** *Transmission of the pulse through the interface(s) of different layers of tissues.*

**c :** *Reflection of ultrasound pulse from the interface(s).*

**d :** *Detection of the reflected echo(s)*

**e :** *Calculation, processing and display of the range of target(s).*

**1-6-5 : A-MODE :**

The A-mode scanning is the simplest technique in echo imaging. As Fig (1-22-a) shows, an ultrasound transducer generates a large burst of ultrasound which propagates through the media. At every interface along the propagation path a portion of the ultrasound wave is reflected back towards the transducer, which is received by it, Fig (1-22-b).

The next step is to rectify the detected signals as illustrated in Fig (1-22-c), and then they will be ready for low-pass filtering which collects the envelope of the rectified signals.

The processes of rectification and smoothing cause the loss of information because during the filtering process some frequency components of the original signal will be rejected. However rectifying and filtering help us in processing of the detected signals by lower bandwidth electronic hardware and software with less sophistication and a lower price.

Therefore, as Fig(1-22-d) shows the final output of the low pass filter is a series of spikes separated by time on the horizontal axis. The vertical height of the spikes is proportional to the amplitude of the original back scattered signal. Hence, this technique is known as the A (for amplitude) mode scanning .

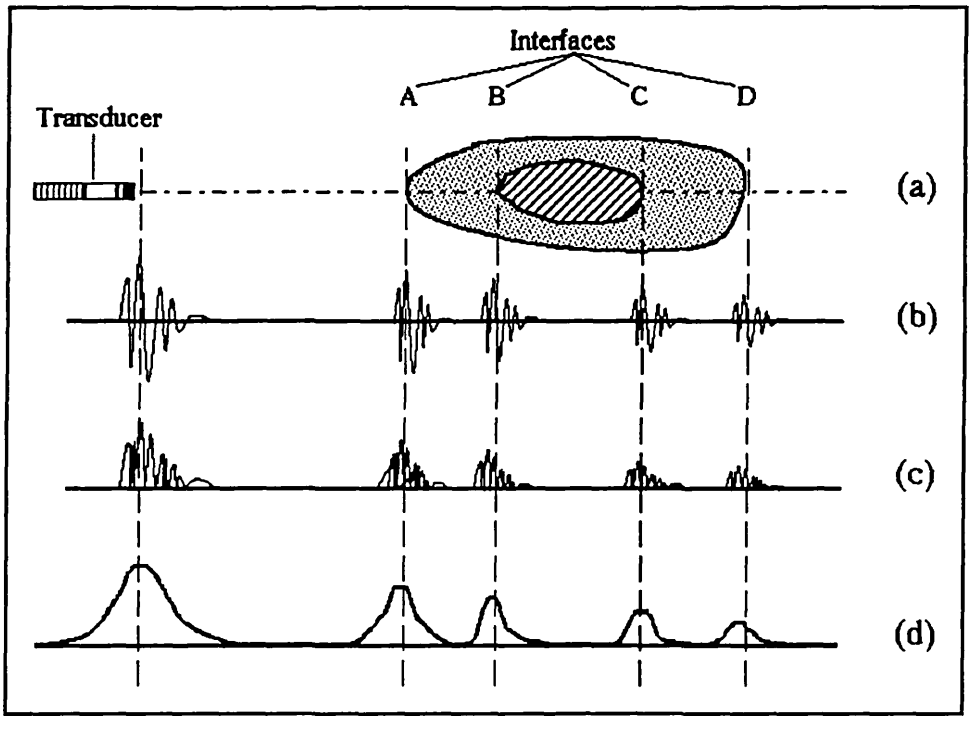


*Fig (1-22) : Formation of A-mode signals at the interfaces through the propagation path.*

By adding a time gain compensation (TGC) stage, the loss of energy in the reflected wave can be compensated. This loss of energy is mainly due to the absorption property of the tissues, which reduces the amplitude of the ultrasound wave in both transmission and reflection paths. As a result, the signals from the deep interfaces will be much smaller and TGC attempts to correct this loss of energy. Therefore, we can expect a better outcome such as what is shown in Fig (1-23-b).

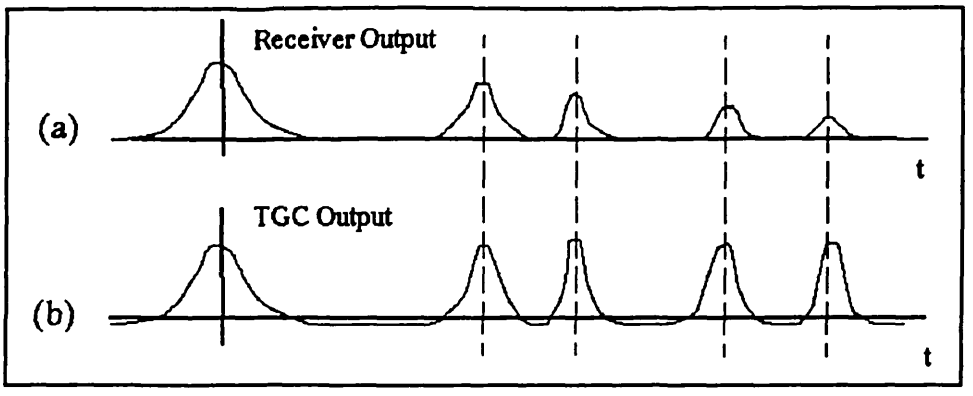


*Fig (1-23) : Time Gain Compensation for A-mode signals. (a) before TGC, and (b) after TGC.*

The A-Mode imaging is mostly used for quantitative measurement of structures lying along the ultrasound beam. Of course A-Mode ultrasound technique is a one dimensional presentation of acquired information and it is very difficult to be interpreted in a qualitative evaluation.

**1-6-6 : B-MODE :**

The B-Mode technique is mainly based on the A-Mode instrumentation, but the raw information of time and amplitude is used to display a two dimensional image of an anatomical structure. In this technique the time interval between every two spikes is used to define the physical dimension of one pixel of an organ and the amplitude of the spike could be converted to its brightness on the screen.

Thus, as Fig (1-24-a and b) show, greater reflection causes a greater spike and consequently a brighter pixel proportional to higher magnitude of intensity will appear on the screen. It is clear that a complete period of transmission and reflection of an

ultrasound wave would only create one line of the two dimensional image. Thus, to complete a single image frame it is necessary to scan the whole area of interest.

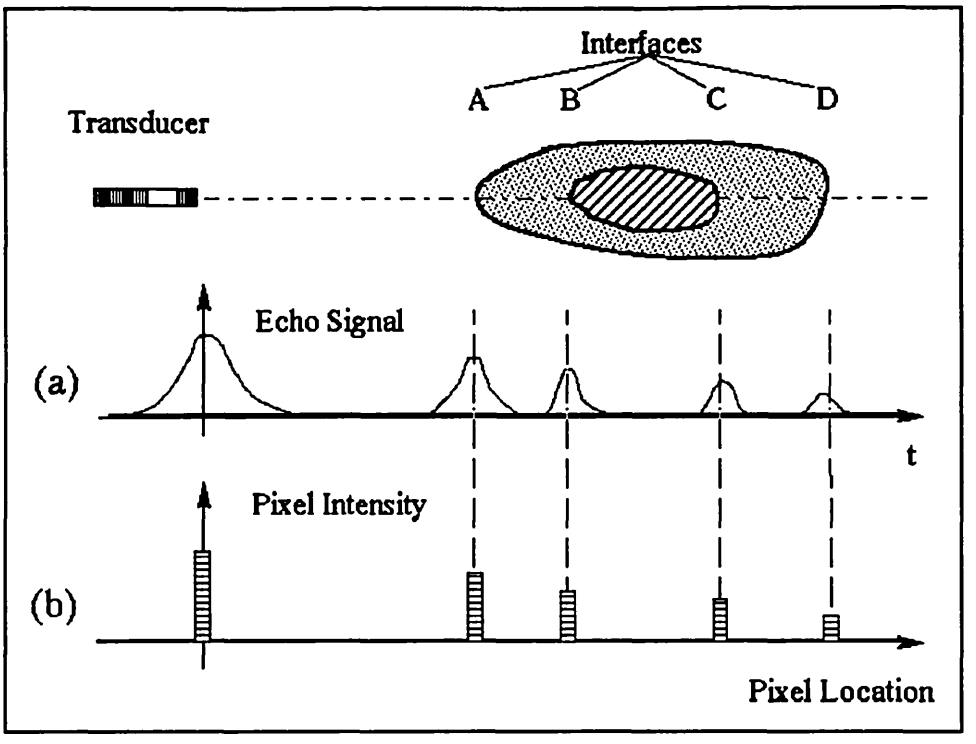


*Fig (1-24) : Formation of pixel intensity in the B-mode image generation. (a) A-mode signals, and (b) pixel intensity in the B-mode imaging.*

Before more discuss ion in details of the B-Mode ultrasound systems, it is necessary to have a brief look at different techniques of image acquisition in the B-Mode ultrasound imaging. These techniques could be categorized into four different classes of scanning procedures. These are classified as :

**a :** *Mechanical Sector Scanning*

**b :** *Mechanical Linear Scanning*

**c :** *Electronic Sector Scanning*

**d :** *Electronic Linear Scanning*

In mechanical scanning there is one transducer and as a consequence there is only one ultrasound beam which is required to be scanned mechanically. The manner in which the transducer is scanned and the configuration of the transducer assembly makes two types of mechanical scanning techniques possible.

In electronic scanning technique there is an array of piezoelectric elements which are triggered sequentially to scan the ultrasound beam in front face of transducer. An electronic circuit conducts the procedure of sequential triggering of piezoelectric elements in the array transducer.

In electronic scanning of an ultrasound beam it is possible to change the direction of the beam and even focus on a desired point. Electronic beam steering is a feature of phased array transducers which are discussed in chapter three. Also a detailed discussion on different types of array transducers and their operation will be given in chapter three.

Fig (1-25) illustrates the block diagram of a B-Mode imaging system. As it can be seen the main body of the system is very similar to the A-Mode ultrasound system, but some additional sections are necessary to be added to it. In this technique after rectification and filtering, the captured signals should be digitized. Then the grey level of every pixel in any line of the image is calculated.

The next task is to apply the necessary processing techniques to convert the polar coordinates of the scanned video signals to rectangular coordinates suitable for display. This is done by digital scan converter which maps each individual point along each scan line into a pixel in the appropriate rectangular coordinate.

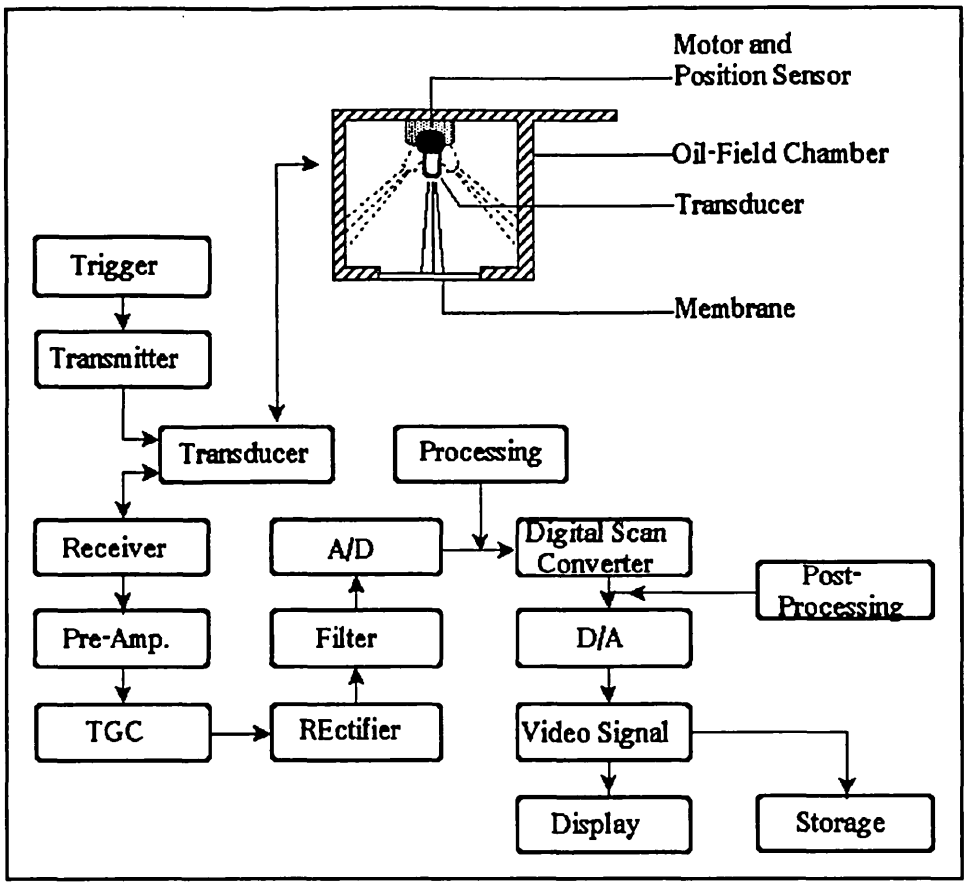


***Fig (1-25) : The B-mode imaging system block diagram.***

Before presentation of the image on the screen any desired image and signal processing can be performed. Then, after digital to analog conversion, the video signal is ready for display, or it can be stored in a mass storage device.

An example of the two dimensional image produced by a mechanical sector scanner is shown in Fig (1-26).

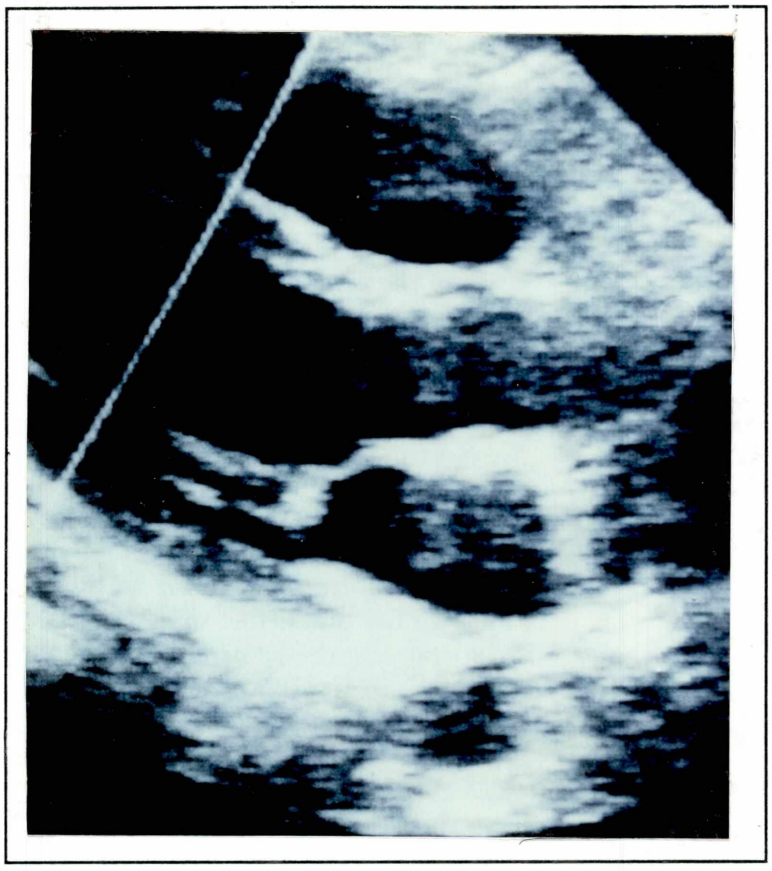

*Fig (1-26) : A B-mode image produced by a mechanical sector scanner.*

**1-6-7 : M-Mode :**

If it is desired to monitor the motion of moving organs inside the body, the M (for motion) -Mode imaging is the choice. In M-Mode imaging one axis represents the depth (proportional to the movement), and the other axis indicates the time. Therefore, the B-Mode display is recorded on a strip of photographic paper.

A set of fine fibre optic lines transfers the pixel intensity from the CRT to photographic paper. The length of this paper is proportional to the time interval and any vertical trace

of light marks the relative line to a movement in any interface inside the organ's tissue. The M-Mode imaging is very popular in echocardiography for monitoring the movements of the heart wall or heart valves.

Fig (1-27) illustrates the schematic diagram of an M-Mode recorder. The signal formation in the A-Mode and the M-Mode systems is being compared in Fig (1-28), and an actual M-Mode signal is shown in Fig (1-29).

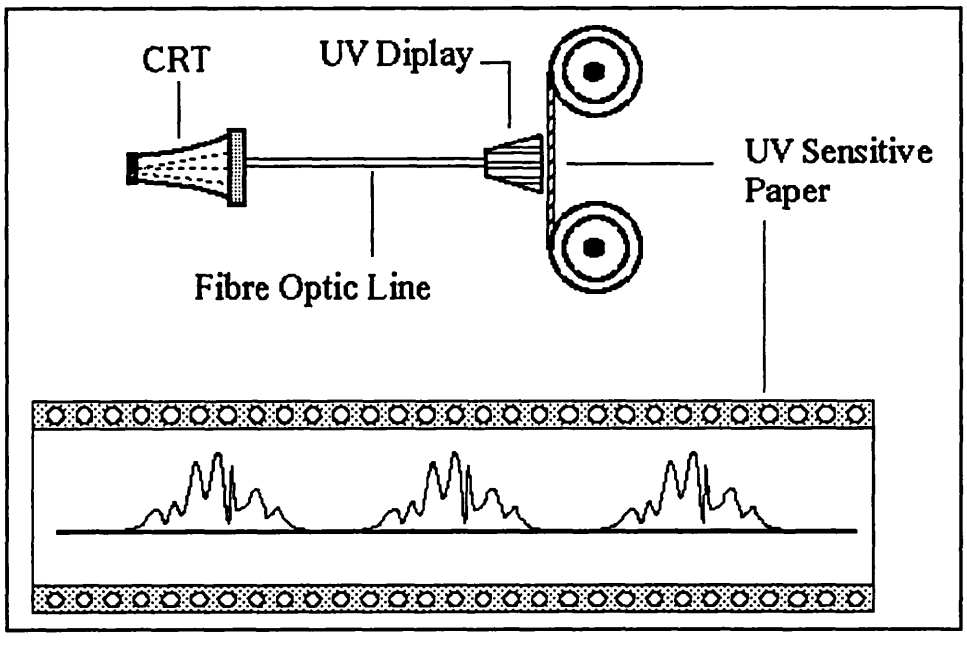


*Fig (1-27) : Schmatic diagram of a fibre-optic chart recorder used in an M-mode ultrasound instrument.*

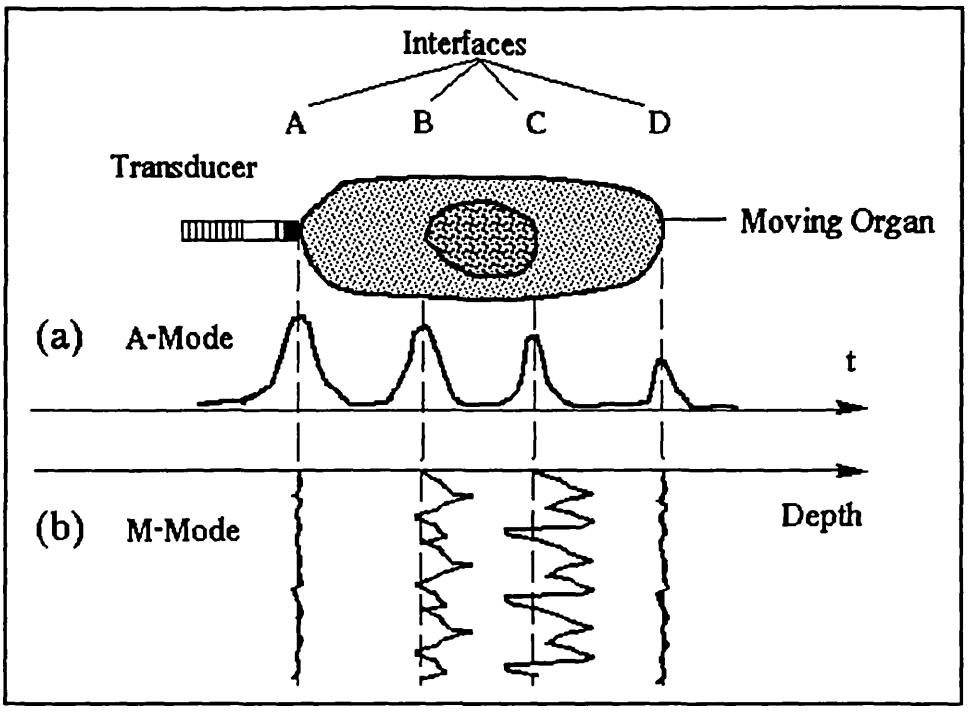


*Fig (1-28) : Formation of signals at static and dynamic interfaces in M-mode scanning technique.*

## 1-7 : Summary :

In this chapter four major techniques in biomedical imaging systems were discussed to provide a general view of each one. In the new techniques of CT scanning or MRI imaging it is possible to provide images of valuable quality. On the other hand we have to consider that patients may face some risks during the procedure of scanning, and specially when the x-ray is employed. For establishment of the x-ray, CT scanning, and MRI imaging systems a high cost for primary investment is necessary which is continued with their maintenance cost. In all of the mentioned techniques we have to consider a special laboratory space which limits them to be used in a dedicated place in the hospital.

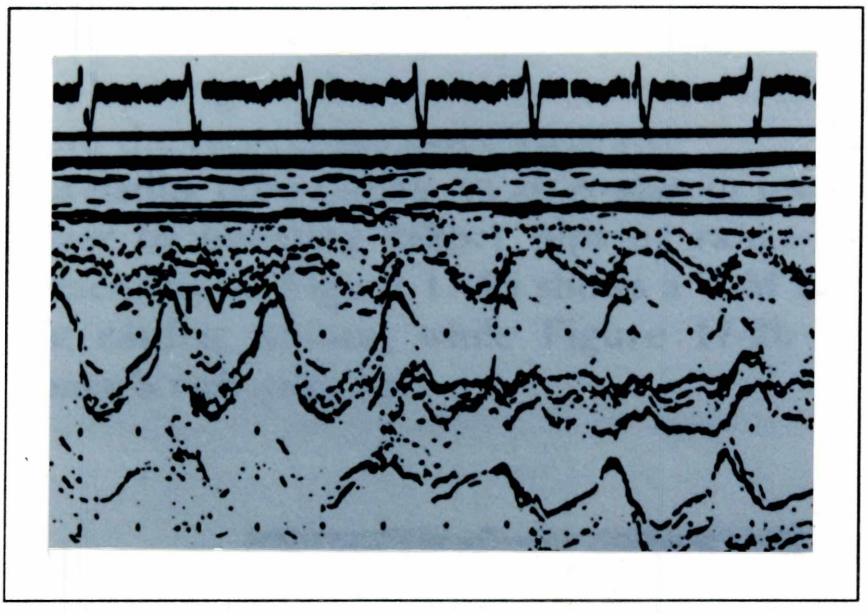


***Fig (1-29) : The actual signal captured in an M-mode scanner.***

On the other hand ultrasound imaging systems with their lower cost, provide handy and portable devices for medical examinations every where. There have been no reports of any sort of risk for biomedical use of ultrasound and this is another point of which is important in consideration of ultrasound as a copletely safe diagnostic technique.

On the basis of our studies and the review presented we chose to carry out this research into the use of ultrasound as an imaging tool. The first encouraging reason was the ability of ultrasound transducer as a miniature tool for itravascular examinations. It is not possible to use the other imaging modalities for intravascular imaging whereas an ultrasound transducer can be easily mounted at the tip of a catheter. Furthermore the low cost of system production, the safety of this technique in biomedical applications, portability of the system as it can be moved from clinic to clinic, and its diversity of use in different applications are other important aspects of ultrasound systems which were considerd at the start of this work.

And finally we should add the simple operation of ultrasound imaging systems which makes them more popular among their users from general practitioners to obstetrician.

*Chapter Two*

# *Ultrasound in Medical Engineering*

## 2-1 : INTRODUCTION :

Ultrasound now has become an important diagnostic tool in medicine. Having a good knowledge of ultrasound and enough study on biological tissues are the first steps in design and development of a medical diagnostic ultrasonic equipment. Therefore, the goal of this chapter is to present a general view of the ultrasound, its associated properties, and a brief study of biological tissues.
At this stage it is perhaps worth restating the importance of ultrasound in this work. As it will be shown later in chapters three and four, the ultrasound system designed in this work utilises the A-mode technique for three dimensional reconstruction of arterial structures. It has been mentioned previously that an ultrasound system lends itself to being very portable, safe and cost effective. This system is set to use the A-mode technique to acquire the data necessary for quantitative measurement of the sectional perimeter of vessels. A number of these cross sectional views are later used with the aid of special purpose software to display a three dimensional image of the vessel.

The first part of this chapter is dedicated to the nature of ultrasound wave, its generation, and its propagation. The beam pattern of the ultrasound waves in near-field and far-field is discussed, and its interactions in a medium and in different conditions are examined. Also in this part the important phenomenon of the ultrasound such as reflection, refraction, scattering, absorbtion and attenuation are studied in details. To provide a practical feeling of the theoretical aspects many tables of measured or calculated data are

included. All efforts have been made to provide further references for those who may be interested in more information and detailed discussion of ultrasound and its properties in direct relation to the presented topics.

In the second part of this chapter a brief study of biological tissues is presented. It has been tried to give simple expression on different types of tissues with more emphasise on their acoustical properties. Then vessels and routes in human body will be explained and the biological construction of arteries studied. Since this work aims to find a solution for visualisation of arteries and arterial occlusions a short discussion on arteriosclerosis and the probable source of their creation will be given at the end of this part.

The final section of this chapter briefs the vital role of ultrasound in a biomedical diagnostic equipment, and particularly as an invasive tool in answering the question of this work.

## 2-2 : ULTRASOUND WAVE PROPAGATION :

Any sound is a sort of mechanical wave. A mechanical wave is generated by the mechanical vibration of molecules in solid, gas or liquid materials. To produce a mechanical wave, it is necessary to vibrate the source of the wave, and it can be propagated if a physical medium is available. Drum skin is an example of a mechanical wave source. As it is beaten, its skin starts to vibrate and its mechanical vibration is propagated through the air molecules in the form of a mechanical wave or sound, which travels away from its source.

The driving force for propagation of sound as a mechanical wave, is provided by

transformation of potential energy stored in the medium particles to kinetic energy in their moving mass.

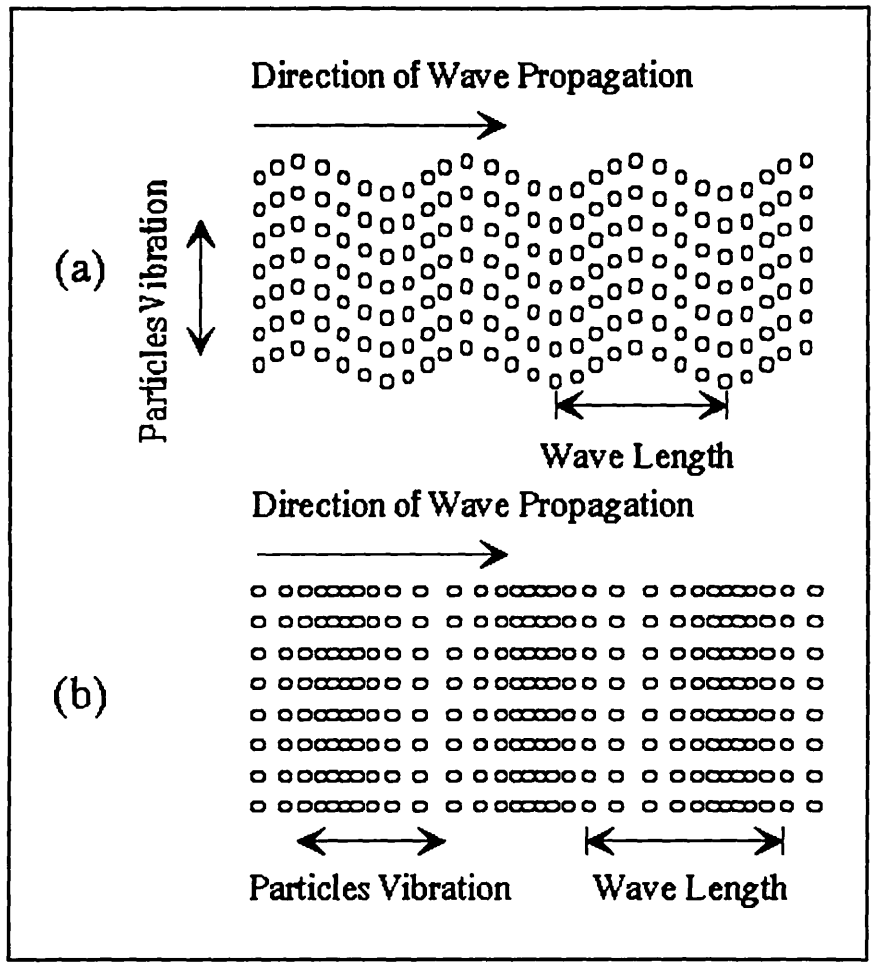


*Fig (2-1) : Propagation of machanical waves. (a) Transverse wave, and (b) Longitudinal wave.*

Considering an infinite medium in which the boundaries are very far from the wave source, two types of mass deformation in the medium's elements are possible, leading to either a compressional stress or a shear stress, Fig (2-1). On the basis of this definition two forms of wave could be generated, pressure waves and shear waves.

Pressure waves, also called longitudinal waves consist of compression and rarefaction of medium particles along the direction of propagation. In the shear waves, which are also called transverse waves, particles are moved up and down perpendicular to the direction of propagation in the medium.

Fig (2-1-a and b) illustrate a representitive appearance of longitudinal and transverse waves, respectively. In both types of waves illustrated in Fig (2-1), a periodic motion or displacement is seen. It implies that any compression and rarefaction of a periodic longitudinal wave or any displacement in a periodic transverse waveHxs repeats after a fixed period of time. Frequency is a qualitative measure of any wave which is expressed in Hertz (Hz). Sound waves with different frequencies produce different tones.

## 2-3 : PIEZOELECTRIC MATERIALS :

Ultrasound can be generated in a number of ways. Early physical studies and researches with ultrasound was performed using natural piezoelectric materials such as quartz, lithium sulphate, and ammonium dihydrogen phosphate. Recent development of ferroelectric ceramics such as the titanate compounds (e.i. PZT, Lead zirconium titanate) led to advantages including higher piezoelectric properties, easier fabrication and even easier shaping.

In early seventies, electromagnetic ultrasound, a new technique for generation and reception of ultrasound in electrically conducting media was introduced. In fact this method is based on Lorentz force transduction, a special case of electromagnetic transduction. For a more detailed discussion on physical aspects of electromagnetic ultrasound transducers refer to Dobbs (1973)[42].

## 2-3-1 : PIEZOELECTRIC CERAMICS :

One of the important classes of piezoelectric materials is synthetic ceramics with piezoelectric properties such as barium titanate, lead zirconate titanate, and lead metaniobate. Those are originally ferroelectric ceramics which are made permanent piezoelectric by applying the process of poling. In this process the elementary dipoles built in the microcrystalline structure of ferroelectric ceramic are aligned by means of a strong electric field. On the basis of poling process conditions, each type of piezoelectric ceramic can be produced in a variety of piezoelectric ceramics with different properties.

In general, piezoelectric ceramics exhibit a relatively high electromechanical coupling factor and good sensitivity to off resonance frequencies. They can be formed into the desired shape and it is easy handling in transducer fabrication process. Their high dielectric coefficient endow them with high sensitivity and enables them to drive high voltage pulses.

For the above mentioned reasons, piezoelectric ceramics have become generally the first choice in the design of the ultrasound transducers and particularly biomedical ultrasound transducers. Among the piezoelectric ceramics the lead zirconate titanate group of piezoelectric ceramics abbreviated to PZT is the most popular material in ultrasound transducer construction.

The PZT ceramics are classified into PZT-4, PZT-5A, PZT-5H, PZT-7A, and PZT-8, Vernitron Ltd(1969)[161]. Each type of PZT ceramic offers a particular feature for a particular application. For example, PZT-5A provides a very high sensitivity to receiving

signals, while PZT-4 has a high driving capacity which makes it a good radiator in high power applications.

In general, PZT ceramics are capable of withstanding high temperatures up to 250° C. They provide a high electromechanical coupling factor and better power handling capacity. From the point of view of transducer fabrication, they can be simply cut and shaped in the desired form. Since they can tolerate high temperatures, the electric electrodes are simply soldered to them without losing their acoustical properties.

Having mentioned the good features of the PZT ceramics, it should be borne in mind that their relatively high acoustic impedance makes them poor in transformation of ultrasound energy to the loading medium and vice versa. Although it is possible to overcome this problem by means of quarter-wave matching layers,Person and Hertz (1985)[131], it still remains a drawback for PZT ceramics in comparison to the piezo films.

Table (2-1) lists the acoustical properties of the different types of PZT ceramics acquired from Vernitron Ltd. (1969)[161], and Lancee et al (1985)[15]. In this table $\mathbf{R}_v$ is the volume resistivity expressed in $10^9$ $\Omega$.m, $\mathbf{C}_T$ is the Curie temperature in °C, $d_{33}$ is the piezoelectric constant representing strain per electric field at constant stress in $10^{-12}$ m/V, $g_{33}$ is the piezoelectric constant representing electric field per stress for constant electric charge in $10^{-3}$ V/m, $k_{33}$ is the longitudinal coupling factor, $\rho$ is the ceramic density in $10^3$ kg/m$^3$ , and $\epsilon$ is he relative dielectric constant in $10^{-12}$ F/m.
Interested readers are referred to Vernitron Ltd. (1969)[161], IRE Committee (1958 and 1961)[76] and [75], and Lancee et la (1985)[15] for more detailed information on PZT ceramics.

**Acoustical Properties of PZT Ceramics**

| PZT Ceramics | $R_v$ | $C_T$ | $d_{33}$ | $g_{33}$ | $k_{33}$ | $\rho$ | $\epsilon$ |
|---|---|---|---|---|---|---|---|
| PZT-4 | 10 | 328 | 289 | 26.1 | 0.70 | 7.5 | 1300 |
| PZT-5A | 100 | 365 | 374 | 24.8 | 0.70 | 7.75 | 1700 |
| PZT-5H | 100 | 193 | 593 | 19.7 | 0.75 | 7.5 | 3400 |
| PZT-7A | 1 | 350 | 150 | 39.9 | 0.66 | 7.7 | 425 |
| PZT-8 | 10 | 300 | 225 | 24.9 | 0.64 | 7.7 | 1020 |

*Table (2-1)*

## 2-3-2 : PVDF AND PIEZO FILMS :

Recently a new type of ultrasound generating material has been introduced. Since early 1970s and after Kawai's discovery of high piezoelectric properties in drawn and poled polyvinylidene fluoride (PVDF), Lovinger (1982)[100], this substance has been used as an ultrasound source in biomedical and industrial applications.

PVDF, is a long chain semi-crystalline polymer of the repeat unit ($CH_2$-$CF_2$), Bloomfield (1987)[13]. Piezo film is a flexible, light weight, tough plastic covered by PVDF.

This piezoelectric material is produced in a variety of thicknesses from 6 to 1000 microns, (Pennwalt Corp. (1987)[130]. The advantage of piezo film as the active element of an ultrasound transducer includes its wide frequency range, near 10 GHz, vast

dynamic range, low acoustic impedance match to that of water, human tissue and adhesives, high voltage output, and high dielectric strength.

Piezo film has some limitations which make it inappropriate for certain applications. Due to its low Q, in comparison to PZT ceramics it shows relatively weak electromechanical coupling in transmitter mode, particularly at resonance and low frequencies. The maximum operating frequency of piezo film is 100 °C. Also exposed electrodes are sensitive to electromagnetic radiation.

**COMPARISON OF PIEZOELECTRIC MATERIALS**

| PROPERTY | UNITS | Pizo Film | PZT | $BaTiO_3$ |
|---|---|---|---|---|
| **Density** | $10^3$ kg/m$^3$ | 1.78 | 7.5 | 5.7 |
| **Relative Permittivity** | $\epsilon/\epsilon_o$ | 12 | 1200 | 1700 |
| **$d_{31}$ Piezo Strain Constant** | $10^{-12}$ C/N | 23 | 110 | 78 |
| **$g_{31}$ Piezo Stress Constant** | $10^{-3}$ Vm/N | 216 | 10 | 5 |
| **$k_{31}$ Electro-Mechanical Constant** | % at 1 KHz | 12 | 30 | 21 |
| **Acoustic Impedance** | $10^6$ kg/m$^2$ sec | 2.7 | 30 | 30 |

*Table (2-2)*

Table (2-2) compares typical properties of piezo film with PZT and $BaTio_3$. For a detailed discussion of PVDF and its applications refer to Richardson (1982)[140], Lewin and Schafer (1988)[96], Murayama et. al (1976)[118], and Bui et al (1976)[22].

The common point in all the ultrasound sources mentioned above is the piezoelectric property for generation of ultrasound. In this work we employed piezoelectric ceramic and therefore, we are interested in generation of ultrasound by it.

Piezoelectric refers to those types of materials which have naturally or synthetically the capability of transforming electrical energy to pressure force (mechanical energy) and vice versa. In other words, as Cady (1947)[23] defines, piezoelectricity is electric polarization produced by mechanical strain in certain crystals, this polarization is proportional to the amount of strain and changes sign with it.

The reverse is also true; that is, an electrical polarization will induce a mechanical strain in piezoelectric crystals. This property is found in natural minerals such as quartz, or produced by synthetic piezoelectric materials such as PZT and piezo film.

## 2-4 : INTERNAL REACTION OF PIEZOELECTRIC MATERIALS :

When an electrical field is applied to a dielectric material, its dipoles are aligned in parallel to the electric field. Due to this dipole alignment, the dielectric material is polarized. This phenomenon is called electrostrictive effect, and disappears in most dielectrics when the electric field is removed. But some materials become permanently polarized after applying the electric field. This group of dielectrics is called ferroelectric. A strong electric field enhances the electrostrictive effect in ferroelectric materials and makes them showing piezoelectric properties, Szilard (1982)[156].

In order to understand the generation of ultrasound by piezoelectric materials, consider a cell of quartz crystal illustrated in Fig (2-2).

As it was mentioned in chapter one, piezoelectric materials contain microscopic ovoid cells. When there is no stress on the crystal cells, they are in resting state and there is no electrical charge on the opposite surfaces of the quartz crystal, Fig (2-2-a).

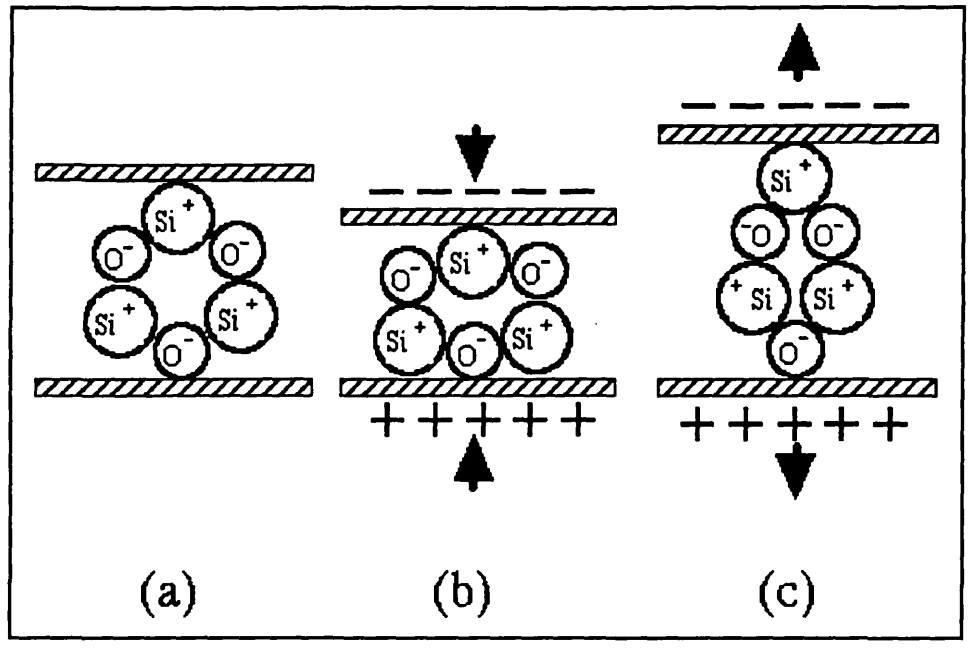


*Fig (2-2) : Piezoelectric behaviour of an elementary cell in a quartz crystal. (a) Unstressed cell, (b) Compressed cell, (c) Extended cell.*

By applying a compressed force, each cell changes its shape to a horizontal ovoid to endure pressure. Due to this deformation the opposite sides of each cell become negatively and positively charged. As a consequence a negative distribution of electric charges is formed on one side of the piezoelectric wafer, and a positive distribution on the opposite side. The same process is accomplished when a piezoelectric wafer is placed in an electric field. Now the ovoid dipoles are aligned and attracted by the electric field and due to this alignment a thinning or thickening process in wafer thickness takes place. This process is shown in Fig (2-2-b).

As Fig (2-2-c) illustrates, in the presence of a tension force the ovoid dipoles are aligned vertically and an apposite distribution of electric charges is formed on the two sides of the piezoelectric wafer.

Therefore, by applying an alternating electric field the piezoelectric wafer starts thickening and thinning, alternatively. In other words it is working as a piston which vibrates with the frequency of the applied electric field, and an ultrasonic wave is generated due to this vibration.In the same manner, a high frequency ultrasonic wave in collision with a piezoelectric material causes alternative compressive and tensile forces on its surface and consequently an alternative electric field is generated on the opposite sides of the piezoelectric wafer.

## 2-5 : POWER AND INTENSITY :

The intensity of ultrasound as mechanical wave is defined as the rate of flow of energy through the unit area in the transmission path. The intensity of ultrasound wave can be related to its pressure amplitude by, Kinsler and Frey (1962)[79] :

$$I = \frac{1}{2} \cdot \left( \frac{p^2}{\rho v} \right) \qquad (2\text{-}1)$$

where $p$ is the pressure amplitude, $\rho$ is the acoustical impedance of the medium and $v$ is the velocity of ultrasound propagation in the same medium. The ultrasound intensity can also be expressed in terms of displacement of particles or their velocities. Therefor;

$$I = \frac{1}{2} \rho v \cdot (\omega^2 x_0^2) \qquad (2\text{-}2)$$

or;

$$I = \frac{1}{2}\rho v u_0^2 \qquad (2\text{-}3)$$

where $x$ represents the particle's displacement, $u_0$ is its velocity, and $\omega$ is the angular frequency of the ultrasound wave.

Another quantitative property of ultrasound is the beam power. The power of ultrasound beam is defined as the rate of flow of energy through the cross sectional area of the beam.To ease the measurement and expression of power and intensity of ultrasound beams, they are normalized and expressed in terms of decibels. Thus ;

$$Output\ Intensity = 10 \log\left(\frac{I}{I_0}\right)\ dB\ (deciBles) \qquad (2\text{-}4)$$

where $I_0$ is the maximum intensity of the ultrasound beam and $I$ is the measured value of intensity in any point in the beam.

The flow of momentum associated with the flow of energy in the ultrasound wave is used to measure the power intensity. This force is directly proportional to the power intensity and for its measurement a small object is placed in front of transducer in a tank of water, Kossoff (1965)[84], Hill (1970)[71],and Rooney (1973)[142].The small object only intercepts a littel part of the whole beam and therefore, it is possible to measure the power intensity at a desired point in the ultrasound field.

## 2-6 : ULTRASOUND BEAM PATTERN :

The behaviour of ultrasound beam pattern has an important role in the spatial sensitivity of the ultrasound transducer, and as a consequence it affects the sensitivity of the imaging

system. The amplitude and phase irregularities due to interference between the contributing wave from all parts of the transducer's face govern the shape of beam patterns in front of the transducer. Another factor which affects the shape of the ultrasound beam is the process of diffraction. As it will be discussed later, diffraction can be found wherever wave approaches to pass through an aperture with dimensions comparable to its wavelength. The front face of an ultrasonic transducer can be considered as such an aperture and therefore, it can strongly influence the formation of beam pattern.

Near the transducer face (the near field), there are many amplitude and phase irregularities,but the lateral width of beam pattern is approximately stable. At the distances far from the transducer face, the ultrasound beam exhibits less irregularity,but starts to diverge laterally, as is shown in Fig (2-4-a).

The axial intensity of a circular transducer with piston-like motion is expressed by, Dekker et al (1974)[36] as:

$$I = 2\rho v V_m^2 \cdot Sin^2\left[\pi\left(\frac{R}{\lambda}\right).\left[\sqrt{\frac{D^2}{R} + 1} - \left(\frac{D}{R}\right)\right]\right] \qquad (2\text{-}5)$$

where $I$ is the axial intensity,$\rho$ is the medium density, $v$ is the velocity of sound in the medium, $R$ is the radius of transducer's element, $D$ is the distance from the transducer's front face, $\lambda$ is the ultrasound wavelength and $V_m$ is the maximum velocity of piston which is given by ;

$$V = V_{max}\, e^{j\omega t} \qquad (2\text{-}6)$$

The normalized presentation of Equ (2-6) can be rewritten as;

$$\frac{I}{I_{max}} = Sin^2\left[\pi\left(\frac{R}{\lambda}\right)\left[\sqrt{\left(\frac{D}{R}\right)^2 + 1} - \left(\frac{D}{R}\right)\right]\right] \qquad (2\text{-}7)$$

where,

$$I_{max} = 2\,\rho\,v\,V_{max}^2 \qquad (2\text{-}8)$$

Fig (2-3) illustrates the axial intensity versus distance ***D/R*** for a circular transducer with ***R/λ*** ratio of 10. It can be shown that for ***R/λ > 5***, Zemanek (1971)[171], the last axial maximum occurs at :

$$Last\ axial\ maximum : \quad D = \frac{R^2}{\lambda} \qquad (2\text{-}9)$$

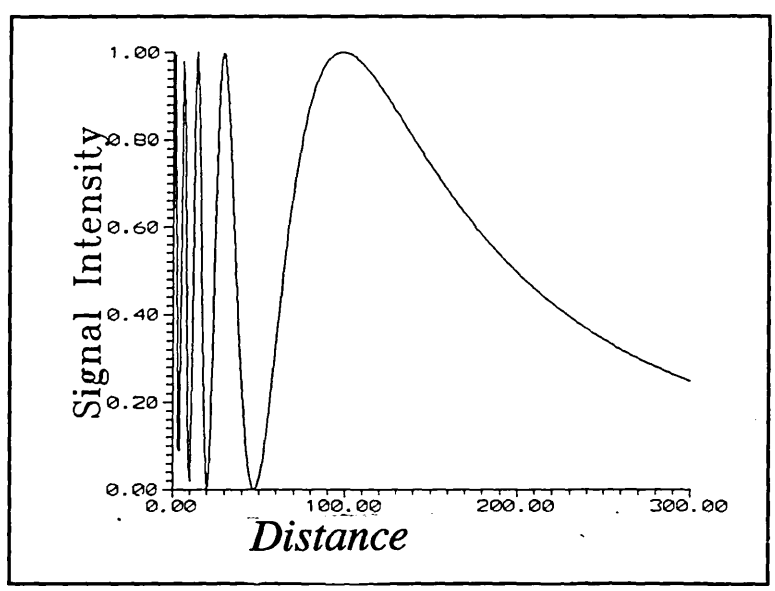


***Fig (2-3) : Axial intensity versus distance for a circular transducer.***

This point is theoretically considered as the beginning of the far field region. Fig (2-4-a) shows the idealized intensity distribution of ultrasound in near-field and far-field. The calculated pressure intensity in near-field and far-field of a circular transducer for **R/λ = 5** is illustrated in Fig (2-4-b). As it can be seen, the beam diameter at the last axial maximum has approximately the same diameter as the source.

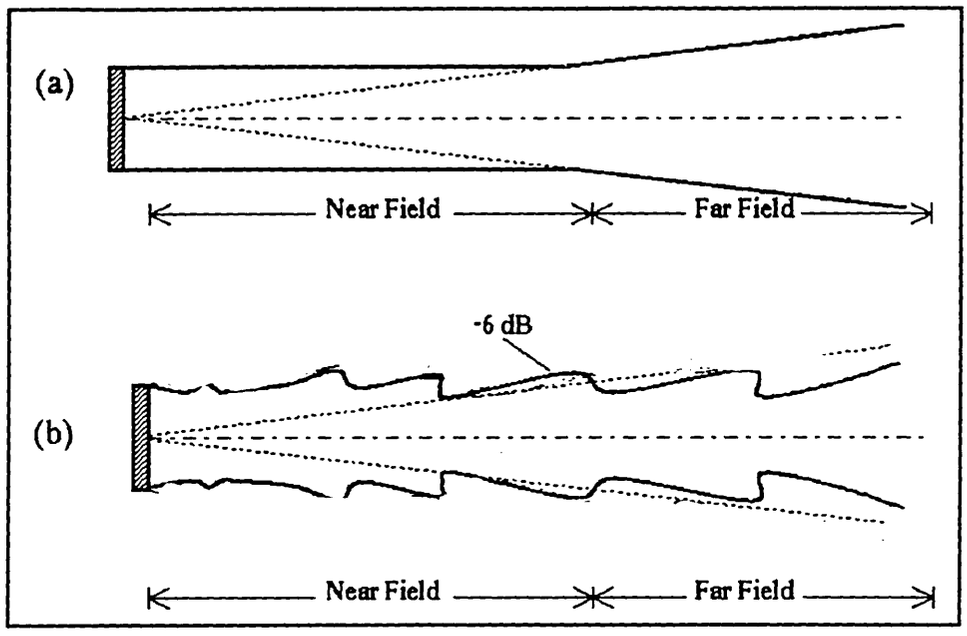


*Fig (2-4) : Beam Pattern of a circular transducer. (a) Under simplified conditions. (b) Mathematically calculated.*

It is necessary to remember that the above mentioned view of the beam pattern has some limitations. In this study it is assumed that the transducer is a circular aperture under continuous excitation of sine wave signals. The beam patterns of real transducers show much more complex behaviours. In the case of rectangular transducers there is a very complex acoustical field in front of it. This field becomes more complex when it is

necessary to reduce the size of the active piezoelectric element, and particularly under pulsed wave excitation.

## 2-7 : ULTRASOUND AND MEDIA EFFECTS :

Propagation of ultrasound in a non-homogenous media such as the human body provides different effects and causes considerable changes in speed, frequency, amplitude and phase of the ultrasound waves. It is a combination of some or all of these effects which makes it possible to produce an image of different layers of tissues and to diagnose any abnormality in a desired point inside the patient body.

### 2-7-1 : PROPAGATION SPEED :

The speed of sound in a medium depends firstly on the type of medium (its density), and secondly on its structure ( gas, liquid, or solid). In gases, sound travels with a velocity of $v$ which is given by:

$$v = \sqrt{\frac{\gamma \cdot P_0}{\rho_0}} \qquad (2\text{-}10)$$

where $\gamma$ is the specific heat ratio, $P_o$ is the static pressure, and $\rho$ is the static density. In fluids the propagation velocity is defined as;

$$v = \sqrt{\frac{\kappa}{\rho}} \qquad (2\text{-}11)$$

where $\kappa$ is the bulk stiffness modulus and $\rho$ is the density of the liquid. For solid media it is possible to generate shear waves, pressure waves, or a combination of them. On the other hand, in a plate or rod the mode and velocity of propagation can also be different.

As a simple case, when there are no boundary effects, the sound velocity for pressure waves is defined by, Szilard (1982)[156] :

$$v_{pressure} = \sqrt{\frac{E}{\rho} \cdot \frac{1-\sigma}{(1+\sigma)(1-2\sigma)}} \qquad (2\text{-}12)$$

and for shear waves is expressed by :

$$v_{shear} = \sqrt{\frac{E}{\rho} \cdot \frac{1}{2(1+\sigma)}} = \sqrt{\frac{G}{\rho}} \qquad (2\text{-}13)$$

where $E$ is the modulus of elasticity, $\rho$ is the density and $\sigma$ is the Poisson's ratio. $G$ is defined as the modulus of rigidity or shear modulus.

The velocity of ultrasound in tissue is defined by, Christesen (1988)[27] :

$$v = \frac{E}{\rho} = \frac{1}{\chi\rho} \qquad (2\text{-}14)$$

where $\rho$ is the density of tissue, $E$ is the elastic modulus and $\chi$ is the compressibility of media. Both the density and the modulus of elasticity are temperature dependent, and therefore in the calculation of velocity this point must be taken into consideration. It can be seen from equation (2-14), that ultrasound velocity varies in the layers of different tissues with different densities. Also this difference in velocity can be due to the restoring force attempting to return the particles to their equilibrium position. Therefore, as the compressibility of tissue increases ( lower modulus of elasticity), the ultrasound velocity drops and vice versa.

There is a direct relation between velocity and wave length which is expressed in Equ(2-15). Therefore, any change in ultrasound velocity has a direct effect on its wave length. This

$$\lambda = \frac{v}{f} \qquad (2\text{-}15)$$

is very important where the axial resolution of ultrasound imaging system is studied.

## 2-7-2 : ACOUSTIC IMPEDANCE :

As we mentioned in equation (2-14), the sound velocity is inversely proportional to the compressibility of the material formed in the medium. In other words the compressibility of a medium is a function of density and wave propagation velocity within the same medium.

This compressibility can impede or even promote the formation of mechanical compressional waves. The characteristic impedance of materials is a defined parameter for evaluation of mechanical wave formation in them. The characteristic impedance of a material is a measure of understanding how well mechanical waves can be formed in a media and what amount of impedance is raised against formation of compressional wave in a medium.

In the study of sound and ultrasound waves the characteristic impedance is called acoustic impedance and expressed as :

$$Z = \rho \cdot v \qquad (2\text{-}16)$$

where $Z$ is the acoustic impedance , $\rho$ is the density of media, and $v$ is the sound velocity in the same media. As it will be discussed later, acoustic impedance plays an important role in the measurement of acoustical reflection and image generation.

Table (2-3) illustrates the approximate values of sound speed, density, and acoustic impedance for some materials of interest in medical ultrasonics.

ACOUSTICAL PROPERTIES OF MATERIALS

| MATERIAL | ($\nu$) m $s^{-1}$ | ($\rho$) kg $m^{-3}$ | (Z) kg $m^{-2}s^{-1}$ |
|---|---|---|---|
| Air (STP) | 330 | 1.2 | 0.0004 |
| Aluminium | 6420 | 2700 | 17.3 |
| Amniotic Fluid | 1510 | | |
| Aqueous Humour | 1500 | 1000 | 1.50 |
| Blood | 1570 | 1060 | 1.66 |
| Bone | 2700-4100 | 1200-1800 | 3.20-7.40 |
| Breast | 1512 | ---- | ---- |
| Brain | 1540 | 1026 | 1.58 |
| Carbon Tetrachloride | 887 | 1595 | 1.415 |
| Castor Oil | 1500 | 953 | 1.43 |
| Ethyl Alcohol | 1119 | 789 | 0.883 |
| Heart Muscle | 1048 | 1548 | 1.62 |
| Fat | 1450 | 950 | 1.38 |
| Kidney | 1560 | 1038 | 1.62 |
| Lens of eye | 1620 | 1136 | 1.84 |
| Liver | 1550 | 1065 | 1.65 |
| Lung | 658 | 400 | 0.26 |
| Muscle | 1580 | 1076 | 1.70 |

| ACOUSTICAL PROPERTIES OF MATERIALS | | | |
|---|---|---|---|
| Perspex | 2680 | 1194 | 3.20 |
| Polythene | 2000 | 920 | 1.84 |
| Polystyrene | 2350 | 1056 | 2.48 |
| PVDF | 1389 | 1800 | 2.5 |
| PZT | 4000 | 7500 | 30 |
| Quartz (x-cut) | 5555 | 2700 | 15 |
| Skin | 1600 | ---- | ---- |
| Soft Tissue (average) | 1540 | 1058 | 1.63 |
| Steel | 5800 | 7900 | 45.8 |
| Tendon | 1750 | ---- | ---- |
| Tetrabromethane | 1041 | 2693 | 3.08 |
| Tooth | 3600 | ---- | ---- |
| Vitreous Humour | 1520 | 1000 | 1.52 |
| Water | 1480 | 1000 | 1.48 |

*Table (2-3)*

## 2-7-3 : REFLECTION :

In a uniform or homogeneous medium where there is no change in density or propagation velocity, the ultrasound wave travels with equal ease in all directions. But when we study a nonhomogenous medium which is a combination of different materials with a variety of densities and propagation velocities, there is a different case. In such a situation, at the interface of different materials the process of reflection takes place, and a portion of

the incident wave is reflected back. The process of reflection of an ultrasonic wave is identical to that of light wave if the interface area is smooth, plane, and laterally large enough relative to the wavelength. At such a reflector the specular reflection occurs which is characterized by the following laws;

**a** : *the angles of the incident wave* $\theta_i$ *and the reflected wave* $\theta_r$, *are equal.*

**b** : *the incident beam and reflected beam are laid in a plane perpendicular to the interface plane.*

Fig (2-5) illustrates the occurance of specular reflection at a specular reflector with normal incidence. The amount of ultrasound energy reflected and transmitted at an interface depends on the changes in the acoustic impedance across the two medium interface.

*Pressure Reflection Coefficient*, ***R***, is a measure for the amount of reflected ultrasound energy relative to the incident ultrasound energy. that is:

$$R = \frac{Reflected\ Energy}{Incident\ Energy} \qquad (2\text{-}17)$$

If we consider two media with acoustic impedances of $Z_1$ and $Z_2$ as shown in Fig (2-5), the *pressure reflection coefficient* for an ultrasound beam travelling from medium **1** to medium **2** is defined as:

$$R = \frac{Z_1 - Z_2}{Z_1 + Z_2} \qquad (2\text{-}18)$$

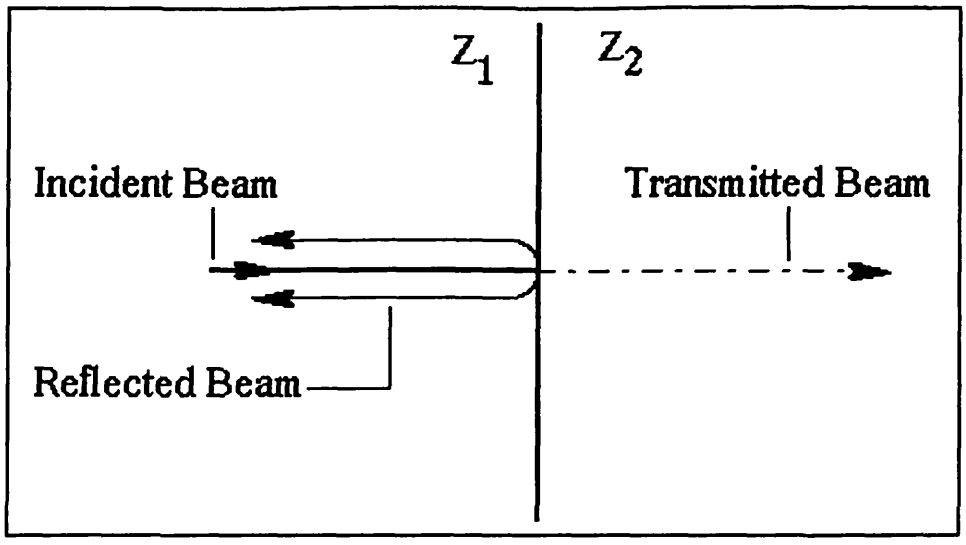


*Fig (2-5) : Interaction of a normal incident ultrasound beam at a specular reflector.*

Therefore, the amount of reflected energy depends on the difference of acoustic impedance between the two media, and is expressed by the magnitude of the ***R***. The sign of pressure reflection coefficient indicates the phase shift of the reflected wave. If the incident wave goes from a medium with a lower acoustic impedance to another medium with a higher one, i.e. , if:

$$Z_1 < Z_2 \qquad (2\text{-}19)$$

then the sign of ***R*** becomes negative, indicating a phase shift of 180° between the incident and reflected beams as shown in Fig (2-6-a).If on the other hand, the ultrasound wave transition is from a high impedance medium to a low impedance one. Therefore:

$$Z_1 > Z_2 \qquad (2\text{-}20)$$

and the sign of ***R*** is positive, indicating that the reflected wave is in phase with the incident wave as illustrated in Fig (2-6-b). The defined reflection coefficient in equation

(2-19) gives a factor of propagationality for the reflected energy. The intensity of the reflected wave is given as :

$$I_r = I_i \cdot \left[\frac{Z_2 - Z_1}{Z_2 + Z_1}\right]^2 \qquad (2\text{-}21)$$

or in terms of pressure reflection coefficient it can be expressed as;

$$I_r = R^2 \cdot I_i \qquad (2\text{-}22)$$

where $I_i$ and $I_r$ represent the intensity of incident and reflected waves respectively.

Also $T$, the *pressure transmission coefficient*, can be defined as:

$$T = \frac{Transmitted\ Energy}{Incident\ Energy} \qquad (2\text{-}23)$$

With this assumption that any energy not reflected must be transmitted into the next medium, we have:

$$T + R = 1 \qquad (2\text{-}24)$$

and therefore:

$$T = \frac{2Z_2}{Z_1 + Z_2} \qquad (2\text{-}25)$$

where $T$ is the pressure transmission coefficient. As Equ (2-25) indicates, the sign of $T$ is always positive and therefore independent of impedance increase or decrease at the interface, the transmitted wave is in phase with the incident wave as shown in Fig (2-6).

Considering Equations (2-16), (2-18), and (2-25) it is possible to calculate $R$, the *pressure reflection coefficient* for a variaty of interfaces.

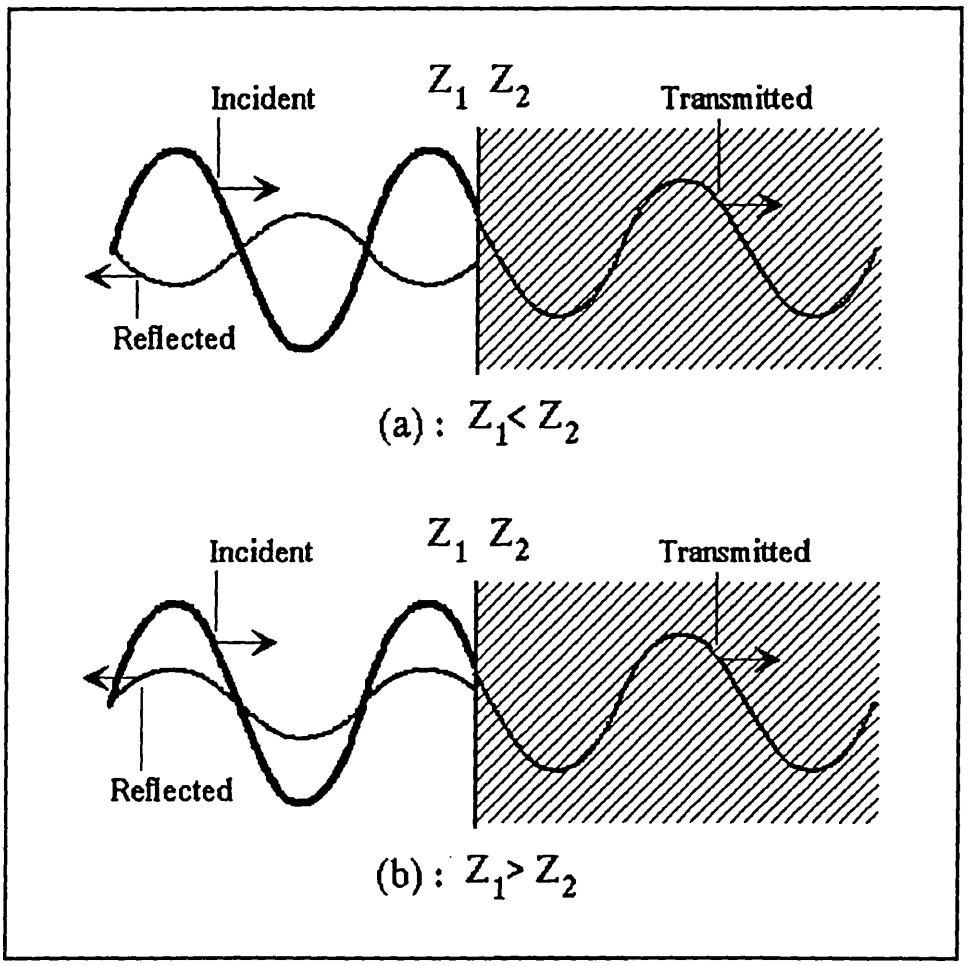


*Fig (2-6) : Interaction of normal incident wave at the interface of two media. (a) $Z_2 > Z_1$, and (b) $Z_1 > Z_2$.*

The listed data from McDicken (1981)[162] in Table (2-4) shows the ratio of reflected wave to normal incident wave, and the percentage of the reflected energy for different interfaces.

| Pressure Reflection Coefficient | | |
|---|---|---|
| **Bone/Fat** | **0.69** | **48.91** |
| **Bone/Muscle** | **0.64** | **41.23** |
| **Fat/Kidney** | **0.08** | **0.64** |
| **Fat/Muscle** | **0.10** | **1.08** |
| **Lens/Aqueous Humour** | **0.10** | **1.04** |
| **Muscle /Blood** | **0.03** | **0.07** |
| **Soft Tissue/Air** | **0.9995** | **99.9** |
| **Soft Tissue/Castor Oil** | **0.06** | **0.43** |
| **Soft Tissue/PVDF** | **0.47** | **0.22** |
| **Soft Tissue/PZT** | **0.89** | **80.00** |
| **Soft Tissue/Water** | **0.05** | **0.23** |

*Table (2-4)*

## 2-7-4 : REFRACTION :

The transmitted part of ultrasound energy continues its jurney but not necessarily in the same direction as it started. Only in the particular case of normal incident, the transmitted beam has the same direction as the incident beam, as was discussed before and shown in Fig (2-5).

When the angle of incident beam $\theta_i$ is not zero, another process at the interface of the two media occurs which is called refraction, Fig (2-7). In this process the transmitted beam in the second media bends from its previous direction having in the first media. Now the transmitted beam has an angle of $\theta_t$ with respect to the normal, and can be estimated from equation (2-26):

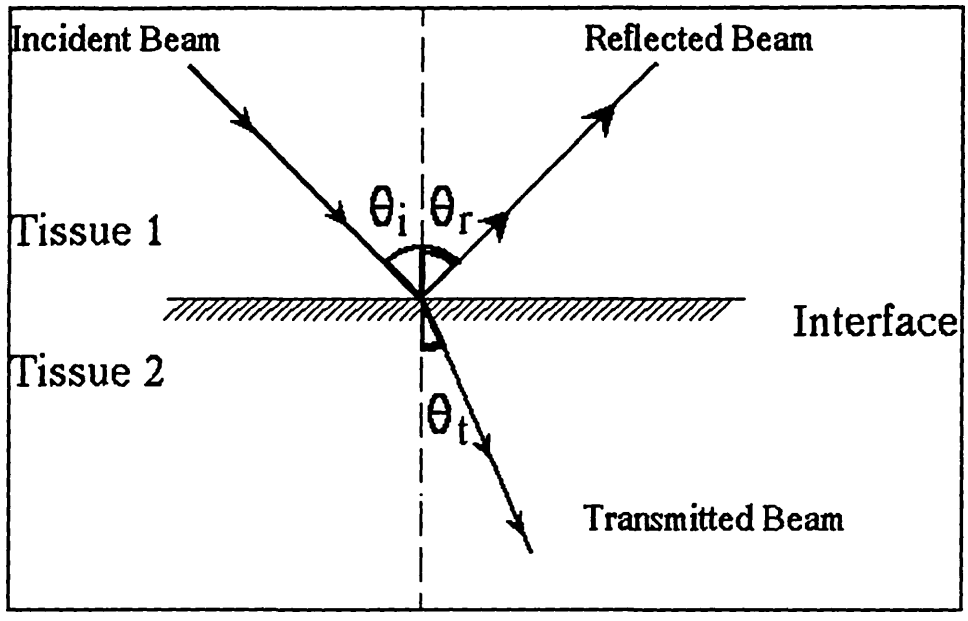


*Fg (2-7) : Interaction of an ultrasound beam with a specular reflecting surface.*

$$\frac{\sin \theta_i}{\sin \theta_t} = \frac{v_1}{v_2} \qquad (2\text{-}26)$$

where $\theta_i$ is the angle of incident beam, $\theta_t$ is the angle of transmitted beam and $v_1$ and $v_2$ are the velocities of propagation in media 1 and 2 respectively.

Equation (2-26) reveals an important point about the velocity variation. It is understood that a large bending in the transmitted beam happens where the velocity of propagation

in medium 2 is very much greater than that of medium 1, i.e., two media have very different densities. Also, for a good refraction the same condition as good reflection is necessary, i.e., having a specular interface in the pathway of the ultrasound beam.

Therefore, it is obvious that although at such an interface the angle of transmitted beam is high but we achieve a strong reflection and a weak refraction. It implies that in biomedical ultrasound imaging, refraction is usually insignificant, although sometimes the processes of refraction and reflection can produce complex results, specially when we are dealing with organs such as heart or lung which provide good specular reflectors.

### 2-7-5 : SCATTERING :

In study of reflection and refraction presented thus far the ultrasound wave is assumed to encounter a smooth, plane and large interface, called specular reflector. But it is also possible for an ultrasound wave to encounter a target relatively rough or small in size on a scale comparable with the wavelength. In biomedical ultrasonography this can be the case in the application of ultrasound in regions such as blood cells, liver, kidney, thyroid, and so on.

In the collision of an ultrasound wavefront with small particles another process occurs which is called scattering. According to Chivers (1977)[28], scattering may be defined as the change of amplitude, frequency, phase velocity, or direction of wave propagation of the wave as a result of spatial or temporal non - uniformity of the medium of propagation.

The process of scattering changes each particle into a new source of ultrasound wave.

Therefore, by transferring energy from the ultrasound wave to the scattering particles, they redirect or in other words scatter the ultrasound wave. The scattered wave is propagated in all directions and of course a part of it is redirected back to the transducer, i.e., the original source of the ultrasound wave. This part of the scattering energy is called back-scattered signal and plays an important role in study of scatterers.

The scattering process depends only on the size of target and the wavelength (frequency) of the incident wave. If we consider targets as small spherical particles with a radius of $r$, the intensity of the scattering signal is directly proportional to the sixth power of the radius of particles and the fourth power of the frequency of ultrasound wave. i.e.;

$$I = 2\pi . f^4 v^4 r^6 \qquad (2\text{-}27)$$

Equation (2-27) shows that by any increase in the size of particle, roughness of surface, or applying higher frequencies, the contribution of the scattering signals is rapidly increased.

The theoritical work of Chivers (1977)[28], agrees with Equation (2-27), but other works done by Goss et al (1979[61] and Polhammer et al (1981)[134] show that the power of the frequency dependency of the scattering-attenuation coefficient is approximately linear as shown in Fig (2-8).

In addition, the experiments done by Lizzi et al (1976)[98], O'Donnel et. al (1981)[126], Reid (1980)[139], Freeze and Lyons (11977)[51], Shung et al (1974)[149], Kadaba et al 1980[78], and Nicholas 1982[123], show that backscatter for soft tissue could be a variable frequency dependency which ranges from one to four.

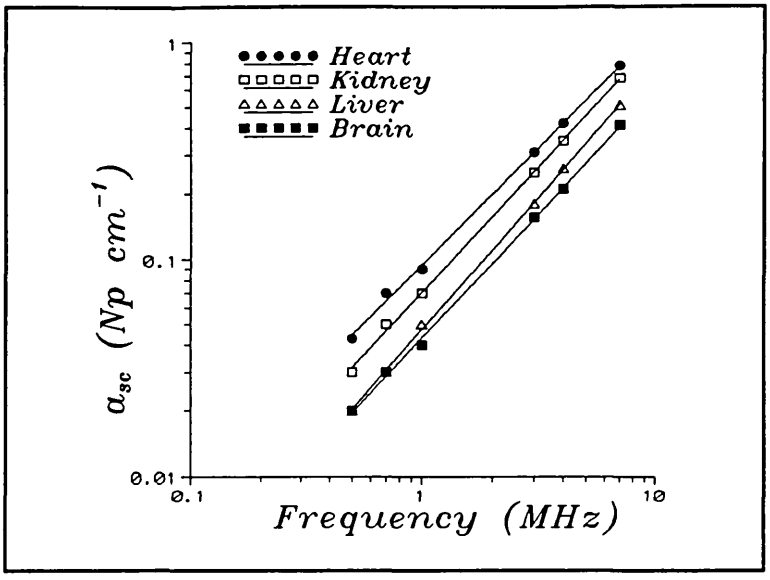


*Fig (2-8) : Frequency power dependence of attenuation due to scattering.*

Table (2-5) illustrates the frequency dependence of backscatter signal wave for different types of tissue collected from [98], [126], [139], [51], [78], and [123].

**FREQUENCY DEPENDENCY OF SCATTERERS**

| TISSUE | FREQUENCY DEPENDENCE |
|---|---|
| Vitreous Haemmorage | 4.0 |
| Blood | 4.0 |
| Heart Muscle (Dog) | 3.3 |
| Heart Muscle (Bovine) | 3.1 |
| Liver (Human) | 1.0 - 1.2 |
| Liver (Bovine) | 1.6 |
| Liver (Canine) | 2.1 |

| FREQUENCY DEPENDENCY OF SCATTERERS | |
|---|---|
| **Brain (Human)** | **1.2** |
| **Spleen (Human)** | **1.7** |

*Table (2-5)*

One important effect of scattering is the creation of interference phenomena. This occurs where the spherical wavefront of to scatterer converge each other. At the points where two waves are in phase they add to each other and make a constructive interference, providing a double amplitude of oscillation. But at the points where two waves are 180° out of phase, destructive interference occurs, causing cancellation of the wave amplitude. These interference patterns can also be detected by an ultrasonic transducer which consequently creates a texture of the ultrasound image. The coarseness of this texture is directly related to the intensity of the scattering signal and therefore a Equ (2-25) shows it can become worse in the case of higher frequencies or larger scatterers.

## 2-7-6 : ABSORPTION :

Absorption is another frequency dependent process in propagation of any mechanical wave. In this process a large amount of energy, usually accounting for about 90% of all energy is converted to heat. This portion of energy loss is the price one pays for overcoming the internal frictional and viscous forces in the medium, to provide easier motion of ultrasound waves.

Intensity Absorption Coefficient, $\mu_A$, is a constant for a specified tissue at a given

frequency. It can be approximately defined by, Evans (1988)[46] :

$$\mu_A = k \cdot f^{1.2} \qquad (2\text{-}28)$$

where $f$ is the frequency of ultrasound and $k$ is a proportionality constant specified by the medium.

The absorption of ultrasound performs a major role in ultrasound beam attenuation. Therefore, the absorption differences between various body structures are important for those instruments which provide transmission images of the body, such as C-mode image scanners, Havalice and Taenzer (1979)[67], Alias and Fink (1977)[124], Alias (1974)[1], and Maginness et.al (1974)[101].

**2-7-7 : DIFFRACTION :**

Diffraction is another interfering process resulting in the addition of several wave fronts to the original wave. This process occurs when a single wave front passes through an aperture. As the number of apertures increases, the multiple wave fronts produced by each aperture converge onto other wave fronts and again a set of constructive and destructive points is created.

Diffraction is a frequency dependent process which makes some limitation on the size and shape of transducers. The diffraction grating produces large off centre lobes called grating lobes. These undesired side lobes are the subject of many studies on multi-element array transducers.

## 2-7-8 : ATTENUATION :

In equation (2-28), it was shown that *Absorption Coefficient* is a frequency dependent parameter. If the *Scattering Coefficient* is presented by $\mu_S$, then the *Total Attenuation Coefficient* in the medium can be defined as, Evans (1988)[46];

$$\mu = \mu_A + \mu_S \qquad (2\text{-}29)$$

where $\mu_S$ is the *Scattering coefficient* and $\mu_A$ is the *Absorption Coefficient* which are both frequency dependent factors and therefore $\mu$, the *Total Attenuation Coefficient* is a frequency dependence parameter.

Representative data from Goss et al (1979)[61], and Segal and Greenleaf (1984)[146] are listed in table (2-4) to illustrate the frequency dependency of *Absorption Coefficient*, *Scattering Coefficient* and *Total Attenuation Coefficient*.

**FREQUENCY DEPENDENCY OF $\mu_A$, $\mu_S$, and $\mu$ as a function of $f^k$**

| TISSUE | $\mu$ | $k$ | Frequencies (MHz) | | | | | |
|---|---|---|---|---|---|---|---|---|
| | | | **0.50** | **0.70** | **1.00** | **3.00** | **4.00** | **7.00** |
| **Brain** | $\mu_A$ | 1.18 | 0.011 | 0.014 | 0.029 | 0.088 | 0.123 | 0.230 |
| | $\mu_S$ | | 0.021 | 0.033 | 0.041 | 0.152 | 0.217 | 0.410 |
| | $\mu$ | 1.14 | 0.032 | 0.047 | 0.070 | 0.240 | 0.340 | 0.640 |
| **Heart** | $\mu_A$ | 1.04 | 0.014 | 0.018 | 0.033 | 0.088 | 0.118 | 0.210 |
| | $\mu_S$ | | 0.046 | 0.086 | 0.070 | 0.322 | 0.442 | 0.790 |
| | $\mu$ | 1.07 | 0.060 | 0.068 | 0.130 | 0.410 | 0.560 | 1.000 |

**FREQUENCY DEPENDENCY OF $\mu_A$, $\mu_S$, and $\mu$ as a function of $f^*$**

| | | | | | | | | |
|---|---|---|---|---|---|---|---|---|
| **Kidney** | $\mu_A$ | 1.02 | 0.014 | 0.017 | 0.033 | 0.086 | 0.115 | 0.200 |
| | $\mu_S$ | | 0.035 | 0.053 | 0.067 | 0.254 | 0.355 | 0.670 |
| | $\mu$ | 1.09 | 0.049 | 0.070 | 0.100 | 0.340 | 0.470 | 0.870 |
| **Liver** | $\mu_A$ | 1.17 | 0.010 | 0.020 | 0.023 | 0.094 | 0.140 | 0.240 |
| | $\mu_S$ | | 0.028 | 0.035 | 0.057 | 0.196 | 0.260 | 0.510 |
| | $\mu$ | 1.13 | 0.038 | 0.055 | 0.080 | 0.290 | 0.400 | 0.750 |

*Table (2-4)*

## 2-8 : ATTENUATION IN TISSUE :

Having studied the various processes affecting an ultrasound wave, we can say that any attenuation in magnitude of ultrasound wave may be due to one, some or all of the following reasons.

1 : *Reflection at planar interfaces.*

2 : *Scattering.*

3 : *Divergence of the wave front.*

4 : *Absorption of wave energy by tissue.*

It is obvious that at any interface inside the tissues with acoustic impedance mismatch, a portion of the ultrasound wave is reflected and causes an attenuation in the propagated wave. Also any localized variation in the acoustic properties of the tissue can cause a broad-angle scattering of the incident wave, and consequently reduce the power density of the propagating wave. Although the reflection, divergence and scattering phenomena

cause reduction in power density, they also transfer some worthy information about the tissues.

The major cause of attenuation is absorption of the wave's energy by tissue and its transformation to heat which of course can not provide any information. The real reason for absorption is not clear but the works done by Bergmann (1957)[10], Hueter and Bolt (1955)[11], Blitz (1967)[20], and Krautkramers (1977)[86] shows that absorption is mainly due to the internal friction or viscousity of the particles, elastic hysteresis, heat conduction, and other factors such as relaxation phenomenoa.

In dealing with a fluid medium, as is the case to a great extent in our studies, other reasons for attenuation may be relevant. One is the transfer of heat from high temperature to low temperature points. In each cycle, heat will diffuse away from that portion of the wave with a higher density towards the region with a lower density. Thus, it causes the dissipation in the wave's organization, and power loss.

Another factor is the transfer of energy from the ultrasound wave into the excitation of the molecules of the fluid. It should be noted that the effect of the last two factors is small compared to that of medium viscosity.

Considering Equation (2-29), the pressure intensity of ultrasound affected by attenuation phenomenon may be expressed as :

$$P = P_0 e^{-\mu z} . \cos(\omega t - kz) \qquad (2\text{-}30)$$

where $\mu$ is the attenuation coefficient.

$P_o$ is the initial incident pressure, and

$k$ is the propagation constant.

$\mu$ itself is defined as :

$$\mu = \frac{\left[\frac{4\eta}{3} + \eta'\right]\omega^2}{2\rho_0 v^3} \qquad (2\text{-}31)$$

where $\eta$ is the dynamic coefficient of shear viscosity,

$\eta'$ is the dynamic coefficient of bulk viscosity,

$\rho_o$ is the density of tissue,

$\omega$ is the frequency of ultrasound wave, and

$v$ is the speed of sound in tissue.

From equation (2-30) we can see that there is an exponential decay in the envelope of pressure wave's amplitude as the wave travels forward in the medium.

The power density of course has a worse condition. The mathematical relation between power and intensity of a mechanical wave can be written as:

$$I = \frac{P^2}{Z} \qquad (2\text{-}32)$$

By substitution of power from equation (2-31) in (2-32), the power density, i.e., the local intensity can be rewritten as:

$$I = \frac{P_0^2}{z} . e^{-2\mu z} \cos^2(\omega t - kz) \qquad (2\text{-}33)$$

or,

$$I = I_0 . e^{-2\mu z} \cos^2(\omega t - kz) \qquad (2\text{-}34)$$

It implies that while the power decays exponentially at a rate of $\mu$, the power density decays at the rate of $2\mu$.

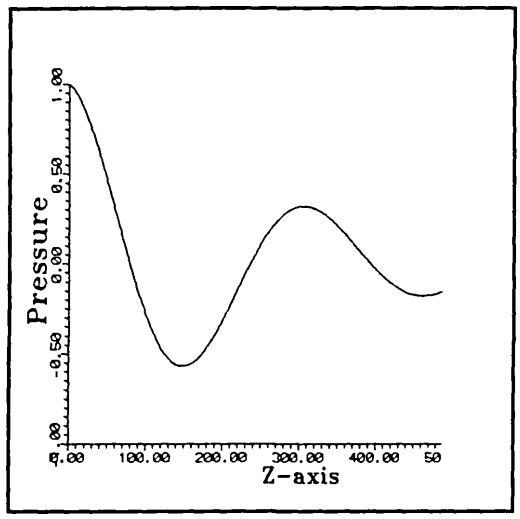


*Fig (2-9-a) : The pressure decrease versus depth of penetration.*

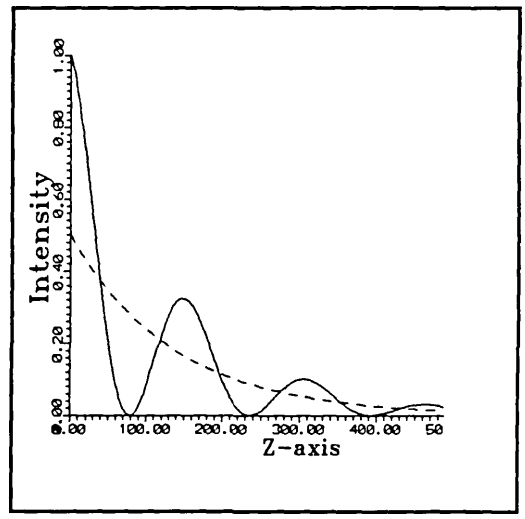


*Fig (2-9-b) : The power intensity decrease versus depth of penetration.*

Fig (2-9) illustrates the normalized exponential decrease in the pressure and power density of ultrasound wave due to attenuation phenomenon in a tissue with attenuation factor of 0.185 $cm^{-1}$.

By averaging the trigonometric equation of power density in Equation (2-34) the average power density can be expressed as :

$$I_{av} = \frac{I_+}{2} . e^{-2\mu z} = I_0 . e^{-2\mu z} \qquad (2-35)$$

Regardless of frequency dependency of the attenuation coefficient, fortunately in most types of tissues the attenuation coefficient $\mu$, is relatively smaller than the propagation constant $k$ and there is little decay per wave length. Therefore, by selecting the correct frequency we can expect enough penetration of ultrasound wave inside the tissues.

## 2-9 : LIMITATIONS, ASSUMPTIONS AND APPROXIMATIONS FOR RECTANGULAR TRANSDUCER :

A good knowledge of energy distribution in the acoustic field of an ultrasonic transducer, and in particular the beam characteristics of near-field and far-field regions, plays a major role in the processing and analysis of the signals received from the acoustical reflectors.

Since in this work it was decided to use rectangular elements of piezoelectric material as transducers, it is important to discuss the limitations of a rectangular transducer regarding its acoustical field. Earlier in this chapter we discussed the near-field and far-field of a circular transducer.

Now let us consider a rectangular transducer with length and width of $b$ and $a$ respectively. For a rectangular transducer, the experimental examinations and obtained results by Hayman and Weight (1979)[68], Marini and Rivenez (1974)[103], and Weins (1980)[166] have shown that for a rectangular aperture the near-field is much more complicated, in comparison with a circular transducer.

The numerical investigations carried out by Weins (1980)[166] show that for a pulsed wave square transducer, the structure of the near-field directly relates to the number of the sine wave cycles participating in the triggering pulse.

Weyns shows that by decreasing the number of cycles, the complexity of near-field is reduced. He also shows that although the focal distance and focal width of the transducer are less dependent on the number of cycles in the triggering pulse, they increase as the number of cycles decreases. It is worth mentioning that the near-field of a square transducer in a plane vertical to transducer and parallel to its sides show less complexity than that of the diagonal plane.

Marini and Rivenez,(1974)[103] , in their theoretical and experimental investigation also show the same result about the rather complex near-field in square and rectangular transducers. They divide the acoustical field of rectangular transducer into three regions. The first one, a very near-field which shows a very complex attitude with rapid and unpredictable variations of ultrasound pressure. This region lies between the transducer and any point at a distance of $a^2/2.88\lambda$.

There is another region between $a^2/2.88\lambda$ and $b^2/2.88\lambda$ which they call it the near-field.

In this region the ultrasound pressure shows less irregular characteristics. After the middle near-field, the far-field starts which shows a completely reliable and steady decreasing attitude.

This work also proves that rectangular transducers have a much more complicated near-field which depends on the width to length ratio , i.e., ***a/b***. In the near field of a rectangular transducer, it may be possible to receive multiple echoes from a single reflector. This is due to the complex distribution of ultrasound pressure in the near-field [124],[14]. Therefore, in pulse-echo observation of reflectors situated in the near-field, careful attention must be taken to perform reliable analysis and interpretation of echo signals. As in circular transducers the strong plane waves produced at the edges could be the source of other artifact signals.

Generally on the basis of the above mentioned works and other theoretical or experimental investigations accomplished by others ,Freeman (1960)[50], one common conclusion can be made. The near-field of a rectangular transducer is a highly complex and unpredictable region. This complexity is determined by the ratio of rectangular sides ***a*** and ***b***, and the number of sine waves participating in the triggering pulse.

Most of the numerical investigations are based upon an infinite, plane, rigid baffle. If we consider the ideality of such assumptions and the non-ideal behaviour of practical transducers, we arrive at the conclusion that the operator of an ultrasonic system, and specially a biomedical diagnostic one, should be made aware of the limitations of the system due to the special shape of the transducer. Misinterpretation of signals particularly in the estimation of dimensions and tissue characterization due to complex pressure distribution in the transducer field may lead to incorrect decision making.

## 2-10 : BIOLOGICAL BACKGROUND :

Various types of tissues with a variety of acoustic impedances, phase velocities, attenuation properties and physical shapes, make a suitable terrain for ultrasound image construction.

The building block of any living tissue is called a cell. Each cell with its small size (typically 10 to 100 $\mu$m in dimension) has independent life processes such as reproduction, metabolism, growth, oxygen consumption, carbon dioxide production and so on. The contents of every cell are surrounded by a tiny membrane and inside is a gel-like material called the cytoplasm.

The reaction of cells to ultrasound depends on their acoustic impedance and the magnitude of the the ultrasound beam pressure. Obviously at low pressure levels, only a little change in temperature or a little mechanical vibration may be experienced by the cell. On the other hand, at very high pressure levels, the cell might be destroyed due to the membrane rupture. Therefore, the safety aspects of ultrasound diagnostic systems is a very important matter of consideration.

## 2-11 : TYPES OF TISSUE :

There are four types of tissues categorised by the function that each type is responsible for. They are called *epithelial*, *muscular*, *nervous*, and *connective* tissues. In the following sections detailed discussion about each type of tissue and its own acoustical properties will be presented.

### 2-11-1 : EPITHELIAL TISSUE :

This type of tissue has a special organization of cells to make a covering layer for any internal or external part of the body. The epithelial tissues are classified on the basis of simplicity of this layer and its thickness. When only one layer of cell is used to construct the tissue it is called simple and is grouped into *squamous*, *cuboidal* and *columnar*, in order of increasing thickness, Christensen (1988)[27]. As an example, the lining of blood vessels and kidney ducts is a simple squamous epithelium, or the tissues in digestive organs and glands are respectively from the simple cuboidal and simple columnar types of epithelial tissues.

Due to the relatively small thickness of lining layers, epithelial tissues have no major effects in determining the acoustical properties of most regions of the body.

### 2-11-2 : MUSCULAR TISSUE :

Muscular tissues are generally formed in groups of elongated units of cells called fibres. They are responsibile for providing motion and are classified into smooth and striated types. Smooth types of muscles which are controlled unwillingly can be seen in the walls of arteries and veins. The striated muscles could be controlled willingly and they are a major part of the skeletal muscles. This latter type of muscle tissue provides force generation and locomotion. For example the cardiac muscle of the heart walls generates the necessary force for blood pumping. During force generation, the fibres are tightly packed, and the density of the muscle increase. Therefore, it can affect the acoustical properties of tissue. The acoustical properties of muscle tissues such as their acoustical impedance, attenuation factor and phase velocity are higher than of other soft tissues, and

somewhat dependent on the direction of ultrasound wave penetration with respect to muscle fibre's orientation.

For better reflection, it is required to provide normal incidence ultrasound beam in respect to the fibre's orientation. From data reported by Goss et. al (1978 and 1980) and Goldman and Hueter (1956) becomes clear that velocity of ultrasound in different muscles ranges from 1560 to 1590 m/sec. Therefore considering the mass density of the muscular tissues their acoustic impedance differ from 1.3-1.6x$10^6$ Rayl (kg $m^{-2}$ $s^{-1}$). The acoustical properties of some muscular tissues is listed in table (2-2), section (2-3-2). For comprehensive information about the ultrasonic properties of mammalian tissues including different types of mascular tissur reffer to Goss 1978 and 1980.

**2-11-3 : NERVES :**

The third kind of tissue is the nervous tissue which has infused almost every part of the body. Nerve cells are the transmission lines between brain, spinal cord and any other part of the body. Because of their separation from each other and their small size, they have no particular effect on the ultrasound waves. Only in the brain and spinal cord the density of the nervous tissue becomes so high that they affect acoustical propagation. For example the reprted velocity for brain tisse of dog is around 1558 m/sec and its acoustical impedence is approximately 1.55x$10^6$ Rayl.

**2-11-4 : CONNECTIVE TISSUE :**

This type of tissue can be found at any point of the body, and in a vast variety of density, structure and composition. The connective tissue fills the space between organs,

and provides support and connection for different parts of body. They also serve as background material for other types of tissue, such a plasma cells for producing antibodies. in terms of density, the connective cells are classified to loose type, Dense type, Bone type and blood.

Loose connective tissues with their weblike structure are usually found among organs to fill their anatomical spaces. Dense connective tissues with greater abundance of fibres, can be found in tendons, organ capsules and nerve sheaths.

Bone is another form of connective tissues with its hard and strong structure. The density of bone is about 1.7 times that of soft tissue. In comparison to soft tissue, because of its low compressibility it has a higher acoustical impedance and acoustic phase velocity. Thus, due to the high difference in acoustical impedance between bone and soft tissues, the reflection coefficient in their interface is very high and the penetration of ultrasound waves is almost impossible.

The last type of connective tissue is blood. Blood transports oxygen from lungs to all tissues to provide their metabolic requirements. Also blood transfers heat from some parts of the body to others to stabilize the body temperature. Blood consists of a combination of plasma, red blood cells and white blood cells. In ultrasound measurement, the red blood cells in plasma act as small scatterers for the incident ultrasonic wave.

Therefore, by means of Doppler frequency shift technique, it is possible to measure the velocity of the blood flow, which is proportional to blood pressure.

## 2-11-5 : VESSELS AND ROUTES :

In the final section of this biological review, we consider the anatomy of the blood vessels and also study the sources of arterial occlusion. The network of blood vessels is responsible for the transportation of blood from heart to the tissues and then its return to the heart. This network starts with two large arteries, which immediately branch to six major arteries as below :

* ***Right Common Carotid Artery*** * ***Left Common Carotid Artery***
* ***Right Vertebral Artery*** * ***Left Vertebral Artery***
* ***Right Subclavian Artery*** * ***Left Subclavian Artery***

Then these arteries branch into medium size arteries through different parts of the body to form the tree of the smaller arteries known as arterioles. the final divisions are capillaries, the microscopic vessels which through their walls oxygen and nutrients are given to body tissues and exhausted materials are taken from them. In returning to the heart, first groups of capillaries reunite to form small veins called venues, which they consequently come together to form veins. For a good explanation of vessels and routes in the cardiovascular system refer to Principles of Anatomy and Physiology by G.J. Tortora and N.P. Anagnostakos,1981.

## 2-12 : ARTERIAL CONSTRUCTION :

Fig (2-10) shows the magnified cross sectioned view of an artery. In general, any artery is constructed from a three-layer wall and a hollow core in the centre. The hollow core is

called the lumen and from inside to outside is surrounded by three coats known as tunica interna, tunica media and tunica externa. The outer coat of the artery's wall is formed from loosely connective tissues. It contains elastic fibres and smooth muscle tissues. Usually an elastic membrane separates the tunica externa from the tunica media. The tunica media consists of elastic fibres and smooth muscles. The Tunica interna or intima is composed of a lining layer called endothelium, an overlying layer of connective tissues, and another outer layer of elastic tissues known as the internal elastic membrane. It is This layer of the vessel's wall which is important in our study of arteriosclerosis.

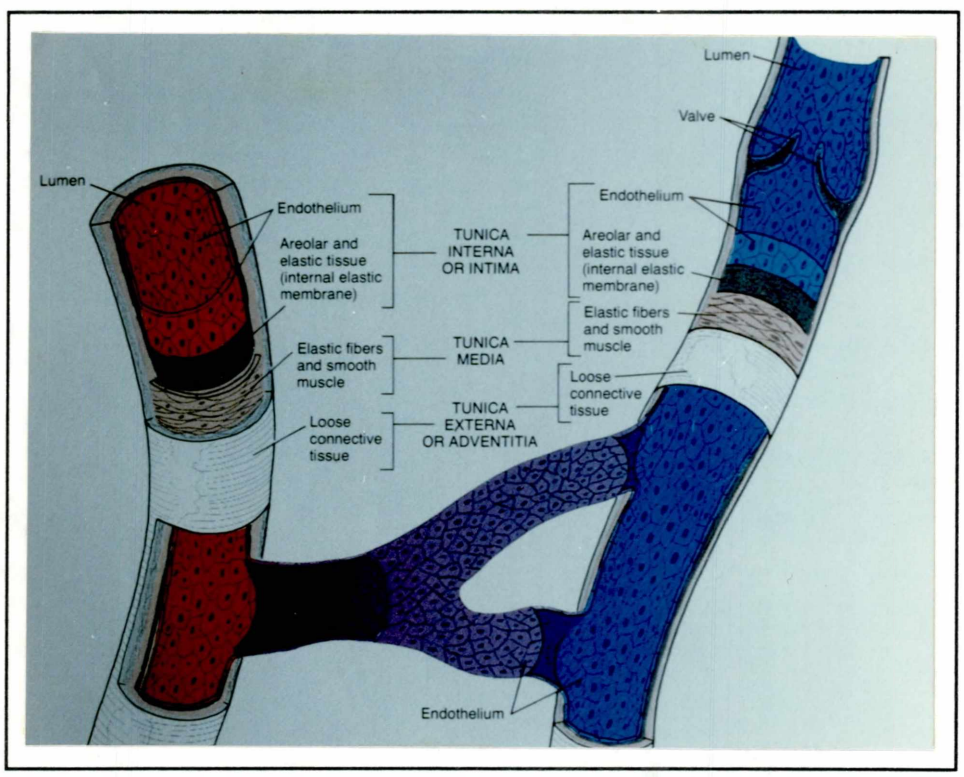


***Fig (2-10) : An imaginary cross sectional view of vascular structure.***

## 2-13 : ARTERIOSCLEROSIS :

Although many researches have investigated the causes of arterial occlusions, none of them have found precise answer to this problem. On the basis of observations accomplished by Virchow and Aschoff, Johnson and Horwitz (1985)[77], in about one hundred years ago, whatever goes wrong with a blood vessel must be due to the blood, blood flow or the vessel itself. There is a strong belief that a sort of volcanic explosion happens in the lumen, [3a].

Also, there is a theory that endothelial injury followed by proliferation of various cells is the key element of this explosion Ashford (1968)[4] On the other hand, various factors such as mechanical injury, injury from viruses, immunologic injury and hypercholesterolemia have been considered as the source of intimal injury. The interested readers are referred to Gresham (1975)[62], Texon (1967)[157], and Fry (1973)[53].

There is another school of thought that the major factors are elevated cholesterol level, blood pressure, saturated fat diets, and smoking, Johnson and Horwitz (1985)[77]. In general we can say that there are many physiological and environmental factors involved in the development of arterial disease.

The arterial occlusion due to the arterial disease in any arterial vessel is considered dangerous, but its risk is most important in coronary and carotid arteries. These arteries are responsible for transportation of blood to heart and brain, and any unusal stenosis puts peoples life in risk. Any stenosis in the coronary artery obstructs blood to myocardium and can cause myocardial infraction, Kritchevsky (1973)[162]. In the same manner any stenosis in carotid arteries can cause sever brain damage.

To make this point clearer let us consider what happens after a coronary artery occlusion. The myocardium of the heart is supplied by three coronary arteries. The ventricular myocardium receives something between 80 to 100 ml of blood per 100 grams of tissue in every minute Johnson anmd Horwitz (1985)[77]. This amount of blood is provided by three coronary arteries and more or less in equal parts. In the basal states, our body needs 10 ml of oxygen which could be provided by the above mentioned amount of blood.

If a significant obstruction is created in the lumen of the coronary arteries, one of its consequences is to restrict the oxygen requirement of myocardium, leading to severe damage in the heart's muscles. Therefore, it is apparent that any diagnostic method of arterial stenosis can save many lives. Although the forward solution to this problem surgical removing of lipid stenosis or bypassing by human blood vessels or synthetic tubes, in rare cases fibrinolysis could be effective, [77].

## 2-14 : CONCLUSION :

The human body is a combination of non-homogeneous types of tissue and even relatively homogeneous tissues, such as the normal liver,exhibits different reactions to ultrasound.These differences in reaction arise from non-homogeneous biological structures. In other words, different types of tissue have different physical properties including variation in acoustical features.

Therefore, ultrasound in its pathway through the layers of tissues provides different acoustical reactions which can be used for tissue characterisation, and type classification, image construction and therapy.

Absorption in tissue is mostly related to the protein content and can be described by a relaxation process in which more than 90% of the acoustic energy is highly attenuated and converted to heat. Ultrasound absorption can be used as both therapeutic and an imaging tool.

It is possible to classify many different types of normal and abnormal tissues in terms of their acoustical properties. For example, tumours with their different biological structures show different acoustical reactions which distinguish them from normal tissue. They could be easily classified according to their acoustical reflection patterns. In reflection study of biological tissues it is important to consider the change of acoustic impedance in the interfaces. This is particularly important when an interface of bone and soft tissue is encountered.

Ultrasound scattering in biological materials is another field of study in diagnostic applications being particularly important in blood flow measurement and tissue characterization.

Absorption, scattering and consequently attenuation are frequency dependent aspects of ultrasound and hence, in work with ultrasound as a diagnostic technique especial attention should be paid to its frequency. Although, ultrasound shows less temperature dependency, in experiments with live human tissue the effects of temperature on the acoustic properties of biological materials should be taken into account.

In pulse-echo ultrasound, one needs to examine the interaction of different types of tissues with various acoustic pulse wave forms. In transducer design it is important to consider the effects of damping, boundary conditions, exciting waveforms, and loading.

In this work we intend to employ the acoustic reflection at the interface of soft tissue of the small vessels to provide A-mode data. This data can later be used to reconstruct the 3D image of the vessel. Of course further development of the current systems and more investigations are necessary to differentiate structural alterations of the vessel wall in normal, fibrous, fibrofatty, and calcified regions.

In continuing our conclusion to this chapter it is worth noting that we decided to use tha A-mode method because of its simplicity in the design of our imaging system. In order to fulfill this aim it was decided to design a ring array transducer with a size small enough to be able to mount it at the distal tip of a catheter. This is because our aim was to investigate the biological structure of small vessels internally.

It will be shown in the following chapters that the system consists of a miniature ring array transducer (MRAT) as the main sensing component and the necessary electronic instrumentation circuitry for data acqusition, storage and interfacing to a workstation.
The sensing device is a catheter mounted transducer with twelve elments which is capable of collecting the ultrasound echo signal from twelve separate points round the cross sectional perimeter of the vessel. The size of this transducer should be as small as possible in order for it to penetrate very small vessels and other conditions of safety, flexibility and robustness should be considered.
The electronic system is responsible for triggering the individual elements in the MRAT, capturing the echo signal, digitising and storing the acquired information in a first-in-first-out (FIFO) buffer memory. At the same time the necessary circuitry for interfacing this system to a workstation should be considered. It is clear that the control signals necessary for organising the operation of different parts of this system should be generated.

*Chapter Three*

# *Miniature Ring Array Transducer*

## 3-1 : INTRODUCTION :

This chapter presents the work done on the design of a miniature ring array transducer. In the first part of this chapter the construction of a simple element ultrasound transducer will be studied to provide a general view about the details of the ultrasound transducer structure and its construction. Then the construction of the ultrasound array transducers will be discussed. This discussion provides enough information about the performance of linear and phased array transducers and reveals the idea behind their construction. In this part it will be shown that how it is possible to produce 2D images using ultrasound array transducers.

Before the design process of the *Miniature Ring Array Transducer (MRAT)* is discussed, a historical survey of intra-vascular diagnostic devices with special emphasis on the catheter based ultrasound transducers will be presented. This review provides a suitable

background to start our discussion about the detail of the *(MRAT)*.

In the next part of this chapter, design and construction of three different ring array transducers will be discussed and step by step construction process of *(MRAT)* will be explained.

The Final part of this chapter presents the experimental results on the acoustical and electrical features of our designed Miniature Ring Array Transducer.

## 3-2 : ULTRASOUND TRANSDUCER CONSTRUCTION :

The simplest type of ultrasound transducer is a single element transducer. The schematic diagram of this transducer is shown in Fig (3-1). The active element of an ultrasound transducer is usually a circular piezoelectric ceramic coated on its two faces with a very thin layer of metallic materials. Electric leads are usually made connected to these metallized faces to pass electrical excitation pulses from the transmitter to the piezoelectric element, and the echo signals from the piezoelectric element to the receiver.

The shape and physical dimensions of piezoelectric elements as well as the excitation signal have the major role in the formation of acoustical patterns in front of transducer. Robinson et al (1974)[141] discussed the effect of short sinusoidal pulses on the near-field of circular transducers. He concluded that most of the energy is confined within a beam having the diameter of the disk. Papadakis and Fowler (1969)[128] showed that in a transducer with increased bandwidth, the maxima and minima of the pressure waves in the near-field become more nearly equal. In other words the pressure is free from sharp zeros or minima.

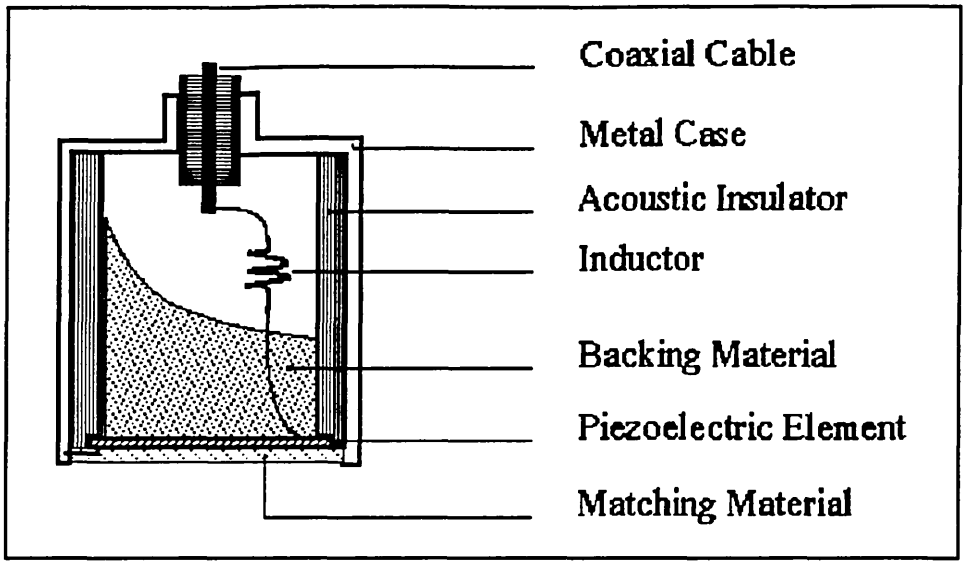


***Fig (3-1) : The general construction details of an ultrasound transducer.***

Weins in his work (1980)[166, 167] described the influence of the transducer shape on the interference phenomena with in the near-field and the far-field. He showed that a decrease in the ratio of transducer radius to wavelength $r/\lambda$ simplifies the near-field structure and reduces the side-lobes.

Dehn in 1960[163] introduced a simple technique for ultrasound beam patterns visualisation. This technique was very useful to examine the wave theory along the propagation axis of the transducer. Marini and Rivenez in 1974[103], described the near-field and far-field for rectangular transducer. Their theoretical and experimental works showed that the pressure waves in front of a rectangular transducers are more complex than those of the circular transducers.

The acoustic impedances of piezoelectric materials have an important role in transferring of the ultrasound energy to the propagating medium. The PZT ceramics have higher

acoustic impedances than those of tissues and therefore, the front face of piezoelectric material should be coated with one or more layers of matching materials to provide a better coupling interface between transducer and loading medium. As a consequence, a better transformation of energy between transducer and transceiver will be achieved.

Many researchers have investigated the thickness and number of matching layers. Kosoff (1966)[85], Goll (1975)[58], and Coates (1988)[29] have all published good reviews of multi-layer impedance matching, while Jung (1985)[35] and Persson (1985)[131] have particularly discussed the acoustic impedance matching of medical ultrasound transducers.

Another ingredient of an ultrasound transducer is its backing layer. The backing layer has different effects on transducer performance. For example, to increase the frequency bandwidth of the transducer it is necessary for the piezoelectric element to be backed by a high acoustic impedance material. On the one hand the backing material increases the frequency bandwidth of the transducer, but on the other hand it decreases its sensitivity. Thus, in the applications where high sensitivity is necessary, the transducer is backed by low acoustic impedance material or just simply by air.

Focusing at a desired range is achieved by using acoustic lenses as Tarnoczy explained in his paper, 1965[159]. It is also possible to make the piezoelectric element concave, and place a convex lens on top of it to provide a flat face for easier coupling to the skin.

The piezoelectric element and its attachments are usually housed in a metal cylinder which is insulated acoustically from the piezoelectric element by a layer of acoustic insulator. To improve the electrical impedance matching between transducer and transceiver circuitry, it is better to connect an inductor in parallel to or in series with the

piezoelectric element. The quantity of this inductance depends on the electrical features of the piezoelectric element and the operating frequency of the transducer, and it is usually mounted inside the transducer body.

## 3-3 : REAL TIME AND DYNAMIC IMAGING :

A single element ultrasound transducer can only provide one line of information in a 2D plane. Therefore, to produced a 2D B-Scan image, it is necessary to scan the ultrasound beam in a desired plane and store every block of data generated from every individual scan line. After one complete scanning cycle is finished, the group of scan lines is used to create one frame of B-mode image. If this process is repeated, then it could be possible to capture more frames and create a real time and dynamic image of the area being scanned.

The ultrasound beam steering can be performed by means of mechanical or electrical techniques. The scanning scheme itself could proceed in a sector or linear manner. Thus, ultrasound beam steering can be categorized in terms of linear or sector format with mechanical or electrical scanning techniques.

### 3-3-1 : MECHANICAL SCANNERS :

In mechanical scanning, the transducer is moved mechanically to produce the scan lines. Fig (3-2) illustrates the schematic diagram of two types of the mechanical scanners. In the rocker type of mechanical scanners shown in Fig (3-2-a), a single transducer rocks forward and backward by means of an electro-motor to produce the scan lines.

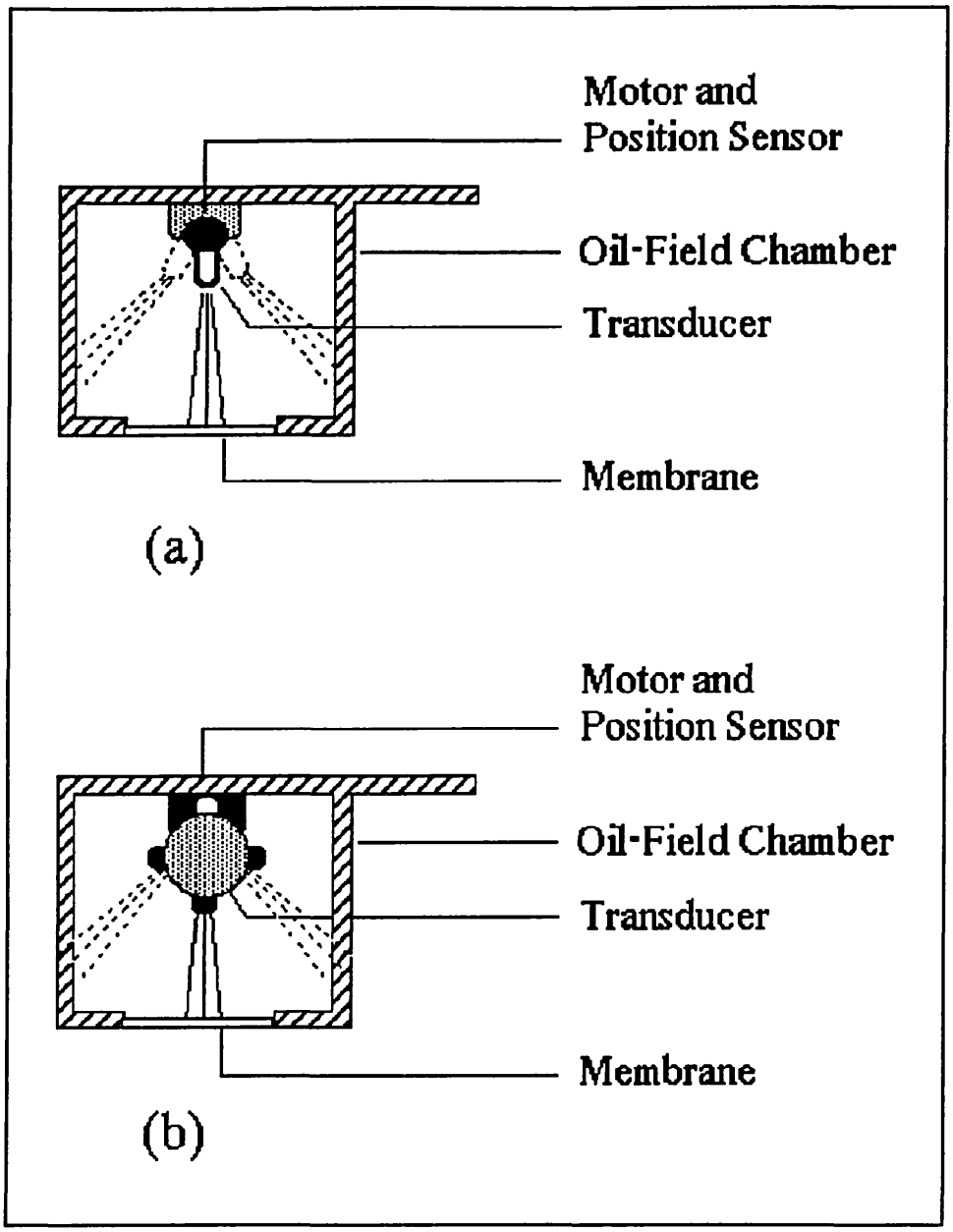


*Fig (3-2) : Two types of the mechanical scanners. (a) Rocker type sector scanner. (b) Multi-element spinner type sector scanner.*

In the spinner type a number of transducers are mounted on a wheel and while they are turning they produce the scan lines, Fig (3-2-b). Due to the constant speed of rotation,

this type of scanner provides an easier way to achieve balance and smooth running of the scan lines.

In the sector scanners, scan lines bunch close to the probe and are taken apart at distances far from the transducer. To solve this problem and to get a rectangular image, it is possible to achieve parallel scan lines if an acoustic mirror is employed. Of course, the geometry of transducer and mirror should be arranged in such a way that all of the reflected beams become parallel.

The major disadvantage of mechanical linear scanners is their large size and it is this which makes them cumbersome and difficult to couple them to the patient's body.

### 3-3-2 : ELECTRONIC SCANNING, LINEAR ARRAY :

Electronic Beam steering is another method for beam scanning. In this technique a number of small and independent piezoelectric elements are arranged in a row to make a linear array transducer. In the first generation of linear array transducers, each element was responsible for the formation of its own scan line and because of the small dimension of each element, the near field was very small. Therefore, at distances far from the transducer the lateral resolution of linear array was very poor.

In the second generation, the new technique of group firing improved the lateral resolution of linear arrays. As Fig (3-3) illustrates, in this technique a group of piezoelectric elements are triggered in such a way that the total active surface resembles a square.

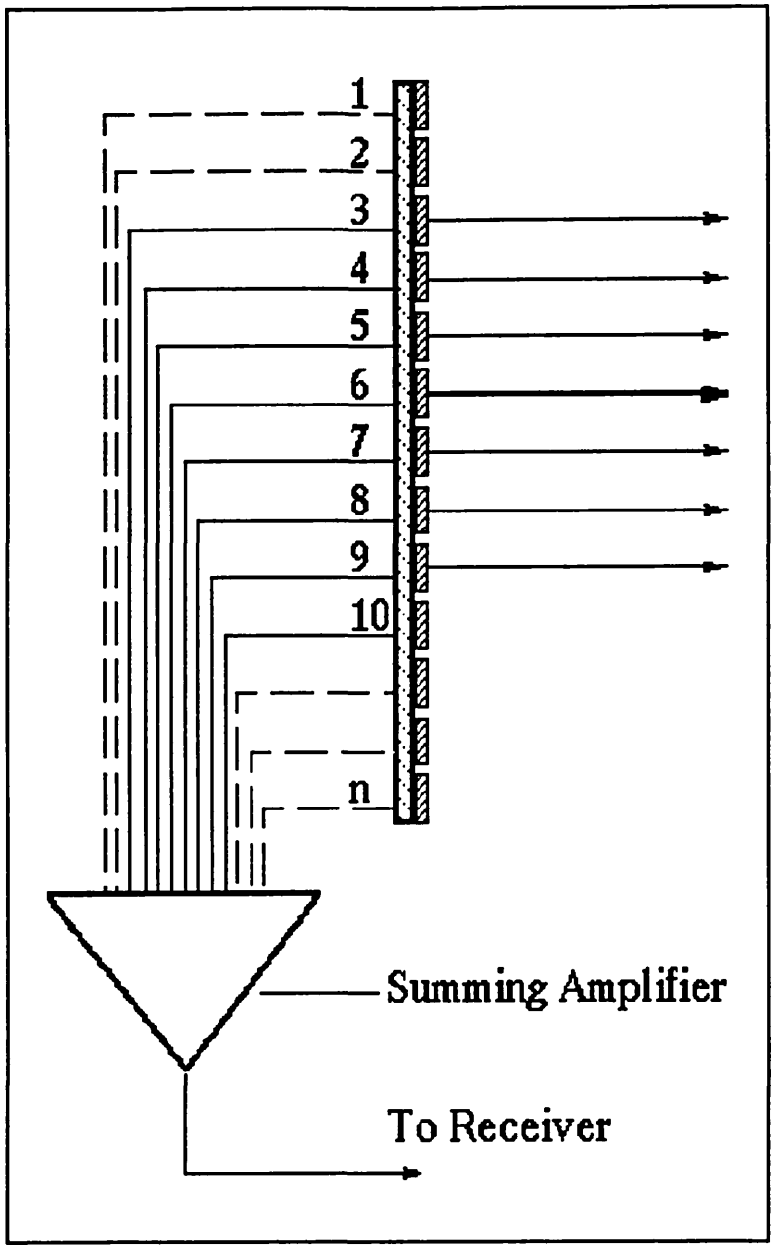


*Fig (3-3) : The group firing in a linear array transducer.*

The area of one element in the array, $A_{PZT}$, is defined as:

$$A_{PZT} = H.D \qquad (3\text{-}1)$$

where $H$ is the height and $W$ is the width of the PZT element.

If it is supposed that $n$ elements of PZT ceramics are fired in one group, then the total area of the firing group, $A_{Group}$, is expressed as:

$$A_{Group} = (n.W) \cdot H \qquad (3\text{-}2)$$

where $n$ is the number of elements in the firing group. Therefore, the length of near field which is proportional to the square of the actual width of the transducer will be improved by $n^2$.

In the third generation, another more important aim was achieved, namely the electronic focusing of ultrasound beams, Somer(1968)[152]. For better understanding of this technique, a desired target at point A in front of the transducer is considered. As can be seen in Fig (3-4), the travelling distance of the ultrasound wave from the excited element to point A and its return to the same element differs for different elements in the array.

For example, the travelling distance for echo signal from point A to elements 3 and 9 is greater than the travelling distance between point A and elements 4 and 8. As a consequence of this difference in the travelling distance, the echo from one target is received and sensed at different times and causes a blurred image. To solve this problem and provide a focused beam at any desired point, it is necessary to delay either the transmitted or the received signals. It is obvious that the outer elements should have no delay while the central element should have the maximum delay. In the next step the delayed signals are added together to produce just one scan line associated with the central element.

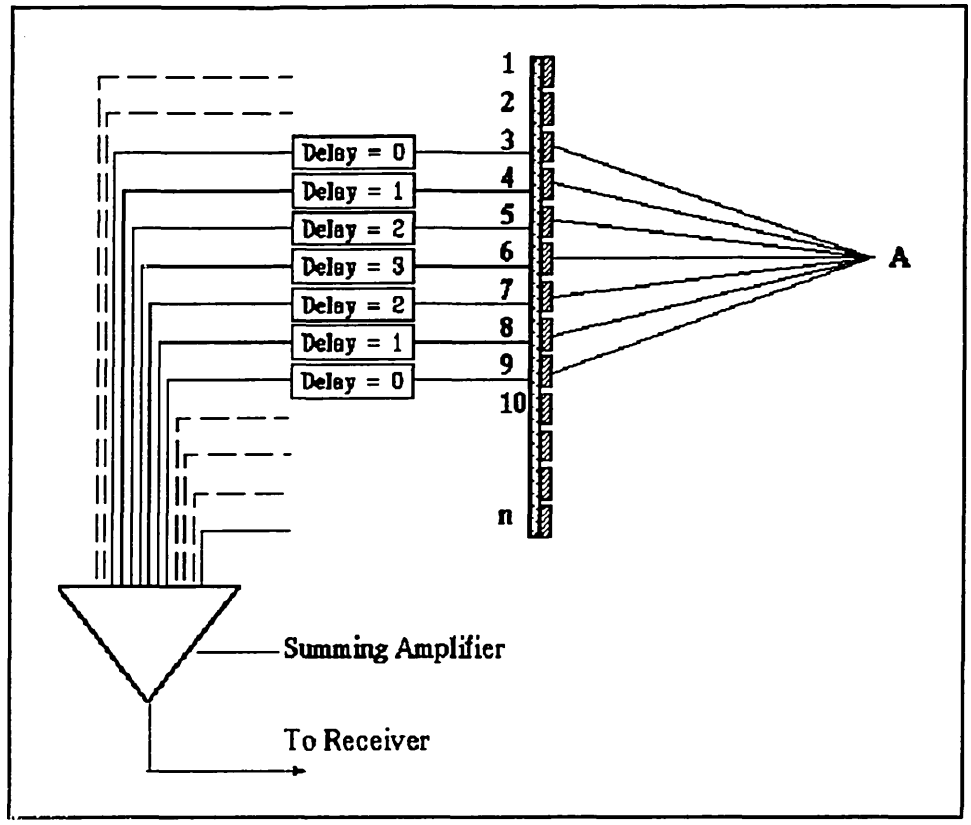


*Fig (3-4) : Group firing in a phased array.*

Therefore, by special arrangement of the delay time for each element the ultrasound beam could be focused at any desired point, at any depth in the body of patient.

Ultrasound linear array transducers are widely used in Doppler flow measurement and echo imaging systems, Vogel (1979)[162]. They are highly reliable and provide good lateral and axial resolutions which make them suitable for obstetric examinations. Some ultrasound linear arrays contain up to 200 piezoelectric elements. The number of elements in a firing group ranges from 8 to 128. Sharpen focusing is achieved by a larger number of elements in a firing group.

### 3-3-3 : ELECTRONIC SCANNING , PHASED ARRAY :

In linear array ultrasound transducers it is not possible to change the focusing point laterally for off axis objects. A phased array transducer is a small linear array transducer usually with 32 to 64 piezoelectric elements, Von Ramm and Thurstone (1976)[163].

In a phased array ultrasound transducer all the elements must be triggered for the generation of every scan line between the centre of the transducer and a desired target.

To examine the performance of phased array transducers, first let us consider a linear array whose elements are triggered successively by a constant time delay relative to each other. The result of this form of firing is a planar wave propagating at an angle which is determined by the duration of the time delay. This planar wave-front could be focused if instead of a constant time delay a different delay time for each element is employed. The complicated triggering procedure of piezoelectric elements is the price which is paid for a small size of phased array transducer and its ability for off axis focusing.

Fig (3-5) illustrates elements of a phased array ultrasound transducer and their associated delay times for focusing on a desired target at point **A**. Since it is difficult to steer a beam without a significant amount of energy being transmitted in directions other than that of the main beam, the ultrasound images produced by phased array transducers are slightly inferior to those produced by linear array transducers, or mechanical scanners. This is the cost one may pay for smaller transucer with capability to provide imaging information from an organ such as heart which is located behind the ribs.

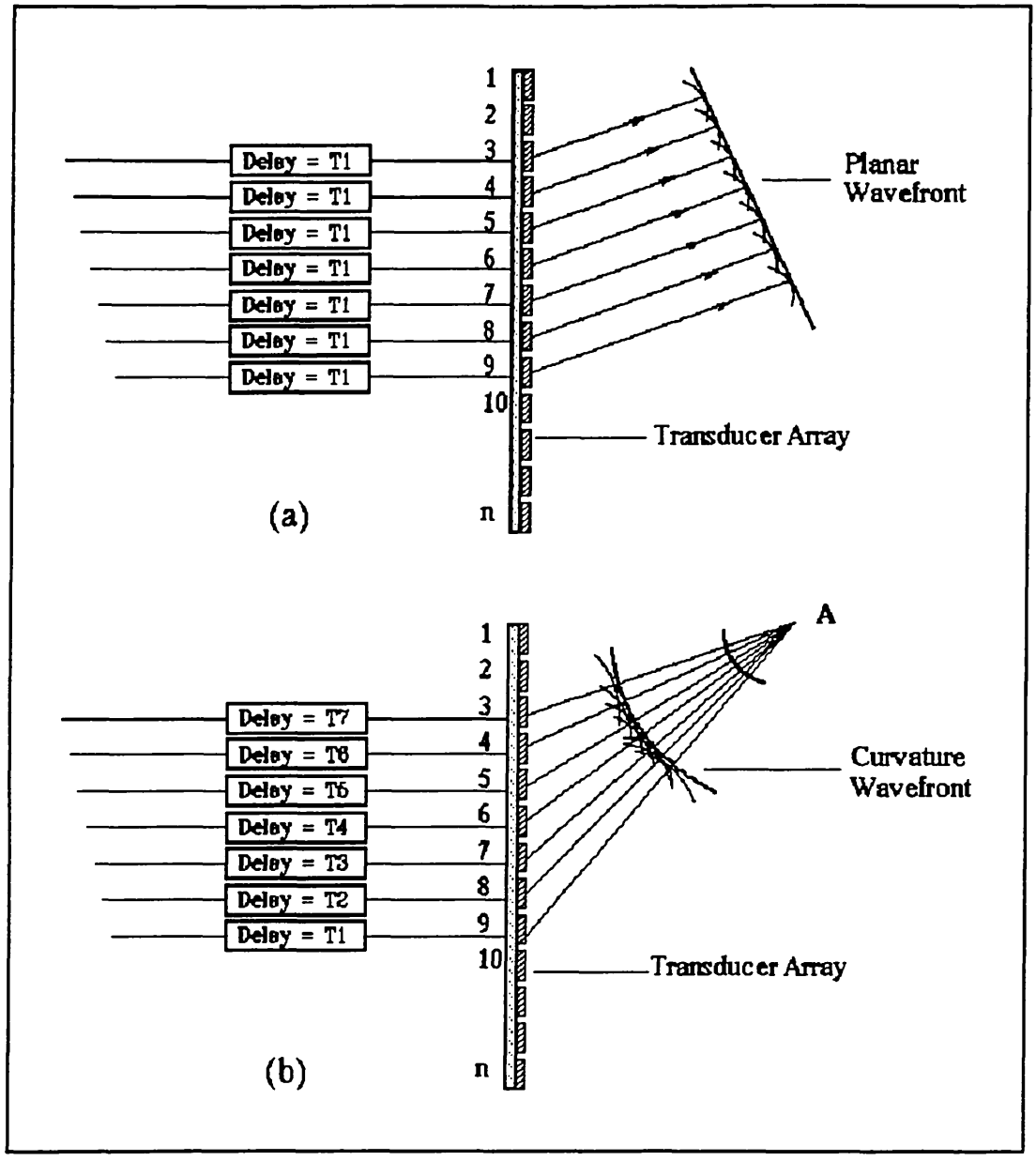


***Fig (3-5)** : Group firing in a phased array ultrasound transducer. (a) Non-focused, and (b) focused.*

## 3-3-4 : ELECTRONIC SCANNING , ANNULAR ARRAY :

Both linear and phased array transducers are only capable of focusing in any direction in the scanning plane , which is perpendicular to the transducer's length. In fact the linear and phased array transducers can provide good resolution only in the scanning plane, and they are not capable of focusing or beam steering outside this plane.

To provide a good three dimensional focusing and beam steering, it is necessary to have a two dimensional source of ultrasound. The simplest construction for such a two dimensional aperture is the annular array transducer.

An annular array transducer is constructed from several concentric annular piezoelectric rings. It can provide a uniform azimuthal resolution around its axis. To obtain ideal focusing in a two dimensional plane it is necessary to increase the number of piezoelectric rings. Theoretical works of Melton and Thurston (1978)[113], Parks et al (1979)[132a], Ariditi et al (1981)[3], and Dietz et al (1979)[41], have shown that the minimum number of piezoelectric rings is five.

At present annular array transducers are commercially made with eight concentric piezoelectric rings. Fig (3-6) illustrates an annular array with eight piezoelectric rings. In annular array transducers (in a similar manner of linear and phased array transducers) the depth of focusing is determined by the number of piezoelectric rings which are employed in transmission and reception modes.

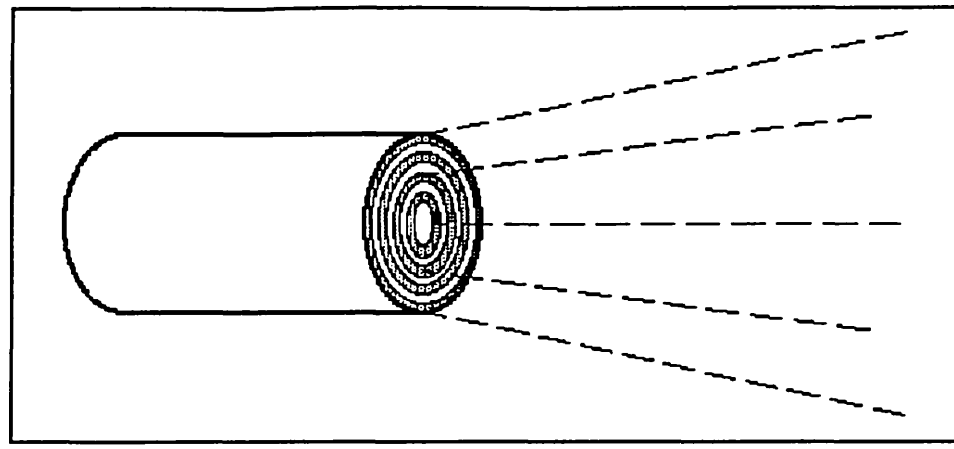

*Fig (3-6) : An annular array transducer with eight piezoelectric rings.*

Obviously to complete the act of focusing in two dimensions, it is necessary to introduce a suitable delay time for every ring in the group of transmission or reception rings.

In addition, to obtain a two dimensional B-scan image the annular array transducer must be scanned mechanically. Annular array transducers can be employed in pulse-echo imaging for both medical diagnostic applications and non destructive evaluation. In medical applications, annular arrays have been used for blood flow measurement, as well as for image generation of rapid moving structures such as heart, Von Ramm and Thurston (1975)[164], and Thurston and Von Ramm (1974)[158]. Interested readers are referred to the works described by Dietz (1979)[41] and [3], and Burckhardt et al (1975)[18], for more details about annular array transducers.

All types of transducers discussed so far are employed in noninvasive examinations. In the next section some of the works related to invasive measurement and imaging applications of ultrasound transducers with an emphasis on catheter mounted transducers will be reviewed.

## 3-4 : CATHETER BASED TRANSDUCERS :

The catheter has been used for many years as a tool for internal investigations in the human body. During the last few years this device has played an important role in the localization of different types of transducers in arteries to provide information from any desired point in the lining layer or even far deep inside the arterial vessel wall.

A catheter is a flexible tube usually made of chemical polymers. The usual length of catheter is about 1 meter and its overall diameter can range from 1.0 to 2.0 mm, depending on the application.

Usually, there are several lumens inside each catheter which are used for different purposes such as anticoagulant injection to avoid blood clotting, injection of contact media, and especially one lumen is dedicated for a tiny guide wire which conducts the localization of catheter inside the branches. Since the catheter material is radio-opaque, its movement and location in the body can be monitored by x-ray fluoroscopy.

Blood pressure measurement in the heart and major vessels of the body is one interesting areas of examination which has involved with the use of catheter-based transducers.

In one of its first applications, the catheter was employed as a hydraulic transmission line to pass pressure waveforms from internal blood vessels to a diaphragm type transducer outside the body, Asmussen et al (1975)[5].

In this technique a liquid filled catheter was used to transmit any changes in blood pressure to a relatively rigid diaphragm. Then the diaphragm deformations caused by

pressure waves, were converted to electrical signals by means of other types of transducers such as linear variable differential transducers Schaevitz (1974)[97], variable capacitors Lilly et al (1947)[145] or strain gauges Lambert (1947)[91].

In the next generation of pressure measuring transducers comprised the development catheter tip diaphragm transducers. This design improved the incoming signal, reduced some of the masking artifacts caused by cardiac and respiratory action, and more importantly increased the resonant frequency of the system Delpy (1975)[37]. Most of these transducers were fabricated on the basis of the same idea of diaphragm transducers but in a miniaturised scale.

The movement of catheter tip diaphragm was usually sensed and changed to electrical signals by means of attached strain gauge or variable inductance (LVDT). Delpy (1975)[37] introduced a new type of miniature pressure sensitive catheter transducer. This transducer had a soft type of diaphragm to make it sensitive and a PVC body to make it rugged against manipulating pressures. The pressure waves are converted to electrical signals by means of a miniature cylindrical capacitor inside the catheter tip. Since this variable capacitor was not attached directly to the pressure sensitive membrane, it was more stable in its features during a long term of use.

Considering the importance of the catheter in our work, the next coming sections present a review on variety of biomedical imaging and non-imaging systems based on catheter mounted transducers.

## 3-5 : ULTRASONIC INTRA-VASCULAR IMAGING :

Ultrasound imaging in intra-vascular applications must go beyond the intimal layer. It can provide information from intima as well as media and externa layers for tissue characterization and diagnostic decision making. Catheter mounted transducers can provide capability to monitor a therapy process after laser angiography by measuring the vessel wall's thickness, Brazilai et al (1987)[7].

Catheter mounted ultrasonic transducers have made it possible to acquire valuable information from the different layers of vessel wall for 3D reconstruction. They also have been used for quantitative and qualitative analysis of arteriosclerosis. It has been proved by Meyer et. al (1988)[115] that in comparison to MRI imaging systems, the ultrasound systems based on catheter mounted transducers can provide images of a quality necessary for angio-plastic procedures. In addition to imaging applications, the catheter-based ultrasound transducers have been used in different configurations for blood flow measurement in arterial vessels.

Although the Doppler technique is a generally accepted method in a non-invasive measurement and the assessment of blood flow, there are several locations where vessels are hidden by other organs, or any received information may be masked by artifacts from other moving organs. The coronary arteries, which supply blood to the heart muscles, are the most important of these vessels. In such cases, and for examination of vessels which are deep within the body, an acceptable alternative could be an invasive catheter mounted ultrasound transducer system.

The catheter mounted ultrasound transducers can be divided into two categories: (*i*) those

for non-imaging applications and (*ii*) those for image formation. In the following sections a review of the work done so far in these two areas is presented.

## 3-6 : NON-IMAGING

## CATHETER MOUNTED ULTRASOUND TRANSDUCERS :

This modality has been used mostly for blood flow measurement. However, recently it has been employed for marking the location of catheter tip in cardiac catheterization.

One of the first attempts for invasive measurement of blood flow in small vessels was the work done by C.J. Hartly and J.S.Cole (1974)[64]. In fact this work was not a catheter based ultrasound system, but an especially designed system for invasive measurement of blood flow. In their system a single piezoelectric crystal was mounted on a small light weight cuff-type plastic probe.

The transducer body consisted of a short length of plastic tube, 3 to 10 mm, with a slot cut parallel to its axis on one side. This slot allowed the cuff shape body of transducer to be slipped around the vessel. The piezoelectric element had been cut from a 20 MHz crystal with 1 $mm^2$ of area. This element was mounted on the cuff-type probe by means of dental modelling wax and had been angled at approximately 45 degrees relative to the transducer body, i.e., to the vessel axis. This transducer was capable of measuring the blood flow in vessels as small as 1 to 4 mm in diameter and it was tested in both acute and chronic studies.

Direct connection of transducer to electronic circuity provided a better feasibility and better signal to noise ratio. In such examinations by means of a coupling transformer, the

exposed wires at the skin surface were eliminated. In this case the connection leads were soldered to the piezoelectric crystal and directed towards the skin surface to form a flat or loop turn of wires, with a diameter of approximately 3 cm in 3 turns.

One of the best outcomes in this work was the idea of applying miniature ultrasonic transducers for invasive blood flow measurement. Cole and Hartley later in 1977[30] developed their catheter based ultrasound transducer. This transducer consisted of a piezoelectric element and it had been cut in a circular shape with a central hole. The outer and inner diameter of the element were 1.6 and 0.5 mm respectively. This element had been epoxied to the transducer body which was a standard No.8 French Sones catheter. Connected wire leads to the piezoelectric element had been brought out from the lumen through a single hole in the side of the proximal luer-lok fitting and were connected to a wire winding coil around the catheter. This wire worked as the secondary winding of a coupling transformer.

To complete the electrical coupling, another moveable winding coil with a larger diameter than that of the secondary winding was used to couple the induced signal from the primary winding to electronic circuit. This winding coil was employed as the primary winding of the transformer. This form of electrical coupling provided complete electrical isolation between the electronic instrumentation circuit and the patient's body. It also provided the mechanical flexibility necessary for catheterization.

The instrumentation system could produce a repetitive pulse with 62.5 KHz of frequency and one microsecond of width. The master oscillator worked at 20 MHz and therefore each pulse contained 20 cycles of the master oscillator frequency. With this system the velocities of up to 100 cm/sec and at a depth of up to 1.2 cm were recorded. Since the

piezoelectric element was mounted at the tip of the transducer and perpendicular to the catheter axis, providing any stable angle between blood cells flow and ultrasonic beam was very difficult. Of course, this problem can be improved by using a guide wire to keep the crystal at a desired angle.

Poor (1979)[135] introduced his catheter tip Doppler probe with a smaller diameter of 1 mm and lower frequency of 10 MHz. He employed a Doppler pulsed wave technique to take advantage of having a single crystal transducer. In this arrangement it was possible to increase the area of the piezoelectric crystal. This increase led to an increase in crystal capacitance and as a result the cable capacitance had less importance. With one crystal the fabrication procedure was also easier. By using a bridge circuit, Poor tried to cancel out the transmitting signal from the receiving signal. The electronic system was isolated from the body by a coupling transformer, which was also part of the tuner.

The probewas introduced into the veins of sheep. It was also used externally to monitor blood velocities in veins and arteries where the small diameter of the transducer enabled superficial vessels to be isolated at very low angles.

In 1970, SWAN and Gans introduced balloon angioplasty or percutaneous trans-luminal coronary angioplasty. In this technique a balloon catheter is advanced across a narrowed artery and inflated to re-open partially blocked vessels. Before the development of this technique catheter based transducers were too large and too stiff to be introduced into small diseased vessels, such as coronary arteries. On the basis of this development Hartley and Miller (1988)[65] produced a very small Doppler catheter based transducer, named Miller DC-101 catheter.

The source of ultrasound in this transducer was a PZT disc with a central hole providing a lumen for a guide wire. The operating frequency of this transducer was selected at 20 MHz which provides a better scattering signal from red cells. The crystal with an overall diameter of 1.7 mm could be positioned into the ostia of the left or right coronary arteries to evaluate total left or right coronary flow, but could not be advanced to sense the flow in smaller branches.

This work and other catheter based Doppler transducers have shown a great capacity for measurement and assessment of blood flow in small vessels. However with a simple single crystal, it is very difficult to measure the absolute volume of blood flow. The final conclusion on the catheter based Doppler probes is that, the newer balloon mounted transducers may provide instantaneous haemo-dynamic information which could be used for improvement of coronary angioplasty.

## 3-7 : CATHETER MOUNTED ULTRASONIC TRANSDUCERS, IMAGING :

Another technique to study the blood flow profile as well as to assess the physical dimension, structural properties and internal image of blood vessels is the use of multi-element or rotating single-element catheter based ultrasonic transducers.

Omoto (1967)[127] described a catheter based system for scanning the inside of the heart. In this system a catheter was mechanically rotated and the echo signal recorded in any position. The transducer in this system was a single crystal.

Carleton et al at the same time developed an A-mode echo measuring system on the basis

of a non-directional cylindrical catheter tip crystal, (1967)[24]. With the system they could estimate the cardiac diameter by means of the travelling time of ultrasound beam from transducer to a desired point in tissue and its return to the transducer.

Eggleton et al in 1969[43] introduced a 4-element catheter mounted ultrasound system. This system was developed for reconstruction of a cross sectional view of the heart in a selected steady state.

One of the pioneers of intra vascular imaging by means of the ultrasound ring array transducer is Bom. He and his colleagues Lancee and Van Egmond started the development of an ultrasound intra-cardiac scanner in 1972[15]. In their attempt they developed a 32-element catheter transducer to study the movement of the cardiac structures.

To fabricate a 3 mm diameter catheter probe, they used a cylindrical ceramic element of barium titanate piezoelectric crystal. The nominal frequency of crystal was chosen at 5.6 MHz to provide a suitable diameter for a cylindrical ceramic to cover 32 single elements of the transducer. First this cylindrical element was bound to the backing material and then cut to 32 elements, with a 0.13 mm gap between them.

Bom and his colleagues employed a phase compensated technique to obtain a directional beam such as the one which would result from an element relatively large compared to the wave length.

Due to the curvature of the circular array it was necessary to apply appropriate time delays to a group of elements to achieve the correct directional beam. The number of

elements selected to generate a phase-corrected beam was eight, and because the system was capable of fast electronic steering with a rate of 160 frames per second, it was possible to display the reflected shape instantaneously.

Although at the time of this work the 3 mm diameter size of catheter probe was a major drawback in the study of small vessels, it however showed a good capacity for diagnostic applications in cardiology and cardiac structure visualization. At the time, this project was too costly to continue and Bom shifted his effort to non-invasive studies.

In 1980[107], Martin and Watkins presented their ultrasonic catheter for intra-vascular measurement of blood flow. This catheter probe was developed to monitor blood pressure and to perform blood flow analysis. More importantly, it was aimed at the measurement of cardiac output and stroke volume during major surgeries.

Martin and Watkins (1980)[107] considered the clinical bio-compatibility and measurement requirements for a catheter probe to fulfil the above mentioned tasks. They decided to chose a flexible catheter with 1.2 meters in length and 2 mm of overall diameter. With this length of catheter, the pulmonary artery from a vein in the extremities is accessible. The number of elements in the circular array of the transducer was decided as six to provide enough points for the detection of the lumen area. Another single disc ceramic was used at the top of the transducer tip to provide a means of pressure or velocity measurement.

Therefore, the artery flow $Q$, could be calculated by measuring the area of the artery $A$, and the velocity of blood flow $V$. Hence,

$$Q = A \cdot V \qquad (3\text{-}3)$$

From the point of view of transducer construction it is worth mentioning that Bom used a diamond cutting tool and a precision milling machine for cutting PZT crystals and making the transducer body. They used the PZT-5A material to achieve high sensitivity and a better coupling factor. The frequency of PZT material was selected at 14.7 MHz to provide narrow angle of radiation for small width of the PZT element and good back scattering from the blood vessel wall.

The overall diameter of the disk element was 1.85 mm. Each element in the circular array was 0.6 mm in length and 2.54 mm wide. The body of the transducer was made from brass and in three separate parts. Therefore, the fixing of elements of the the circular array and disc element was carried out separately on different parts, [107].

Martin and Watkins used solder cream for binding crystals to the body of transducers, and micro coax UT-8 with overall diameter of 0.8 mm was used for electrical connection of piezoelectric elements to the instrumentation system.

This system was capable of recording distinct wall echoes from pulmonary arteries. This transducer was employed to do tests on a dog, and ample scattering signals from the blood cells were recorded. Although this system had not been designed as an ultrasonically imaging system, the resulting measurements proved the capacity of ultrasound as a tool for intra-vascular measurements with capacity for more progress, as an imaging system.

The latest work done by Martin et al (1988)[105] is a B-mode and Doppler ultrasonic

catheter for use with fibre optic endoscopes. This catheter probe combines the ability of fibre optic for lumen surface visualisation with the penetrating capacity of ultrasound for structural visualization of the vessel wall. The difference between Martin's work and other available fibre-optic and ultrasound catheter systems is in the technique of using an insertable ultrasound probe in an ordinary fibre optic endoscope. Martin and his team developed a miniature ultrasonic probe that can be used with standard endoscopes, by passing them through the biopsy channels rather than the ultrasound transducer element(s) built into or on the endoscope.

They have developed two types of probe called Doppler and Echo probes. The Doppler probe was constructed by means of a cylindrical PZT ceramic to overcome the problem of angle alignment. This probe radiated in 360° instantaneously and perpendicular to the catheter axis. The echo probe had a single element crystal which could be rotated manually by means of an excellent torsional flexible cable from the proximal end of the catheter.

In both probes the PZT elements were backed by air to avoid ultrasonic energy reverberating in the small tip of the probe which could be an undesired artifact on the signals received from the tissue. The biopsy catheter had different channels ranging from 1-2 meters in length and 2.5 to 3.7 mm in diameter. The length of the Doppler probe was 2 meters and the outer and inner diameters of the PZT element were 1.8 mm and 1.00 mm, respectively. The operating frequency of this probe was 8 MHz.

The Echo probe was made in 2 meters long, but its element had a diameter of 2.9 mm and operating frequency of 20 MHz.

Results recorded with 123 patients by means of more than 40 Doppler probes and 10 Echo probes proved good sensitivity. The Doppler probes had a good capacity for identifying vessels as either artery or vein. Also assessment of the vessel's size was possible. It was found that the cylindrical element does not provide satisfactory radiation, due to its multiple side-lobes. The most hopeful point in this work was that good images were obtained with the single element Echo probe. Once again Martin and his team had shown the capacity and necessity of ultrasound in intra-vascular imaging systems.

In (1988)[114],[115],[114a], experiments conducted by Meyer et al proved the capability and feasibility of ultrasound for intra-vascular imaging and as a competitive tool to MRI imaging systems. Their results indicated that high resolution B-Mode ultrasound images could be obtained at higher frequencies, which shows a great potential not only for quantitative intimal roughening measurement, but also visualisation beyond the intimal lining of the vessel.

These results showed the possibility that tissue attenuation estimation could lead to tissue histology identification. It is obvious that by having detailed information about media and adventitia it would be easier to examine atherosclerosis, or to obtain quantitative estimates of surface roughness, degree of calcification and scarring or thickness of lipid deposits.

Meyer et al (1988)[114] decided to use a 30 MHz piezoelectric material to improve the lateral resolution. In their system the piezoelectric element was mounted coaxially aligned with a right angle acoustic reflector. By manually rotating the transducer assembly around its long axis, they could acquire data from the vessel wall over 360°. The captured ultrasonic signal was digitized by an 8-bit, 50 MHz digitizer. The digitized data

was stored in a 300 K byte video scan converter memory organized as 480 "look" directions, or lines. Each line contained 640 bytes of data.

With this system features an angular resolution of 0.75° at a depth of 1 cm inside the tissue was possible. The prototype transducer used by Meyer was not really a catheter mounted transducer, but the achieved results indicated that in comparison with MRI images, it is possible to acquire high resolution B-Mode images of valid quality.

For further development of this work, it is necessary to reduce the size of the transducer and therefore the thickness of piezoelectric element. Consequently, it leads to an increase of resonance frequency of the piezoelectric element and band width frequency of the receiver. Considering these parameters it is possible to avoid broadband noise by using a high frequency narrow-band transducer or bearing the expense of highly sophisticated and expensive instrumentation.

Recorded results, [115], of in-vitro human arterial samples presented excellent correlation between the ultrasound images and high resolution magnetic resonance images. Presence of any small calcification was easily identified by its strong scattering. In addition, the quality of the ultrasonic images may be useful for staging atherosclerosis based on the presence of healthy media and plaque position.

Hartley et al (1988)[66] also in the same year made another attempt to prove the feasibility of producing close range and high resolution images using a small single element transducer. They developed different transducers of small aperture size PZT-5A piezoelectric material. The body of the transducer prototype was a 17 gauge needle with an overall diameter of 1.5 mm. The piezoelectric element was cut from a 20 MHz PZT-

5A ceramic crystal into rectangles of 0.5 mm by 1.0 mm.

The piezoelectric element was mounted in a cuff cut needle and backed with styrofoam to provide a low acoustic backing. To increase the lateral resolution, different types of cylindrical and spherical lenses were tested on top of the transducer element.

Once again from the achieved results it became clear that a high frequency catheter mounted ultrasound transducer is capable of producing high resolution intra-vascular images. This work showed that the cylindrical lens can provide a good combination of resolution and signal strength. Although satisfactory results were obtained for prototype transducers, in reality it is necessary to bear in mind the fact that mechanical scanning has inherent problems with position sensing and the driving mechanism.

Sacharoff et al (1988)[143] presented another demonstration to prove the feasibility of ultra sound in intra-luminal imaging. They used a 6F catheter as the base for their ultrasound transducer. They claimed a good axial and lateral resolution of 0.25 mm and utilisation of the system in intra-vascular image reconstruction as small as 4.0 mm of internal diameter.

They achieved good results in experiments to detect artificially created stenosis or actual stenosis in canine vessels. Also, they could detect atherosclerotic lesion in human cadaver tissue. From the results obtained by Sacharoff and his team, the use of their invasive ultrasound tool for internal diameter determination, wall thickness visualization and tissue differentiation is validated.

Further work in this area was carried out by Ellis et al (1988)[44]. They also developed

a 6F catheter mounted mechanically scanned ultrasound transducer. The instrumentation system and catheter transducer were capable of producing two dimensional images of small vessels in B-mode.

To avoid image distortion due to dislocation of acquired data, the accurate position control of the transducer element is very important. To perform such accurate position sensing, they used a flexible and torsional drive shaft between the transducer element at catheter tip. The motor and position sensing components at the proximal end of the catheter. They used high acoustic impedance backing to provide high attention to obtain high damping and shorter pulse duration.

In this work the results show less clear images. This was due to the lower amplitude signals which is the consequence of high impedance material used for backing of piezoelectric element. However, the catheter transducer made by Ellis et al showed an ability for data acquisition in vessels as small as 4 mm internal diameter.

A further interesting example of catheter transducer is that of Martinelli et al (1988)[108]. They employed an 0.8 mm catheter mounted ultrasound probe to capture data from an artery with its intervening space filled with flowing blood. They also develpoed a software programme capable of processing the captured data to extract the arterial thickness, together with a programme for 3D reconstruction of the arterial wall. Their results proved that highly calcified atherosclerotic plaques, as well as non-calcified plaques, could be traced by catheter mounted ultrasound transducers.

In the next sections first the preliminary steps which were taken to achieve the necessary information and experience for making the final miniature ring array transducer are

presented. Then the full details of the construction procedure for the final work, a *Miniature Ring Array Transducer*, will be discussed.

## 3-8 : PRELIMINARY PROBLEMS AND DESIGNS :

In this section first the basic problems associated with the construction of a Miniature Ring Array Transducer are discussed. One of the most difficult problems in the design of the miniature transducers was cutting the piezoelectric crystals to the very small dimensions necessary for them. It was decided to place twelve separate elements in the ring array which could provide relatively better lateral resolution, Martin (1980)[193]. Also, it was necessary to consider the overall diameter of F8 catheter, i.e. 2.1 mm, which was selected as the localisation tool for the transducer body. It is obvious that the width of the piezoelectric elements had to be something less than 1 mm.

As a first step it was decided to determine to what extent we can reduce the size of PZT crystal and still have reasonable pressure in the reflected echoes. Three pieces of the PZT ceramics were cut from two 6x6 $mm^2$ PZT-5A ceramic plates. These three pieces had different dimensions of 1x3, 2x3 and 3x3 $mm^2$. To cut the PZT crystal we employed the Macrotome 2, a precision cutting machine.

To stop movement of the PZT plates during the cutting process it was necessary to stick them to a microscope slide by means of Double sided adhesive tape from RS Components, [RS 555-033]. Aseton solvent cleaner was used to separate the pieces from the microscope slide after the cutting process. Then by means of a brush the surface of the microscope slide was washed and PZT pieces were separated.

Figure (3-7) shows these three pieces before placing on their own simple transducer body. The body of the transducers are made of brass and machined to provide an air gap as backing material. Each PZT element was placed on the transducer body by means of silver loaded epoxy resin. This epoxy with its high electrical conductivity, completed the electrical connection between one face of PZT elements and the transducer body.

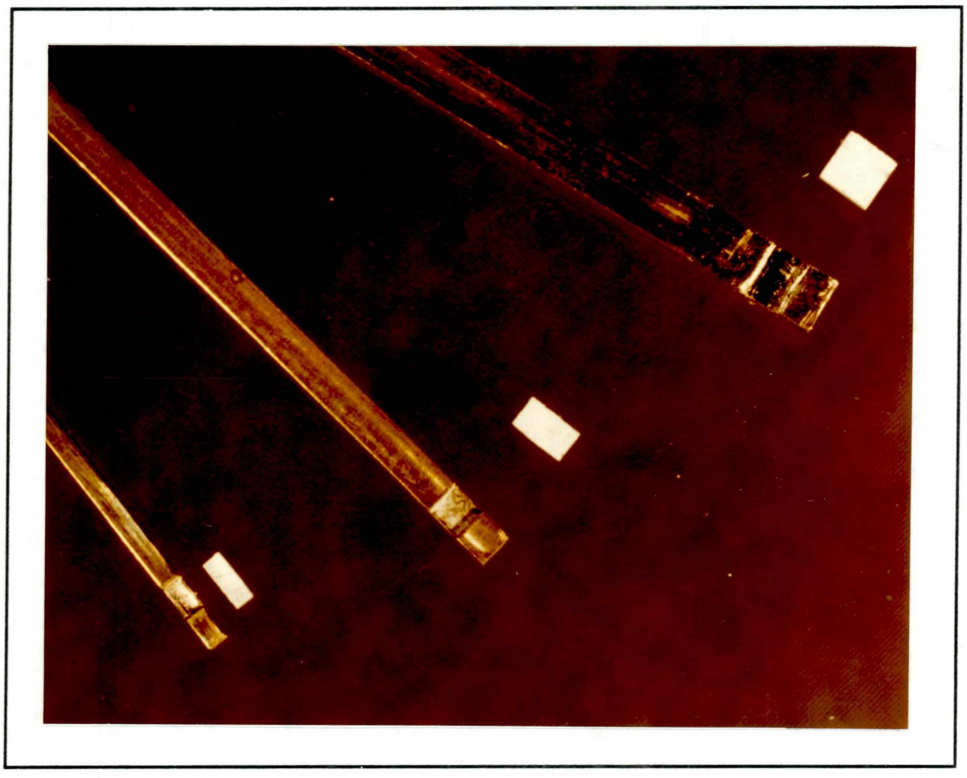

***Fig (3-7)** : Three different single element transducer body and their PZT elements.*

Therefore, the transducer body was employed as the common lead to the PZT element. To complete the electrical connection of PZT elements, the other face of each one was connected to the central conductor of a miniature coaxial-cable.

To ease the soldering process and to provide better flexibility in the handling of such a small transducer, a miniature coaxial cable with overall diameter of 1 mm was prepared, RS Components [RS 388-530].

Fig (3-8) shows the schematic diagram of a single transducer body and the completed transducers are shown in Fig(3-9).

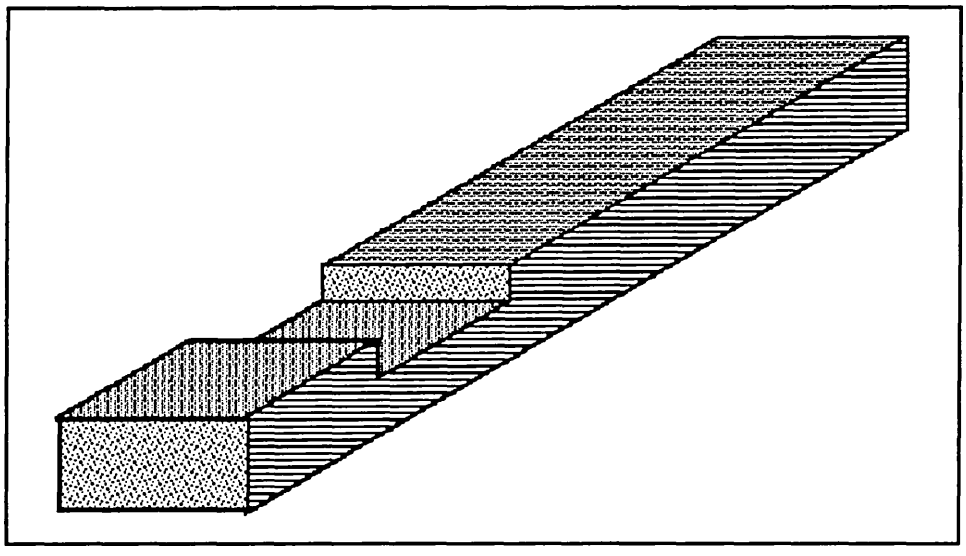

*Fig (3-8) : The schematic diagram of the single element transducer.*

To examine these transducers, a simple ultrasound transceiver was designed. This transceiver was continuously triggered by a 1 $\mu$sec pulse with a repetition frequency of 10 KHz. Therefore, the receiver was listening to the back scattering echoes for 100 $\mu$sec. To obtain a relative relation between pressure intensity and the crystal size each transducer was tested in a water tank. The target was a piece of plane perspex with a thickness of 1 cm.

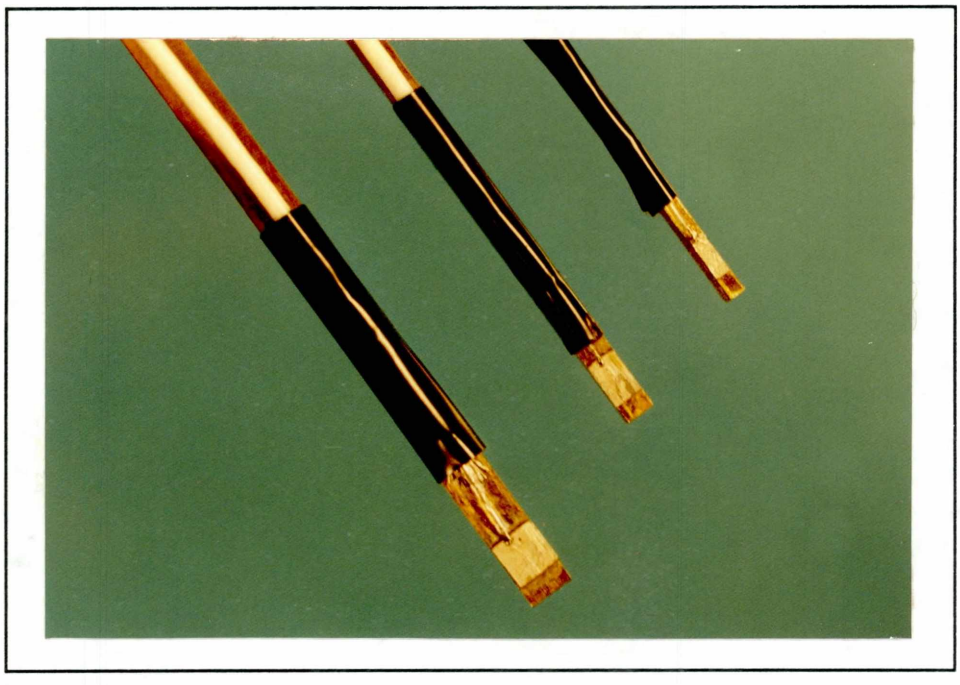

***Fig (3-9)** : The completed single element transducers.*

Fig (3-10) shows the result of this experiment for all three transducers. Each graph illustrates the normalized pressure intensity of ultrasound echo signal versus travelling distance between each transducer and target.

The results obtained confirmed that a reduction in the size of the piezoelectric elements leads to a relatively lower pressure amplitude. However, it is still possible to obtain good reflected echoes with a relatively strong amplitude.

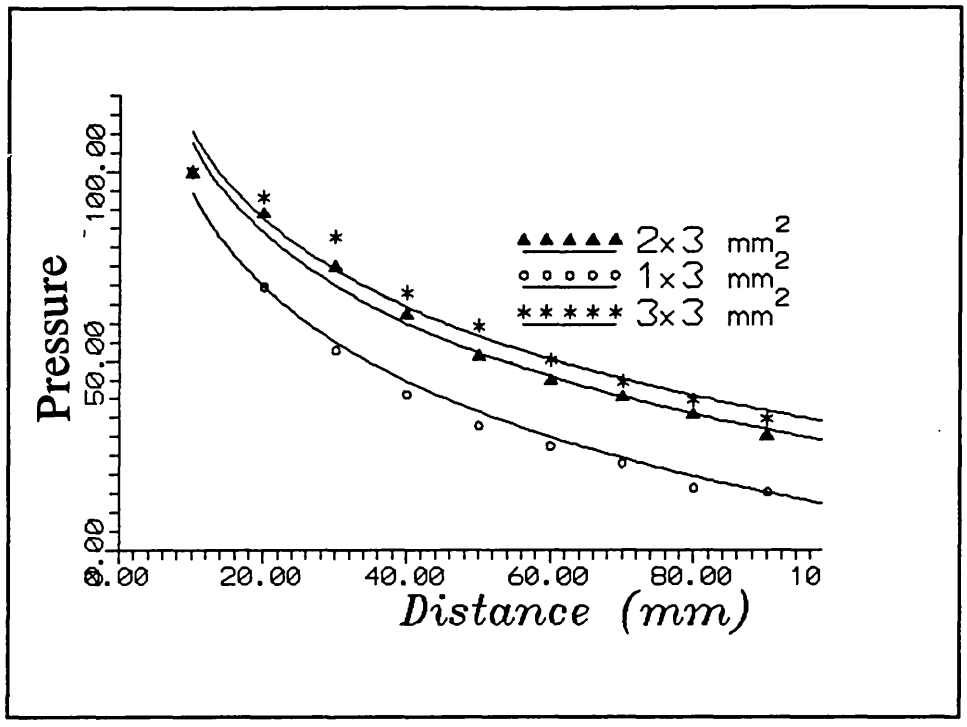


*Fig (3-10) : Normalized pressure versus distance for the single element transducers.*

Work was then shifted on the design and fabrication of a dodecagon ring array transducer. To calculate the actual precision details of the transducer body it was necessary to know the thickness of PZT elements. This parameter is directly related to the resonance frequency of the PZT material. In this work it was decided to use 6 MHz PZT ceramic plates. At this frequency we could achieve better penetration of ultrasound waves and consequently less loss of pressure, but at the price of lower axial resolution. On the other hand at a nominal frequency of 6 MHz it is possible to avoid a sophisticated instrumentation system.

After consideration of the above mentioned factors it was decided to use 6 MHz PZT-5A ceramic plates as active elements of the *Ring Array Transducer.* The thickness of PZT-5A at 6 MHz is 0.37 mm and it was necessary to consider that every two elements of the *Ring Array Transducer* are placed opposite each other. Of course we accounted some tenths of millimetres for adhesive which was required for sticking of PZT elements to the transducer body. Also we had to think about the overall circumference of dodecagon.

After all the necessary considerations, we arrived at the first design with an overall diameter of 2.62 mm. Therefore, our final design led to the first version of the dodecagon ring array transducer. This design which is shown in Fig (3-11) was machined from perspex. The reason for using perspex for the transducer body was to provide a uniform impedance backing material for the PZT elements.

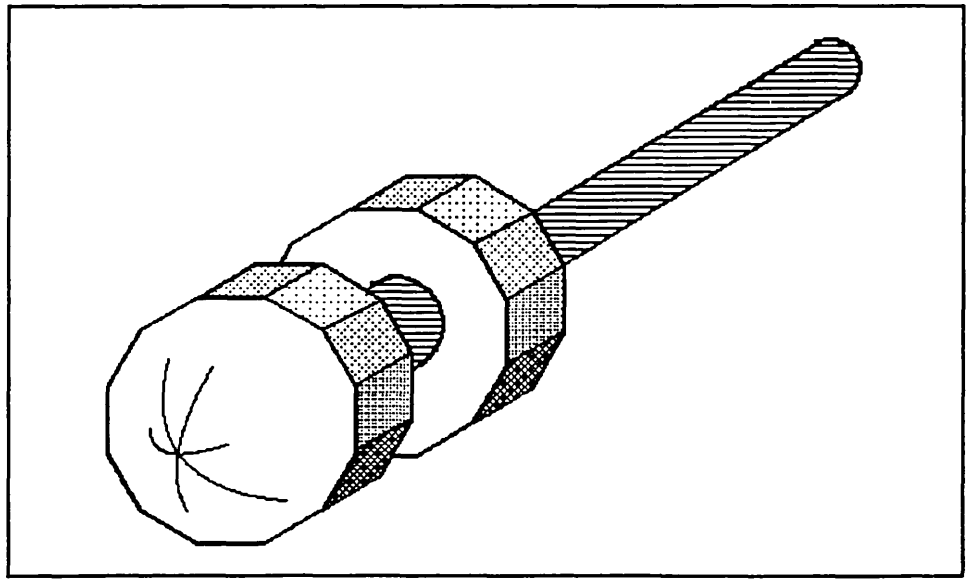

***Fig (3-11)** : The schematic diagram of the first dodecagon transducer.*

As Fig (3-11) illustrates, in this design each PZT element was separated from its

neighbouring element by a blade of perspex which would provide a good acoustical insulation between the PZT elements.

Even though this was a useful experience, we encountered a major problem which forced us to stop working on this design. We had to find an electrically conductive adhesive with high viscosity to stick the PZT elements on the transducer body. At the same time a very tiny wire had to be lied down between each PZT element and the transducer body to act as one of the two electric leads of the PZT element. Unfortunately at the time of this work we could not find any solution to this problem and therefore we concentrated on other materials. Fig (3-12) illustrates the actual body of the first dodecagon transducer made from perspex.

Next it was decided to modify the design of the transducer body and to chose brass as the base material.

## 3-9 : 4 mm DODECAGON RING ARRAY TRANSDUCER :

Due to the problems encountered with the small size of the previous design, It was decided to design and build a larger transducer with an overall diameter of 4 mm. As already mentioned in section (3-8), brass was chosen as the base for the construction of the transducer body. This material in addition to its cheap cost, has several important features which make it a suitable choice for building a miniature ultrasound transducer. First, it can be easily machined. Also, it is a compound of copper and therefore it has a very good electrical conductivity which makes it capable of handling electrical signals and act as one of the required electrical leads for PZT crystals. The mechanical connection between PZT elements and transducer body could be easily fulfilled by silver

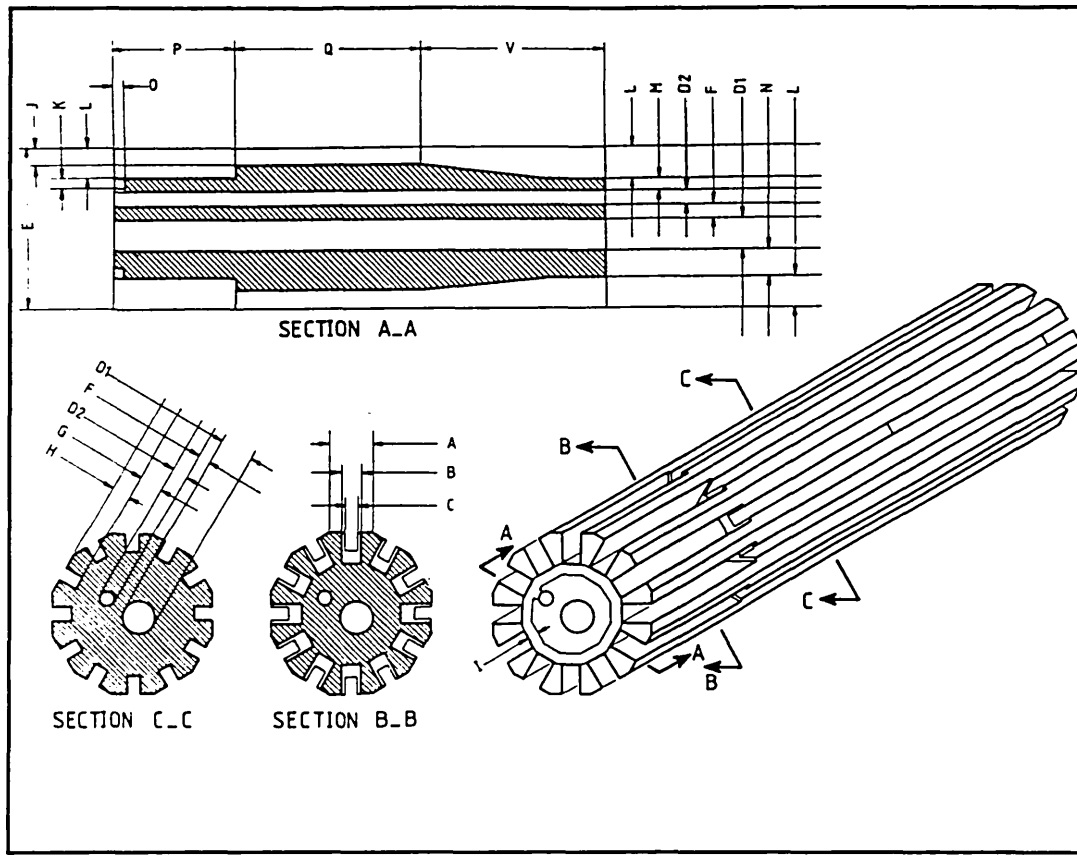


*Fig (3-12) : The first design of miniature ring array transducer made from perspex.*

epoxy resin or low temperature solder cream. Finally brass shows a very good strength against corrosion which makes it ideal for biological environment such as blood vessels in a practical experiment.

In comparison to the work done by Martin [107] and Bom [15], the dodecagon *Ring Array Transducer* provides enough lateral resolution in less complexity of model making and electronic system. Although at this stage the size of transducer may have been a drawback for our *Ring Array Transducer*, we later managed to reduce the overall size of the transducer and it became an important aspect of this transducer with respect to those made by Martin or Bom.

Fig (3-13) illustrates the completed body of this transducer. It contains of twelve sides, each one with a dimension of 0.8 mm by 3.8 mm. The PZT elements were cut from a 10x10 $mm^2$ plate of PZT-5A produced by Verniteron Ltd, [160]. To avoid cross talking between crystal elements, they were cut into 0.55 mm by 3.0 mm. Silver epoxy resin was employed to stick the PZT elements in their place on the transducer body. After all the elements were mounted, they were heated together for 45 minutes to 80° C, to strengthen the mechanical joint between the PZT crystals and transducer body. Then the electrical insolation between the transducer body and the front face of each element was examined.

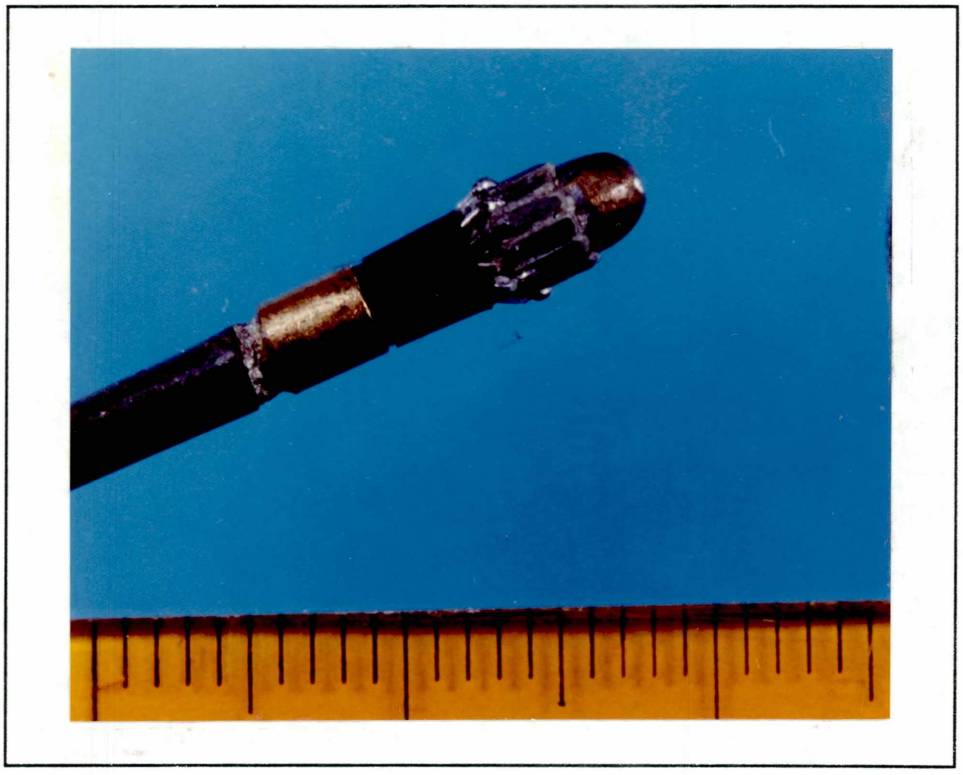

***Fig (3-13)** : The finished body of the 4 mm dodecagon transducer. The ruler is scaled in mm.*

Next, the micro-coaxial cables were made ready for connecting to the front face of the PZT elements. These-micro coaxes were prepared from Suhner Micro-Coax Ltd, [109]. The selected micro-coax was UT-8 type with overall diameter of 0.8 mm. During the process of soldering to avoid heating more than maximum rated temperature of the PZT elements and to protect them against high temperature, a low temperature solder cream from Multi-core Solders Ltd [81], was used. This solder has a relatively low temperature melting point of 170° C which is 180° C lower than the Courie Temperature. After all elements were connected to their associated micro-coax cables, once again the electrical connection between each element and inner conductor of micro-coax cables and electrical insulation between each inner wire of micro-coax and the transducer body were examined.

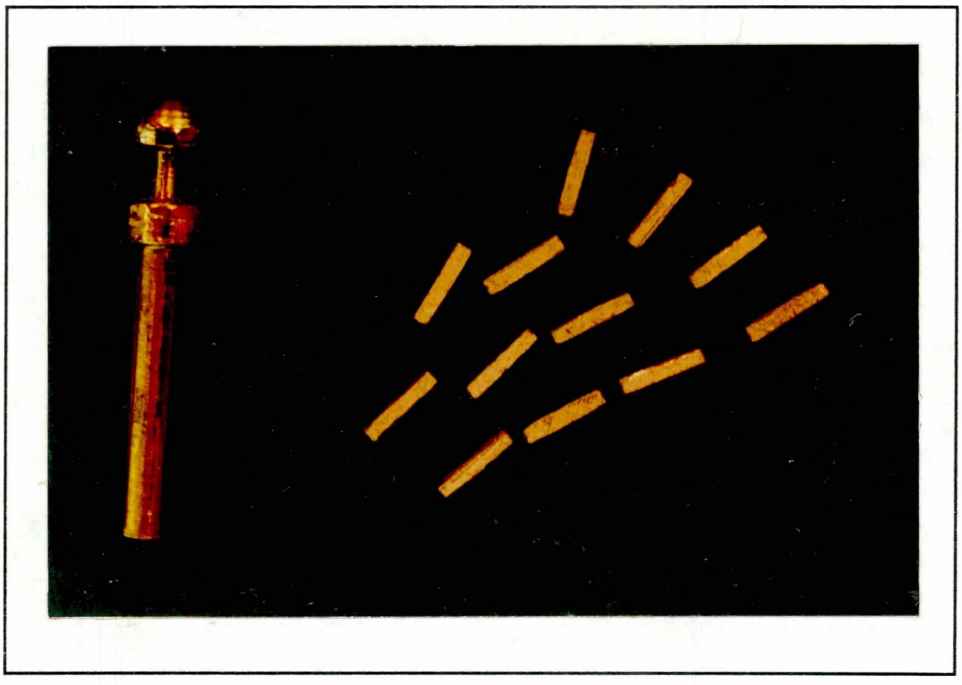

***Fig (3-14)** : The machined body of the 4 mm dodecagon ring array transducer.*

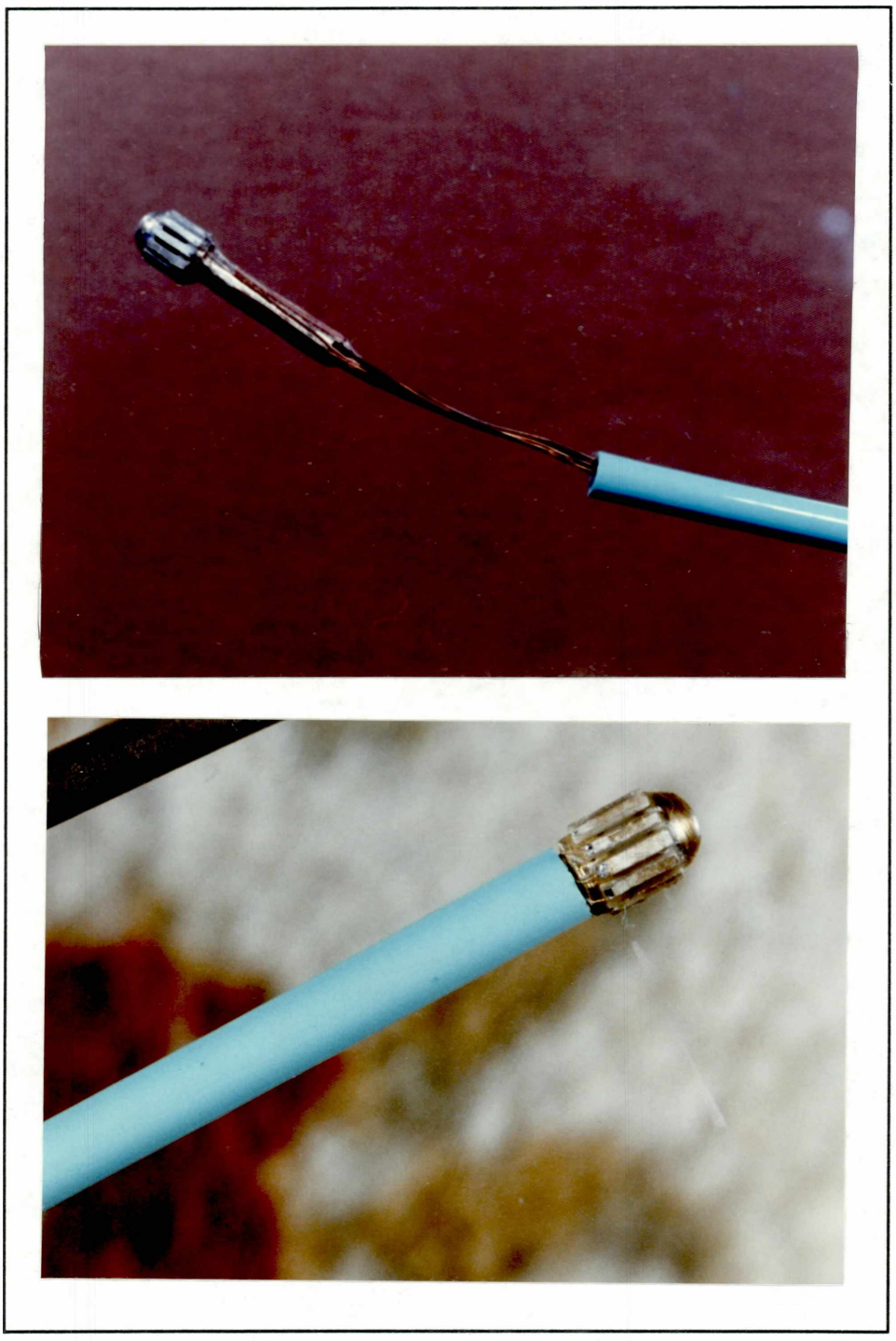

***Fig (3-15)** : Two different stages in costruction of the 4 mm Ring Array transducer.*

Fig (3-14) shows the bare body of the transducer along with its PZT elements. Fig (3-15) illustrates the 4 mm Ring Array Transducer in other stages of its fabrication process.

After all PZT elements were connected to micro-coax cables, completed transducer was dipped in melted wax. Through the gaps between the crystals, the wax filled the space behind the PZT elements. Therefore, wax was used as a low acoustic impedance backing to provide a better sensitivity for transducer elements.

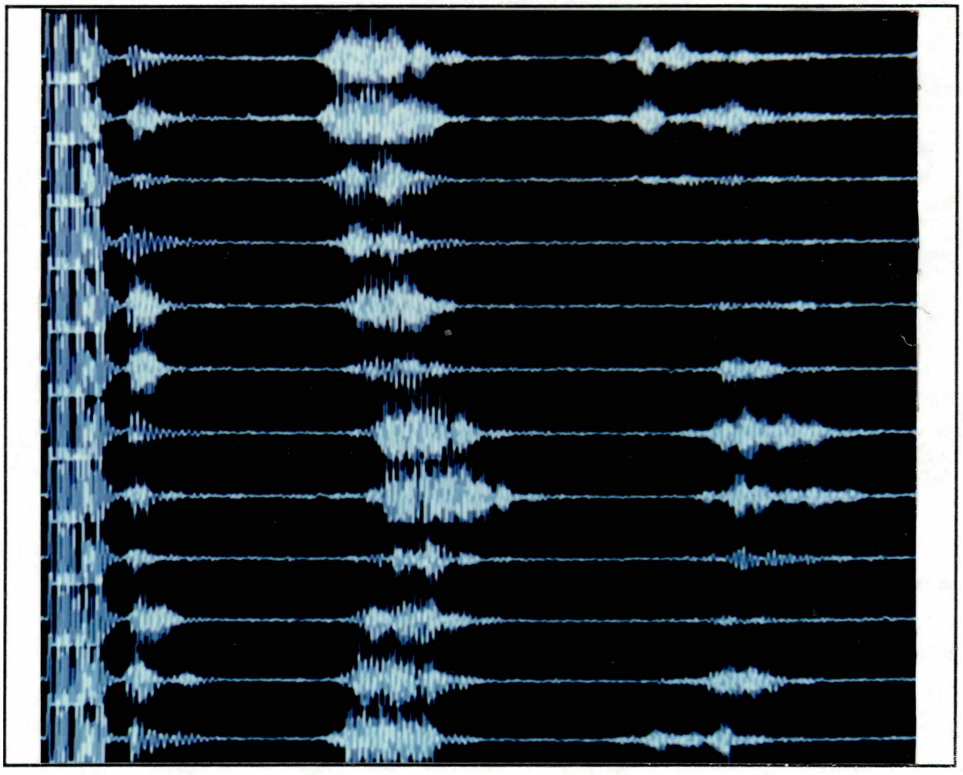

***Fig (3-16)** : The ultrasounic signals captured by the 4 mm Ring Array Transducer.*

To be assured about the performance of each of the PZT elements, they were tested by the ultrasound transceiver test circuit. Fig (3-16) illustrates the ultrasound signal

generated by each element of the *4 mm Ring Array Transducer*. The test object was a cylindrical perspex phantom with an internal diameter of 30 mm and a thickness of 1.0 mm. This phantom was filled with water and placed in a water tank. The results obtained from this experiment proved that transducer and electronic circuit have adequate capacity for accurate data acquisition in such an experiment.

## 3-10 : MINIATURE RING ARRAY TRANSDUCER :

After successful results was achieved with the 4 mm probe, it was decided to decrease the size, and in particular the overall diameter of the transducer. In the new design it had been planned to provide a lumen for a guide wire which added another limit to design of a smaller transducer. In the following sub-sections we will examine the detailed process of design and fabrication for our *Miniature Ring Array Transducer*.

### 3-10-1 : TRANSDUCER BODY:

Fig (3-17) illustrates the schematic diagram of the *Miniature Ring Array Transducer*'s body. On the basis of our design the body of the transducer was machined from brass by Allbon Saunders Ltd, [2]. For better conducting and control of catheter tip in a clinical practice, the head of the transducer was designed conically. Also, for easier fitting of transducer at the end of catheter, the end part of transducer is also a narrow cone.

There are two dodecagons on the transducer body which are separated by a gap of 1.5 mm. These dodecagons provide twelve pairs of opposite platforms for twelve PZT elements. The depth of this gap is 0.7 mm which was limited by the necessary space for

lumen in the transducer body. The gap between the dodecagons and its possible depth give enough space for the backing material.

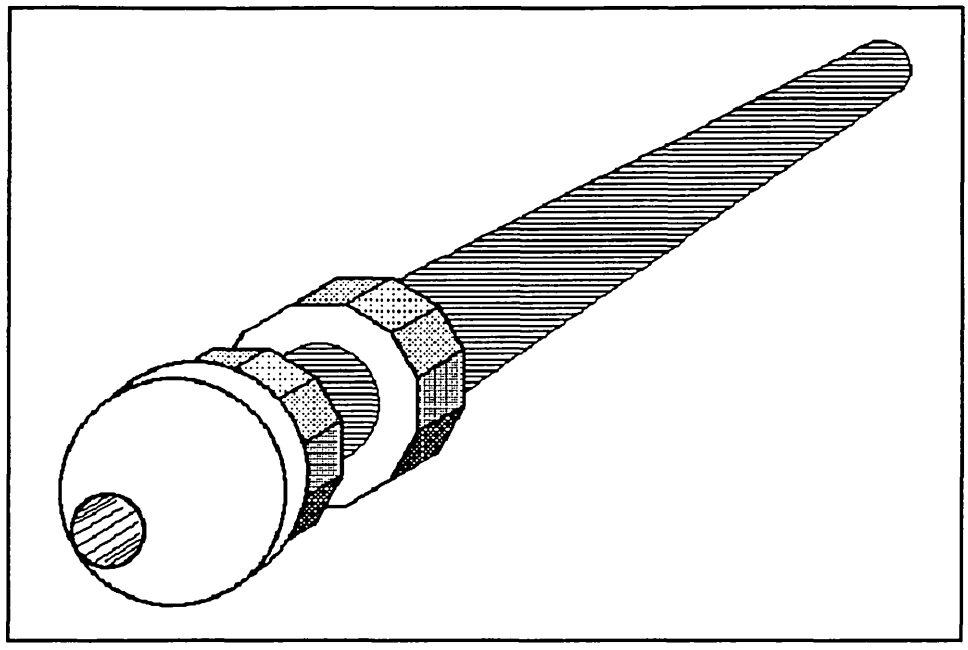

*Fig (3-17) : The schematic diagram of the Miniature Ring Array Trandsducer.*

The lumen for the guide wire is a hole through the transducer body with a diameter of 0.5 mm. To make the catheter tip smoother the conical head of the transducer body has a base with a radius of 1.05 mm.

### 3-10-2 : PZT FABRICATION :

The PZT-5A was chosen as piezoelectric material for this transducer. This material has a very high sensitivity to reflected echoes which was of great importance for us. Several 6x6 $mm^2$ plates of 6 MHz PZT-5A were prepared by Verniteron [160]. Each side of

dodecagon on the transducer body has 0.5 mm of width. Therefore, to avoid acoustical coupling between the transducer elements, the width of each element had to be less than 0.4 mm. By using a precision cutting machine macrotome 2, [82], the PZT plates were cut to the smaller size of 6 mm length and approximately 0.4 mm width. Then all pieces were polished to reduce the size of the elements to 0.35 mm. Next each piece was cut into pieces with a length of 2.7 mm.

During the cutting process the PZT plates were held tight on a microscope slide by means of double sided adhesive tape [RS 555-033]. After the cutting process was finished, aceton solvent cleaner was used to separate the pieces from the microscope slide. Before the fabrication procedure, all PZT elements, micro-coax cables and the transducer body were cleaned with aseton to remove dust and greasy substances from their surfaces.

Now the PZT elements were ready for mounting on the transducer body. The silver loaded epoxy was used as an electrically conductive adhesive to stick PZT elements to the transducer body. Therefore, the transducer body was employed as the common line of transmission or reception for all twelve elements. Due to the small size of the transducer we had to stick one or two elements at the same time.

The transducer was then heated to 70° C to speed up the process of hardening. After two hours, the electrical insulation between adjacent elements and upper and lower faces of each element were tested. Fig (3-18) illustrates the Miniature Ring Array Transducer after all the twelve PZT elements were mounted.

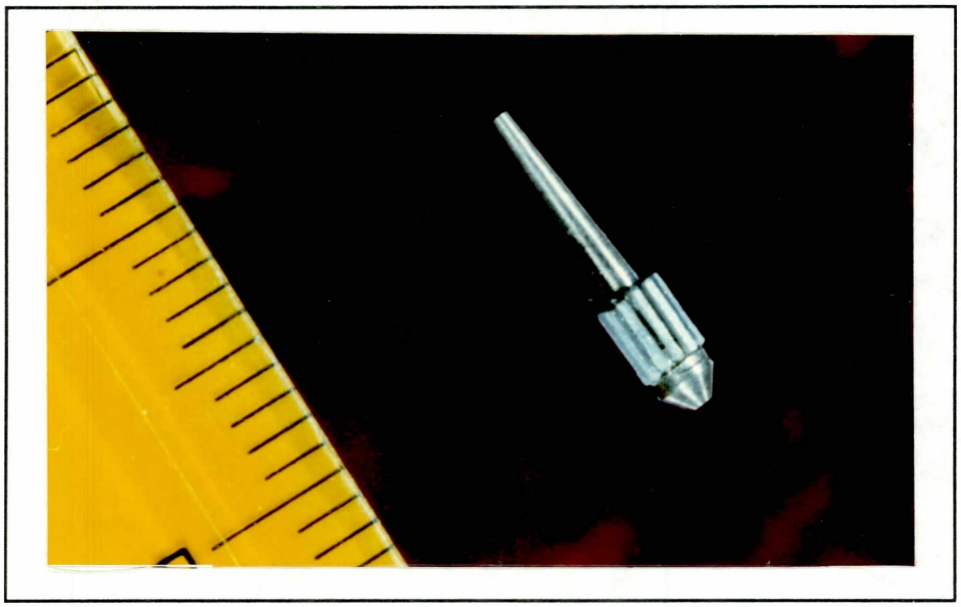

***Fig (3-18)** : The body of the Miniature Ring Array Transducer after all twelve crystals were mounted on it.*

The next stage was to connect the upper face of each element to a tiny micro coaxial cable. Once again the UT-8 micro-coax was employed to make electrical connection between the instrumentation system and the transducer's elements. This micro-coax has an overall diameter of 0.5 mm and enough flexibility for practical examinations.

The inner conductor of micro-coax was soldered to the upper face of each element in the ring array transducer. The solid shields of all micro-coax cables were connected to the transducer body to act as the common line for the transmitting and receiving signals.

Fig (3-19) shows the *Miniature Ring Array Transducer* after the connection of all micro-coaxes to the PZT elements were finished. To protect the PZT elements during the soldering process, a low temperature solder cream with melting point of 170°C was used, [81].

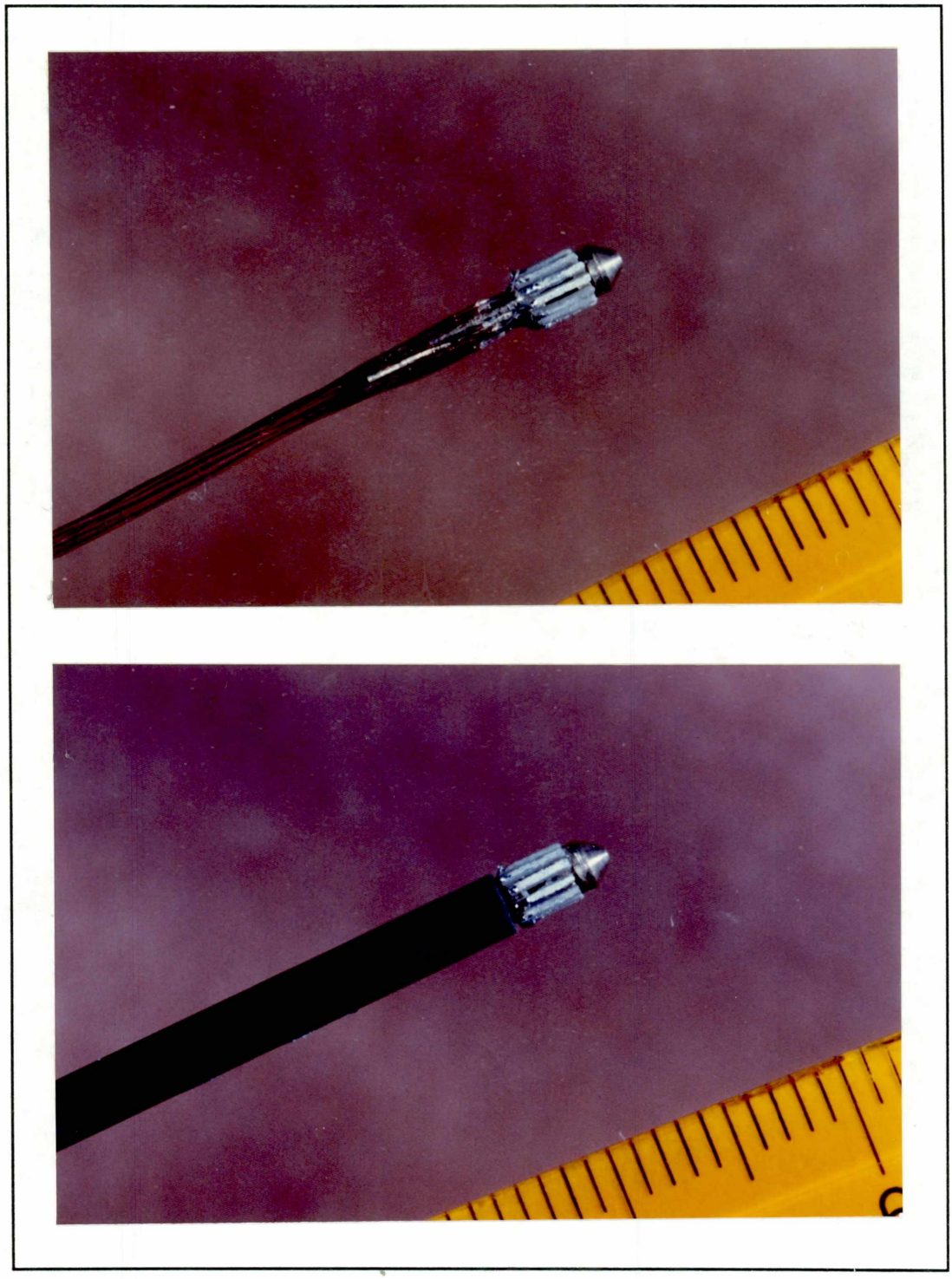

***Fig (3-19)** : The Miniature Ring Array Transducer in its final stages of construction.*

In the next stage of transducer fabrication it was necessary to place the backing material behind each element and finally to cover them by a suitable matching layer.

### 3-10-3 : BACKING AND MATCHING :

The purpose of the backing and matching layer is to improve the performance of the ultrasonic transducer. Backing of transducer is used to dampen the vibration of piezoelectric element after triggering by electrical signal or acoustical wave. The higher the density of the backing material the faster it dampens the vibration of the piezoelectric elements. It is ideal to have the same density as the one of the piezoelectric material for the backing materia to provide a good acoustical interface between the piezoelectric elements and the backing material.

Low acoustical impedance provides less dampening for piezoelectric elements and narrow bandwidth and higher sensitivity for the transducer. Thus, it was decided to use a low density material as backing substance. This was achievedby mixing brass powder with wax to obtain a wax loaded brass backing material. The reason that wax was utilised as the backing material is its low melting point which makes it a good choice for injection into small spaces such as what we had between each element of the *Miniature Ring Array Transducer* and its body. The mixture of wax and brass powder was injected into the space behind the array elements through the guide wire lumen and the small holes on the two sides of the transducer body. The injection was continued until wax started to leak from the gap between the PZT elements.

The matching layer is used to prepare a good interface between the piezoelectric element of a transducer and the loading medium (examination environment). Although in the

pulsed wave ultrasound there is a spectrum of sine waves which makes a good matching interface difficult, some studies have shown that still there is some improvement by using matching layers.

In this work, our catheter mounted transducer was to be examined in human vessels. Therefore, we had to consider three important points in the selection of material for the matching layer. Firstly, the matching layer had to provide a good biological compatibility. Secondly, it had to be spread over the PZT elements in a very tiny thickness. And Thirdly it had to be electrically a good insulator. To fulfil all of the above mentioned points, it was decided to cover the transducer and all its elements with Op-Site spray dressing made by Smith & Nephew Ltd., [120]. This spray is a dressing material which is usually used for surgical or surface wounds.

The final examination of the transducer was to test the completeness of matching layer. First the electrical resistance between front face of each element and the other end of micro-coax cables were measured. The high resistance measured in this examination assured us that dressing spray had covered the complete surface of each element. Then each element of the transducer was examined by an electronic microscope to inspect any bubble air between dressing cover and front face of the piezoelectric elements.

## 3-11 : ELECTRICAL AND ACOUSTICAL FEATURES OF MRAT :

In this section the electrical and acoustical measurement and obtained results are presented. These results provide enough information for ones who are interested in development or application of the small rectangular ultrasound transducers.

### 3-11-1 : EQUIVALENT CIRCUIT AND ELECTRICAL FEATURES :

The equivalent circuit of an ultrasound transducer has been discussed in many articles (Persson and Hertz 1985[131] , Hunt et al (1983)[73], Posakony(1975)[136], Desiletes et al (1978)[38] and Krimholtz (1970)[87]).

Most of these approaches are based on the equivalent circuit described by Mason (1948)[109]. The Mason's equivalent circuit for a high-frequency (thickness-mode) transducer is shown in Fig (3-20). In this circuit an ideal transformer couples the electrical port to the mechanical one.

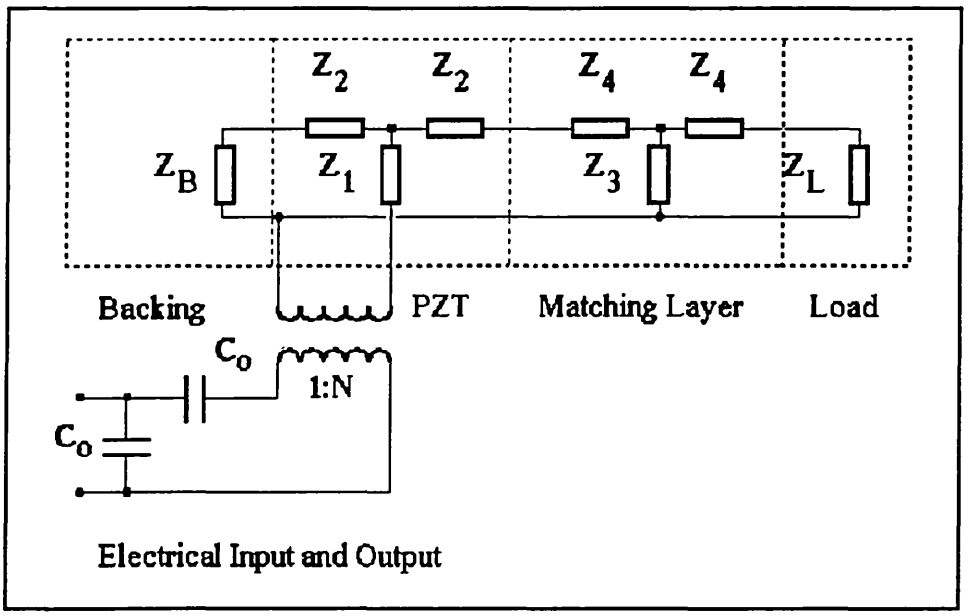


*Fig (3-20) The equivalent circuit of an ultrasound transducer.*

On the basis of information collected from Hunt et al (1983)[73] and Persson and Hertz (1985)[131], the appropriate components associated with the equivalent circuit of Fig(3-20) are listed in table (3-2).

| COMPONENTS OF THE EQUIVALENT CIRCUIT OF A TRANSDUCER | | |
|---|---|---|
| COMPONENT | DEFINITION | COMMENT |
| $C_o$ | $A.\epsilon_{33}^{S}/d$ | Clamped capacitance of the piezoelectric element. |
| $v_T$ | $(C_{33}^{D}/P)^{1/2}$ | Speed of sound in the transducer. |
| $A$ | ..... | Area of the piezoelectric element |
| $N$ | $C_o.\ h_{33}$ | Transformer Ratio |
| $Z_T$ | $A.Z_o = A.P.v_T$ | Acoustic Impedance of the transducer (kg/sec) |
| $Z_1$ | $Z_T.cosec(\pi f/f_o)$ | Delay Impedance of the transducer |
| $Z_2$ | $Z_T.tan(\pi f/2f_o)$ | Delay Impedance of the transducer |
| $d$ | ..... | Thickness of the transducer |
| $f$ | ..... | Frequency (Hz) |
| $f_o$ | ..... | Fundamental frequency of the transducer (Hz) |
| $h_{33}$ | ..... | Piezoelectric constant, electric field/strain at constant charge or stress/charge density at constant electric field (C/m) |
| $\epsilon_{33}^{S}$ | ..... | Relative dielectric constant of piezoelectric element backing or matching materials. |
| $Z_o$ | ..... | Characteristic acoustic impedance of the transducer, backing or matching layers ($kg/m^2.sec$, Rayls) |
| $Z_3$ | $Z_M.cosec(\alpha_n)$ | Delay Impedance of matching layer |

| COMPONENTS OF THE EQUIVALENT CIRCUIT OF A TRANSDUCER | | |
|---|---|---|
| $Z_4$ | $Z_M \tan(\alpha_n)$ | Delay Impedance of matching layer |
| $\alpha_n$ | $k.d_n$ | Phase shift in radians in the n-th layer |
| $K$ | $2\pi/\lambda$ | Wave number |
| $d_n$ | ..... | The thickness of the nth matching layer. |
| $Z_B$ | ..... | Acoustic Impedance of the Backing Material |
| $Z_L$ | ..... | Acoustic Impedance of the Loading Medium. |

*Table (3-1)*

Fig (3-21) shows a simplified equivalent circuit for an ultrasound transducer. This circuit is particularly useful in approximate estimation of the electrical behaviour of the transducer.

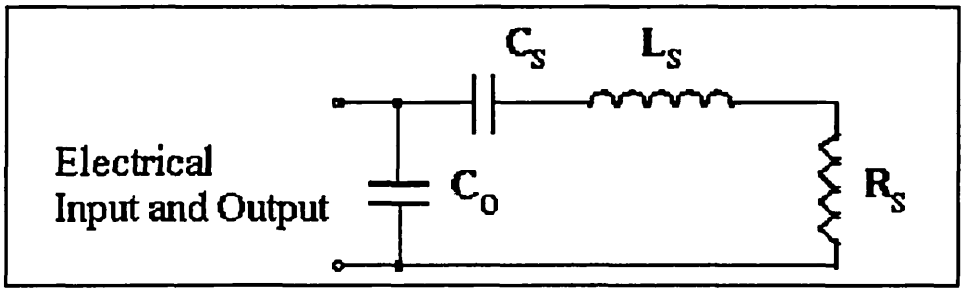


*Fig (3-21) : The simplified model for near resonance ultrasound transducer operating at high Q.*

The components in this equivalent circuit are calculated from the following relationships (Hunt (1983)[73]) :

$$C_o = C' - C_s \tag{3-4}$$

$$C_s = C_o . \frac{(f_p^2 - f_s^2)}{f_s^2} \tag{3-5}$$

and,

$$L_s = \frac{1}{(2\pi f_s)^2 . C_s} \tag{3-6}$$

In the above equations, $f_s$ is the series resonance frequency in which the total impedance of the transducer reaches its minimum value, i.e.

$$R_s = Z_{min} \qquad at: \ f_s \tag{3-7}$$

$f_p$ is the parallel or anti-resonance frequency at which the total impedance is at its maximum value, and $C'$ is capacitance of the transducer at a frequency well below $f_s$.

To measure the actual components associated with one element of the *MRAT* a single element transducer with the same dimensions of an element in the array was examined. This transducer was connected to a Phillips bridge which can measure resistive, capacitive and inductive quantities of any passive network connected to its input.

| Electrical properties of the MRAT | Measured | Calculated |
|---|---|---|
| $C_o$ | 175.5 pF | 169 pF |
| $R_s$ | 4.58 KΩ | 6.1 KΩ |
| $C_s$ | 175.2 pF | 198 pF |
| $L_s$ | 4 μH | 25 μH |
| $R_p$ | 479 MΩ | 286 MΩ |
| Q | 195 | 226 |

*Table (3-2)*

Table (3-2) illustrates the electrical specifications for one element of the MRAT.

## 3-11-2 : ACOUSTICAL CHARACTERIZATION :

In this part of the project the acoustical properties of the *MRAT* was examined. First a single element transducer was employed to measure the acoustical response of this transducer at different angles of radiation and to find out its capability in ultrasound echo capturing.

Then the same transducer was used to measure the acoustical patterns in the planes parallel to its face or intersect to its horizontal and vertical axis.

### 3-11-2-A : HORIZONTAL MISALIGNMENT :

Since the final aim of this project is the application of the *MRAT* as an intravascular diagnostic tool, it is necessary to examine its efficiency under unwanted misallignment of the transducer tip. To fulfil this job a single element transducer with the same PZT element of the ring array transducer was examined. This transducer which is shown in Fig (3-22) was mounted on a flat piece of perspex and placed in front of the flat surface of a water tank.

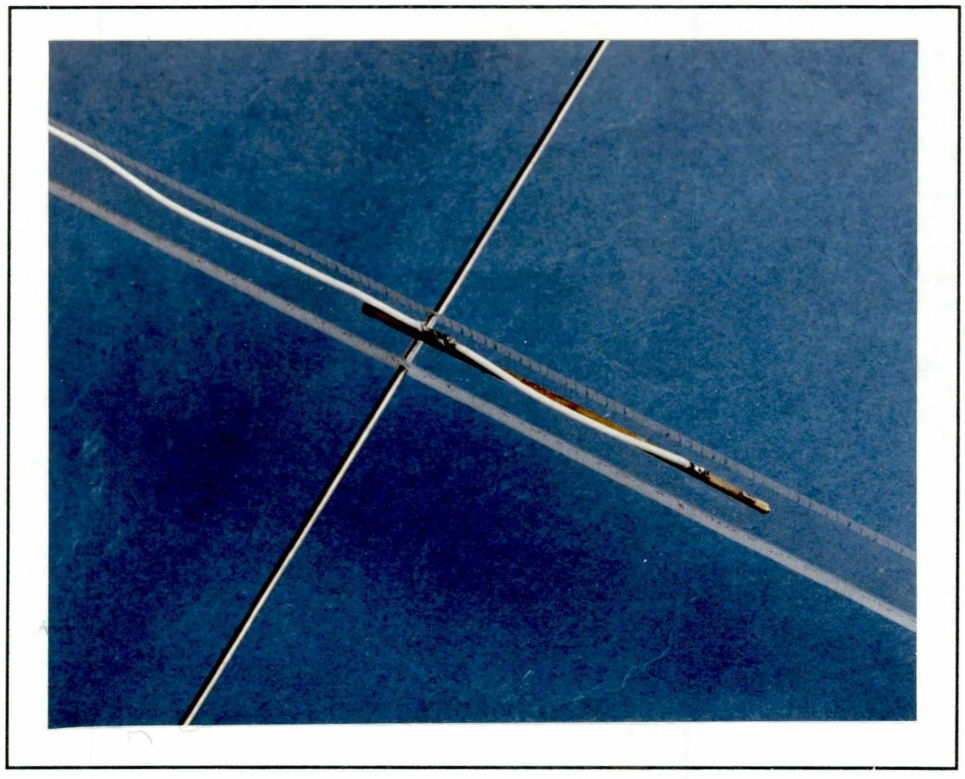

***Fig (3-22) : A sample transducer and its assembly employed in alignment examination***

This transducer was connected to the ultrasound test circuit and its output was connected to an oscilloscope. The transducer was initially aligned by eye such that its acoustic axis

was adjusted along the z axis. Then we tried to optimize the position of the transducer for maximum reflection echo.

After positioning the transducer for maximum reflection, it was aligned around its vertical axis and the amplitude of the reflected echo was recorded at 5°intervals. Fig (3-23) shows the normalized pressure of the reflected echoes versus different angles of radiation for horizontal misalignment of the transducer.

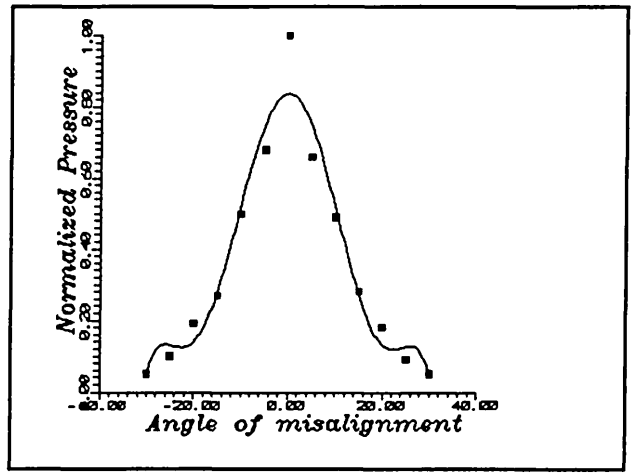


*Fig (3-23) : Ultrasound pressure versus angle of horizontal misalignment of the radiation beam. The graph was plotted using a least mean squares polynomial fitting curve with a degree of 6.*

### 3-11-2-B : VERTICAL MISALIGNMENT:

The same experiment was carried out with the same transducer to examine its ability in echo capturing under vertical alignment. This time the transducer was tilted around its horizontal axis and the ultrasound echo was monitored at every 5° of misalignment. Fig (3-24) illustrates the normalized pressure intensity of reflected echoes versus angles of radiation for vertical misalignment of the transducer.

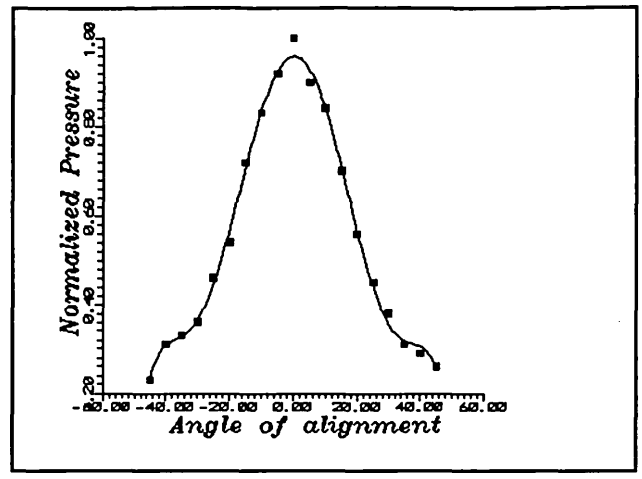


*Fig (3-24) : Ultrasound pressure versus angle of vertical misalignment of the radiation beam. The graph was plotted using a least mean squares polynomial fitting curve with a degree of 6.*

## 3-11-2-C : ACOUSTIC PRESSURE MEASUREMENTS:

In order to capture information on the acoustical pressure inside the ultrasound beam, it is necessary to measure the amplitude of the pressure in three directions of X,Y and Z axis in front of the transducer. This measurement should be carried out in a manner such that the perturbation on the acoustic field is minimized.

A PVDF membrane hydrophone is a suitable alternative for acoustical pressure measurement of an ultrasound transducer. The PVDF hydrophones present a significant performance characteristics in comparison to the ceramic hydrophones. Their acoustic impedance is relatively close to that of water ( typically 4 x $10^6$ $kg.m^{-2}$ $S^{-1}$); this makes them transparent to acoustic waves. Ideally, a hydrophone should have stable performance properties, it should have an active element of a size comparable to or smaller than the acoustic wavelength, and it should have an adequate and sufficiently broadband sensitivity with little variation of frequency over the range from 0.5 MHz to

15 MHz. Interested readers are referred to a draft IEC standard prepared for Technical Committee 29D for more detailed performance characteristics (The characteristics and calibration of hydrophone for operation in the frequency range 0.5 MHz to 15 MHz).

To study the acoustic pressure behaviour in front of the elements of the MRAT, a single element transducer with similar size and shape of the array's element was examined.

This transducer was placed in a water tank against a PVDF membrane hydrophone of nominal diameter 0.2 mm. to acquire pressure intensity data in a plane parallel to the transducer face, raster scans were performed at different positions.

Much efforts were employed in acquiring reliable data from the acoustical behaviour in the near-field. However, due to the complex attitude of the rectangular transducer in the near-field and especially the small size of our transducer, recording of stable and reliable results were possible. Also, the time available to us did not allow the construction of the scanning rig and highly sensitive hydrophones that would have been necessary for pressure measurements in the near field of such a small transducer.

Therefore, it was decided to perform our experiment the positions further from the transducer, with the hydrophone located at 15 mm and 30 mm from its face. Fig (3-25) shows the schematic diagram of the position of the transducer's element, the hydrophone, and the vertical and horizontal scan lines.

At the two measurement points the voltage waveform proportional to the acoustic pressure was generated by the hydrophone which was processed to provide information on the axial variation of acoustic pressure, and contours of the pressure distribution in a plane parallel to the transducer face.

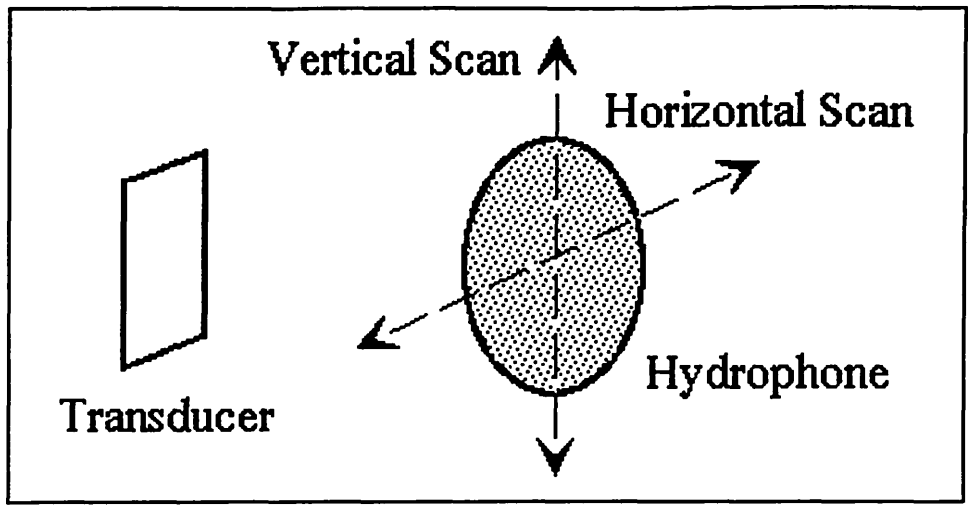


***Fig (3-25)** : Spatial position of the hydrophone and the transducer's element.*

Fig (3-26) and (3-27) shows the contour plots of the pressure distribution in front of a single element (0.35 mm x 2.7 mm) rectangular transducer at two distances of 15 mm and 30 mm, respectively. To provide these results, the hydrophone was scanned in an area of 9.0 x 9.0 mm with a step size of 0.2 mm. Each closed cvrve in these graphs is a contour of pressure which was normalized in terms of maximum measured pressure and is presented in different colours.

It is possible to obtain an estimate of acoustic pressure in any point close to the acoustical axis of the transducer. It is also possible to make an approximate estimate of the ultrasound beam angle associated with any particular pressure contour at the distance of 15 mm or 30 mm of the transducer face.

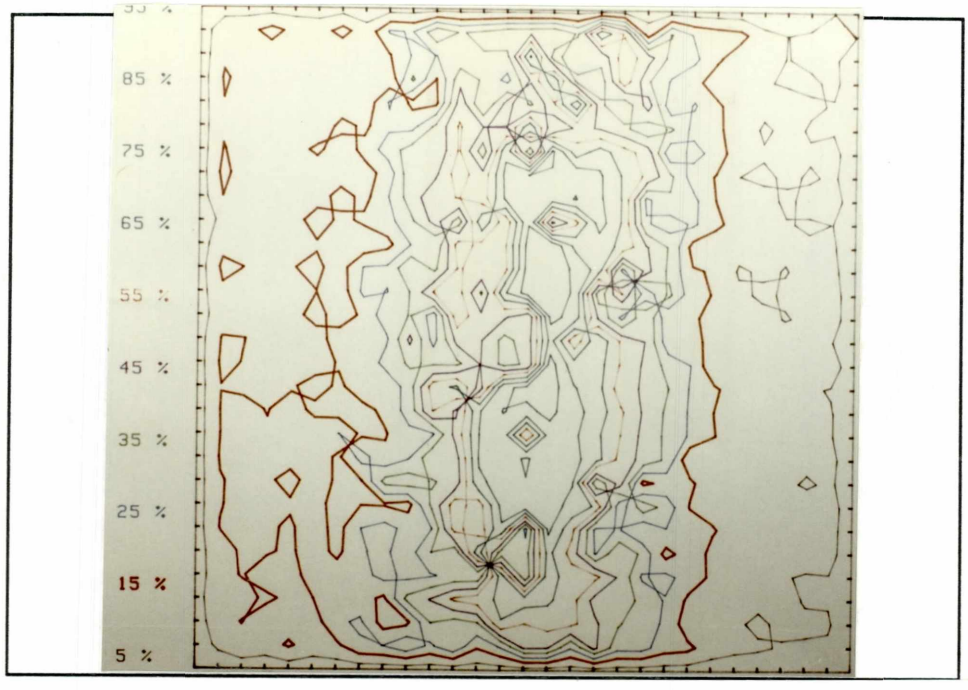


***Fig (3-26)** : Two-dimensional Raster scan of the acoustic pressure in the measurement plane 15 mm separated from the transducer face. The colour key to the acoustic pressure is related to the numbers at the left hand side of the graph. The existence of several high pressure regions signifies the complexity of acoustic pressure behaviour in front the rectangular transducer.*

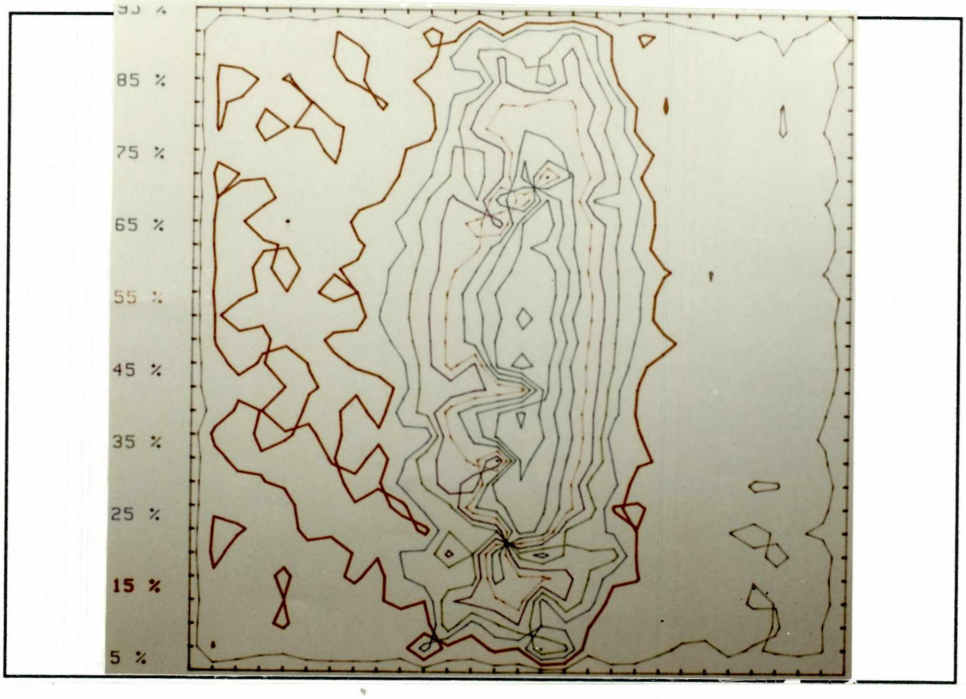


***Fig (3-27)** : Two-dimensional Raster scan of the acoustic pressure in the measurement plane 30 mm separated from the transducer face. The colour key to the acoustic pressure is related to the numbers at the left hand side of the graph.*

The ambiguity of contours, proves the complex behaviour of the rectangular apertures. However from the comparison of these results it becomes evident that the acoustic pressure shows less disturbance as the acoustical waves enter the far-field and in particular at considerable distances from the transducer.

To study the effect of the transducer size on the complexity of the pressure contours, another single element transducer with a width of 1mm and length of 3mm was made.

This transducer was examined at the same positions, 15 mm and 30 mm from the transducer face. The results obtained are illustrated in Fig (3-28) and (3-29). These results reveals that an increase in the size of the rectangular transducer provides a more uniform distribution of acoustic pressure.

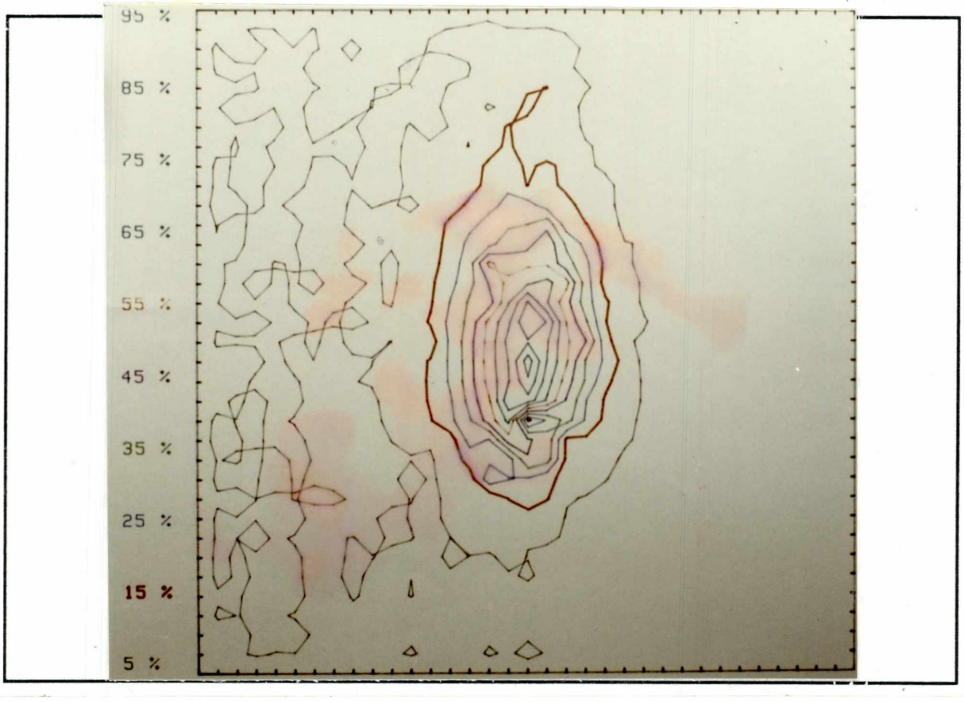


***Fig (3-28) :*** *Two-dimensional Raster scan of the acoustic pressure in the measurement plane 15 mm separated from the transducer face. The colour key to the acoustic pressure is related to the numbers at the left hand side of the graph.*

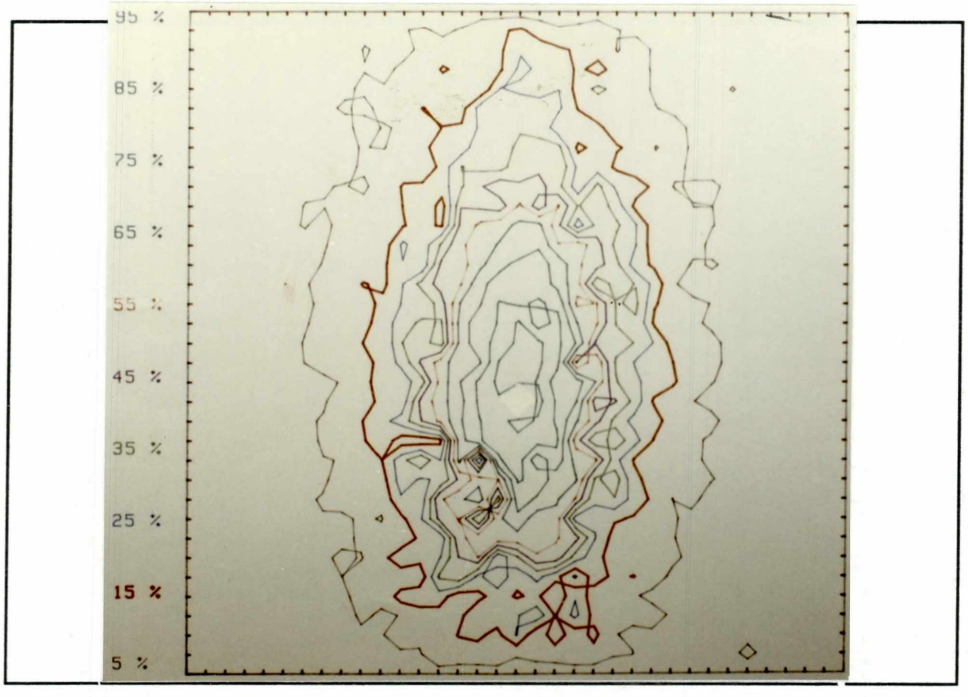


***Fig (3-29) :*** *Two-dimensional Raster scan of the acoustic pressure in the measurement plane 30 mm separated from the transducer face. The colour key to the acoustic pressure is related to the numbers at the left hand side of the graph.*

In the next set of experiments the peak-positive acoustic pressure and the pulse-pressure squared integral were measured. The results give a good and sensible estimate of the acoustic pressure along the acoustic axis in vertical and horizontal directions.

Fig (3-30) shows the peak-positive acoustic pressure versus distance along the vertical axis and the pulse-pressure squared integral of the signal power to the noise power. This information is a value in determining how to map the physical world to a 3D image. This is presented in Fig (3-31). (The detailed use of this parameter lie beyond the scope of this thesis.

The same experiment was repeated to provide information about the acoustic pressure along the horizontal axis of the transducer. The results obtained in this experiment are presented in Fig (3-32) and (3-33).

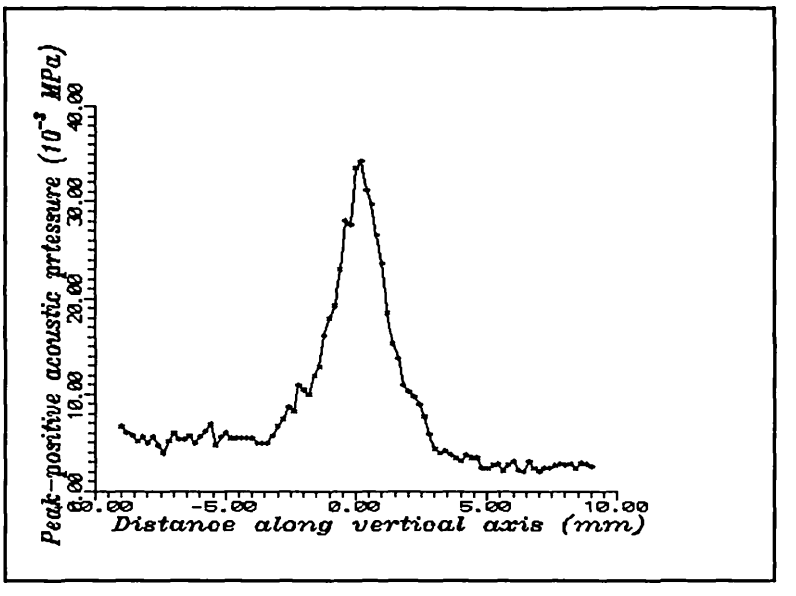


***Fig (3-30)** : Peak-positive acoustic pressure along the vertical axis measured at 15 mm from the transducer.*

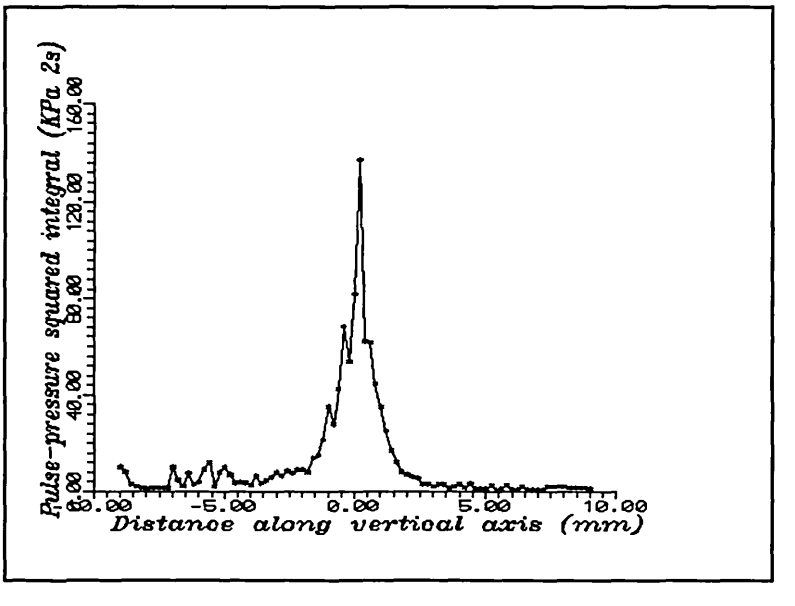


***Fig (3-31)** : Pulse-pressure squared integral along the vertical axis measured at 30 mm from the transducer.*

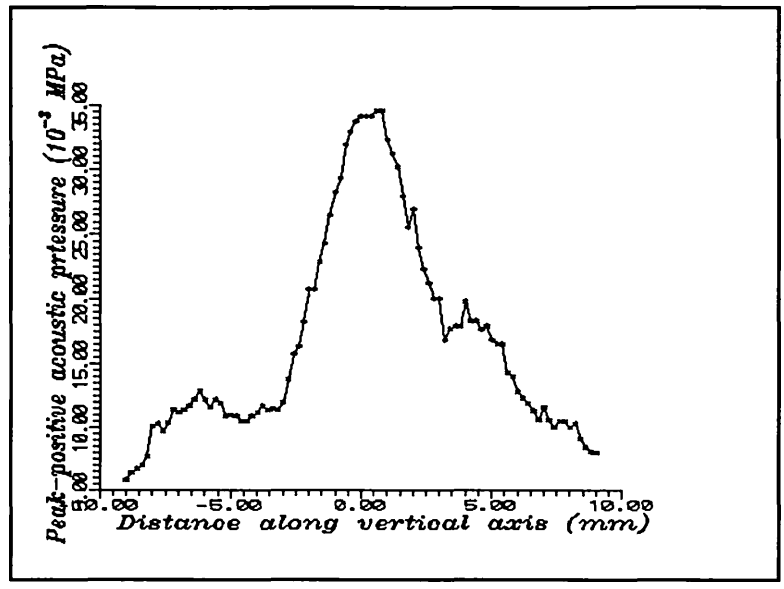


***Fig (3-32)** : Peak-positive acoustic pressure along the horizontal axis measured at 15 mm from the transducer.*

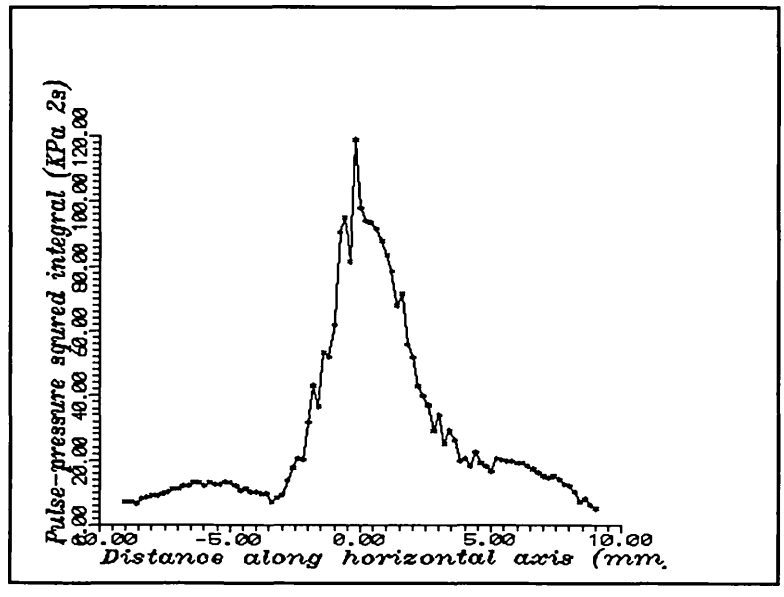


***Fig (3-33)** : Pulse-pressure squared integral along horizontal axis measured at 30 mm from the transducer.*

## 3-12 : SUMMARY :

In this chapter first construction details of an ordinary circular element ultrasound transducer was discussed to provide the necessary background for the following subjects. Then different types of the array transducers employed in biomedical application were studied. In this part the Linear Array, Phased Array and Annular Array Transducers were examined by particular emphasis on their construction.

In the next part of the chapter, a technical review on the catheter based transducer was presented. It was tried to prepare the essence of the related works done during the last two decades.

In this part the catheter based transducers were divided into two categories of non-imaging and imaging applications, and they were surveyed separately.

The review of the related researches to this work provided a good knowledge base for continuation of our investigation in construction of the Miniature Ring Array Transducer.

Following to the mentioned studies, the procedure of design and construction for different types of the ring array transducers were presented. First the general and special problems in construction of the miniature transducer were examined and then three different designs were discussed.

It was notified that construction of perspex-base transducer was stopped due to the difficulty in process of PZT fabrication. The step by step discussion on construction procedure of 4mm dodecagon ring array transducer, and later the Miniature Ring Array

Transducer (MRAT) provided complete information about the design and constructin of miniature trnasducers made in this project.

At the final part of this chapter the obtained results from the technical examinations carried out on a prototype single element transducer were presented. In order to provide these results a single element transducer with a rectangular element of the same size of an element of the MRAT was made and examined. These examination provided some useful information about the acoustical pattern and pressure intensity of any element of the MRAT.

*Chapter Four*

# *Ultrasonic Instrumentation System*

## 4-1 : INTRODUCTION :

The electronic instrumentation system developed for ultrasound wave generation, data acquisition, digital to analog conversion and data storage will be outlined in this chapter. The different parts of these systems are explained and examined in the following sections.

The instrumentation system is responsible for the triggering of the *Ring Array Transducer*, reception of echoes, and finally saving the digitalized captured signals in a FIFO ( First In First Out ) memory buffer. To fulfil this task, it was necessary to design the different parts of the instrumentation system as illustrated in Fig (4-1).

The heart of the data acquisition system is an ultrasound transceiver which provides a high frequency signal for each element of the *ring Array Transducer.* It also listens to

the back scattered echoes and receives them. To fulfil the operation of the transceiver part it was necessary to design a digital triggering circuit to perform several tasks. It produces a pulse of short duration to trigger the transceiver. It also controls the twelve channels of a multiplexer which conducts trigger signal to twelve elements of the *ring Array Transducer.*

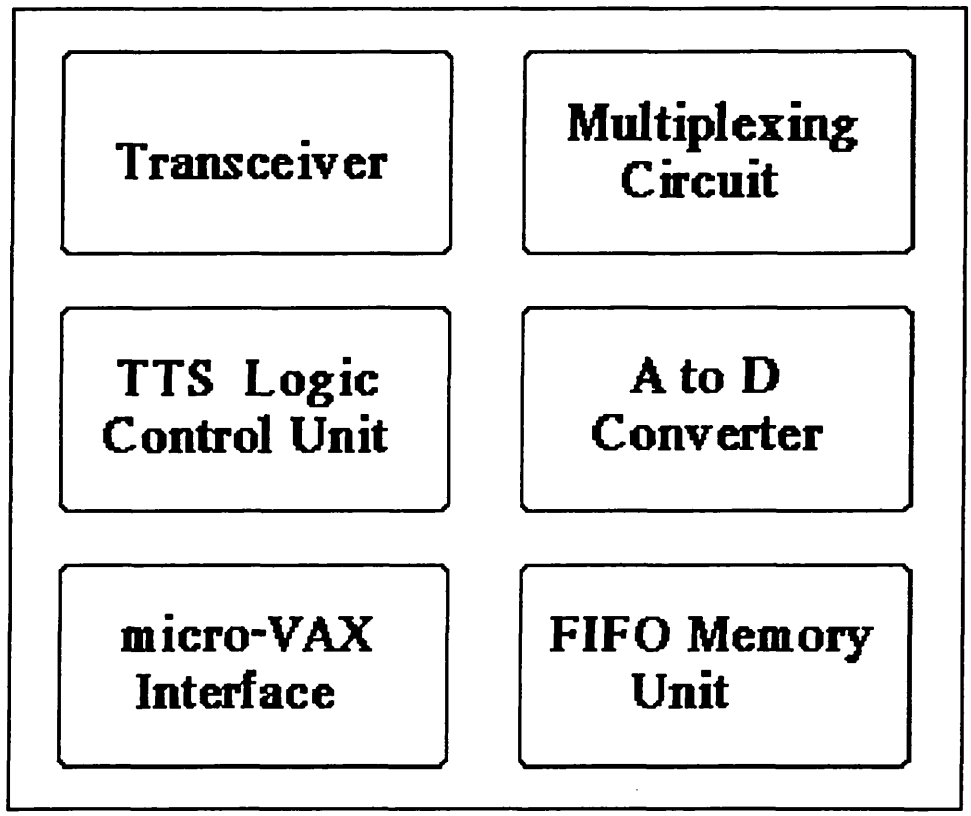


*Fig (4-1) : The principal elements of the ultrasonic instrumentation system.*

Another part of the instrumentation system is the multiplex circuit which transfers the high frequency triggering signal from the transceiver to each element of the *ring Array Transducer* and back scattered echo signals from each element to the transceiver. The Analog transmitted and received signals are digitized by a fast A to D converter and finally the digitized signals are saved in a FIFO memory buffer for further processing.

This system needed to be interfaced to a micro-VAX and therefore necessary hardware and software requirements needed to be considered.

## 4-2 : ULTRASOUND TRANSCEIVER :

The ultrasound transceiver comprises an LM1812 chip and associated components to keep it in operation.

The LM1812 [173] is a complete ultrasonic transceiver on an 18 pin chip capable of performing a variety of pulse-echo ranging applications. This chip needs a short duration pulse to produce the necessary burst for the oscillation of the transducer element. After the oscillation burst is transmitted, LM1812 changes its mode to receiver and listens to the returned echoes. The sound decoder in LM1812 generates a pulse approximately with the same width as the original echo. The only condition for detection of the returning echo is its amplitude which should be sufficiently large.

Fig (4-2) illustrates the schematic circuit diagram of the ultrasonic transceiver in the transmitting mode. The transmitter output is pin 6 of LM1812. To determine the operating frequency an LC network consisting of $L_1$ and $C_1$ is connected to pin 1. Another LC tank which is connected between pin 6 and 13 works as a band-pass filter. The relation between L,C and the operating frequency $F_0$ , is expressed in equation (4-1);

$$f_0 = \frac{1}{2\pi\sqrt{L_1 C_1}} \qquad (4\text{-}1)$$

Therefore, by selecting correct values for the inductor and capacitor it is possible to arrive at the required resonance frequency. There is an on chip 1 $\mu$sec one-shot which is triggered by each cycle of the oscillator and in turn drives a power amplifier at pin 6.

To turn ON the one-shot circuit, it is necessary to activate pin 8 with a short pulse of 1 $\mu$sec width. A 12 K$\Omega$ resistor was connected between pin 8 and the pulse generator as a current limiter to protect the input amplifier at pin 8.

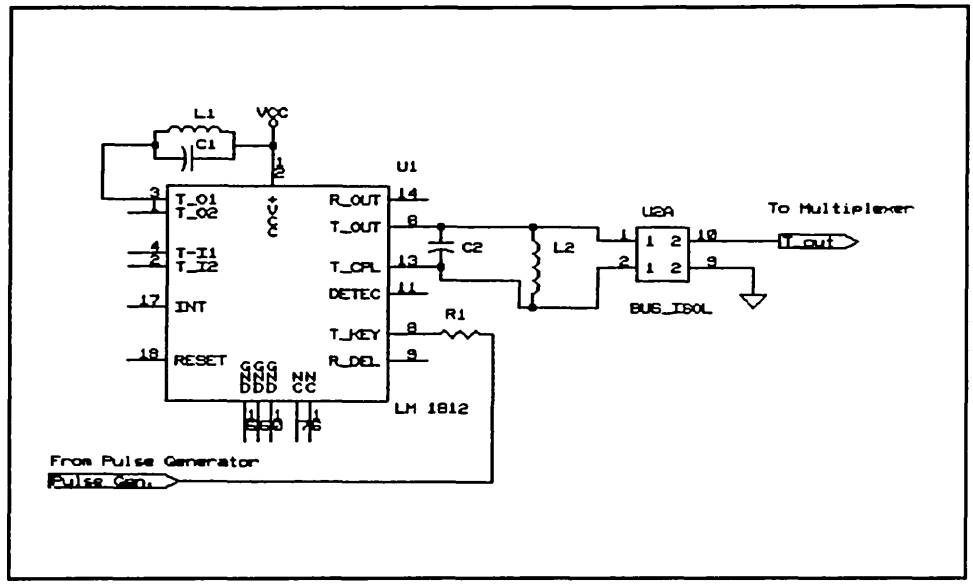


*Fig (4-2) : The ultrasound transceiver circuit in transmitting mode.*

To couple the transducer to the transmitter output, a bus isolator transformer with a 1:1 ratio was employed. It was necessary to tune the primary winding of this coupling transformer at the operating frequency and hence capacitor $C_2$ was selected in such a way to be tuned with $L_2$ and the primary winding of transformer.

The key pin to switch the LM1812 into either the transmission or reception mode is pin 8. When this pin is held High, the transceiver acts as transmitter and when pulled Low it changes to a receiver. The key pulse has a width of 1 $\mu$sec at High level and 100 $\mu$sec in Low level. A train of twelve repetitive cycles of this pulse is input to pin 8 through the current limiter resistor $R_1$. Therefore, the transceiver for 1 $\mu$sec transmits the

ultrasonic waves and for 100 $\mu$sec listens to back scattered echoes. This process is repeated for all twelve elements of the *Ring Array Transducer.*

The receiver section of the LM1812 contains two separate gain stages. When pin 8 is held Low, the receiver input pin 4 listens to the incoming signal. Fig (4-3) illustrates the schematic diagram of the transceiver in the reception mode. To protect the first gain stage of the receiver section, the capacitor $C_7$ was connected as a current limiting reactance. The value of this capacitor was selected in a manner to provide about 5 K$\Omega$ of reactance at the resonance frequency of 6 MHz.

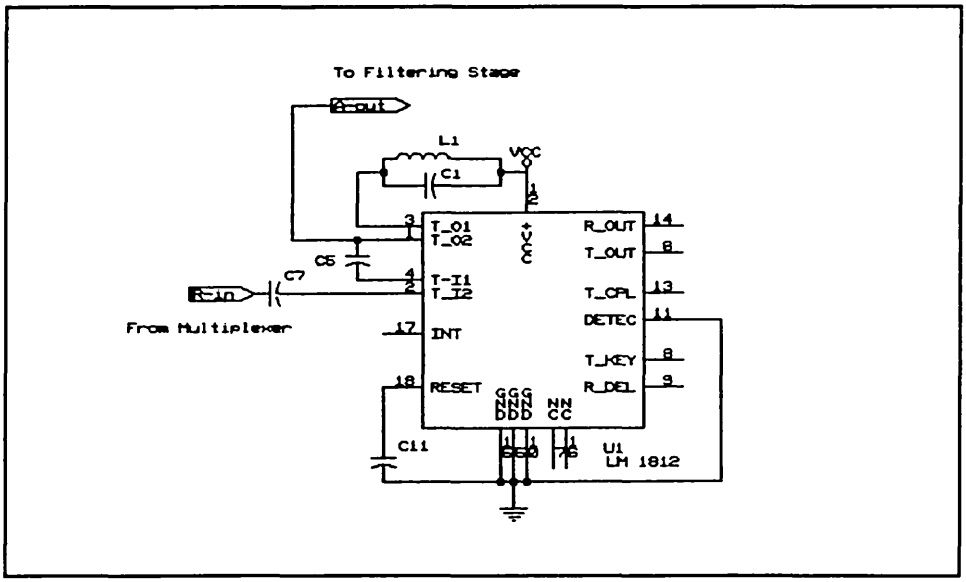


*Fig (4-3) : Transciver circuit in Receiving mode.*

The $L_1C_1$ network is shared by both transmitter and receiver sections. During the receiver mode this LC tank circuit is tuned at the same operating frequency, determining the gain factor of the second gain stage of the receiver section.

Fig (4-4) shows typical waveforms at pins 6 and 8. As it is seen, at the start of the

transmission mode the transducer starts its vibration and continues its ringing sometimes after being switched to reception mode.A part of this ringing is due to the mismatching between piezoelectric element and the transmitting medium.

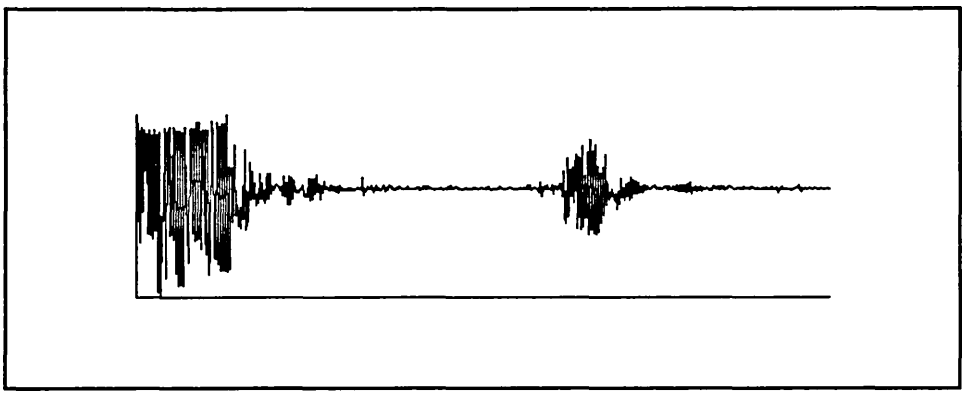

*Fig (4-4) : Ultrasound signal on pin 6 of the transceiver.*

Also, some part of the ringing phenomena is produced by low density backing material. Another factor could be a loose connection between the piezoelectric element and the transducer body.

## 4-3 : FILTERING :

To provide a preliminary band-pass filtering the NE592 video amplifier was employed to pass through the original incident and reflected signals. This filter which is illustrated in Fig (4-5), was tuned on 6 MHz.

At this stage, by means of a variable resistor $R_4$ between pin 4 and 11, it is possible to control the gain of the amplifier to obtain a suitable output from either weak or strong echoes.

[175]

The NE592 provides a pair of differential outputs at pins 7 and 8 which are directed to the next stage for A to D conversion.

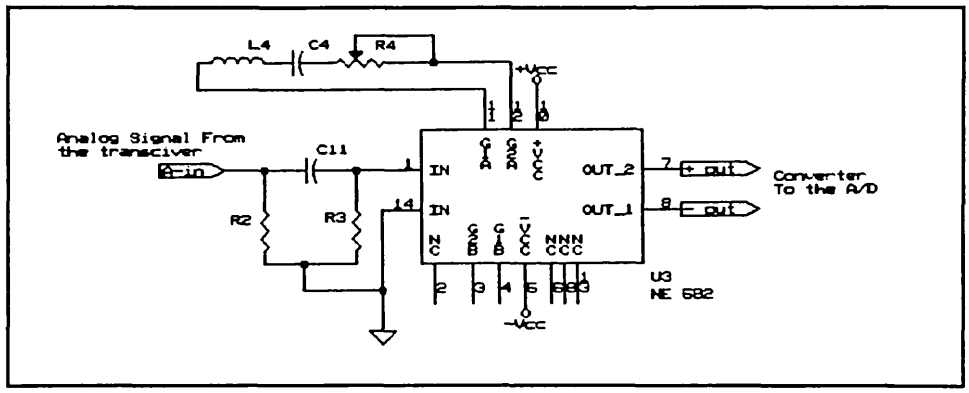


*Fig (4-5) : A 6 MHz band-pass filter with differential outputs.*

## 4-4 : TTS LOGIC CONTROL UNIT :

The logic control unit of the *Transceiver Triggering System (TTS)* is the centre of producing all necessary commands for communication with the multiplex circuit, A to D converter, and FIFO memory unit. It is necessary to mention that for the digital circuits we used TTL low powered Schottcky devices to have a fast circuit with low power consumption.

The task of the *Logic Control Unit* is to provide the START signal for the beginning of the process and the END signal to finish it. It was also considered that the electrical burst for the transceiver unit should be produced by this unit. During the active cycle of each channel of the multiplexer, it is necessary to determine the duration of the electrical burst and that of listening to each PZT element in the *Ring Array Transducer.* Finally, it should be possible to provide the necessary signals for the A to D converter and FIFO Memory Unit to broadcast the start and end of one complete data capturing process.

The above mentioned control signals are achieved in three sections reffered to as *Resetting Circuit, Timing Circuit and Addressing Circuit.* In the following sections each of these circuits are discussed in more details.

## 4-4-1 : RESETTING CIRCUIT :

Fig (4-6) illustrates the schematic diagram of the *Resetting Circuit.* The RESET and $\overline{\text{RESET}}$ signals are turned to High and Low levels by a normally open foot switch.

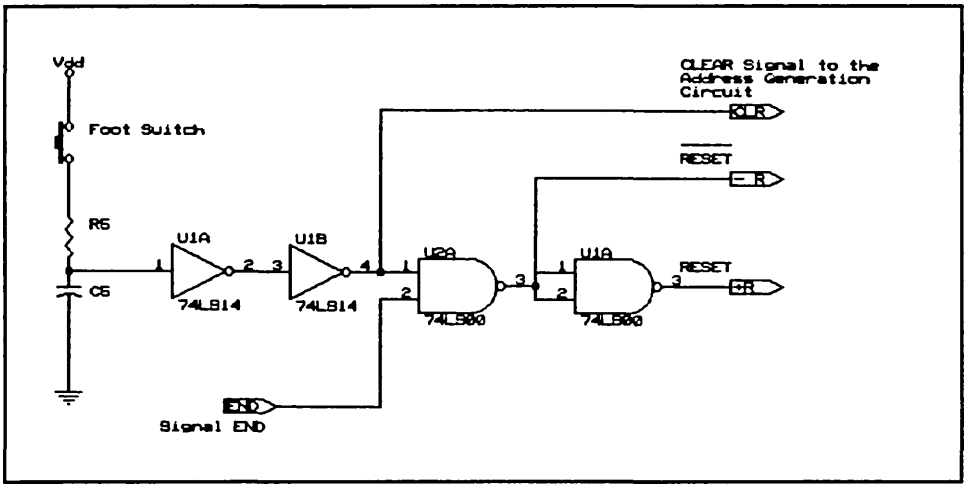


*Fig (4-6) : RESETing circuit.*

After the foot switch is pressed the RESET signal at the output of the NAND gate U1A goes High and remains at this level up to the end of the capturing process. When all twelve crystals in the *Ring Array Transducer* are triggered an END signal is produced which brings the RESET signal to Low level, making the system ready for another capturing process. The signal END is created by the *Addressing Circuit* which is discussed later.

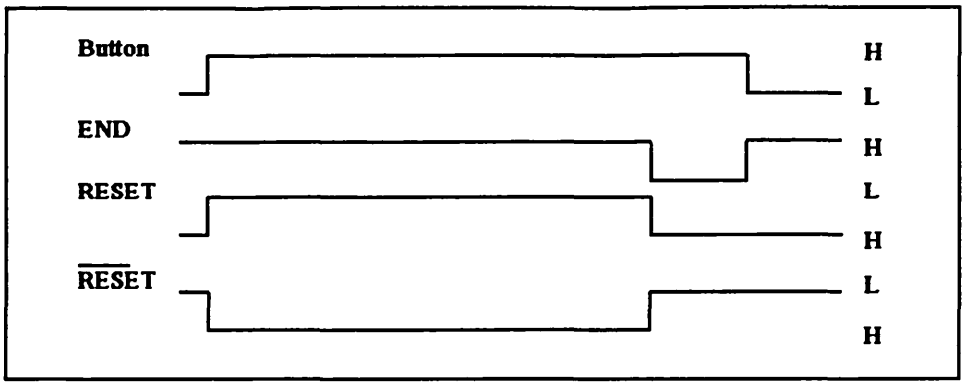


*Fig (4-7) : Generation of RESET Signal*

Fig (4-7) shows the timing diagram of the *Resetting Circuit*. It can be seen that before the foot switch is pressed, the BUTTON signal is Low and the END signal is High. Therefore, the RESET and $\overline{\text{RESET}}$ signals remain at Low and High levels, respectively. At the end of the capturing process signal END goes down and causes the RESET and $\overline{\text{RESET}}$ signals to change their levels. Thus, all activities in the control unit will be stopped. After a short period of time the END signal will return to its High level, and the electronic circuit will be ready for the next capturing process. The release of the foot switch returns the BUTTON signal to its Low level again.

The duration of SET and RESET signals is counted by the *Clock Generation Circuit* to provide enough time for twelve individual triggering and capturing processes of twelve elements in the *Ring Array Transducer*.

### 4-4-2 : TIMING CIRCUIT :

The *Timing Circuit* provides the required timing signals for the triggering of any individual element of the *Ring Array Transducer* and listening to reflected echoes. It also

provides the START pulse which is used to initiate the A/D converter and the *FIFO Memory Unit*. The timing signals are two very similar train of pulses called **T1** and **T2**. Fig (4-8) shows the waveforms associated with these signals. **T1** is a train of twelve pulses which is used to generate the necessary control and address signals for the multiplex circuit. **T2** is very similar to **T1** and is used for the triggering of the *Transceiver Circuit* to produce twelve electrical bursts for the twelve piezoelectric elements.

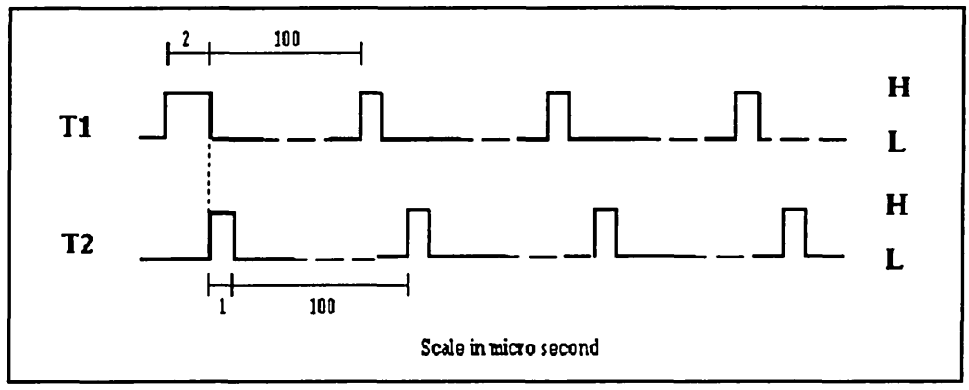


*Fig (4-8) : T1 and T2 digital waveforms.*

It is obvious that before the transmission of any electrical burst, the associated channel through the PZT element should be ready. Therefore, it was decided to generate **T1** to lead **T2** by 1 $\mu$sec. Thus, any desired channel could be opened 1 $\mu$sec before the transmission of the electrical burst.

At the start of any capturing process it is necessary to re-initialise the micro-VAX and its associated hardware and software. To fulfil this idea the first pulse of **T1** is prolonged for 2 $\mu$sec , and finally as will be discussed latter, **T1** is added to the received signals

from the transceiver to produce an output signal containing all the necessary information for re-initialisation of the micro-VAX and image formation.

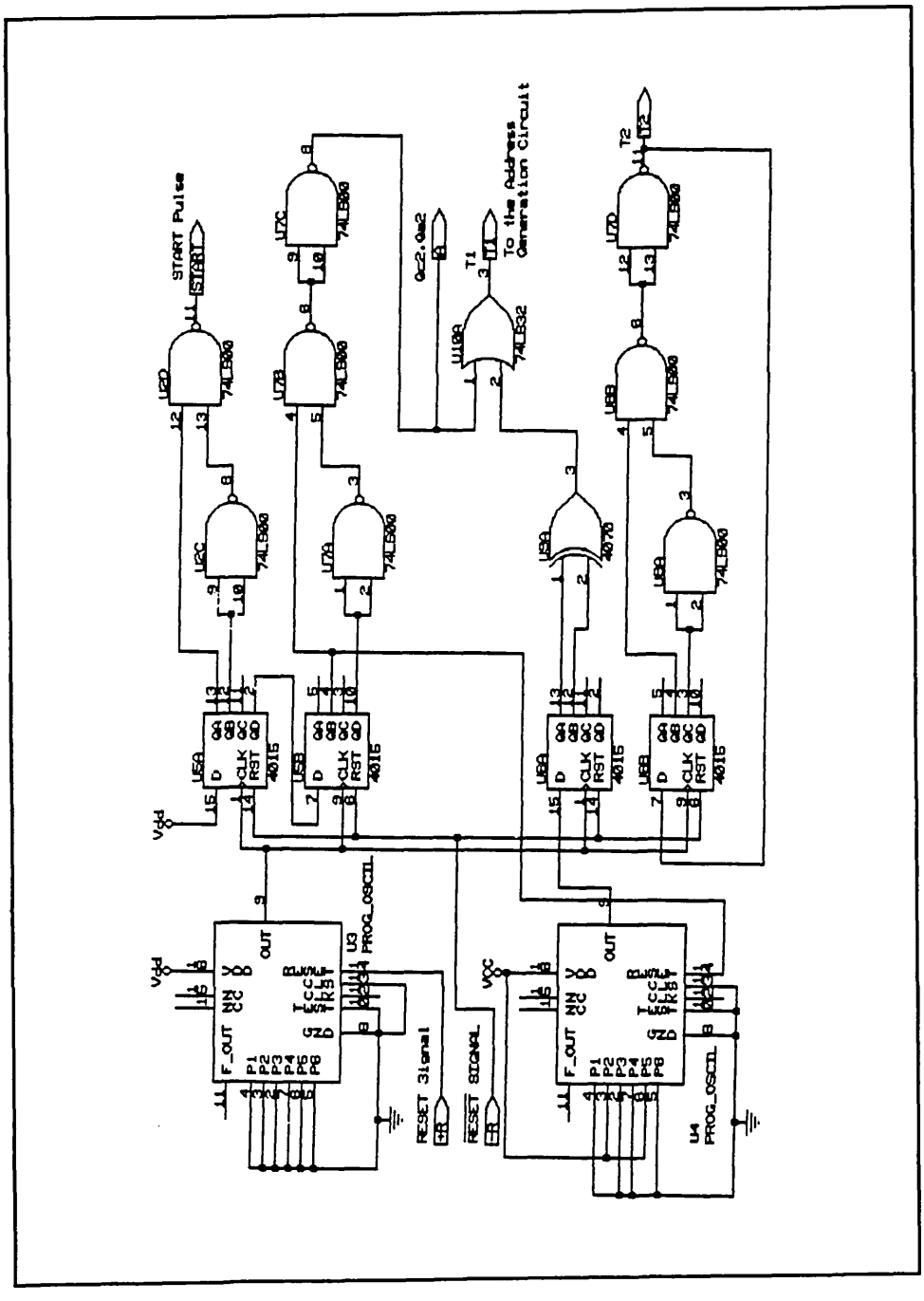


*Fig (4-9) : The schematic diagram of the clock generation circuit.*

Fig (4-9) illustrates the schematic diagram of the logic circuit for generation of **T1** and **T2**. The heart of the timing circuit is a pair of programmable oscillators set at 1 MHz and 5 KHz. By pressing the foot switch the RESET signal goes High and enables the 1 MHz oscillator. Then its output is used as the clock signal for a pair of dual four bit shift registers, in U5 and U6. These shift registers are enabled at the same time by the $\overline{\text{RESET}}$ signal. A combinational logic circuit consisting of ordinary logic gates combines the output of these shift registers to create **T1**, **T2**, and the START pulse as shown in Fig (4-8).

As it can be seen the 1 MHz signal is used as the clock signal for all four shift registers in U5 and U6. Therefore, by the first, second ,third and fourth rising edges of the 1 MHz signal the outputs of the U5A shift register changes. Since the input to this shift register is tied to $V_{DD}$, its output will remain steady for the rest of the capturing process. Therefore the outputs $Q_A$ and $Q_B$ of U5A could be used to create the START pulse which is defined as :

$$START\ Pulse = \overline{Q_{A_{U5A}} \cdot \overline{Q_{B_{U5A}}}} \qquad (4\text{-}2)$$

U5B, the other half of the U5's shift registers is used to create signal **A** which is used later to create T1. The input to the shift register U5B is $Q_D$ the output of U5A. This choice assures us that all outputs of the second shift register are at zero level for 3 $\mu$sec after the beginning of the START pulse to give enough time for preparation of A/D and micro-VAX units. After $Q_D$ is set to High level, the next rising edges of 1 MHz clock have no effect on the outputs of U5B. Therefore $Q_A$, $Q_B$, $Q_C$ and $Q_D$ will go to and remain at High level. The combination of $Q_B$ and $Q_D$ creates the **A** pulse which is defined as;

$$A = \overline{Q_{D_{U5B}}} \cdot Q_{B_{U5B}} \qquad (4\text{-}3)$$

U6B, the second pair of shift registers in U6, is also clocked at 1 MHz. The input to U6A is the 5 KHz clock. Therefore, its four outputs will remain at Low level until the 5 KHz signal goes High. Then each of its outputs will go to and remain High by the next rising edges of the 1 MHz clock.

The logical combination of $Q_A$ and $Q_B$ of U6A makes a train of eleven pulses with 1 $\mu$sec of duration separated with a 100 $\mu$sec time interval. This signal is called as the **B** pulse. The **B** pulse is the result of EXclusive ORing of $Q_A$ and $Q_B$ of U6A expressed as;

$$B = Q_{A_{U6A}} \oplus Q_{B_{U6A}} \qquad (4\text{-}4)$$

Now simply by combining **A** and **B** through an OR gate, the timing pulse T1 is created. Hence;

$$T1 = A + B \qquad (4\text{-}5)$$

As it was mentioned earlier, T1 is used to produce the necessary control and addressing signals for the multiplexing circuit. The first pulse in T1 has a duration of 2 $\mu$sec necessary for the preparation of the micro-VAX.

Finally, by using T1 as the input signal for the U6B shift registers, we can obtain T2 from the logical combination of $Q_B$ and $Q_C$. Equ (4-6) expresses the timing signal T2.

$$T2 = Q_B \cdot \overline{Q_C} \qquad (4\text{-}6)$$

The timing signal T2 was used as the triggering signal for the Transceiver Unit. T1 and T2 were shown in Fig(4-8).

## 4-4-3 : ADDRESS GENERATION CIRCUIT :

For transmission of electrical bursts to the PZT elements of the *Ring Array Transducer* a 16-channel multiplexer was employed. In our multiplexing circuit only twelve of the sixteen channels are required. To generate a 3-bit address bus for selection of any channel in the multiplexing circuit, a 74LS191 binary counter was used. Fig (4-10) shows the schematic diagram of this counter with the associated logic circuit to provide a 3-bit address bus and a 1-bit enabling line for the multiplexing circuit.

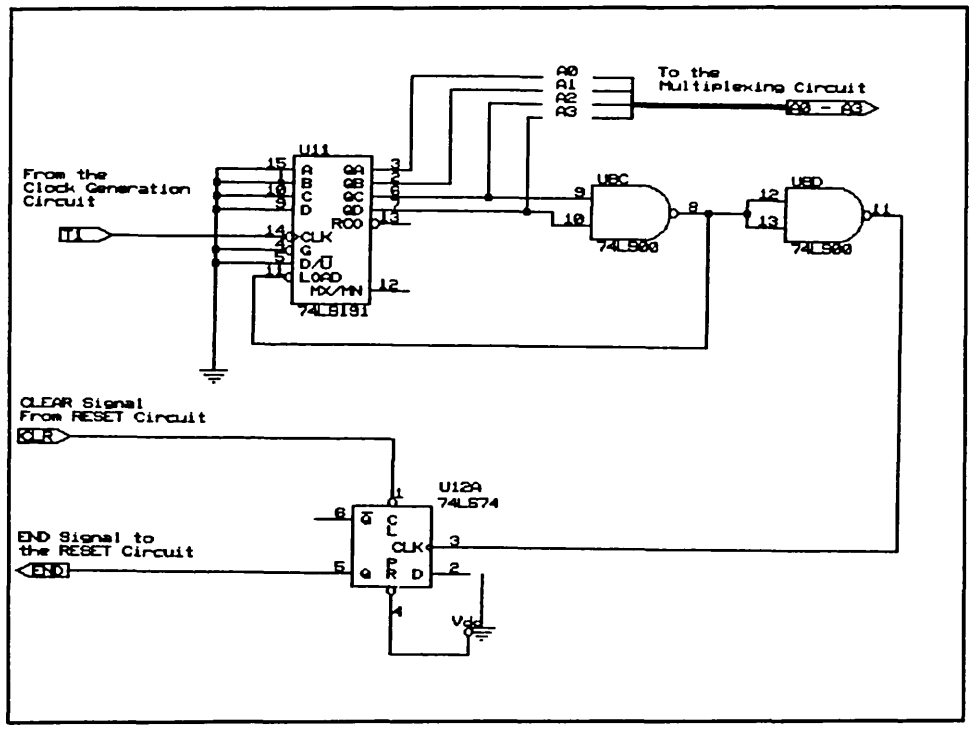


*Fig (4-10) : The schematic diagram of the multiplex-address generator.*

74LS191 is a 4-bit binary counter. In our design it is necessary to stop the counter after the twelfth count and at the same time an END signal should be created to stop the whole process of data capturing. To start the counting from zero, all of the four inputs of

74LS191 (A, B,C and D), were tied to ground. The clock signal is T1 which causes counting to be started 2 $\mu$sec earlier than ultrasonic transmission.

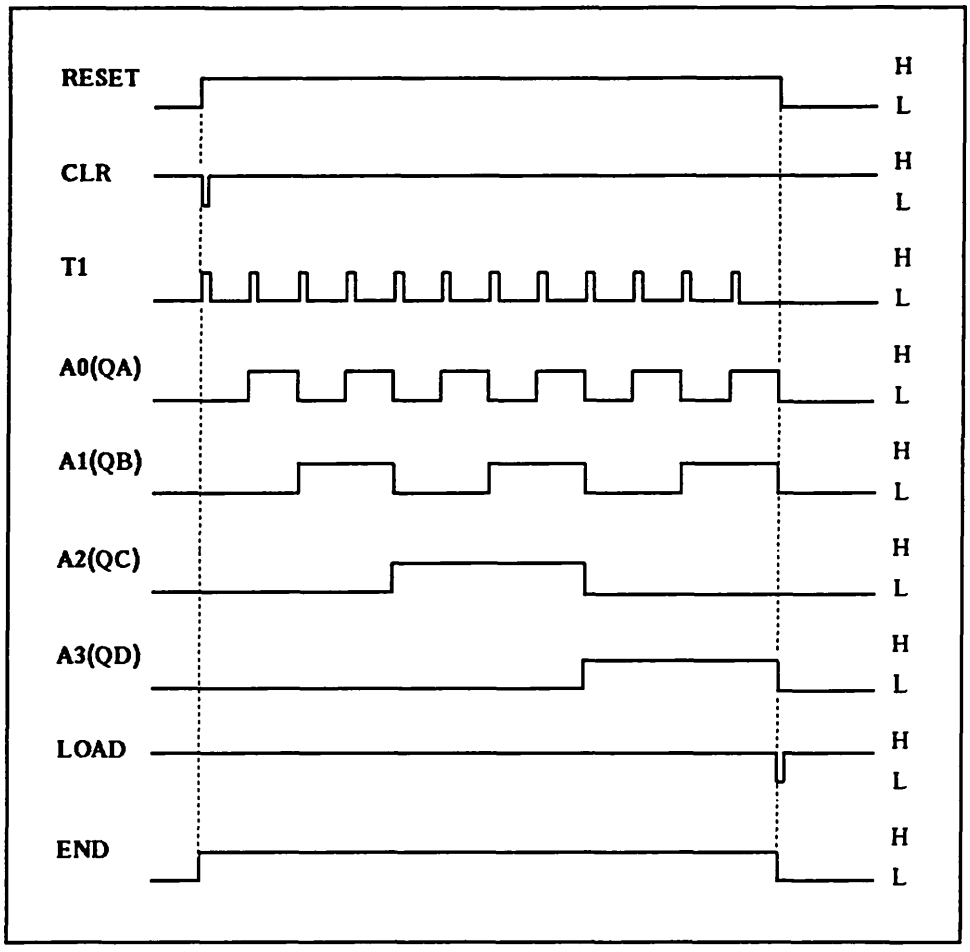


*Fig (4-11) : END and Addressing Signals.*

By the first rising edge of T1 the counter starts counting and after the twelfth count, and at the beginning of the thirteenth count, it will stop. At this moment both $Q_C$ and $Q_D$ are about to change their state to the High level and consequently the output of the NAND gate connected to them goes Low. This signal is the END signal which turns the SET and RESET signals to High and Low levels, respectively, and as a consequence disables all parts of the *Logic Control Unit.*

The timing diagram of the *Address Generation Circuit* is shown in Fig (4-11). $Q_A$, $Q_B$ and $Q_C$ are directly used as the address lines for the multiplex circuit. The END signal is also used as the enabling signal for the multiplex circuit which is discussed later.

## 4-5 : MULTIPLEX CIRCUIT :

As the *Ring Array Transducer* contains twelve piezoelectric elements, it was necessary to design a multiplex circuit for transmission of electrical bursts to all the PZT elements of the *Ring Array Transducer* and the reception of all the back scattered signals to the *Transceiver Circuit.* In the current design a 16 channel analogue multiplexer, HI506 was used. Fig (4-12) illustrates the schematic diagram of the multiplex circuit. As a safety point in medical examinations and to insulate the PZT elements from DC voltage, insulating transformers with a 1:1 ratio were placed between each element of the *Ring Array Transducer* and the associated channel of the multiplex circuit.

It is obvious that for proper performance of the multiplexing circuit it is necessary to address the appropriate channel at the appropriate time. The addressing commands are generated by the *Logic Control Unit* which provides three lines for addressing and one line for enabling of the *Multiplexing Circuit.*

By considering the timing signal T1, and the enabling signal EN it becomes clear that each channel can be open for 100 $\mu$sec which is divided into two timing segments. At the first instance for 1 $\mu$sec the electrical burst triggers the piezoelectric element and the transceiver acts as a transmitter. Then for 99 $\mu$sec the transceiver works as a receiver to listen to the back scattered echoes.

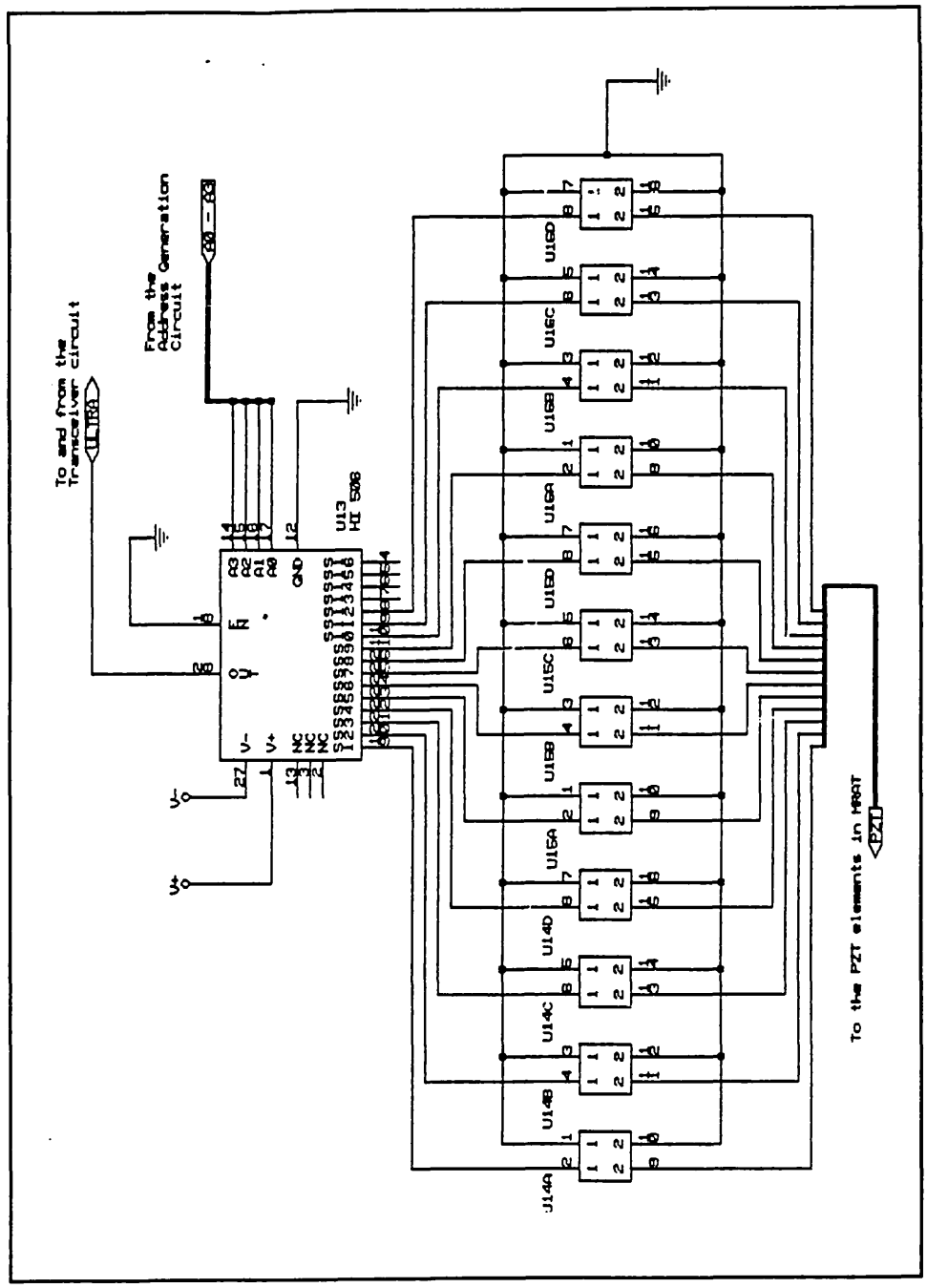


*Fig (4-12) : The schematic diagram of the Multiplexing Circuit.*

## 4-6 : OUTPUT STAGE :

The final stage before A to D conversion consists of three inverting amplifiers all at unity gain. The purpose of this circuit is to produce a readable code for the micro-VAX along with the actual analog signal containing the electrical burst and reflected echoes.

To provide the required frequency capability, [1721] 5539 high speed operational amplifiers with a gain-bandwidth product of 110 MHz were chosen as both inverting and summing amplifiers.

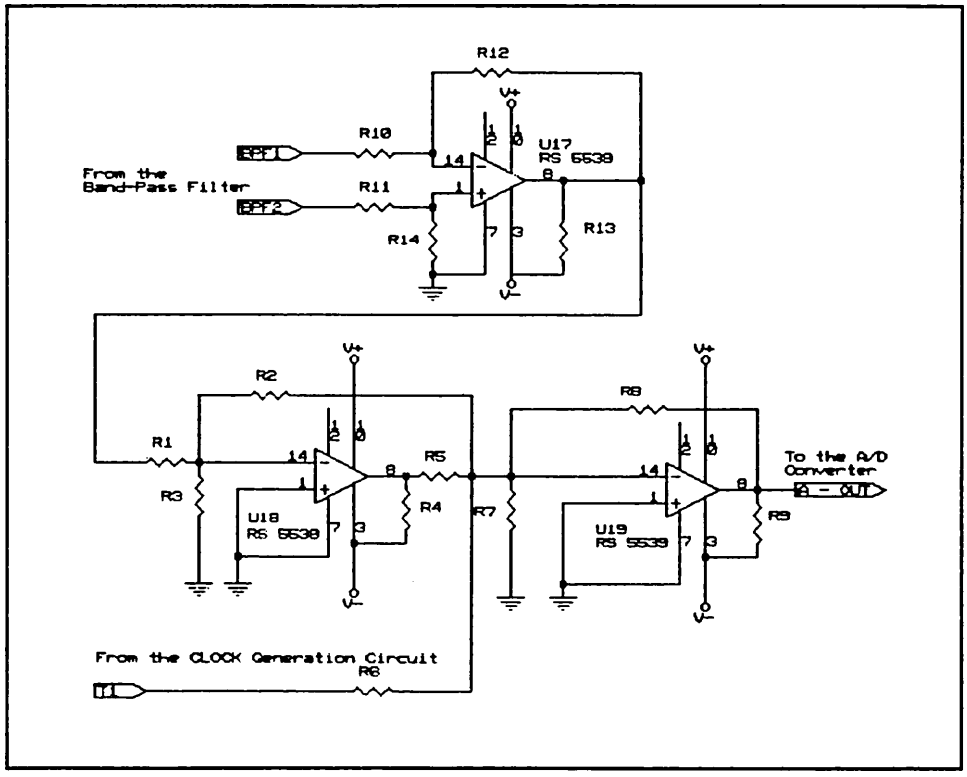


*Fig (4-13) : The schematic diagram of the Summing Circuit.*

As Fig (4-13) shows the first stage containing U17 and U18, works as an inverter for the incoming signals from the transceiver. First the two differential signals are added and

then the output of the U17 is inverted. The second stage, also in inverting mode with unity gain, works as a summing amplifier to add the clock signal T1 and burst-echo signal which is coded by a negative 1 $\mu$sec pulse advancing each burst. These negative pulses after being saved in FIFO memory storage will be read and recognized by the micro-VAX. The micro-VAX will interpret each negative pulse as the start of one individual block of data captured by each element of the *Ring Array Transducer.*

## 4-7 : A TO D CONVERSION CIRCUIT :

For post processing of the ultrasound signals, it is necessary to digitize and save them. To avoid losing information, the sampling frequency of the A to D converter should be at least twice that of the highest frequency component in the signal. Since the ultrasonic [174] elements of the ring array are operating at 6 MHz, it was decided to use TDC1048, an 8-bit A to D converter with sampling rate of 20MS/s. It is clear that in an accurate measurement it is necessary to consider higher harmonics of the nominal frequency which will appear at opproximately 18 MHz, 30 MHz. At the time of this work providing faster memory chips was a limiting factor in increasing the sampling frequency. On the other hand, blood has the property of absorbing signals related to high frequency harmonics. This was a fortunate point which in turn justified not worrying about these higher frequncy signals. The schematic diagram of the A to D converter is shown in Fig (4-14). This unit contains an input buffer amplifie, a voltage refrence, the A to D converter, and an output buffer.

### 4-7-1 : INPUT BUFFER AMPLIFIER :

To provide a suitable input buffering for high frequency signals, an HA2539 [175] high frequency amplifier has been used. This amplifier was optimized for 50 $\Omega$ input resistance. The input voltage level could be 1 $V_{p\text{-}p,}$ and with a gain factor of 2, the A to D converter receives a full-scale input signal from 0-2 V.

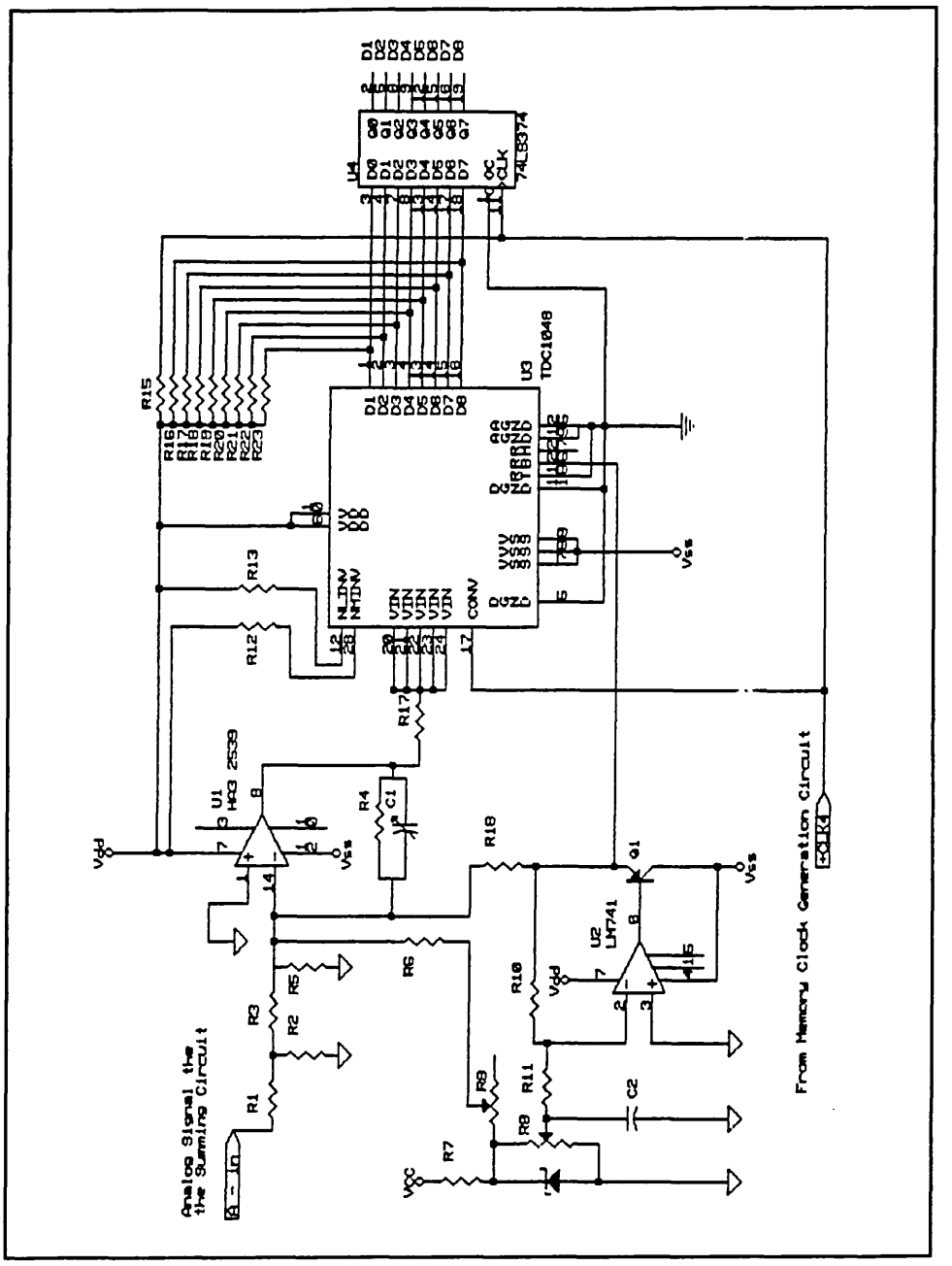


***Fig (4-14) : Complete schematic diagram of the A/D converter.***

The low gain factor of the buffer amplifier provides a higher band-width which is of great importance to us. To optimize the input resistance to 50 Ω at 2 volts of input voltage range, R1 and R2 were selected as 24.9 Ω and 24.3 Ω, respectively.

### 4-7-2 : VOLTAGE REFERENCE :

By means of the potentiometer R9, it is possible to adjust the gain of the 741 operational amplifier and therefore to control the reference voltage of A to D converter as illustrated in Fig(4-14).

LM313 is a precision low voltage reference source which provides a highly reliable constant voltage at 1.220 volts. This constant voltage is fed through the R9 potentiometer to a 741 operational amplifier which employs a PNP transistor in its output to supply the reference current required for the TDC1048 A to D converter. R9 provides a gain adjustment tool to control the reference voltage over a range of 0.0 to -2.4 volts.

### 4-7-3 : TDC 1048 A TO D CONVERTER :

The TDC1048 is an 8-bit fully parallel (flash) analog to digital converter capable of digitizing its analog input signal at a selected rate up to 20 Mega-samples per second. To provide 8 bit of resolution, 255 sampling comparators have been used in parallel in the input stage of the TDC1048. This converter also contains the necessary logic encoding circuits and a latched output register. To start and control the conversion cycles, only a single control signal is necessary. This signal which also determines the conversion rate is a square pulse at a desired sampling frequency and is applied to the CONV pin of the A to D converter. On the rising edge of the CONV signal the analog data is sampled, the comparators are latched and their outputs are encoded. By the next rising edge of the CONV signal the encoded data is transferred to the outputs of the TDC1048,i.e., pins,1,2,3,4,13,14,15 and 16.

To produce the square wave signal of CONV a 40 MHz oscillator was employed and its output was divided by two. This oscillator was located in the *FIFO Memory Unit* which will be discussed later.

### 4-7-4 : A to D OUTPUT BUFFER :

[175]
To improve the output drive and to protect the output of the TDC1048, a 74LS374 octal edge-triggered latch was utilized. This latch provides complete TTL compatible output for interface between the *A to D Converter Unit* and the *FIFO Memory Unit*. The clock pin of 74LS473 is clocked by the CONV signal. Therefore, on the same rising edge of the CONV signal the data would be available at the output pins of TDC1048 and at the same time it would be latched into the 74LS374.

## 4-8 : FIFO MEMORY UNIT :

The FIFO Memory Unit was designed to store 64 Kilo Byte of sampled data captured by the A to D converter. It was necessary to consider that after a complete process of storing each byte of data, the FIFO Memory Storage should be read by the micro-VAX. The different functions of this unit are illustrated in the block diagram of Fig (4-15).

As Fig (4-15) shows the memory unit contains five major parts. *FIFO Address Generation Circuit, FIFO Input Interface, FIFO Storage Memory, FIFO Output Interface* and *Control Unit*. In the following sections different parts of the *FIFO Memory Unit* will be discussed in detail .

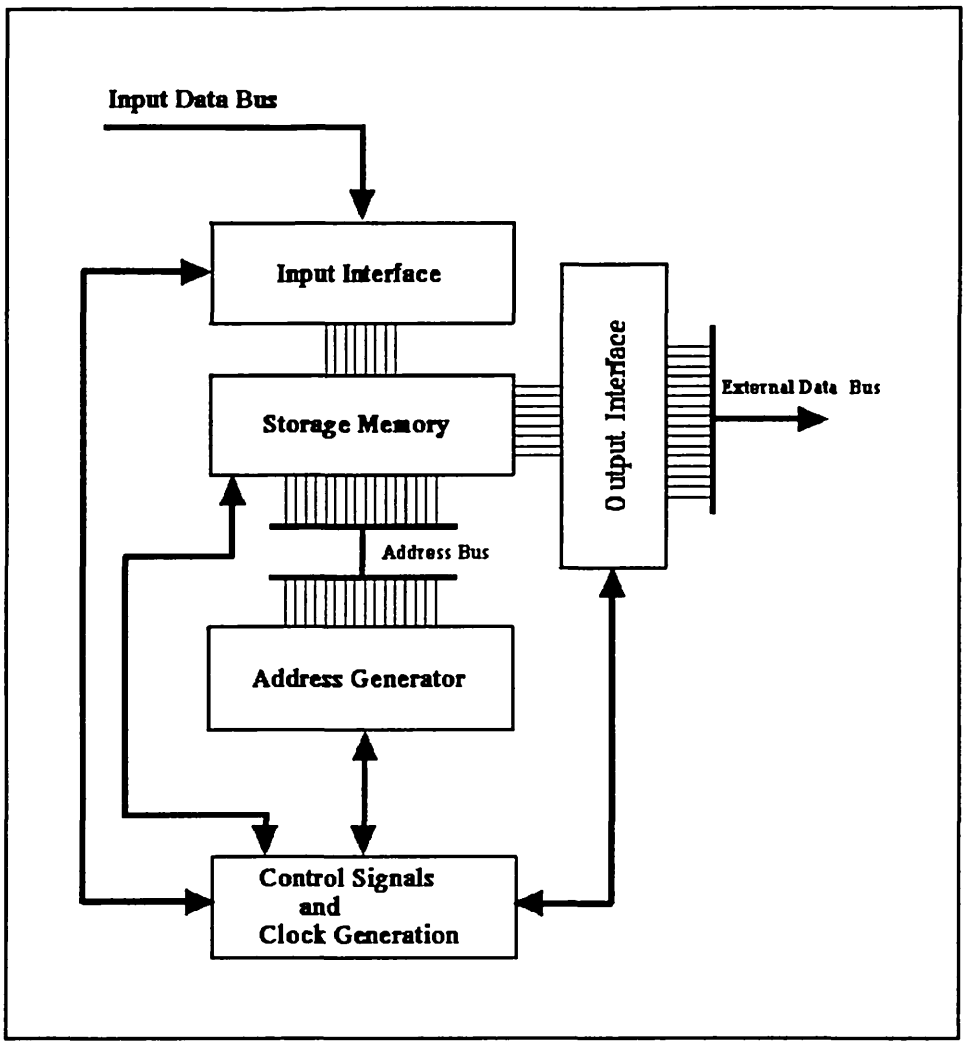


*Fig (4-15) : FIFO Memory Unit Block Diagram.*

## 4-8-1 : CLOCK GENERATION CIRCUIT :

As mentioned in section (4-6) it was decided to select the sampling frequency of the A to D converter at the rate of 20 MS/s, ( 20 MHz ). It is obvious that the *A to D Converter* and *Memory Unit* should be clocked at the same rate of 20 MHz. To generate the clock signal it was decided to use a 40 MHz TTL Oscillator. Then by using a simple

JK flip flop its output was divided by two, giving an even mark/space signal with a frequency of 20 MHz.

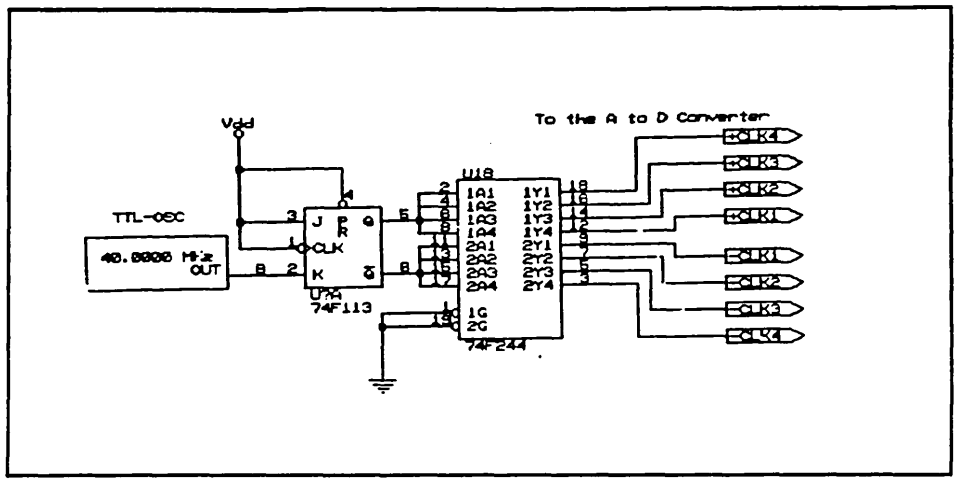


*Fig (4-16) : Clock Generation Circuit for the FIFO Memory Unit.*

Fig (4-16) illustrates the schematic diagram of the *Clock Generator Circuit*. As it is seen, to improve the output drive of the *Clock Generation Circuit* a 74LS244 was employed to buffer the outputs of the JK flip flop. Therefore, four CLK signals were generated for different parts of the FIFO Memory Unit. One of these clock signals is CLK4 which is directed to the CONV pin of the A to D converter as it was mentioned before.

## 4-8-2 : FIFO INTERFACE CIRCUIT :

There are two input data buses connected to the *FIFO Memory Unit*. The first data bus comes from the A to D converter which is used for writing the captured data into the *FIFO Memory Storage*. The second data bus is connected to the *Address Generation Circuit*. This data bus is used to perform the test procedure for the *FIFO Memory Unit*.

In fact it is possible to generate the data from the counters in the *Address Generation Circuit*, load them into the *FIFO Memory Storage*, and finally read them by the micro-VAX to test the performance of the *FIFO Memory Unit*. To perform this test it is enough to use half a word of the address bus as the data bus. Hence, the loaded data should display a saw tooth waveform when it is read by the micro-VAX.

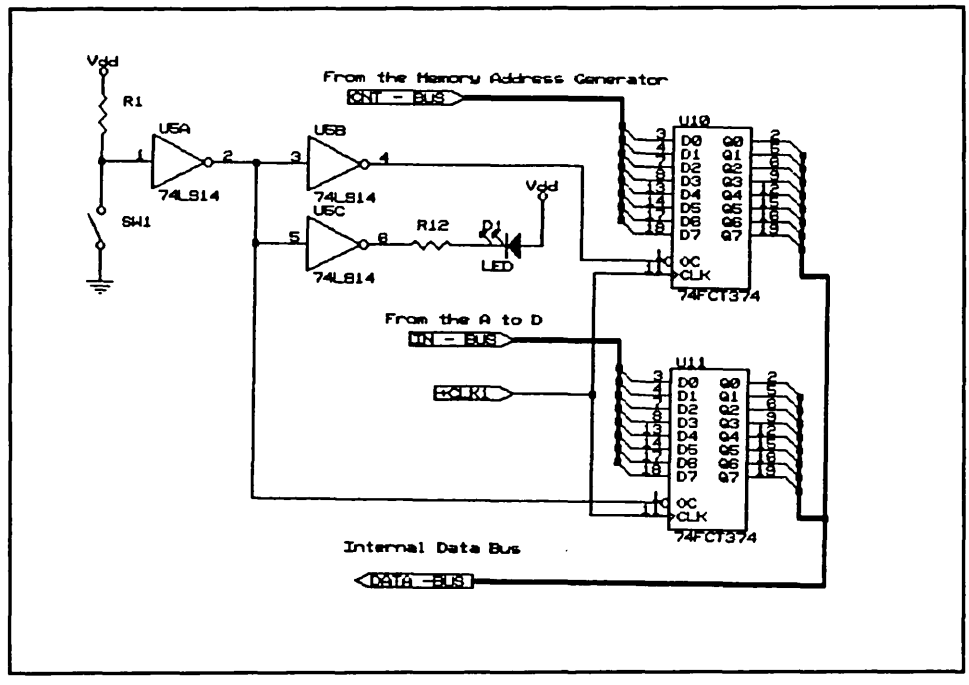


*Fig (4-17) : Input Interface Circuit in FIFO Memory Buffer.*

Fig (4-17) shows the schematic diagram of the input interface. It simply contains two 74FCT374 octal edge-triggered latches, which are both clocked by the CLK1. To select the TEST mode the signal TEST should be turned High which enables the 74FCT374 for the test signal and disables the interface between the *FIFO Memory Storage* and the *A to D converter*. When the signal TEST goes Low the interface between the *A to D*

*Converter* and *FIFO Memory Storage* is enabled and the captured data is written into the *FIFO Storage Memory.*

## 4-8-3 : ADDRESS GENERATION CIRCUIT :

The *FIFO Memory Unit* has a capacity of 64 Kilo-Bytes. Therefore, it is necessary to generate a 16-bit address bus to access all the locations of the *FIFO Storage Memory*. Fig (4-18) shows the schematic diagram of the *Address Generation Circuit.*

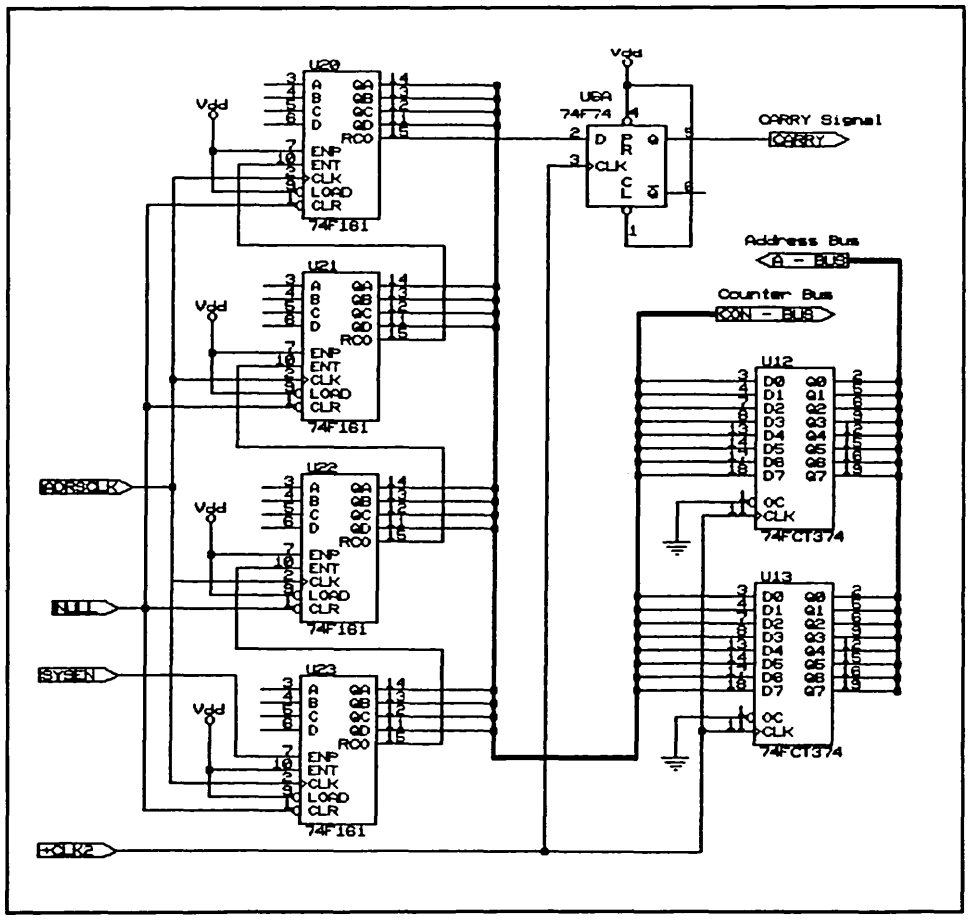


*Fig (4-18) : The schematic diagram of the Address Generation Circuit.*

Four 74F161 binary counters are responsible for the generation of a 16-bit address bus. Each counter is responsible for four bits of the address bus. They count from 0000 to FFFF. Counting should be started at the same time as the A to D converter starts the digitization of data. SYSEN provides the control line for the start of counting. When SYSEN ( SYStem ENable) goes High the first counter starts counting. After completing its counting, a carry bit on pin 15 of the first counter goes High and enables the second counter. Now both the first counter and the second one are enabled. The same procedure continues until all four counters are enabled. The carry signal of the fourth counter is used to null all counters. The NULL signal will be discussed later in the *Control Unit* section. The clocking of counters in the *Address Generation Circuit* is provided by ADRSCLK. This signal has the exact configuration of the 20 MHz CLOCK signal, but it is necessary to consider some other control commands associated with its preparation. The ADRSCLK will be discussed later in the *Control Unit* section.

### 4-8-4 : CONTROL UNIT :

In this section we discuss the external and internal control lines which are required to organize the process of data acquisition and data transfer from the *FIFO Memory Unit* to the micro-VAX. In fact there is no individual control unit for the generation of control signals.

Although, whenever it was necessary, one or more control lines were generated. In the following sections the digital circuits and associated waveforms for the generation of control signals will be discussed in detail.

### 4-8-4-1 : MICRO-VAX CONTROL LINES :

All together 3 input and 2 output control lines provide the communication bus between the micro-VAX and *FIFO Memory Unit.* Fig (4-19) shows the schematic diagram of the circuit associated with the input and output control lines. The first two input control lines are the IBUSY (I/O Busy) and IREADY (I/O Ready) lines which are used to declare the situation of I/O interface between the micro-VAX and *FIFO Memory Unit.* When the micro-VAX has no communication with any external device, it sets the IREADY line in High level. The $\overline{\text{DRST}}$ line is used to signal that the micro-VAX is waiting for a new set of data.

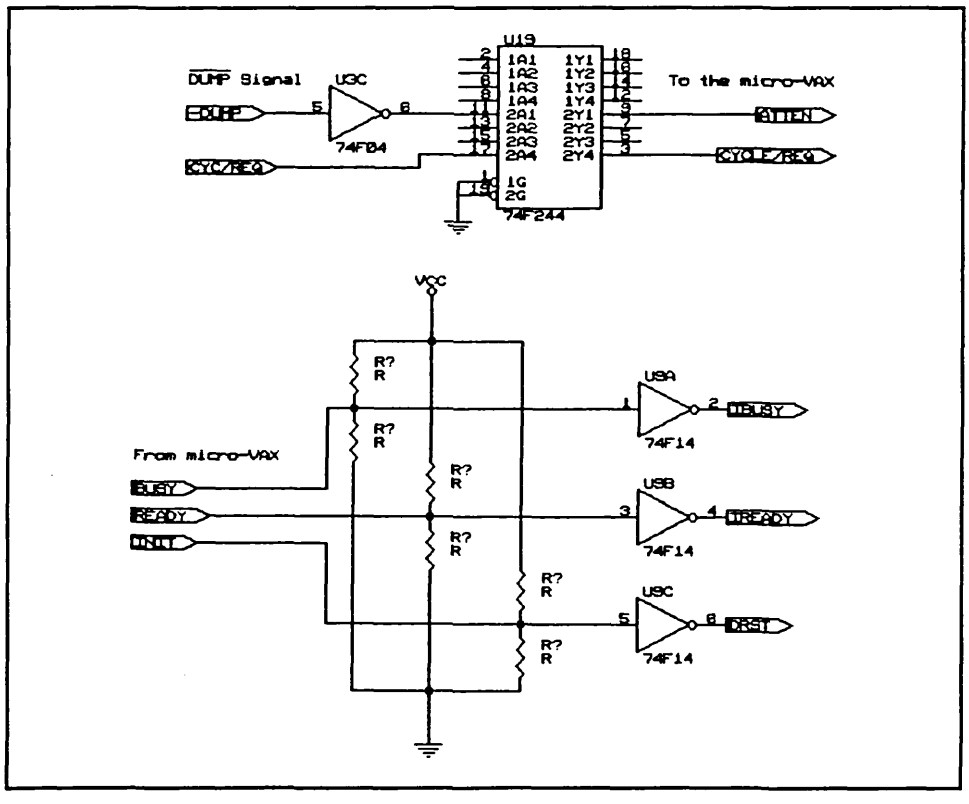


*Fig (4-19) : the input and output control lines to and from the micro-VAX.*

It should be noted that the micro-VAX will not start reading of data until a signal from the *FIFO Memory Unit* declares its readiness. This signal is provided by the CYCLE/REQ output control line. When the micro-VAX receives a High level signal on this line it sets the $\overline{\text{DRST}}$ signal Low and starts reading of data. Another output signal is ATTEN (Attention) which is generated by the $\overline{\text{DUMP}}$ signal of *FIFO Memory Unit*. The ATTEN signal is used to keep the attention of the micro-VAX until the end of data acquisition process.

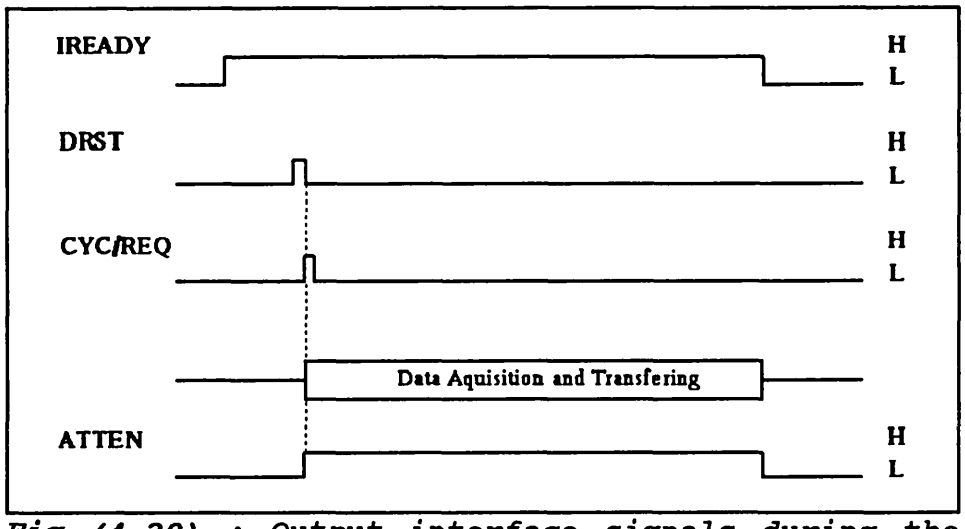


*Fig (4-20) : Output interface signals during the data capturing process.*

Fig (4-20) illustrates the input and the output control signals during data acquisition procedure. To provide an easy way for the generation of CYCLE/REQ (Cycle Request) signal a DRV-11PAL Programable Array Logic (PAL) was employed.

Fig (4-21) illustrates the PAL and its inputs and outputs. Some of the signals input to PAL are generated by the *FIFO Memory Unit* which will be discussed later.

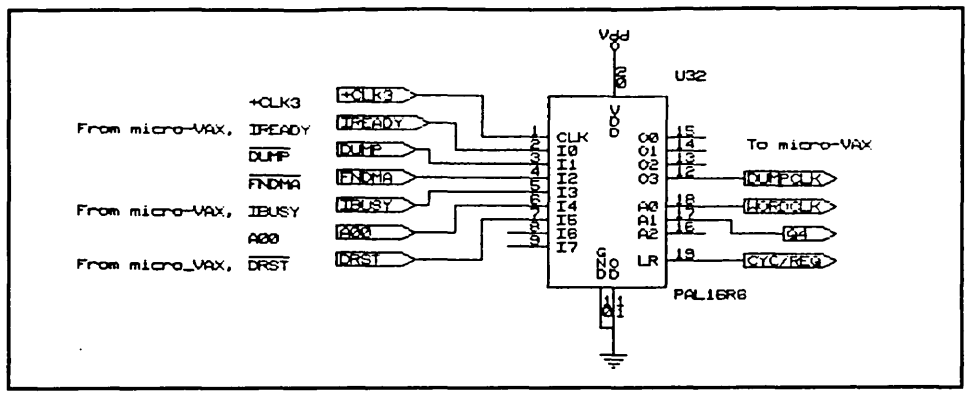


***Fig (4-21) : Programable array logic.***

Also WORDCLK and DUMPCLK signals are internal control lines which are utilized in *FIFO Memory Unit* itself. All of these signals will be examined and discussed in more detail in the following sections.

**4-8-4-2 : SYSTEM ENABLE SIGNAL :**

As mentioned earlier, there are two signals which are sent from the *TTS Logic Control Unit* to the *FIFO Memory Unit*. These signals were introduced already as END and BUTTON (RESET) signals.

As Fig (4-22) shows, after buffering through a GN137 dual Op. Amp., these signals are directed to the *FIFO Control Unit*. Signal $\overline{\text{MPRIME}}$ is used to provide two important signals of SYSEN (System Enable) and $\overline{\text{PRIME}}$ which are employed as internal control lines for the *FIFO Address Generation Circuit* and the *FIFO Storage Memory*.

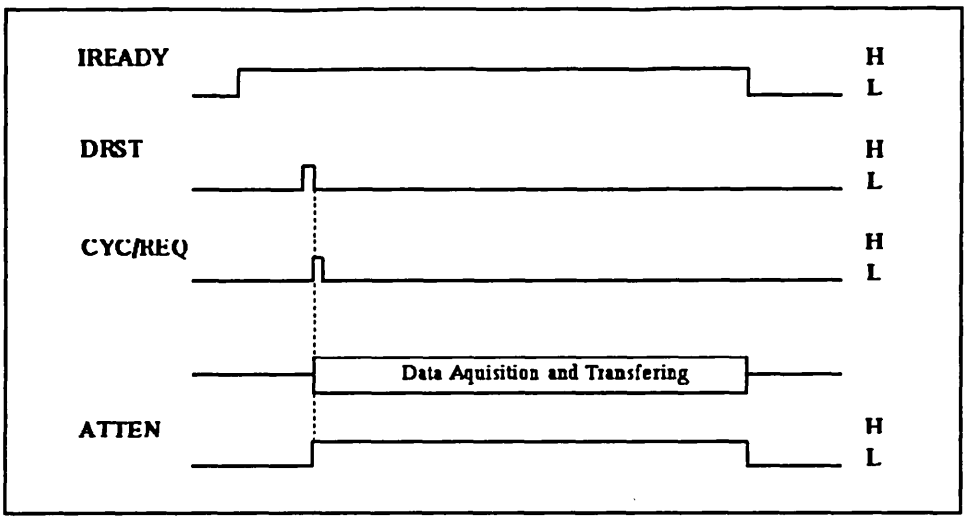


*Fig (4-22) : Control Signals for Output Interface Unit.*

The signal SYSEN is used to enable the first 74F161 counter in the *FIFO Address Generation Circuit*. This signal is generated at the Q output of a D flip flop as shown in Fig (4-23).

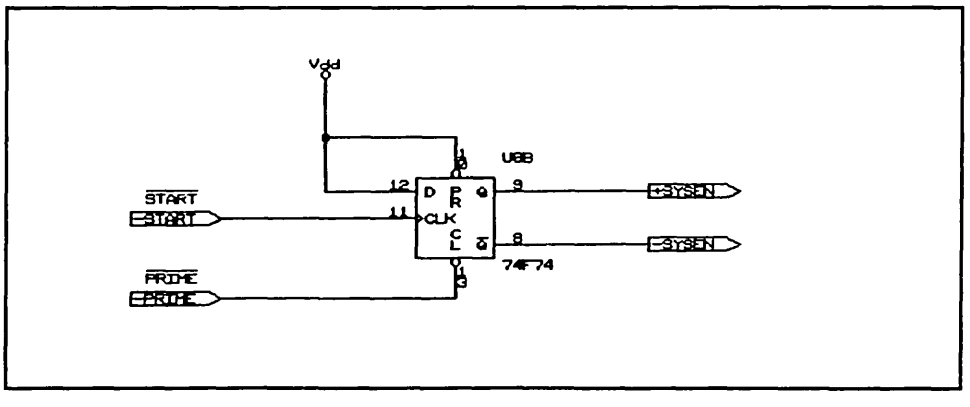


*Fig (4-23) : The schematic diagram of the circuit for generation of SYSEN signal.*

Before the *Address Generation Circuit* starts doing its task it is necessary to fulfil some conditions. First it is necessary to have complete access to the *FIFO Memory Storage*. This implies having no DMA. This is established by the $\overline{\text{FNDMA}}$ signal which declares the ending of Direct Memory Access (DMA). Then a command must come from the user. This command is $\overline{\text{MPRIME}}$ which is in fact the END signal coming from the *TTS Logic Control Unit* having passed through a buffer.

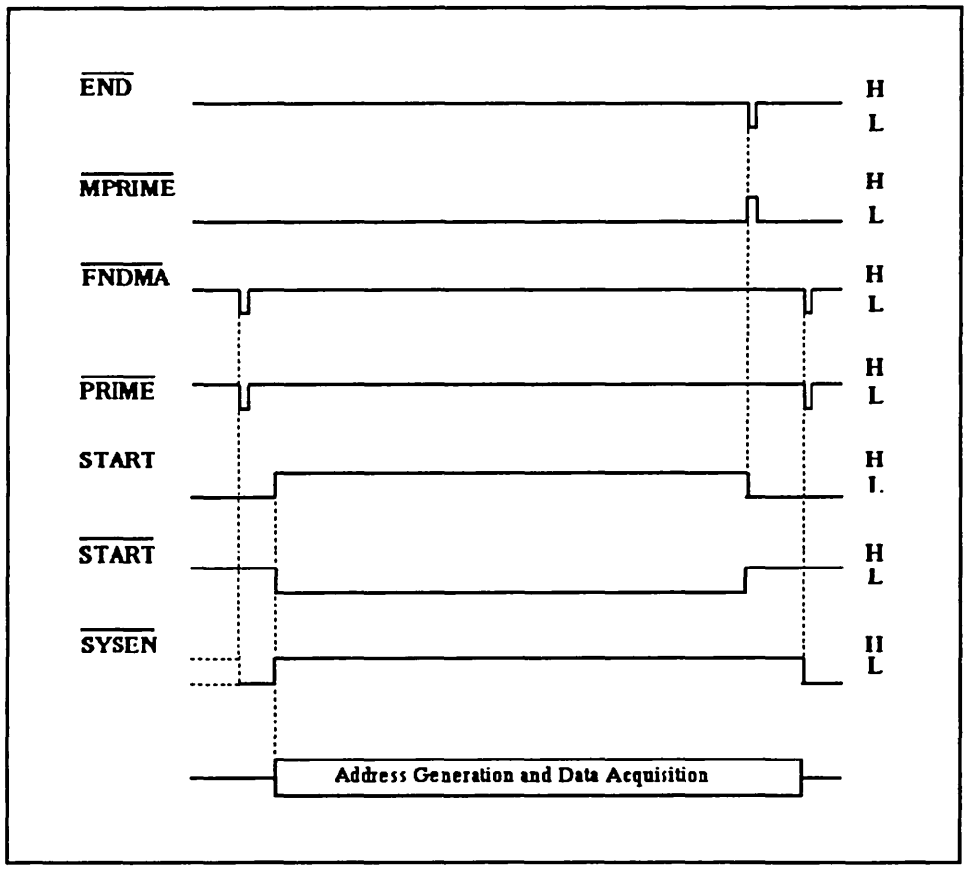


*Fig (4-24) : Generation of SYSEN Signal.*

As Fig(4-24) shows during the process of data capturing by means of one element of the *Ring Transducer Array* this signal is High and at the end of the process goes momentarily

Low. Therefore, when $\overline{MPRIME}$ is Low and $\overline{FNDMA}$ goes Low, the signal $\overline{PRIME}$ will go Low and clear the D flip flop in U6B.

Since PRESET pin of the flip flop has been tied up to the $V_{DD}$, the Q and $\overline{Q}$, or in other words SYSEN and $\overline{SYSEN}$ will be set to Low and High levels respectively. Hence, primarily the 74F161 counter is disabled and when the foot switch is pressed the $\overline{START}$ signal goes High. At this moment the D input of flip-flop will be clocked into the Q output and therefore the first counter is enabled and counting will start.

Fig (4-24) shows the END, START, $\overline{MPRIME}$, $\overline{START}$, $\overline{FNDMA}$, $\overline{PRIME}$, and SYSEN control signals before and during the data capturing process.

### 4-8-4-3 : NULL SIGNAL :

The signal $\overline{NULL}$ is a control signal for resetting the counters in the *FIFO Address Generation Circuit*. It causes data to be written in the *FIFO Memory Storage* from location zero. As Fig (4-25) shows the $\overline{NULL}$ signal can be generated in two ways.

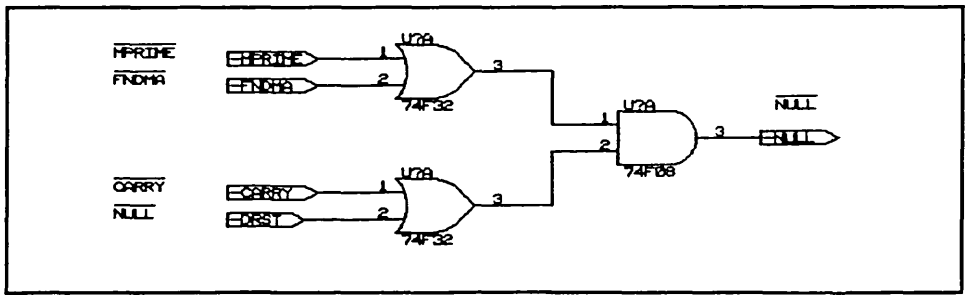


*Fig (4-25) : The NULL signal generator.*

The first way is when the DMA process is finished or the reset Switch SW2 is pressed. It implies that after every completion of data capturing and transferring to the micro-VAX or whenever SW2 is pressed $\overline{\text{FNDMA}}$ goes Low and because $\overline{\text{MPRIME}}$ is also at Low level, $\overline{\text{PRIME}}$ and consequently $\overline{\text{NULL}}$ signals are set to Low level and hence all counters are reset. Fig (4-26) shows the situation of $\overline{\text{MPRIME}}$, $\overline{\text{FNDMA}}$ and $\overline{\text{NULL}}$, when the $\overline{\text{FNDMA}}$ signal is used for NULLing.

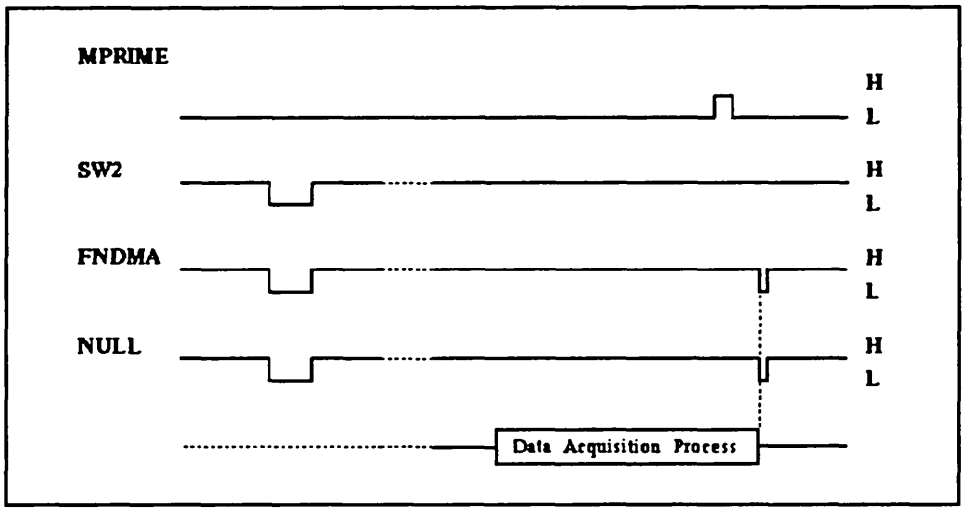


*Fig (4-26) : The NULL signal generation and its situation before and after the data capturing process.*

The other situation in which NULL signal is generated is when the address generation process ends at FFFF. At this moment pin 15 of the fourth 74F161 counter goes High and changes the input level of the D flip-flop in U6A from Low to High.

Therefore, as Fig (4-27) shows, on the next rising edge of CLK2, Q and $\overline{\text{Q}}$ are set at High and Low levels respectively. It means that now the $\overline{\text{CARRY}}$ signal in Fig (4-28) is Low and because $\overline{\text{DRST}}$ is also Low, $\overline{\text{NULL}}$ will be set to Low and again all counters are reset. This action naturally returns pin 15 of the fourth counter and consequently the CARRY and $\overline{\text{CARRY}}$ to their previous levels.

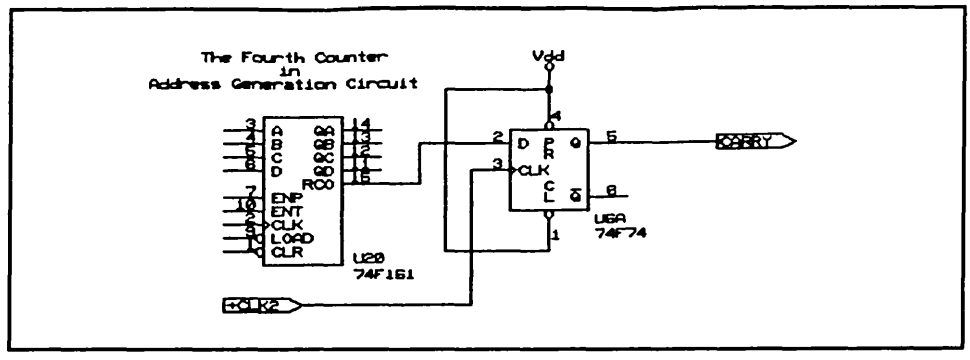


*Fig (4-27) : The CARRY signal generator.*

Fig (4-28) illustrates the wave forms associated with $\overline{\text{CARRY}}$, $\overline{\text{DRST}}$ and $\overline{\text{NULL}}$ signals before and after the NULLing process.

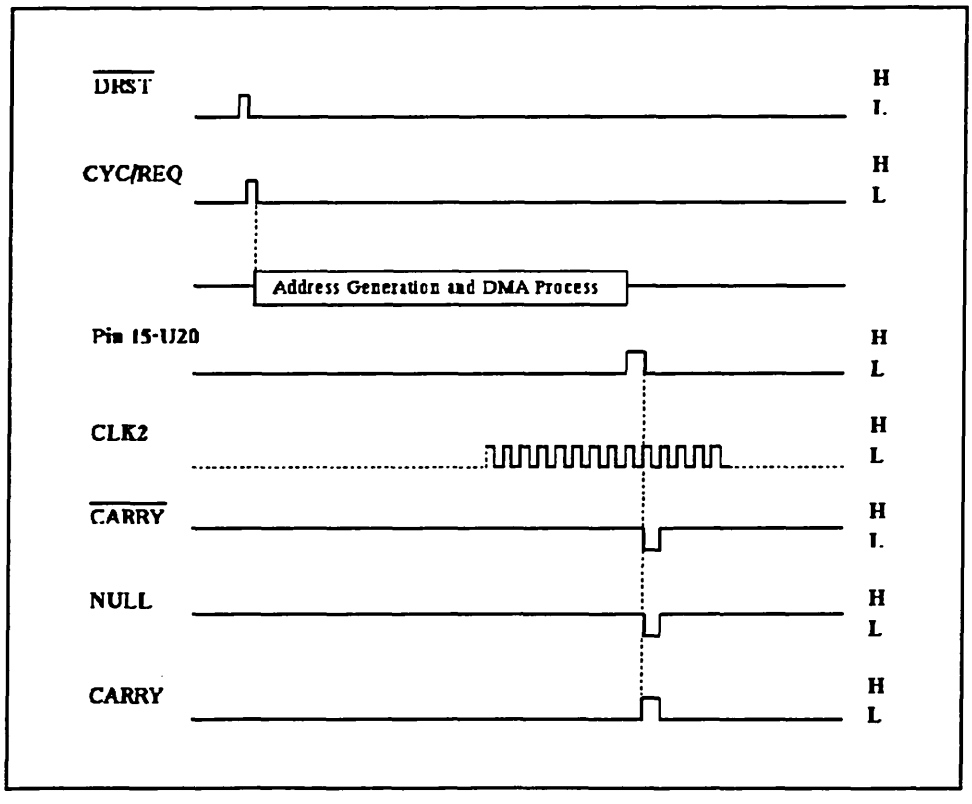


*Fig (4-28) : Generation of NULL Signal at the end of the address generation process.*

### 4-8-4-4 : $\overline{\text{CAPTURE}}$ SIGNAL :

This signal declares the start and continuation of the data capturing process. Fig (4-29) illustrates the schematic diagram of the logic circuit for generation of $\overline{\text{CAPTURE}}$ and $\overline{\text{DUMP}}$ signals. To start the capturing process it is necessary to reset the $\overline{\text{WE}}$ (Write Enable) signal to Low level. This action causes all memory chips to be put into the write mode position.

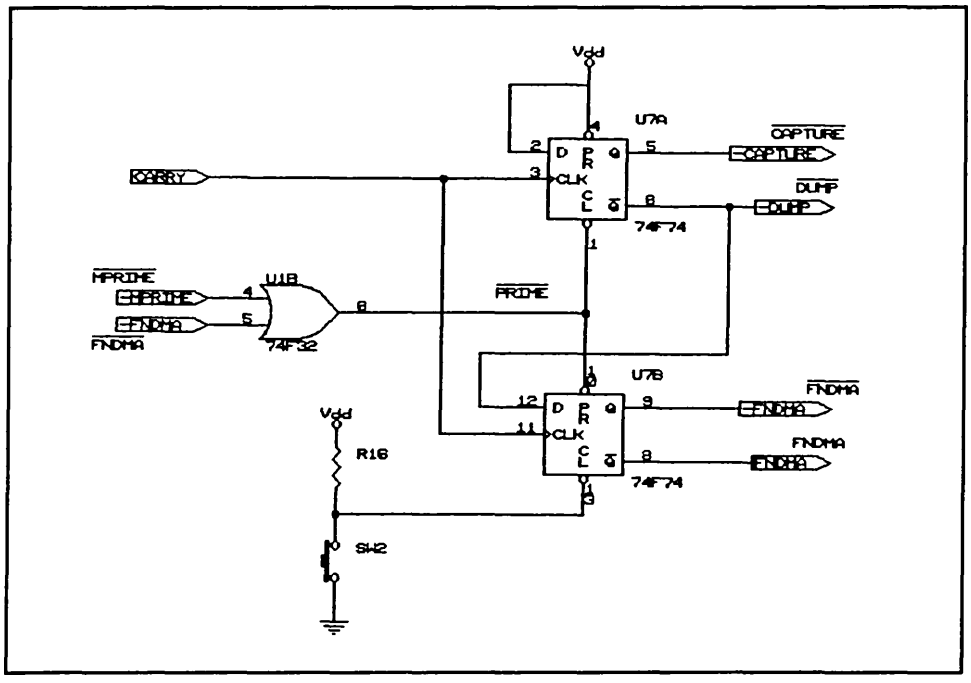


*Fig (4-29) : The schematic diagram of the circuit for generation of CAPTURE and DUMP signals.*

As we will discuss later, the logical combination of $\overline{\text{CAPTURE}}$ and CLK1 provides a Low level for $\overline{\text{WE}}$.

It is necessary to keep the $\overline{\text{CAPTURE}}$ signal at Low during the capture process, and this is done when the signal $\overline{\text{MPRIME}}$ is Low and $\overline{\text{FNDMA}}$ is pulled down for a moment.

In other words, after pressing the foot switch, $\overline{MPRIME}$ is Low and if $\overline{FNDMA}$ is momentarily set Low the $\overline{PRIME}$ signal will go Low and clear the D flip flop U7A. By clearing the flip-flop regardless of its clock and input signals, its Q and $\overline{Q}$ outputs will be set to Low and High levels, respectively. This situation is exactly what we need for bringing the $\overline{CAPTURE}$ signal and as a consequence the $\overline{WE}$ signal to the Low level.

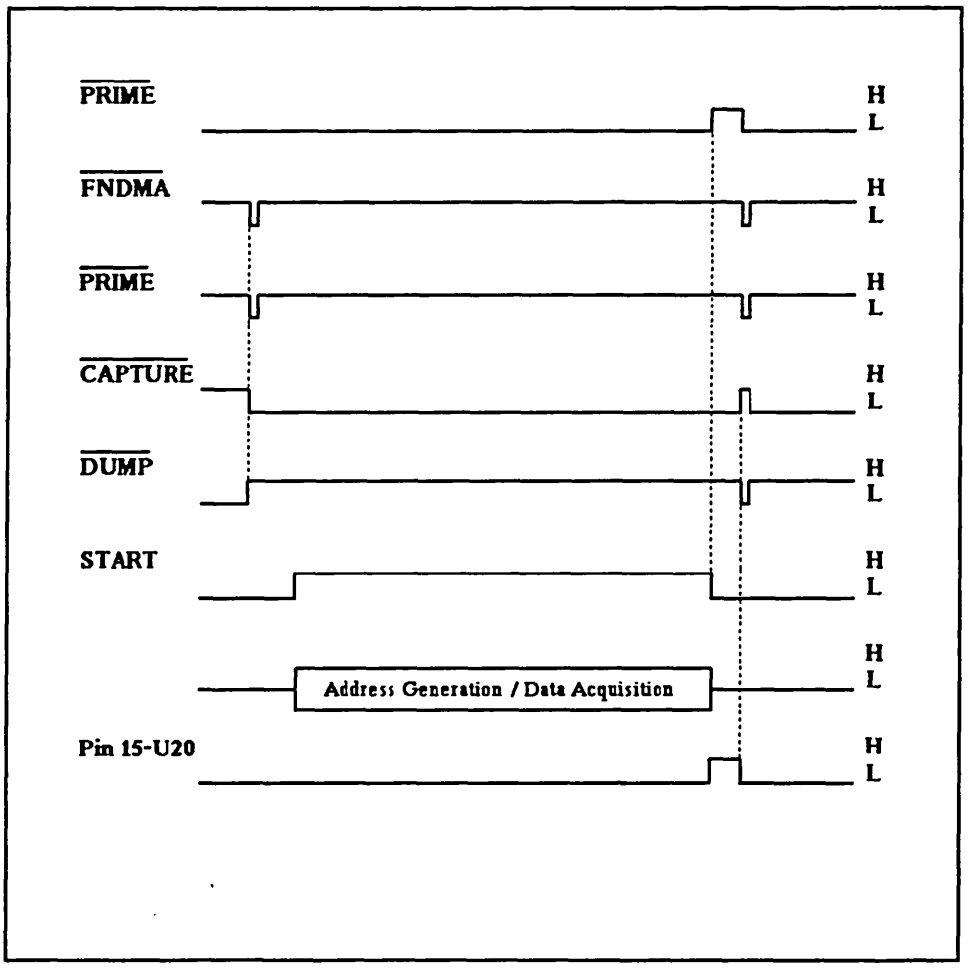


*Fig (4-30) : Generation of CAPTURE and DUMP Signals.*

The process of data capturing will start after the foot switch is pressed and the $\overline{START}$ signal goes High. It will be finished when $\overline{CAPTURE}$ goes High and this will happen

when $\overline{\text{CARRY}}$ goes High and clocks a High input D to Q, that is,when the fourth 74LS161 counter ends its counting and produces a carry flag on pin 15.

The $\overline{\text{DUMP}}$ signal which is the complement of the $\overline{\text{CAPTURE}}$ signal is used to produce the $\overline{\text{FNDMA}}$ and DUMPCLK signals which are discussed in the following sections. Fig (4-30) illustrates the digital waveforms associated with the generation of the $\overline{\text{CAPTURE}}$ signal.

### 4-8-4-5 : $\overline{\text{FNDMA}}$ :

This signal is used to declare the end of DMA (Direct Memory Accessing) process. As Fig (4-31) shows only one D flip flop is necessary for the generation of $\overline{\text{FNDMA}}$, but there are several different situations which should be discussed in more detail.

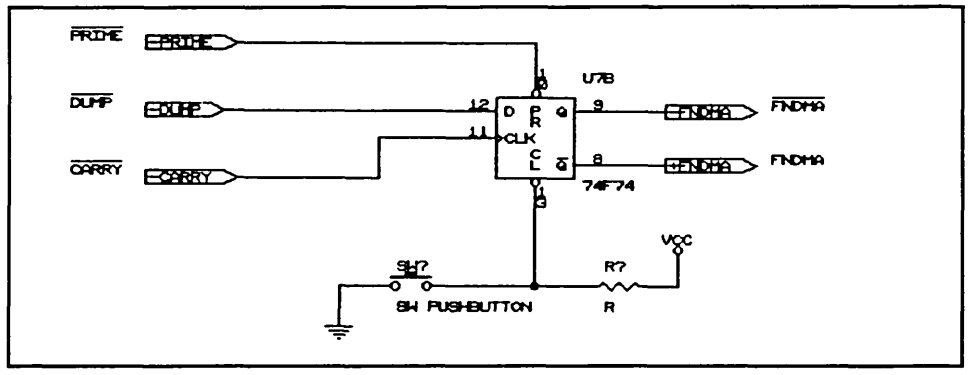


*Fig (4-31) : The schematic diagram of the FNDMA generator.*

The first point to consider is how to stop the DMA at any desired moment. To fulfil this aim it was decided to use a normally open single pole push button to clear the D flip flop.

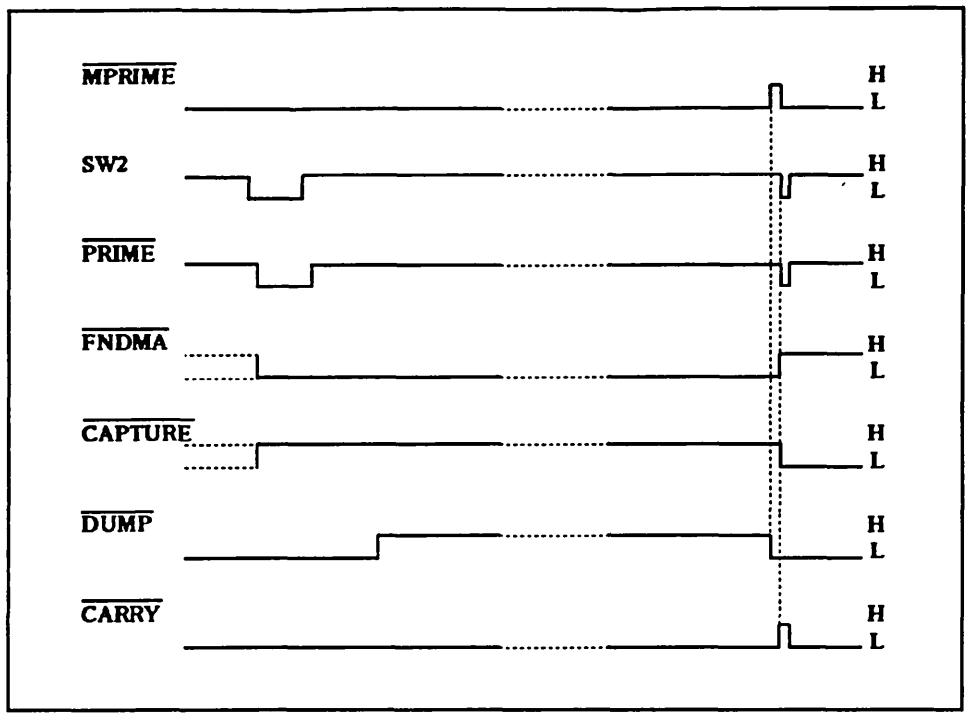


*Fig (4-32) : Generation of FNDMA Signal.*

This action causes Q and $\overline{Q}$ which are the $\overline{FNDMA}$ and FNDMA signals, to be set at Low and High levels respectively. As discussed earlier, it means that the DMA process has finished and the system is permitted for data capturing process.

In Fig (4-32) first the generation of FNDMA and $\overline{FNDMA}$ by pressing the SW2 Switch are shown and then the digital wave forms associated with $\overline{DUMP}$ and $\overline{FNDMA}$ signals and their interactions are illustrated.

### 4-8-4-6 : $\overline{WE}$ SIGNAL

The $\overline{WE}$ signal is the control signal to establish the write mode for the memory chips in FIFO Memory Storage. Fig (4-33) shows the simple logic circuit necessary to provide the $\overline{WE}$ signal. During the data acquisition process, the signal $\overline{CAPTURE}$ is Low and

therefore in every negative half of CLK1, the $\overline{WE}$ goes down and data is written into the memory chips.

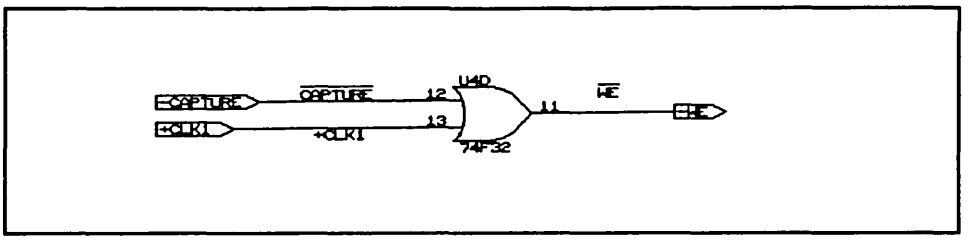


*Fig (4-33) : Generation of WE signal.*

## 4-8-4-7 : ADRSCLK SIGNAL:

As described previously, only in a half cycle of CLK1 data is written into the memory chips. In the other half data can be read and transferred to the micro-VAX. Therefore, it is necessary to examine the required conditions before the address bus is increased. The schematic diagram of the logic circuit for generation of ADRSCLK is shown in Fig (4-34). ADRSCLK is used as the clock signal for all 74F161 counters in the *FIFO Address Generation Unit.*

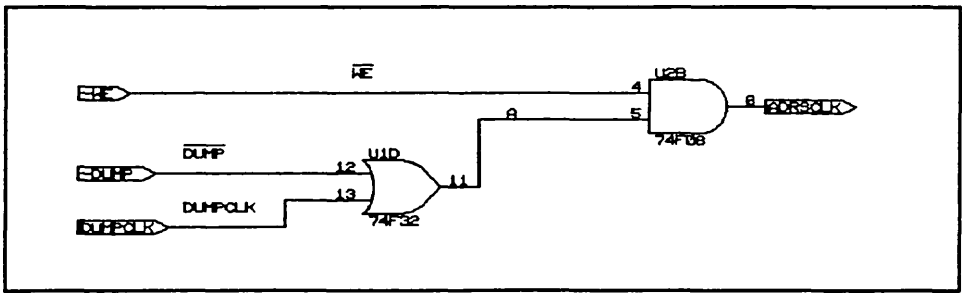


*Fig (4-34) : The ADRSCLK generator.*

As Fig (4-34) and the waveforms illustrated in Fig (4-35) show, it is obvious that during the writing process of data into the memory chips, ADRSCLK is Low and there is no progress in address generation. In the positive half of CLK1, and at the rising edge of $\overline{WE}$ signal the address bus increment is started.

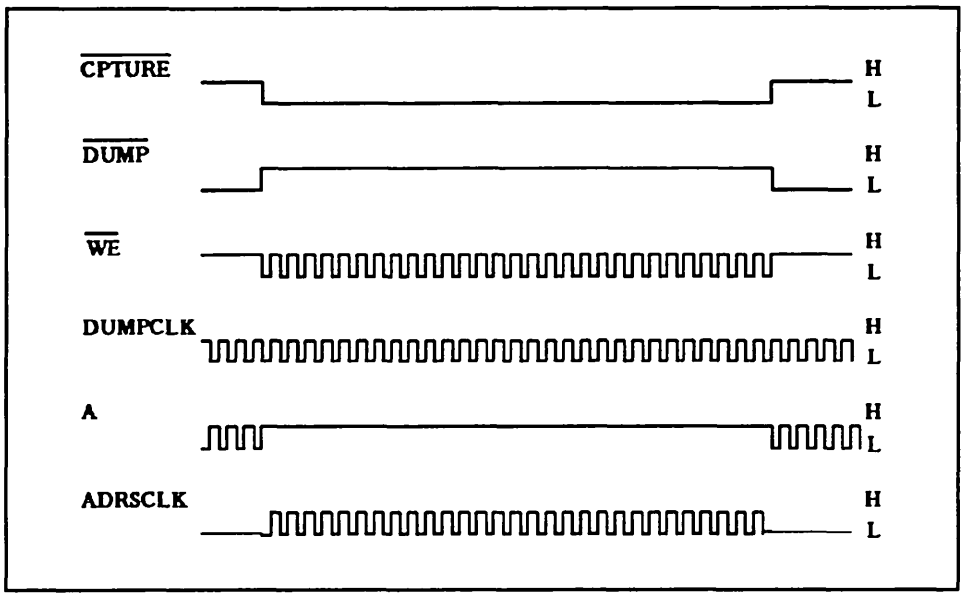


*Fig (4-35) : Generation of ADRSCLK Signal.*

During the data acquisition process, the $\overline{DUMP}$ signal is High and DUMPCLK has no effect on ADRSCLK. But when the data acquisition process stops, $\overline{DUMP}$ goes Low and puts the complement of DUMPCLK at the output of OR gate. This signal is the complement of $\overline{WE}$ and therefore ADRSCLK remains Low and address increment will be stopped.

### 4-8-4-8 : CTRLCLK SIGNAL:

The CTRLCLK signal is employed as the clocking signal for 74LS548 which transfers the 8-bit internal data bus to the 16-bit external data bus. CTRLCLK has a repetition rate

of 20 MHz and is controlled by the WORDCLK and DUMPCLK signals. Fig (4-36) illustrates the logic circuit diagram and associated signals for the *FIFO Output Interface Circuit*. These control lines will be discussed later in more detail in the *FIFO Output CIRCUIT* section.

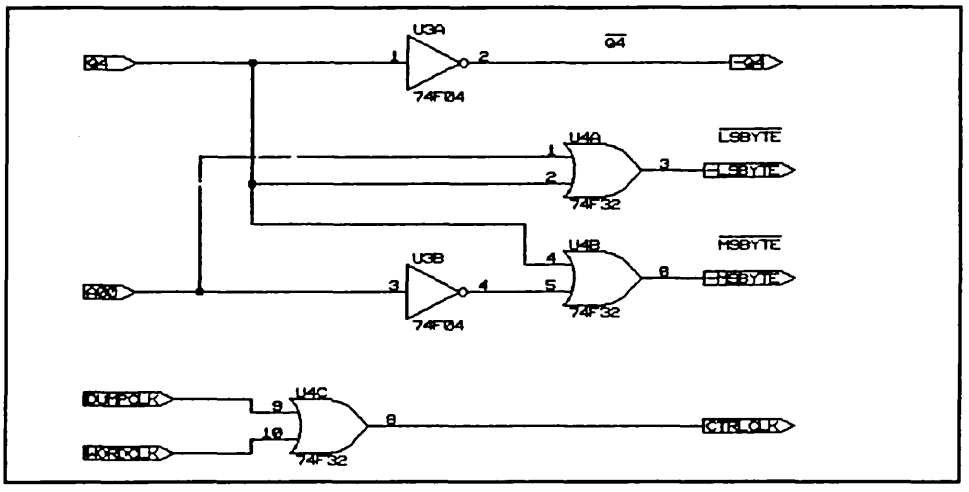


*Fig (4-36) : The schematic diagram of the LSBYTE and MSBYTE generator.*

## 4-8-5 : FIFO MEMORY STORAGE :

*FIFO Memory Storage* consists of eight Am99C641-35[176] static CMOS memory chips. Every chip has been organized as 65536 words with 1 bit per word. Therefore, to provide an 8-bit word memory organization, an array of eight Am99C641's were employed. To cope with the high speed of the A to D converter the memory chips were required to have access time of 35 nsec, which easily makes them capable for being written at the speed of 20 MS/sec.

Fig (4-37) shows the schematic diagram of *FIFO Memory Storage*. Each Am99C641 has separate input and output pins which along with the two control pins $\overline{CE}$ (Chip Enable) and $\overline{WE}$ (Write Enable) provide ease of writing and reading of data as well as expansion in an array organisation arrangement.

The only control signal to activate the memory chips is $\overline{WE}$. As we explained earlier in sections (4-7-4-6) and (4-7-4-7), $\overline{WE}$ signal is exactly the same as CLK1 and provides half a cycle for writing of data in the memory and another half for reading of data from it.

**4-8-6 : FIFO OUTPUT INTERFACE :**

The *FIFO Output Interface* is responsible for the transformation of 8-bit internal data bus to the 16-bit external bus readable by the micro-VAX. It consists of two 74LS548's and two 74LS244's. The 74LS548 [175] is an 8-bit two stage pipeline registers and the 74LS244 is an octal buffer. Each 74LS548 contains a pair of 8-bit high speed registers which can be programmed to perform in a variety of pipeline functions. By means of the control lines CE1 and CE2 a pair of internal multiplexers are governed to produce several useful data paths.

The arrangement of registers within the 74LS548 can be thought of as two 8-bit storage ranks, named Rank 1 and Rank 2. The clock signal is common for both ranks but they have their own enable lines, called as CE1 and CE2.

The presented data at the $D_0$-$D_7$ inputs are stored in Rank 1 on the rising edge of the CLK (clock) signal, provided that CE1 has already been asserted.

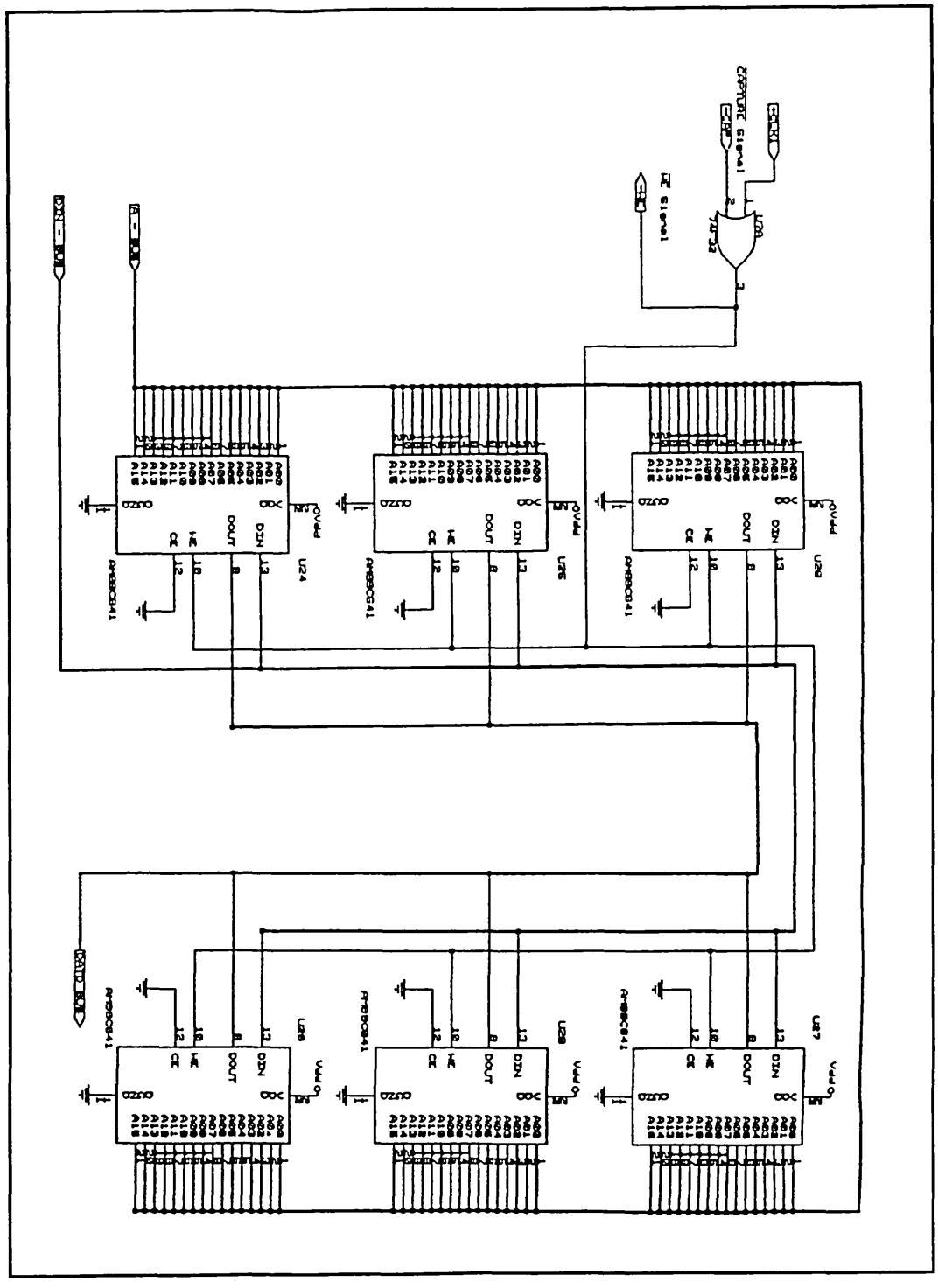

*Fig (4-37) : The schematic diagram of the FIFO Memory Storage.*

Similarly data are stored in Rank 2 on the rising edge of the CLK signal if CE2 already has been set to Low. There are other control lines to present the contents of any of two internal ranks at the output pins.

The OSEL (Output Select) line is used to select either Rank 1 or Rank 2 and to present its contents at the output. When the OSEL is Low, Rank 2, and when it is High , Rank 1 is selected. The $\overline{OE}$ (Output Enable) is another control line which governs on the output pins. When the $\overline{OE}$ is High all output pins are set in the high impedance mode. By pulling $\overline{OE}$ down the contents of one of the internal ranks will be presented at the output pins.

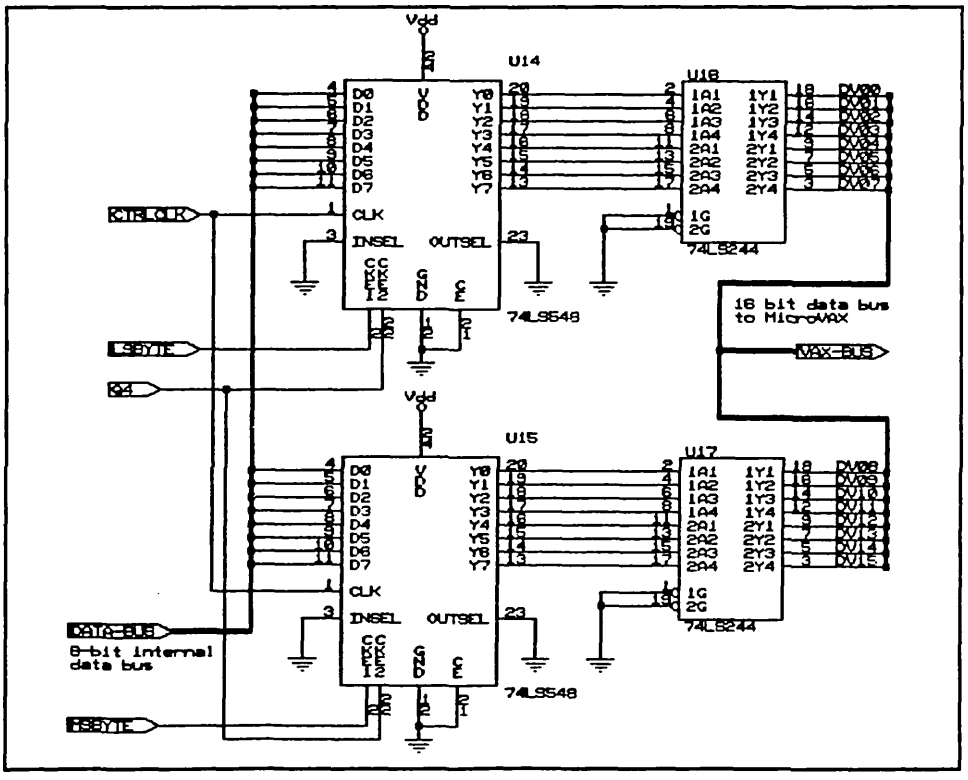


*Fig (4-38) : The schematic diagram of the Output Interface Circuit.*

As it was explained earlier, when $\overline{WE}$ control signal is Low the captured data is written into the memory chips, and on the High level of $\overline{WE}$ the data could be read from the memory chips.

Fig (4-38) illustrates the schematic diagram of the FIFO Output Interface along with its input control lines. The $\overline{OE}$ and OSEL lines are both tied to ground. Therefore, in both of 74LS548 pipeline registers, the contents of Rank 2 are presented at the output pins. Transfer of data from inputs $D_0$-$D_7$ is controlled by the LSBYTE control signal for the lower 74LS548 and the MSBYTE control signal for the higher 74LS548.

Considering the digital waveforms illustrated in Fig (4-39), it becomes clear that the LSBYTE is shifted exactly 180° with respect to the MSBYTE signal. When LSBYTE is Low, at the rising edge of CTRLCLK data is read and stored in the Rank 1 of the lower byte 548, U14. Then LSBYTE goes High and disables the inputs of U14.

At the second rising edge of CTRLCLK two events will happen in parallel. In U15, the data bus is read and its contents are stored in Rank 1 of the higher byte 548,i.e. U15. At the same time the contents of Rank 1 in U14 is transferred to Rank 2 of the same chip, leaving its Rank 1 ready for the next data reading.

At the third rising edge of CTRLCLK once again data are read and stored in Rank 1 of U14 and at the same time the contents of the Rank 1 in U15 is transferred to Rank 2 of the same chip. Hence, after the third rising edge of CTRLCLK, two successive 8_bit data have been stored in the Rank 2's of U14 and U15, the lower and higher byte 548s.

Between the third and the fourth rising edges of the CTRLCLK signal data is transferred

to the micro-VAX and on the Fourth rising edge of CTRLCLK every thing will be repeated.

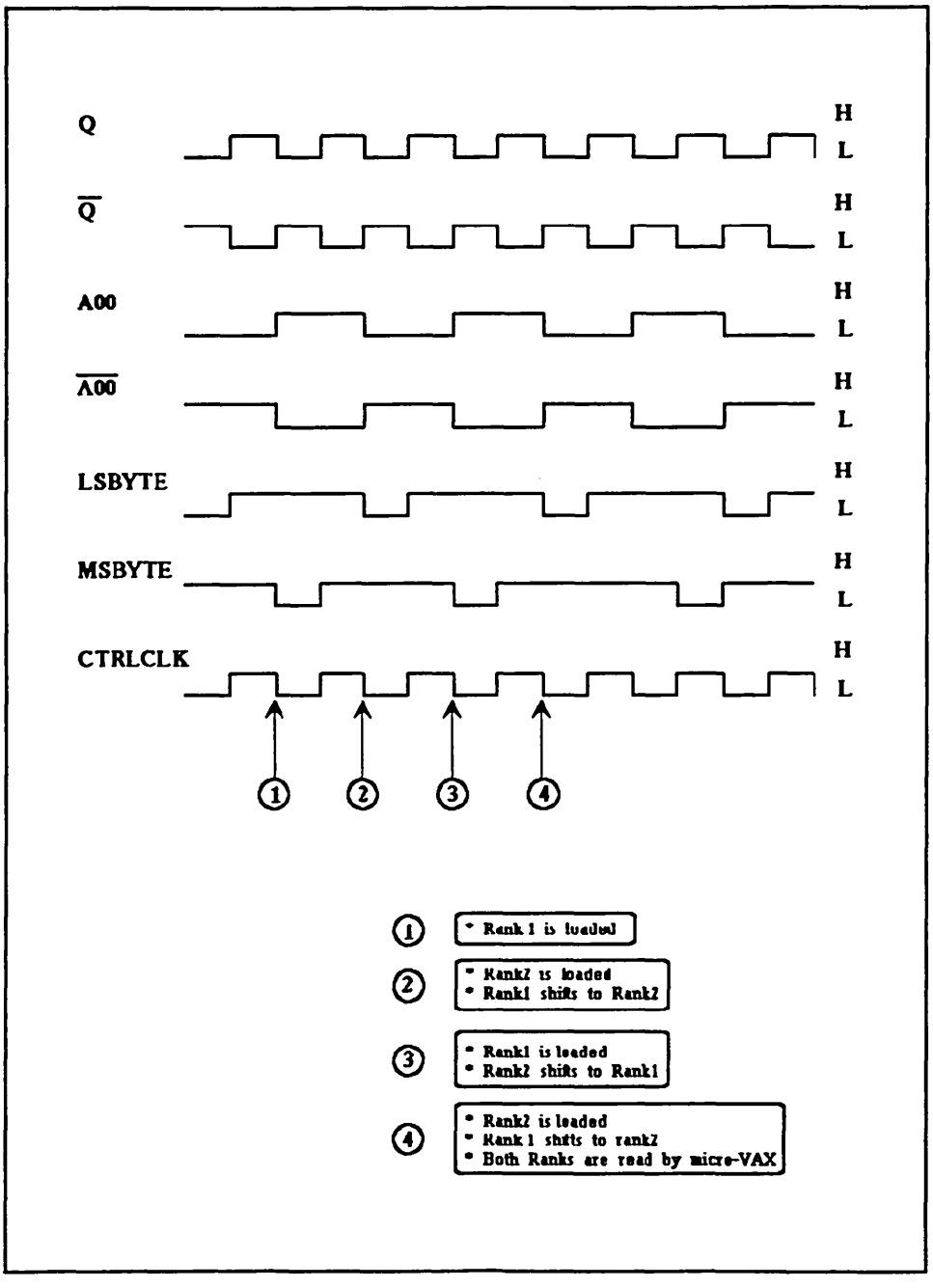


*Fig (4-39) : The timing diagram associated with the Output Interface Circuit.*

## 4-9 : CONCLUSION :

This chapter outlined in detail the different parts of the ultrasound hardware system. These included , ultrasound generation and detection, data acquisition, A to D conversion, data buffering and output interface to the micro-VAX.

We explained the actual analog and digital circuits and performance of each unit was examined. It has been attempted to present the complete schematic circuit diagrams and the associated timing waveforms.

It is perhaps worth mentioning that from the beginning of this project continuous progress has been made in VLSI production and many new fast static memories, multiplexing chips, and pipeline registers have been produced. Therefore, those interested in developing this work should bear in mind that some necessary changes could make cheaper, faster and more portable circuits from the device available today.

At the end of this section the complete technical specification of the entire system designed can be summarised as follows.

Ultrasound transceiver: Operating at 6 MHz this transceiver triggers each pizoelectric element of the transducer for 1 micro second and listens to the incoming echos for 99 micro seconds. The operating system of this transceiver can be adjusted by means of an LC tank connected to pin 3 of the LM1812 chip.

TTS logic control unit: This unit is responsible for gererating all the necessary signals for triggering, reseting and stopping the process of data capturing by means of the transceiver circuit. This unit generates a 3 bit address bus for the multiplexing circuit.

Multiplexing circuit: Using HI506 a 16 channel analogue multiplexer we are capable of directing the ultrasound signal to all channels. In this work the first 12 channels of the HI506 were used and every channel was isolated from the PZT elements by an insulating transformer with a 1:1 ratio.

A to D conversion circuit: This circuit is capable of sampling at the rate of 20 MS/s using TDC1048. It was decided to provide an input buffering stage for high frequency signals by

means of an HA2539 which has been optimised for 50 Ohms input resistance. To improve the output drive and to protect the output of the TDC1048, a 74LS374 octal edge-triggered latch was utilized. This latch provides complete TTL compatible output for loading devices.

FIFO memory unit: This unit consists of 8 Am99C641-35 static CMOS memory chips. Every chip has been organised as 65536 words with 1 bit per word. Therefore, the total available memory is 64 KBYTES arranged as 8 bit words. The access time of this memory buffer is 35 nano seconds which is capable of responding to the A/D convertor at the rate of 20 MS/s.

FIFO output interface: This circuit is responsible for the transformation of the 8 bit internal data bus to the 16 bit external bus readable by the micro-VAX. It consists of two 74LS548's 8 bit two stage pipe line registers. Each of these chips contains two separate 8 bit storage named Rank1 and Rank2 which can be selected for proper transfer of data.
The complete block diagram of the system is shown in Fig (4-40).

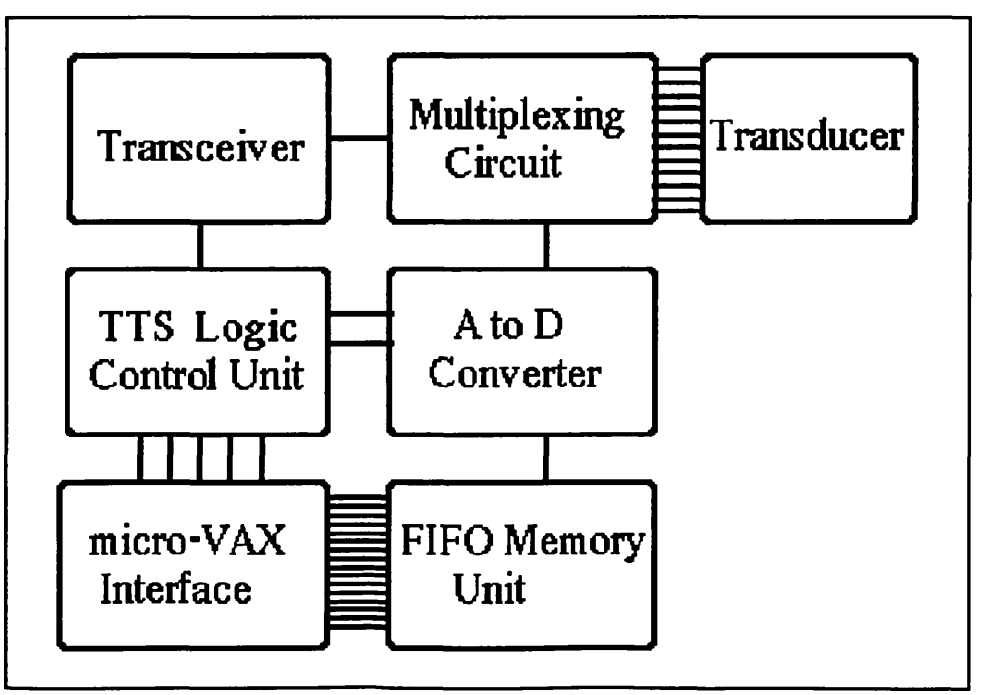


*Fig (4-40) : The block diagram of the ultrasonic system.*

*Chapter Five*

# *3D Visualisation of Vascular Structures*

## 5-1 : INTRODUCTION :

In the last two chapters we first presented the full discussion on the electronic circuity associated with our intravascular system. Then the especially designed MRAT necessary as an original sensor of that system was discussed.

To illustrate the capability of the electronic instrumentation in conjunction with the *Miniature Ring Array Transducer (MART)* different experiments with Phantom and real tissue were performed. This chapter presents the results obtained in some of the experiments done with our intravascular system.

First a short discussion is presented to explain the performance of the software part of this system. In this section it is shown how a block of data is read by the micro-VAX and translated to a slice of the object under examination. It will be explained, how the

created slices are put together for reconstruction of a 3D image of the object. After clarification of the software's performance, the results associated with different types of phantom are presented. Then the 3D reconstruction of arterial fragments is examined and the associated results are presented.

## 5-2 : BASIC APPROACHES TO 3D MODELLING :

Most computer-based 3D reconstruction systems create either wire-frame or solid models using computer-selected shapes (primitives) for graphical representation Kitney et al (1987)[82]. These systems are relatively easy to implement, but for medical applications tend to be unrealistic and, unless a very large amount of processing time is used, lack adequate detail.

Two other methods of modelling have been developed. In one, boundary representation, the object volume is defined by the surfaces which delimit it, as a series of polygonal facets. This method is most suitable when the structures to be modelled are smooth i.e. when not too many facets are required to represent the volume adequately.

For complex, irregular structures, we prefer a method based on volumes, as opposed to surfaces, in which 3D models are reconstructed using volume-elements (voxels), Kitney et al(1988)[81]. In these models, the entire volume, including any hidden surfaces, is represented. As a consequence, the model will remain physically consistent after any manipulation.

The voxel can be seen as an extension to 3D space of the digital picture-element, or pixel. The 3D depth of the object is reconstructed from a series of 2D pixel planes by

placing them one behind the other. Any plane of the voxel space can be seen as a digital 2D image.

## 5-3 : 3D IMAGE RECONSTRUCTION :

As it was explained in chapter 4, this intravascular system works on the basis of A-mode ultrasound instrumentation. In other words, the most important information acquired is the amplitude of the echo signal and time of flight.

To create a 3D image first it is necessary to produce consecutive slices which are then exploited in the construction of a volume of an object.

In this work in order to create every individual slice needed in a 3D reconstructed image of the phantom or a piece of arterial vessel, the *Miniature Ring Array Transducer (MRAT)* is employed as the original component for data capturing.

As explained in chapter 3, the *MRAT* contains 12 crystals placed on a cylindrical body of the transducer in equal angular spaces from each other. Fig (5-1) shows twelve assumptive points in the pathway of ultrasound waves around the *Miniature Ring Array Transducer*. When the instrumentation system triggers an individual element of the *MRAT*, an echo signal is receieved by the same element. This echo can determine the distance between the element's face and the interface of two media which produces that echo. In our study this interface is the inner surface of a phantom wall or the inner surface of intima layer in an arterial vessel. This distance can be estimated as :

$$R = \frac{v \cdot T}{2} \qquad (5\text{-}1)$$

where $v$ is the speed of the ultrasound waves in blood (approximately 1500 m/sec) and **T** is the necessary time for the ultrasound wave to travel from the transducer to interface and return to the transducer. Therefore, by calculation of the radius, point **A1** can be determined which is located in distance **R** from an assumptive origin, **O**.

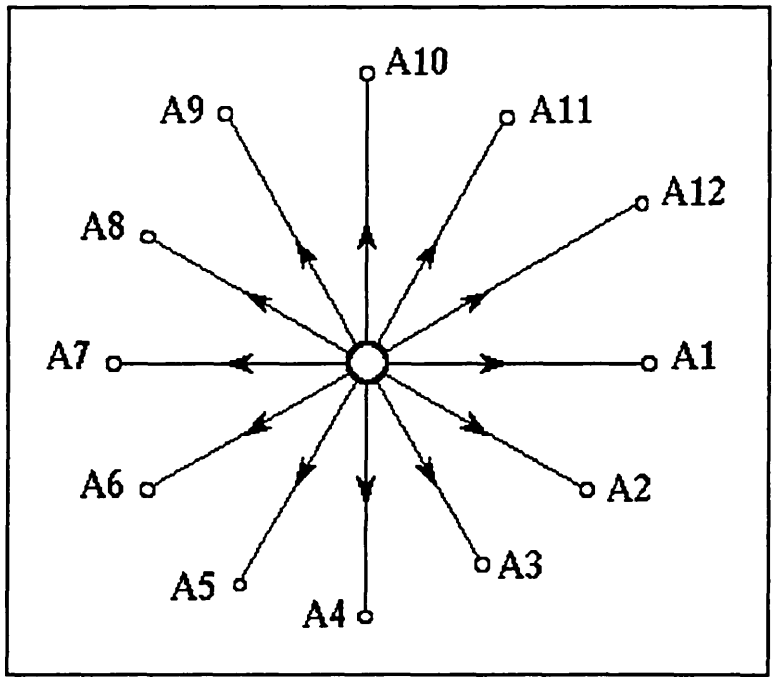


*Fig (5-1) : The Miniature Ring Array Transducer surrounded by twelve points in the pathway of the ultrasound beams.*

In the same manner it is possible to calculate the other points lying on the perimeter of the phantom or vessel sectional cavity surrounding the *MRAT*. Next it is necessary to connect these points to each other to create a closed connected curve coinciding to the original sectional view of the object.

In the simplest method it is possible to connect these points by straight lines. The result is a dodecagon similar to the one illustrated in Fig (5-2-a).

To create a smooth closed connected curve, it is possible to calculate the radius of the pie which is approximately coincided with origin **O**, and any two neighbouring points, such as $A_1$ and $A_2$. Fig (5-2-b) illustrates the same slice shown in Fig (5-2-a) after the smoothing process.

It is possible to create an even smoother closed connected curve, but it is necessary to consider the joining of the two curves for the separate segments. This requires further mathematical analysis. After applying such an algorithm, the curve obtained for the same points of Fig (5-2) is the completely smoothed curve shown in Fig (5-3).

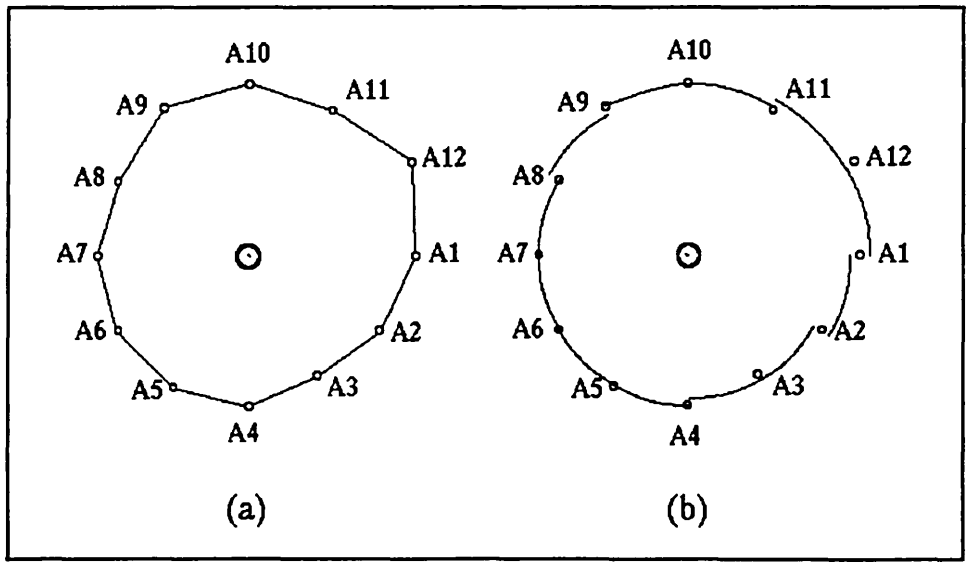


*Fig (5-2) : The same points as in Fig (5-1) with unsmoothed and semi smoothed closed connected curves.*

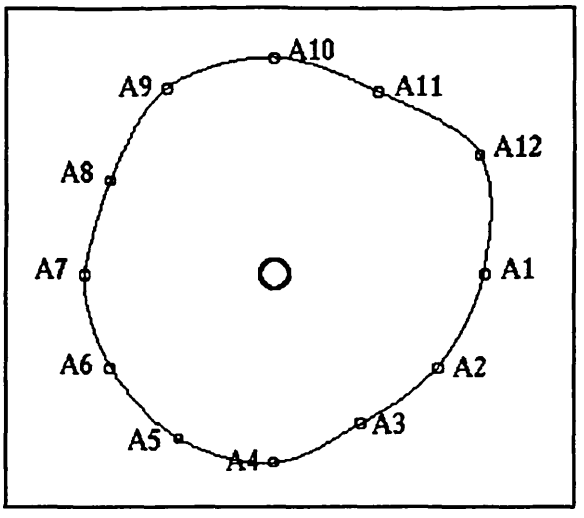


*Fig (5-3) : Completely closed connected curve for the same points as in Fig (5-1).*

To create a 3D image the created slices are placed on top of each other. Of course there are precise technical and mathematical aspects which are necessary to consider in the generation of the 3D images. Readers interested in 3D graphics and image reconstruction can refer to Foley (1984)[3Y], and those interested in 3D Image Generation package associated with this work are referred to Moura (1989)[3Z].

## 5-4 : PHANTOM RESULTS :

Fig (5-4) shows four different types of phantom which were examined to evaluate the capability and accuracy of the *MRAT* and the hardware system.

The first three phantoms are simply cylindrical hollow objects having different radii of 5 mm, 7.5 mm and 10 mm, respectively. The fourth one (d) has a wide bore in its two ends and a narrow bore in the middle. This phantom resembles a symmetrical stenosis in a cylindrical pipe.

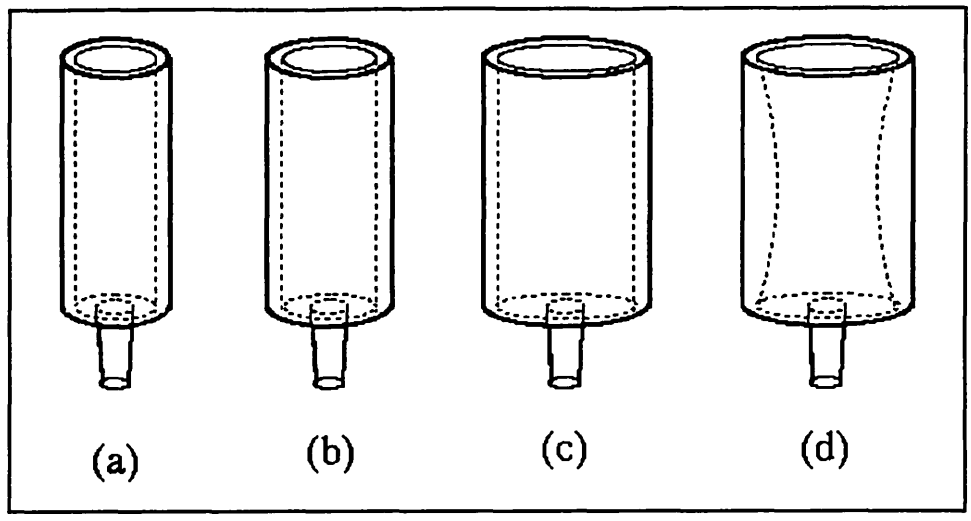


*Fig (5-4) : Four different types of phantom beakers used in 3D image reconstruction.*

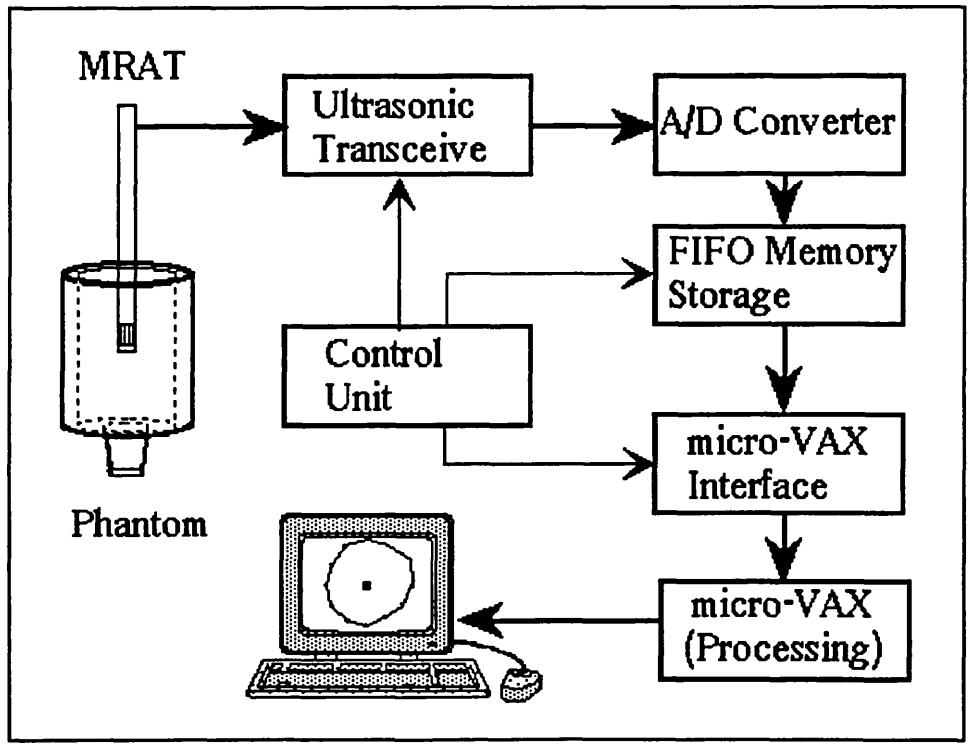


*Fig (5-5) : The block diagram of the ultrasonic system for data acquisition from a perspex phantom.*

The block diagram of the data acquisition system along with the *Miniature Ring Array Transducer* which were assembled to establish the necessary experiments is illustrated in Fig (5-5). To capture a complete block of data for the generation of a contour, the ring array transducer was placed in the centre of each phantom beaker and triggered by the electronic circuitry. Each block of data contains twelve individual ultrasound signals related to twelve elements of the *MRAT*. To capture a readable echo signal and avoid its saturation it is necessary to adjust the gain of the video amplifier located in the transceiver module.

Fig (5-6) illustrates the twelve ultrasonic signals associated with the twelve elements of the transducer. Even though we tried to place the transducer in the centre of the beakers to obtain equally strong reflection echoes, some echoes such as these associated with elements 7,8, and 9 show a greater distance between the transducer and the inner layer of the breaker wall.

It should be noted that some reflected echo signals have smaller amplitudes. This is due to the misalignment of the PZT elements associated with them. This misalignment is mostly caused by the misaslignment of the transducer tip, although it can also be due to the element itself. If this misalignment is caused by the element it is due to unequal amount of the material used for connecting it to the body of the transducer. Therefore more care must be taken during the fabrication of the transducer and particularly in sticking the PZT elements to the transducer body and the amount of the silver epoxy which is laid down beneath the PZT element.

To solve the problem of weak echo due to the misallignment of the transducer a guide wire in the centre of the transducer can be helpful.

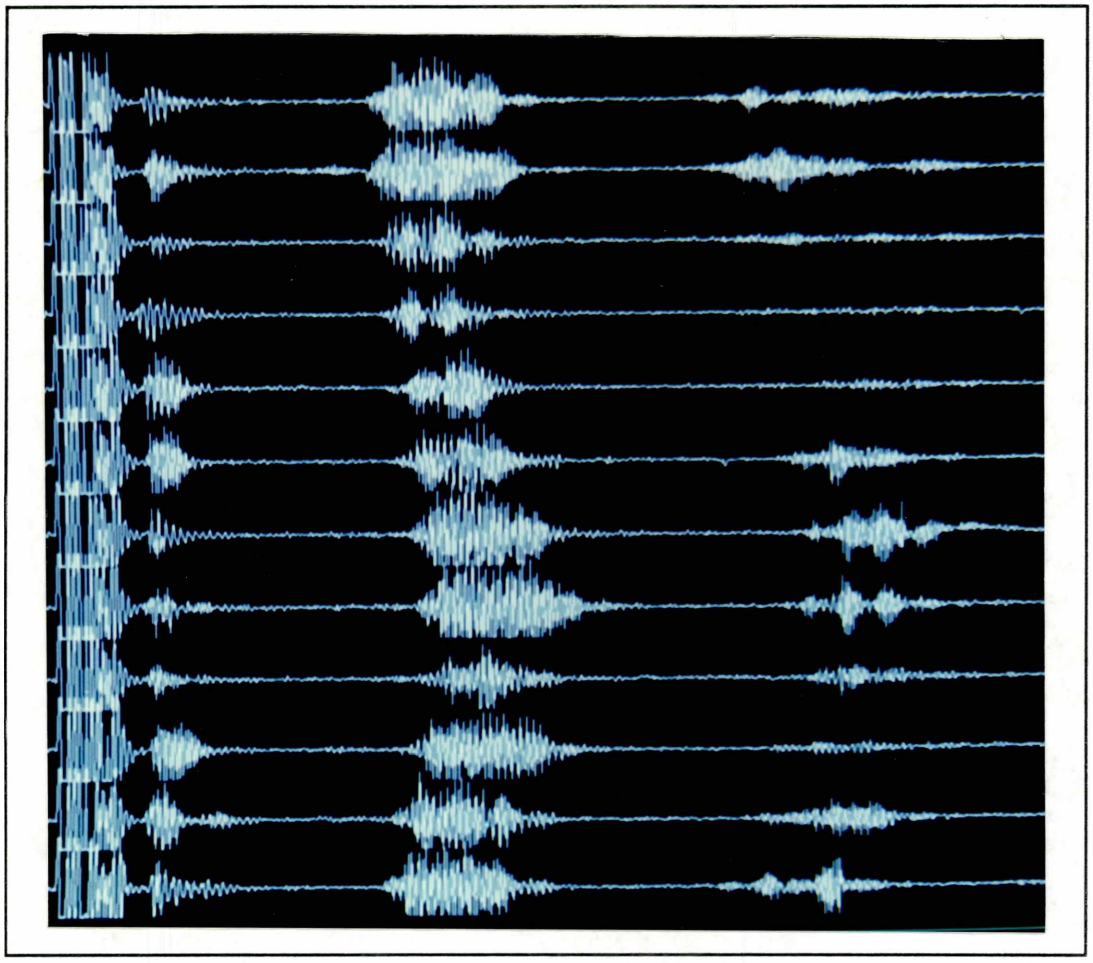

***Fig (5-6) : The ultrasonic signals associated with one phantom slice.***

The next stage was to detect the peak value of the reflected echo signals coming from the interface between water and perspex, which is the inner surface of the beaker wall.

First the captured signals provided by the array transducer were filtered through a Butterworth band pass filter centred at 6 MHz. Fig (5-7) shows all twelve signals after filtering. Then the peak value of the filtered signals were marked. If the echo signals are saturated, then it leads to two or more similar peak values.Therefore, it is necessary to pay a great deal of attention to the output signal of the electronic circuits to avoid saturation. In addition,

it is necessary to provide warning messages in the software package to stop the creation of wrong images based on the incorrect data.

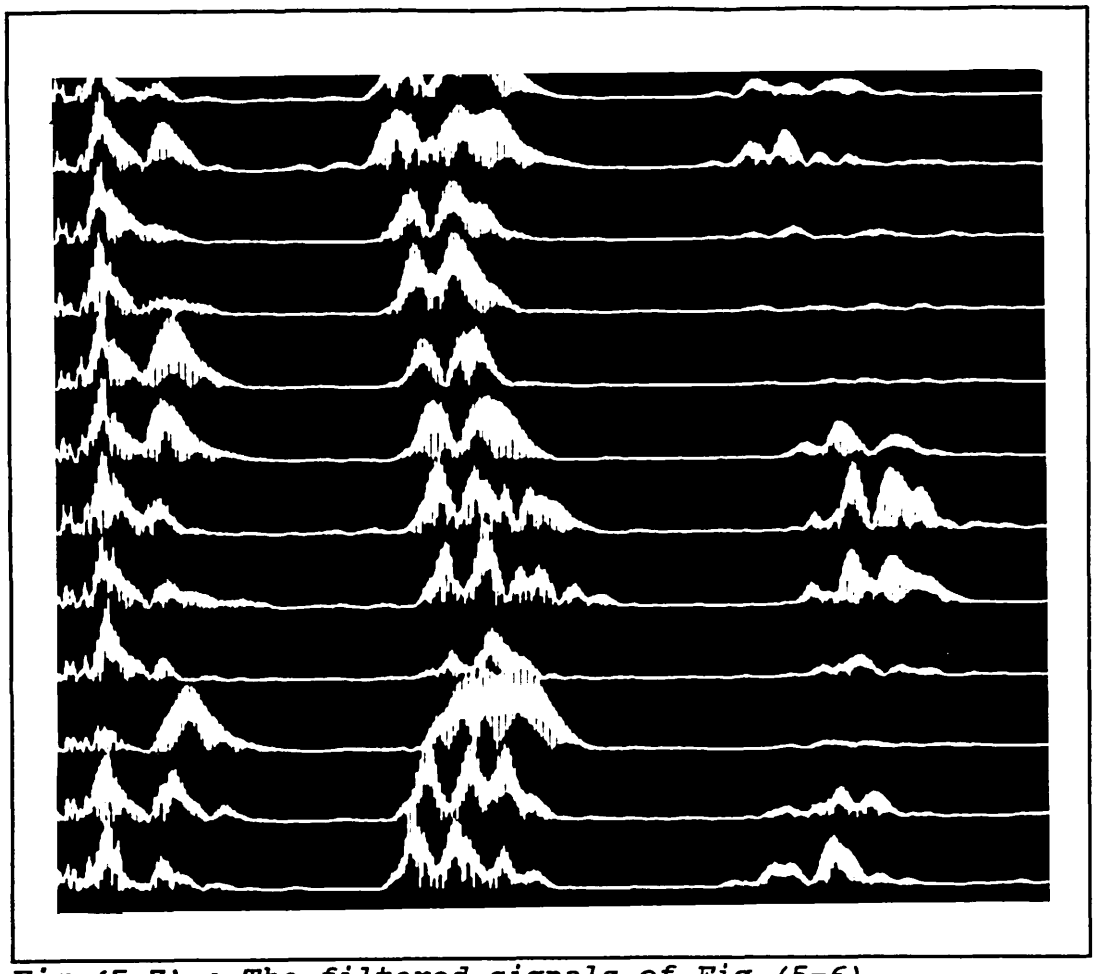

***Fig (5-7) : The filtered signals of Fig (5-6).***

Fig (5-8) illustrates the detected peak values of the twelve signals of Fig(5-7). Because of the inability to distinguish the signal from the noise at the beginning of an echo signal back scattered to the transducer, it is necessary to decide an approximate level of the signal as the start point. On the basis of the experiments carried out and comparison of the results with the physical dimensions of the phantoms, we were able to conclude that choosing the level of 60% of the maximum amplitude is usually a good measure. The effect of this choice is to introducve a geometric error into the image.this is calculated to be less than 0.3 mm. which is not considerable. To capture data from different cross sectional parts of the phantom beaker, the phantom was lifted up while the transducer was fixed in its position. Eight samples of data were taken in 2.5 mm steps and saved by micro-Vax. The same processes of signal filtering and

peak detection were performed for every set of data. Then by means of a dedicated routine, a closed connected curve was created, reconstructing the slice associated to a set of data.

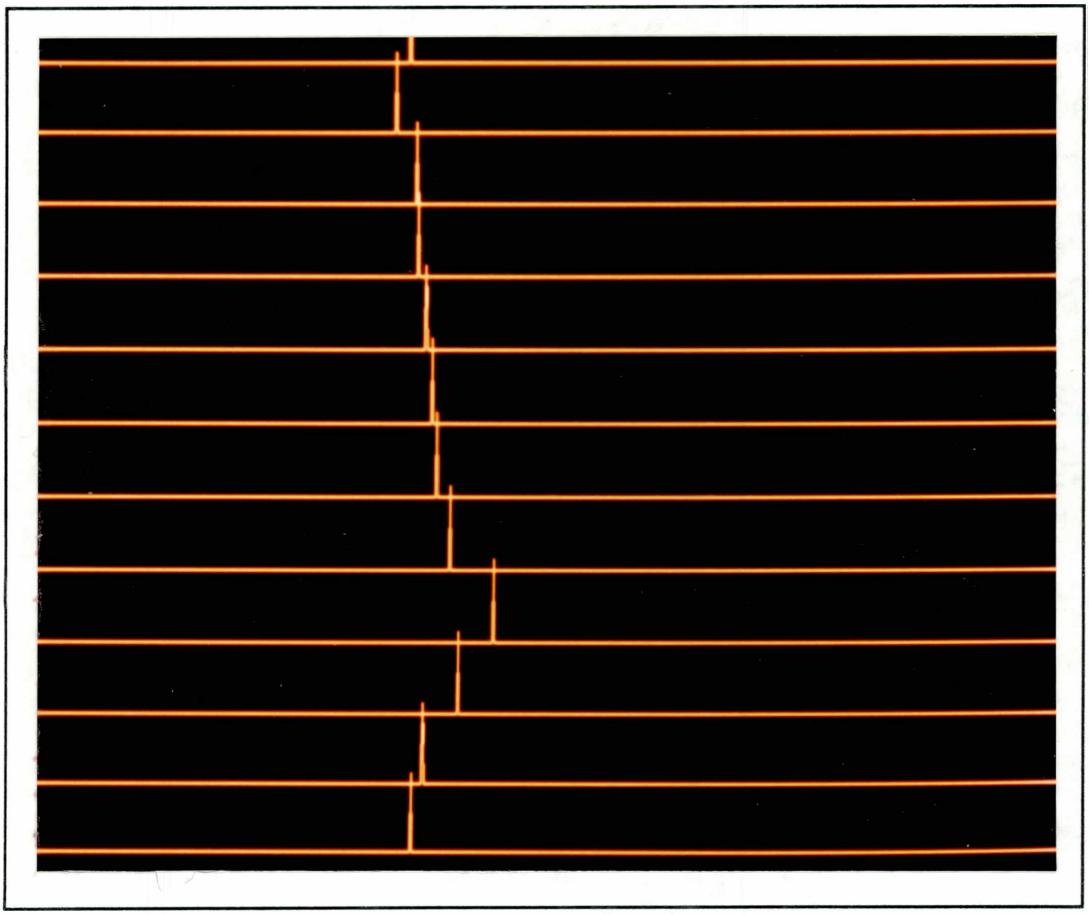

***Fig (5-8) : Peak detection on the signals of Fig (5-7).***

To illustrate the accuracy of the *Miniature Ring Array Transducer* and the electronic instrumentation system in 3D image reconstruction, a perspex phantom such as one shown in Fig (5-4-c) was examined. The data was captured every 2 mm along the axis of the phantom. Three sets of data and the associated generated contours are presented in Fig (5-9-a, b, c, d, e, and f). These contours were later employed in the reconstruction of a 3D image which is shown in Fig (5-10).

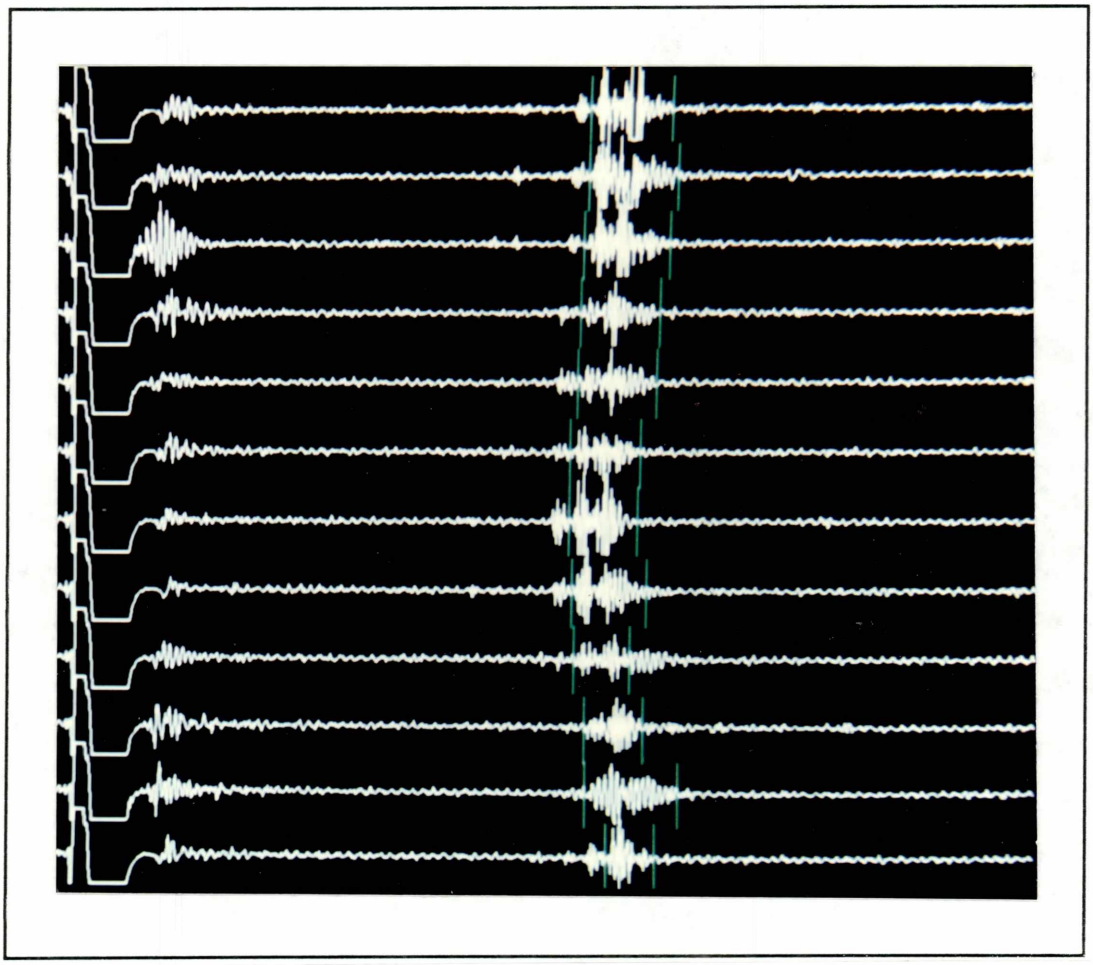

***Fig (5-9-a)*** *12 ultrasound signals captured by the miniature ring array transducer.*

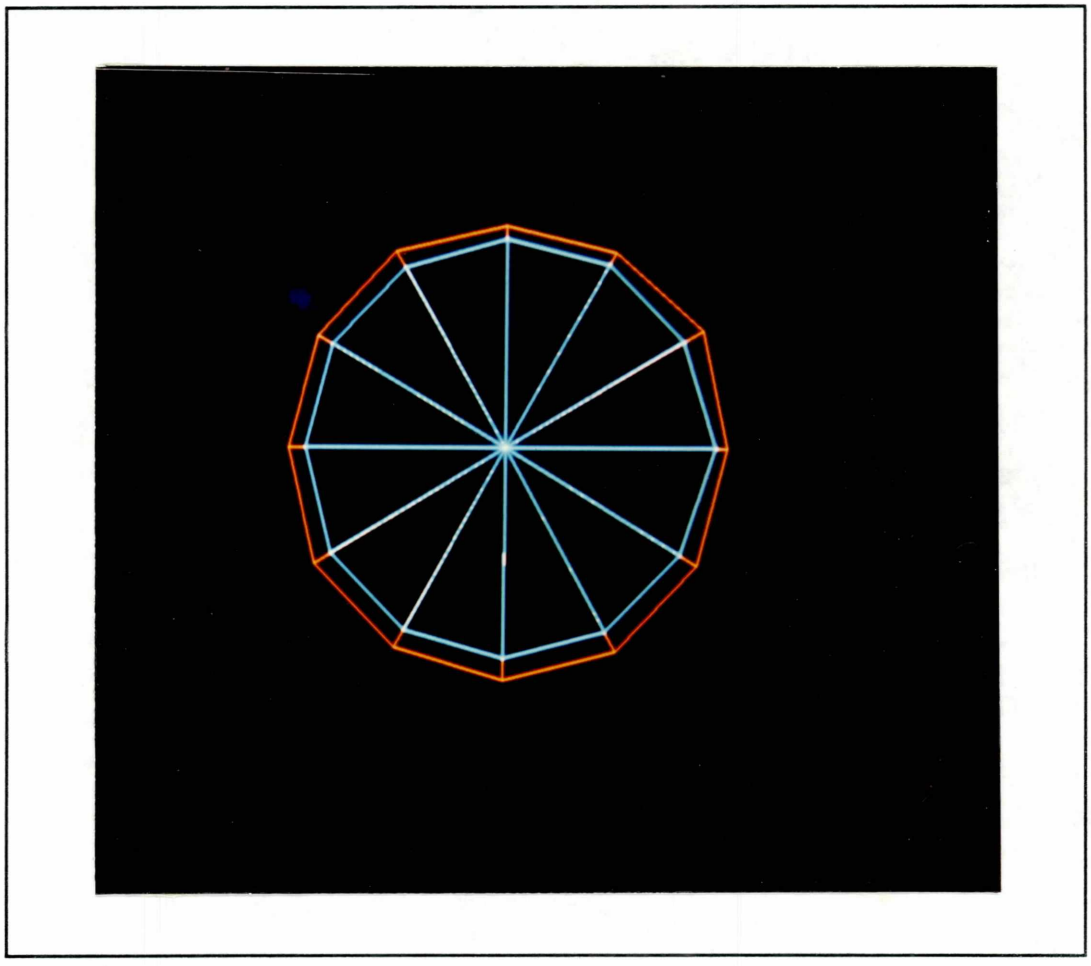

***Fig (5-9-b)*** *Contours generated from the signals shown in figure (5-9-a).*

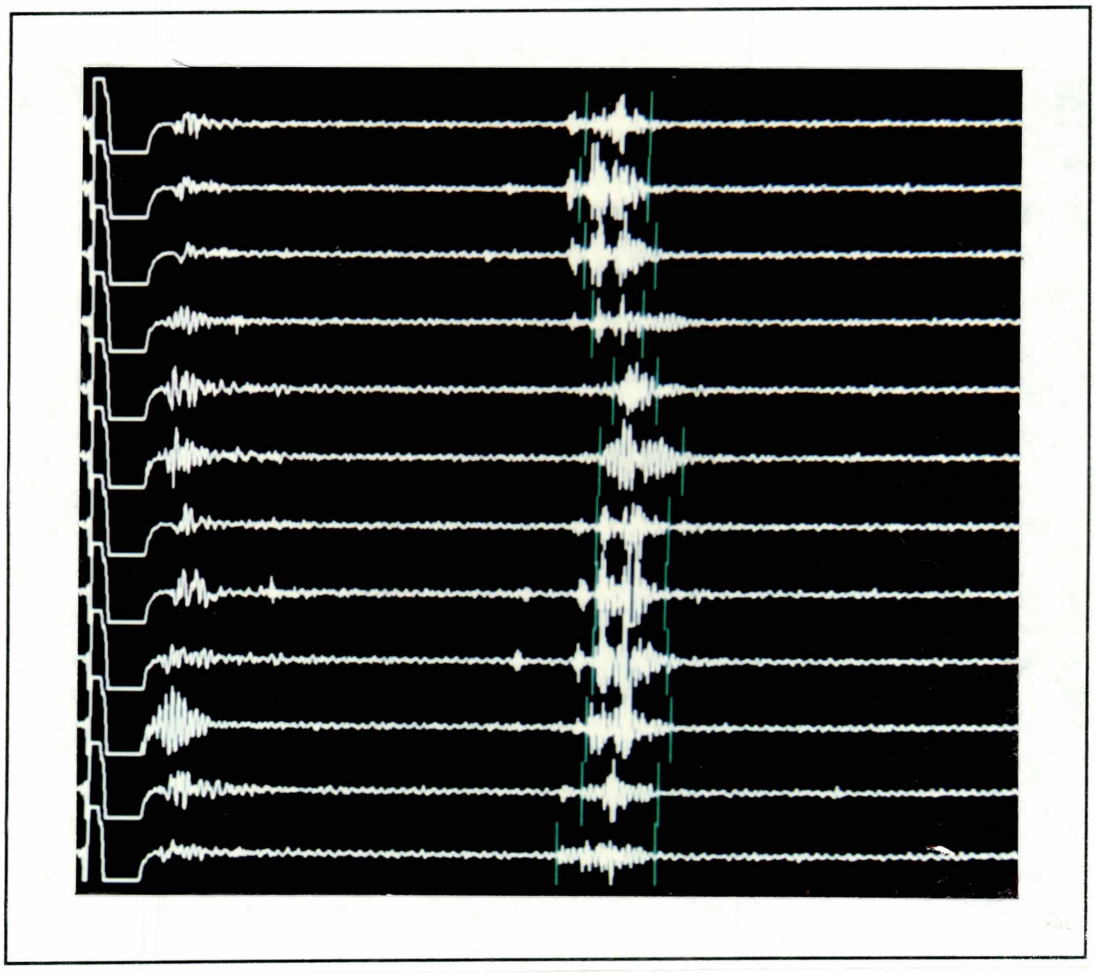

**Fig (5-9-c)** *12 ultrasound signals captured by the miniature ring array transducer.*

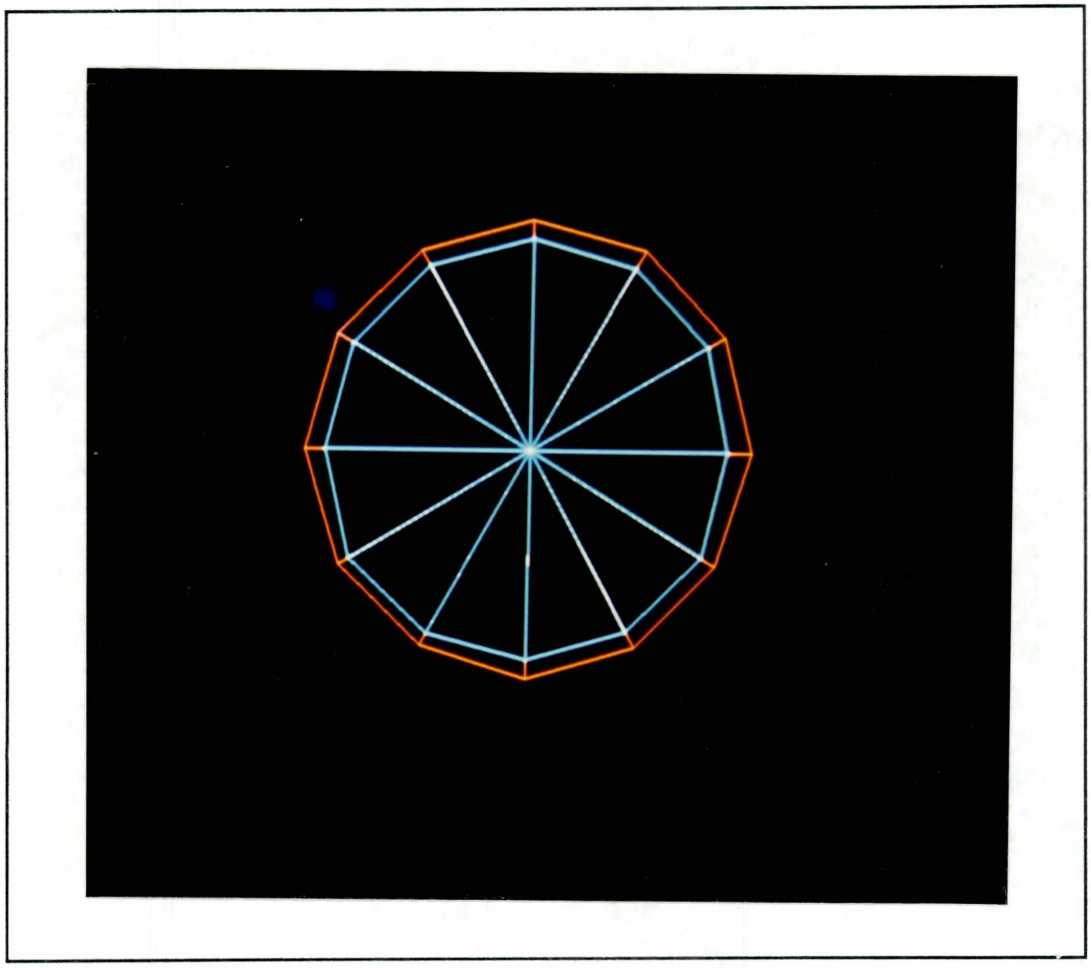

**Fig (5-9-d)** *Contours generated from the signals shown in figure (5-9-c).*

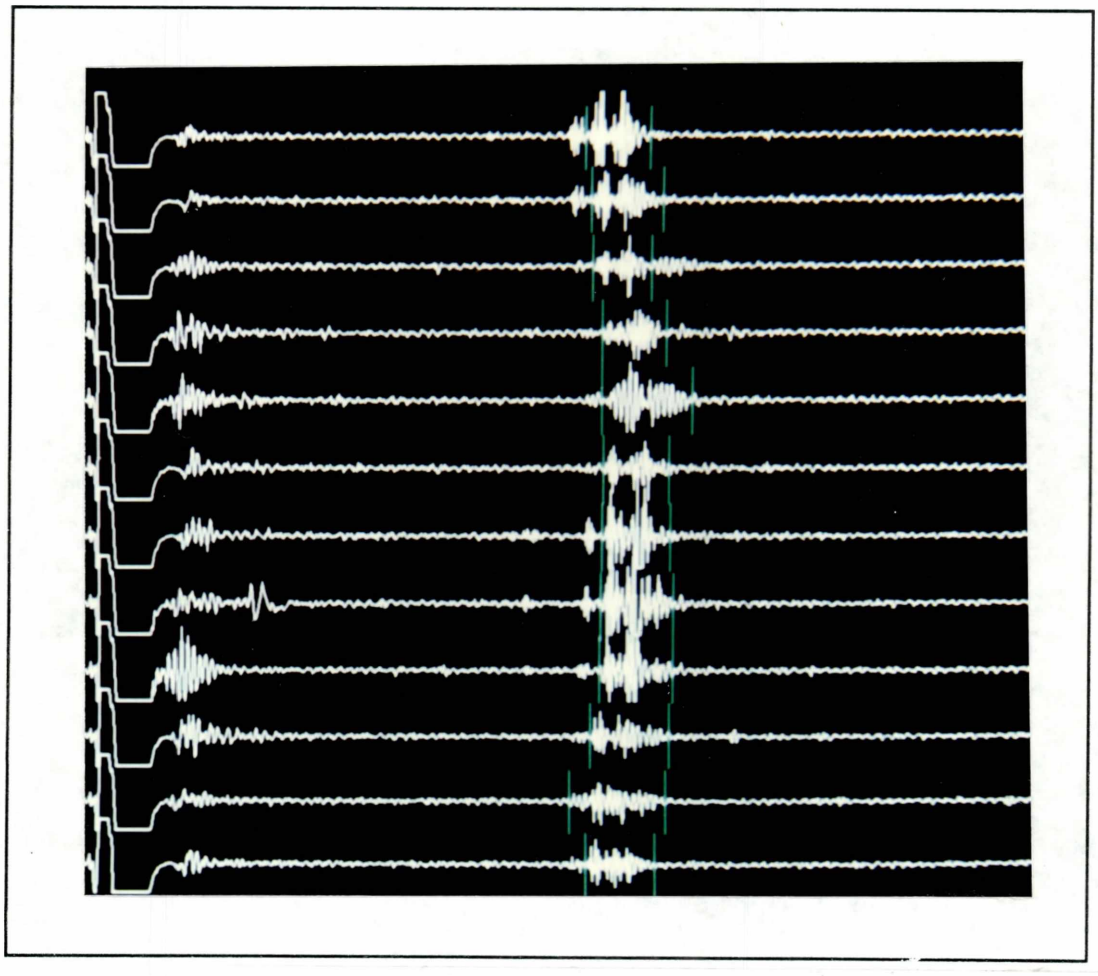

**Fig (5-9-e)** *12 ultrasound signals captured by the miniature ring array transducer.*

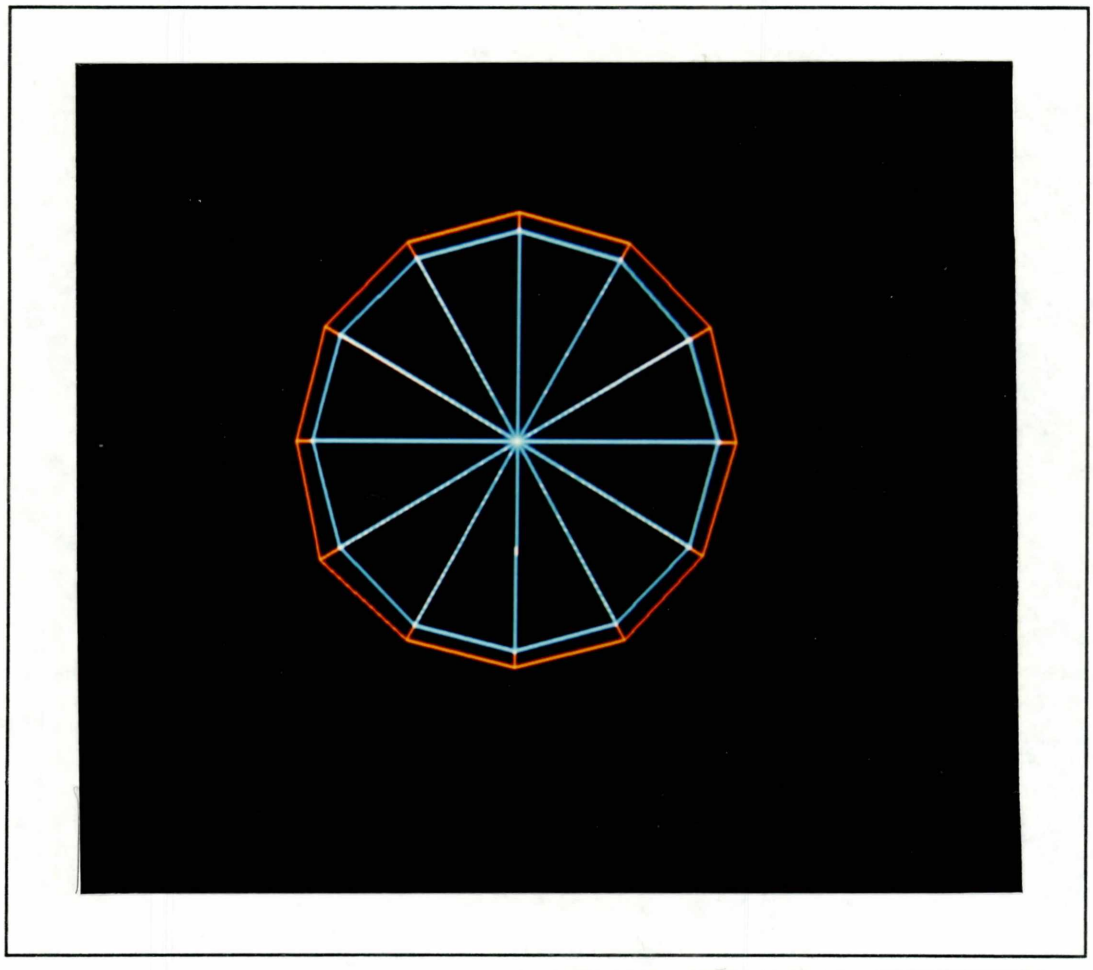

***Fig (5-9-f)*** *Contours generated from the signals shown in figure (5-9-e).*

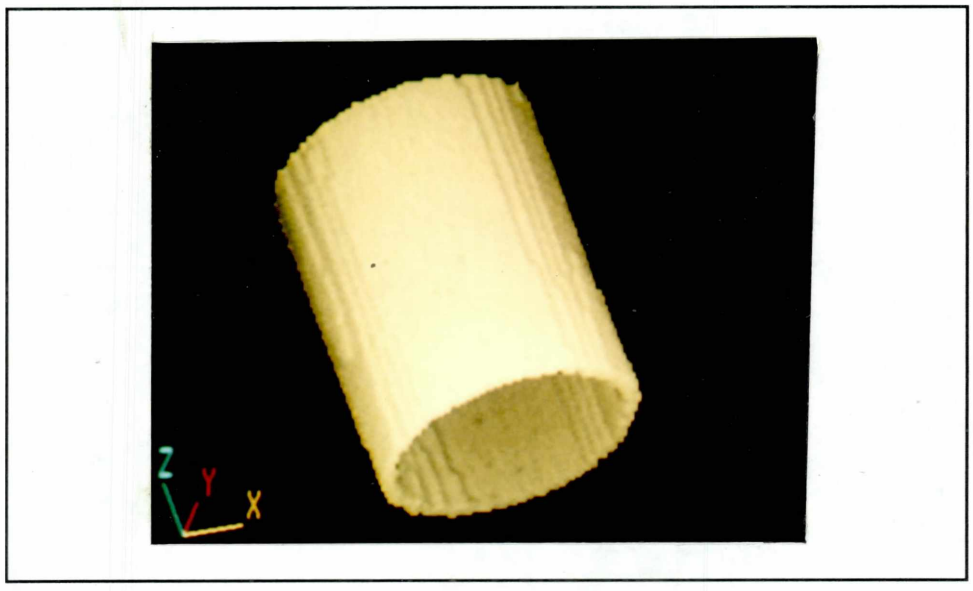


***Fig (5-10) :*** *The reconstructed 3D image of the perspex phantom.*

It should be noted that in carrying out this experiment our aim was to demonstrate the capacity of this system for the generation of valuable data. As the software system was not capable of marking out the beginning and end of the echo signal associated with the thickness of the perspex phantom, it was decided to mark the signals mannually. This can sometimes lack the necessary accuracy.

The same examination was carried out on the smaller phantoms. Fig (5-11) and Fig (5-12) present the captured signals for the other two beakers shown in Fig (5-4-a and b). During the experiments with the smaller phantoms it was necessary to reduce the gain to avoid saturation of the echo signal.

With the same procedure explaind previously, eight contours were produced from eight slices of the phantom shown in Fig (5-4-b). These contours are illustrated in Fig (5-13-a and b). The reconstructed 3D image associated with these sets of data is presented in Fig (5-14).

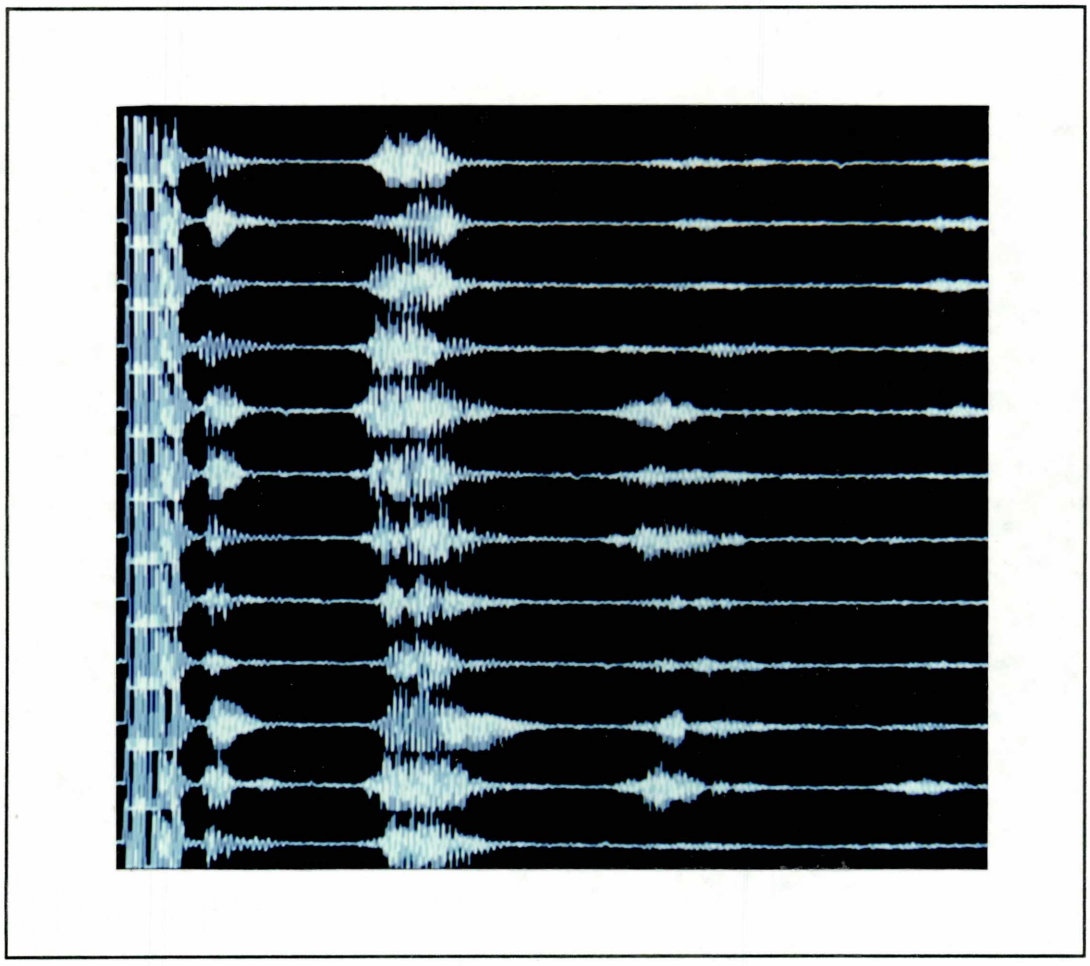

***Fig (5-11)*** *: The ultrasound signals captured from the MEDIUM phantom shown in Fig (5-4-b).*

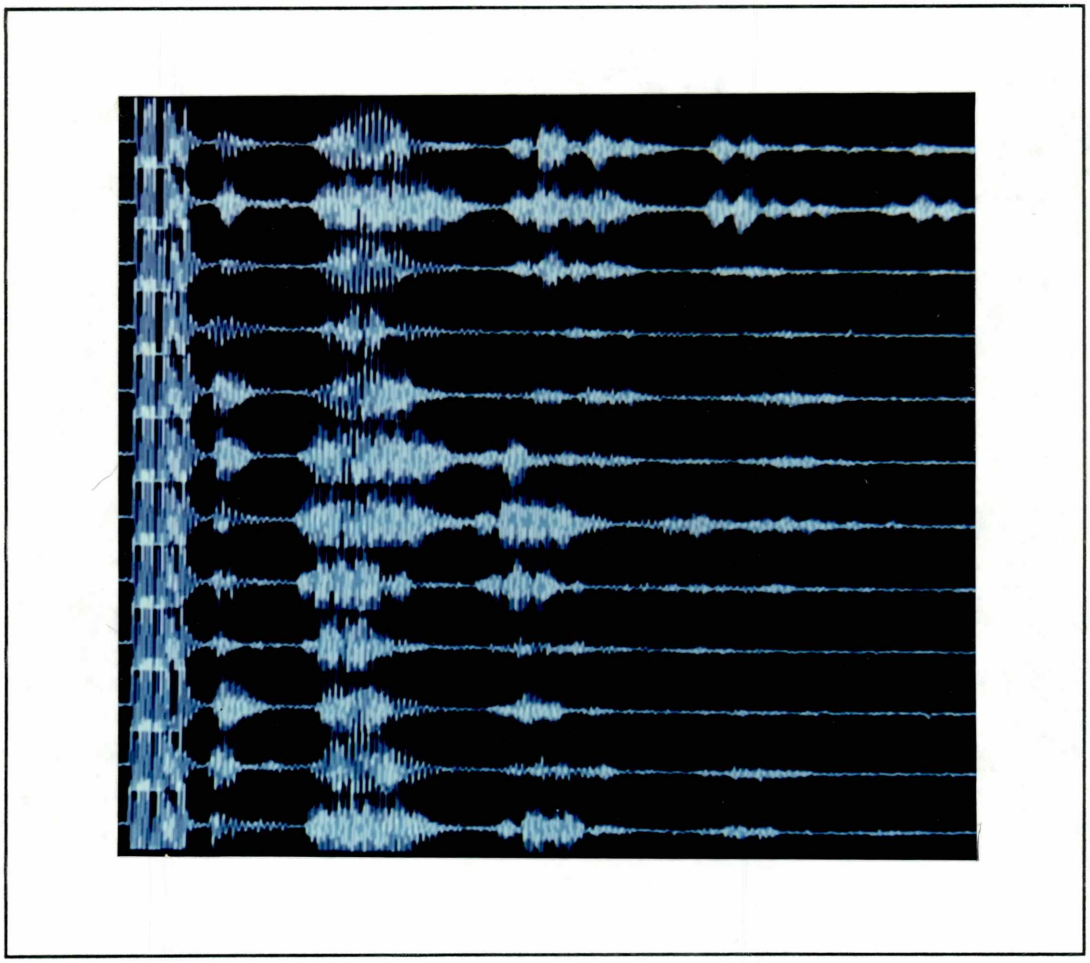

***Fig (5-12)*** *: The ultrasound signals captured from the SMALL phantom shown in Fig (5-4-a).*

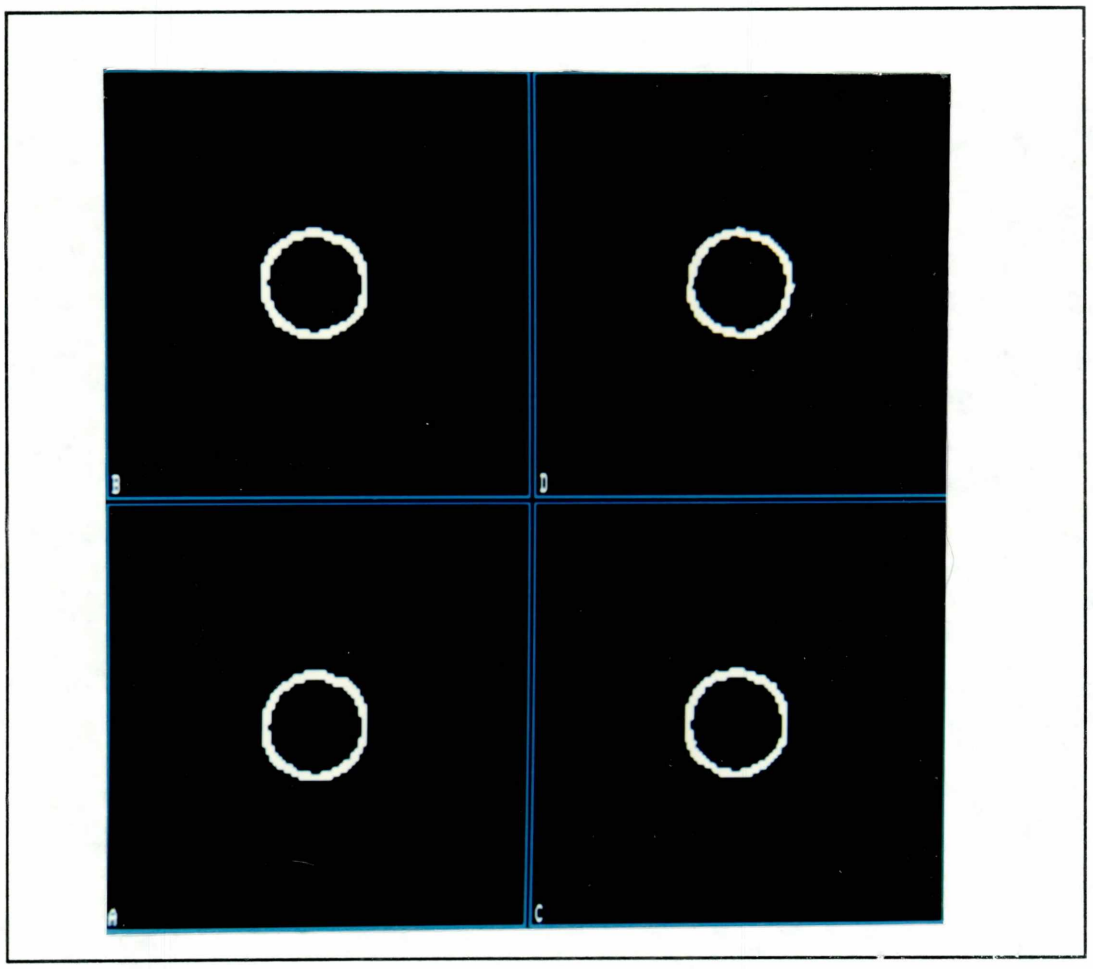


***Fig (5-13-a)*** *: Contours A-D relating to the SMALL phantom.*

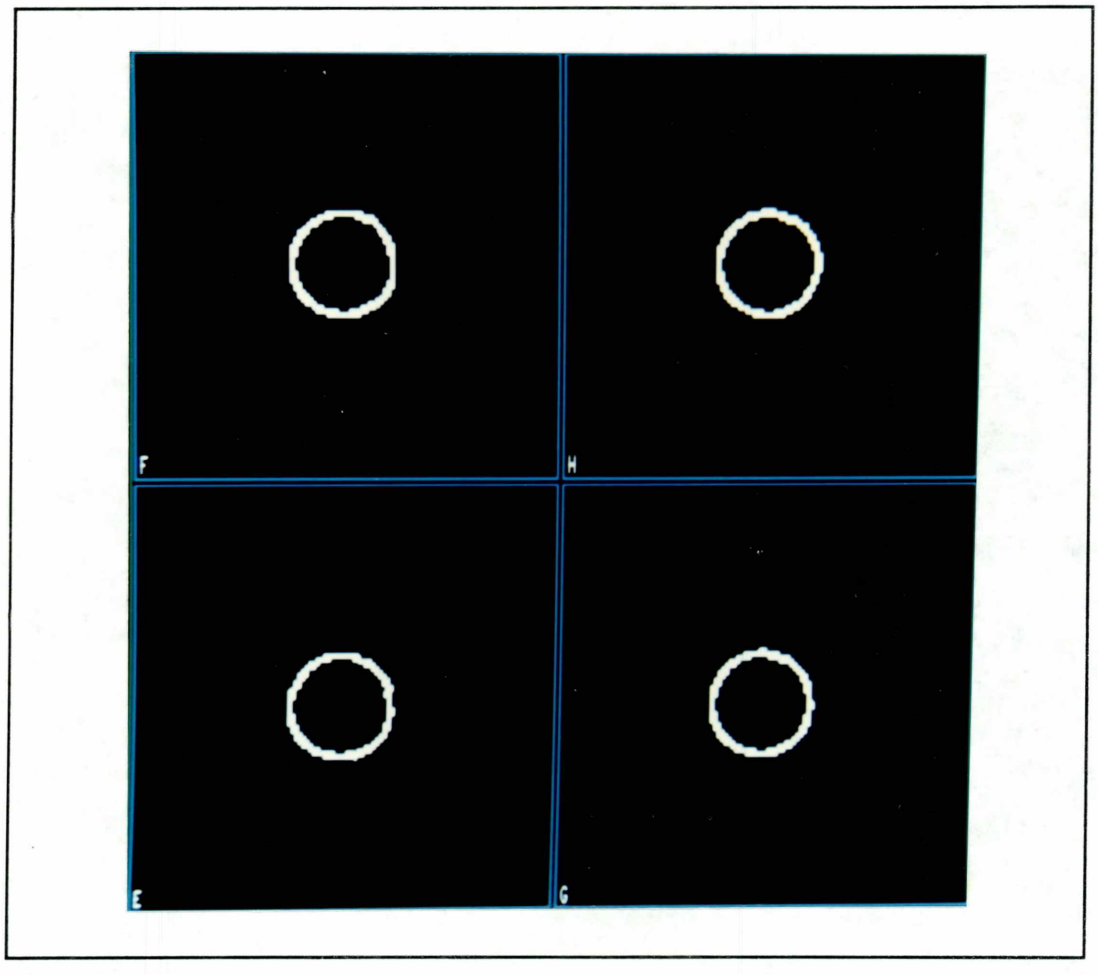


***Fig (13-b)*** *: Contours E-H relating to the SMALL phantom.*

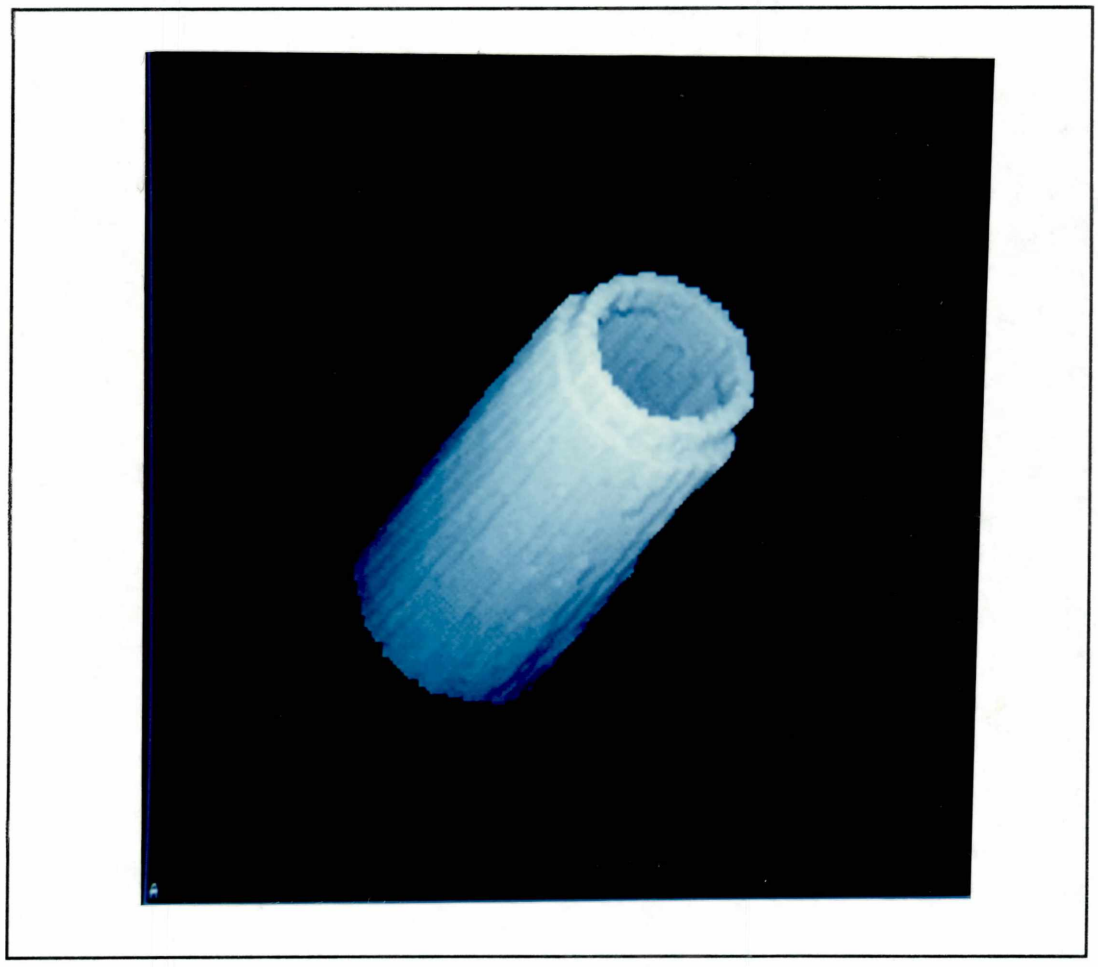

***Fig (5-14)*** *: The 3D image of the SMALL phantom reconstructed from the contours A-H shown in Fig (13-a and b).*

Another examination was carried out with the narrowed phantom beaker. As Fig (5-15) shows this beaker was lifted up and the data was captured in 9 different positions of it.

The procedure of 3D image reconstruction was the same as before. To illustrate the accuracy of the data aquisition system and the transducer, nine sets of data along the axes of the phantom were captured.

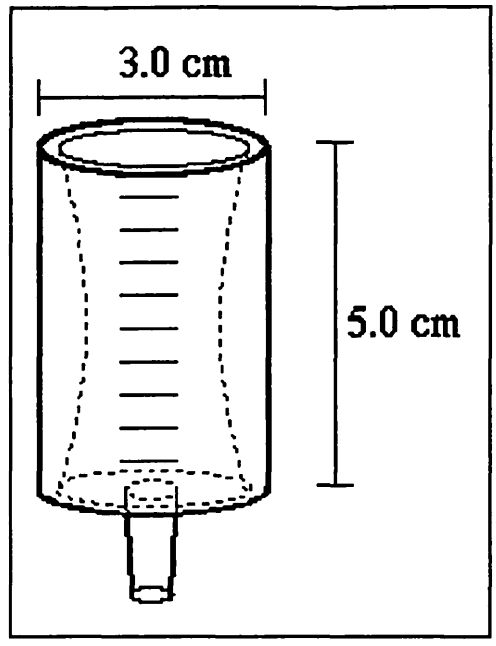


*Fig (5-15) : The narrowed beaker with nine cross sectional layers used in its 3D image reconstruction.*

Four slices related to different positions of the narrowed phantom along with a cross sectional view of it are shown in Fig (5-16). The slices shown in this picture prove the capacity of this system for reliable data acquisition from the inner surface of a narrowed phantom beaker.

In another part of our experimental work an arterial model was fashioned from a small (2cm diameter) plastic beaker within which adhesive putty ("blu-tac") was used to simulate atheromatous plaque encroaching into the lumen of the vessel. Using the catheter-mounted ultrasound probe positioned within the lumen of this model, a series of 2D slices of the model were reconstructed. By the method described above, these data seta were then used to recostruct a 3D image of the model in full voxel space. Fig (5-17a and b) illustrate the 2D slices of the beaker. The 3D reconstructed image of the beaker is shown in Fig (5-18).

In this example, the two different layers of the beaker wall and the adhesive putty are

represented in different colours on the computer screen, illustrating how colour-coding may be used in these models to differentiate between tissue layers with different acoustic properties.

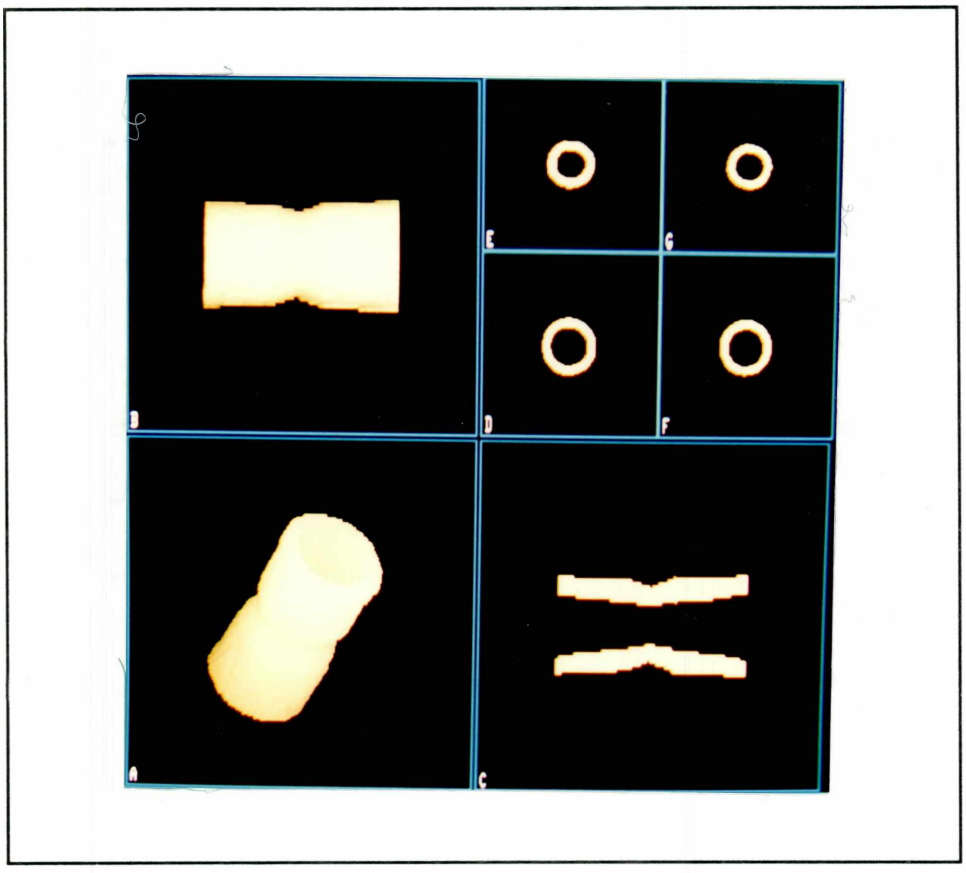

***Fig (5-16) : The 3D image of a narrowed phantom and its associated cross sectional views.***

The software can also be utilised in a number of ways to demonstrate regions of interest within the reconstructed 3D volume. For example, the model may be split longitudinally and opened out showing the "plaque" volume more clearly.

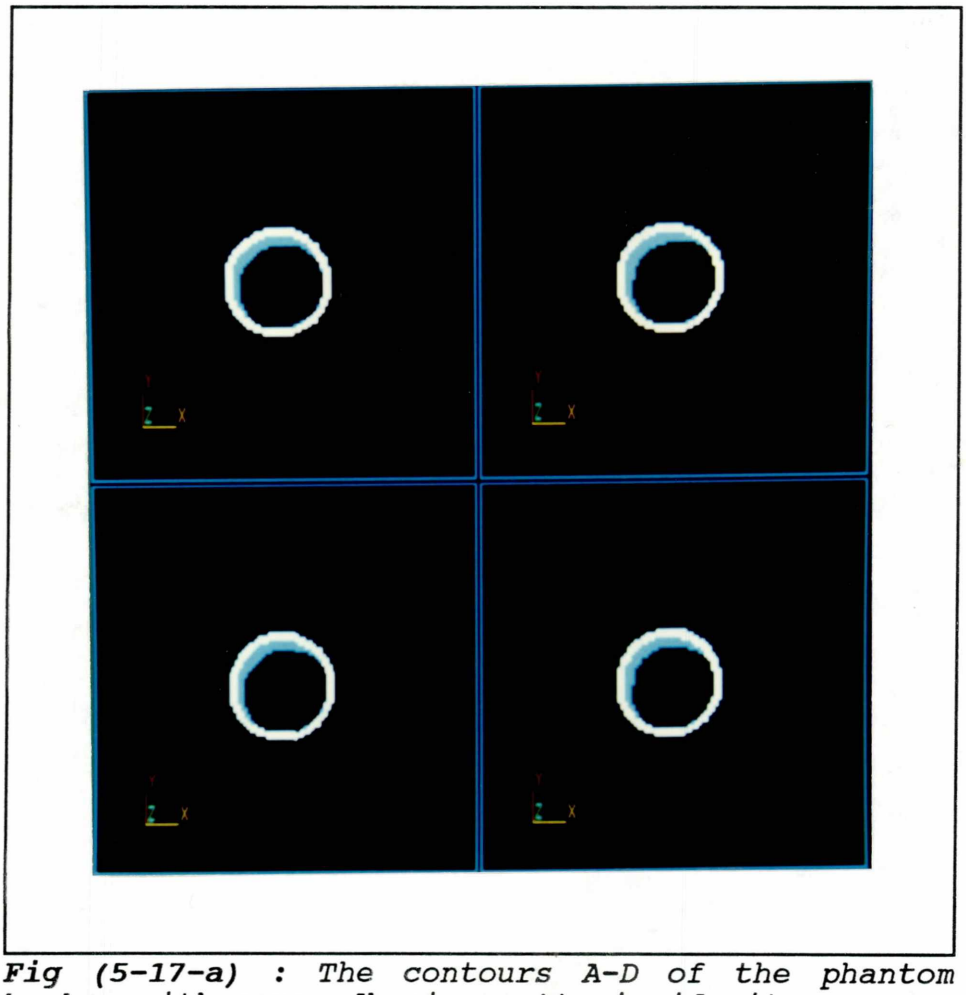

***Fig (5-17-a)*** *: The contours A-D of the phantom beaker with some adhesive putty inside it.*

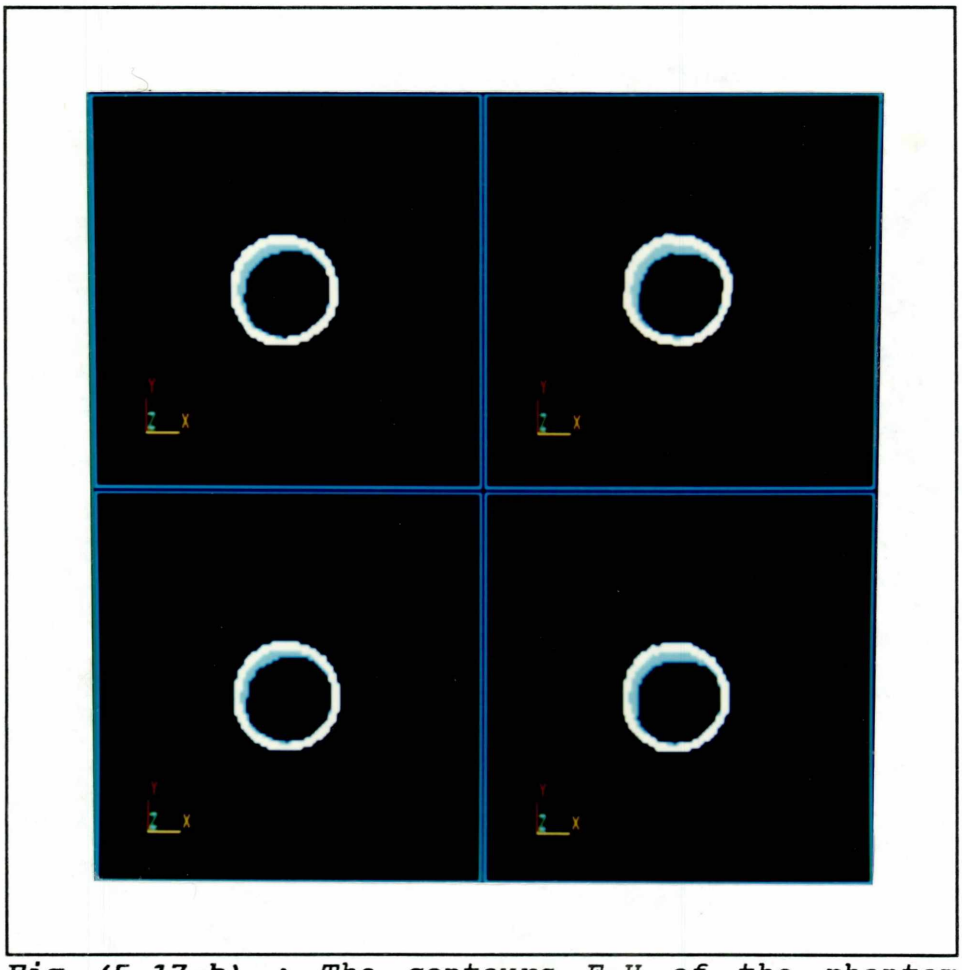

***Fig (5-17-b)*** *: The contours E-H of the phantom beaker and some adhesive putty inside it.*

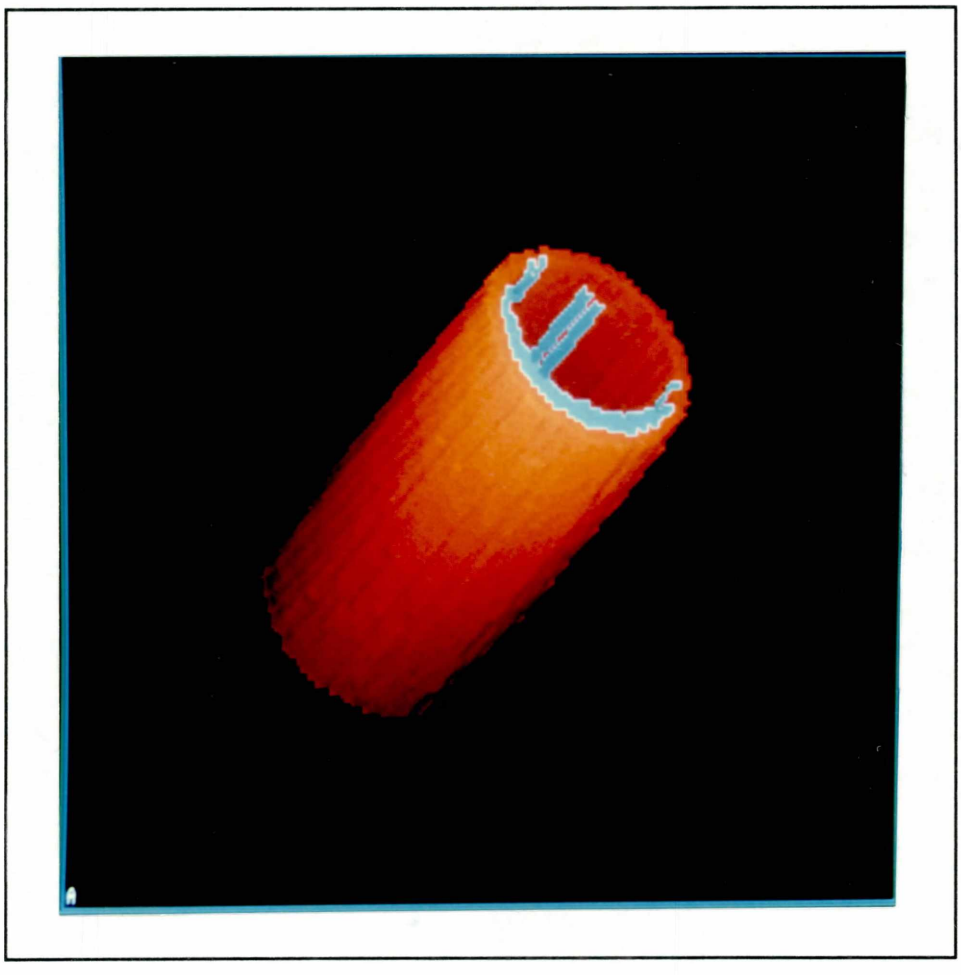

***Fig (5-18) :*** *A 3D image of the phantom beaker reconstructed from the slices shown in Fig (5-17).*

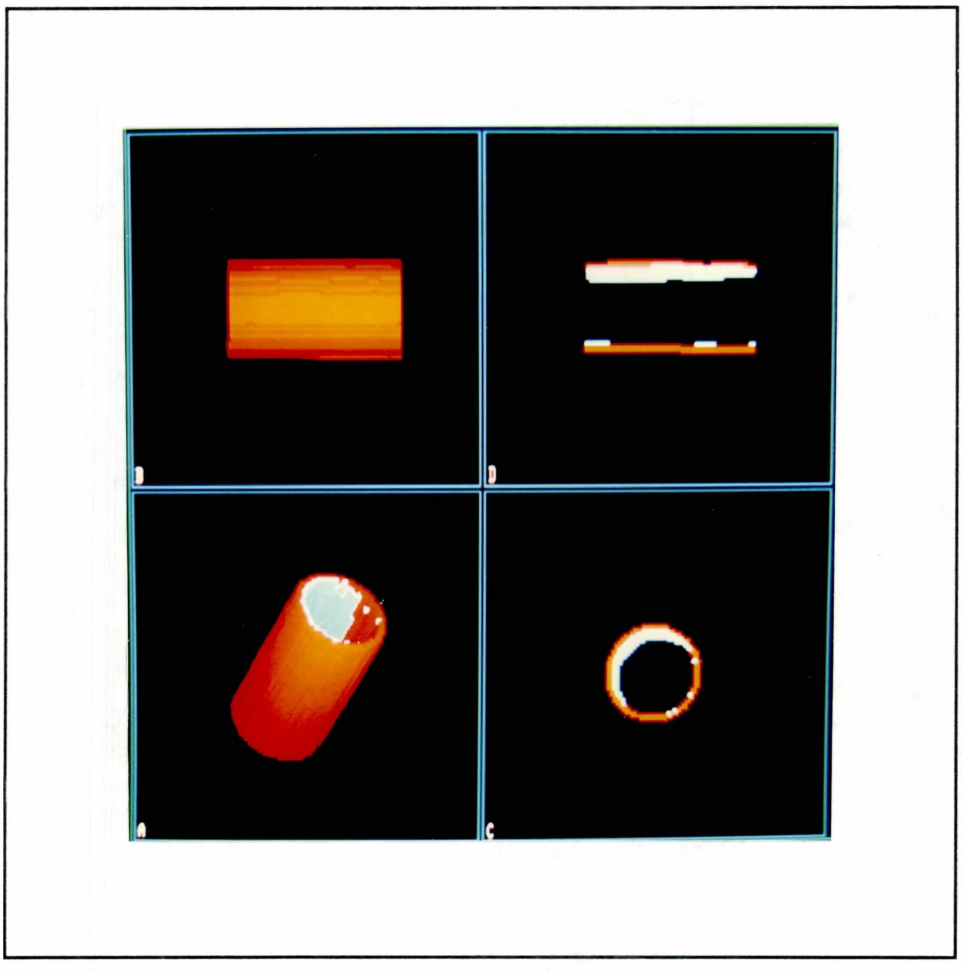

***Fig (5-19)*** *: Another reconstruction of the beaker of Fig (5-18) and its longitudinal cross sectional view.*

## 5-5 : IN-VITRO RESULTS :

In the previous section we considered the visualisation of phantoms, including these with "plaque". This section will consider the application of the visualisation system to example arterial sections. To create a similar enviroment to what is around the transducer in a real examination, the pieces of arterial samples were placed in a water tank. Due to the lower density of the arterial wall, the amplitude of the reflected echo signals were lower in comparison the those previously taken in examinations with perspex phantoms and beakers. Therefore, it was necessary to consider more precautions in hardware as well as software. In all cases the tissue samples were supplied by the department of pathlogy at the Royal London Hospital.

### 5-5-1 : AN EXAMPLE OF HEALTY TISSUE :

The visualisation of a 3 cm section of a healthy common carotid artery is shown in Fig (5-20). The first two panels of Fig (5-20-a and b) show eight examples of cross-sections of the artery taken along its entire length. The 3D model which is constructed from the complete set of 2D cross-sections is presented in the Fig (5-20-c).

### 5-5-2 : AN EXAMPLE OF DISEASED TISSUE :

Fig(5-21-c) illustrates an example of a 4 cm section of a deseased aortic tissue.

Fig (5-21-a and b) show a set of exemplar cross-sections. The reconstructed 3D model of this example is shown in Fig (5-21-c). Figure (5-22) shows the same section of aorta after it has been subjected to planar cutting (after 3D reconstruction), followed by

rotation. Inspection of these figures reveals that there is a significant incursion into the lumen by the plaque. Unlike the previous example "Figure (5-18)" where a phantom had been visualised with plaque, colour coding of plaque in real arterial specimens is not currently possible with our system. To do so it would be necessary to have automatic methods of tissue charactrisation. These have not yet been developed. Nevertheless, visual inspection of the arterial model provides an effective means of identifying plaque in most circumstances.

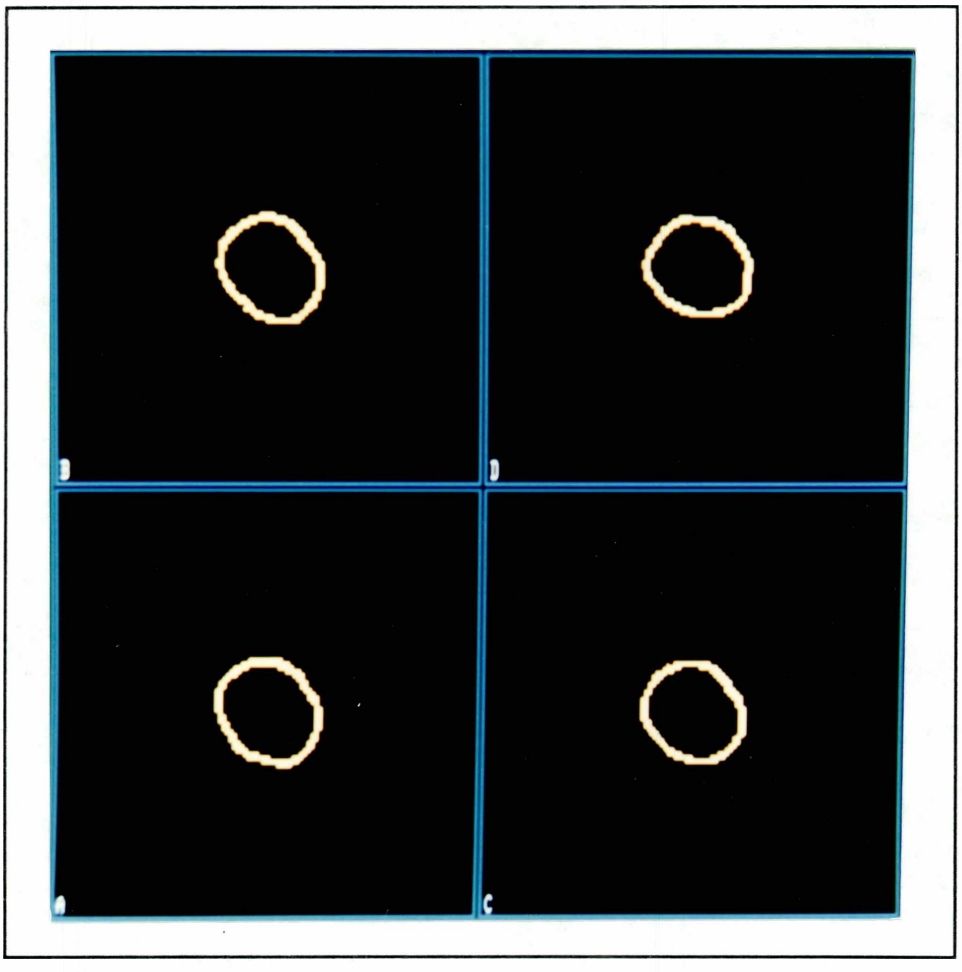

***Fig (5-20-a) : The 2D reconstructed slices (A-D) of a carotid artery.***

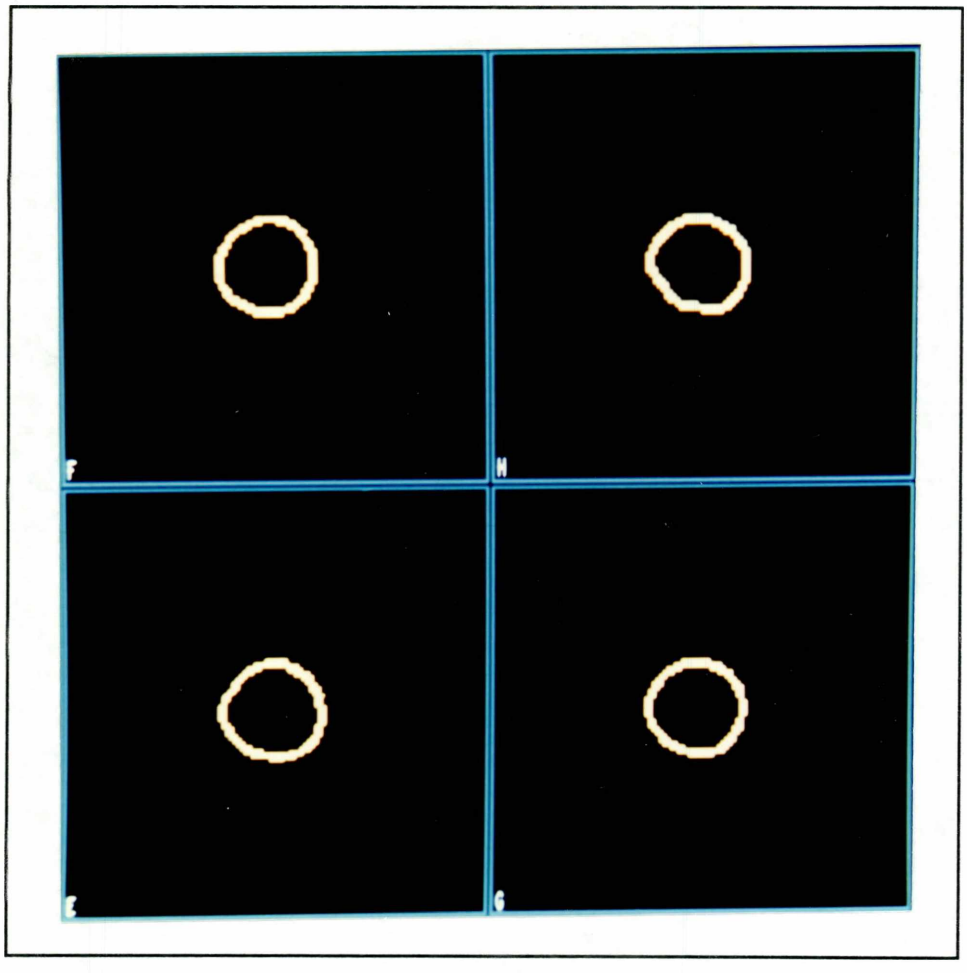


***Fig (5-20-b)*** *: The 2D reconstructed slices (E-H) of a carotid artery.*

***Fig (5-20-c)*** *: A 3D image of the carotid artery reconstructed from the slices shown in Fig (5-20-a and b).*

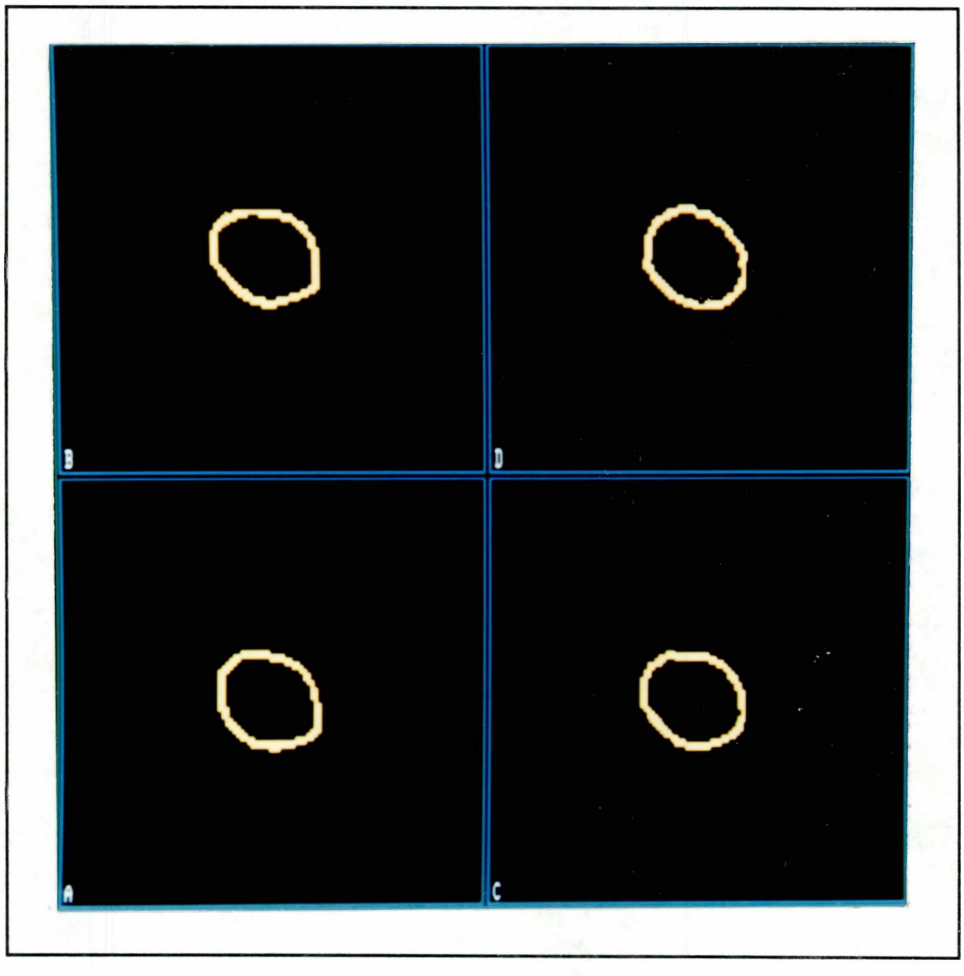


***Fig (5-21-a)*** *: The 2D reconstructed slices (A-D) of a diseased aortic tissue.*

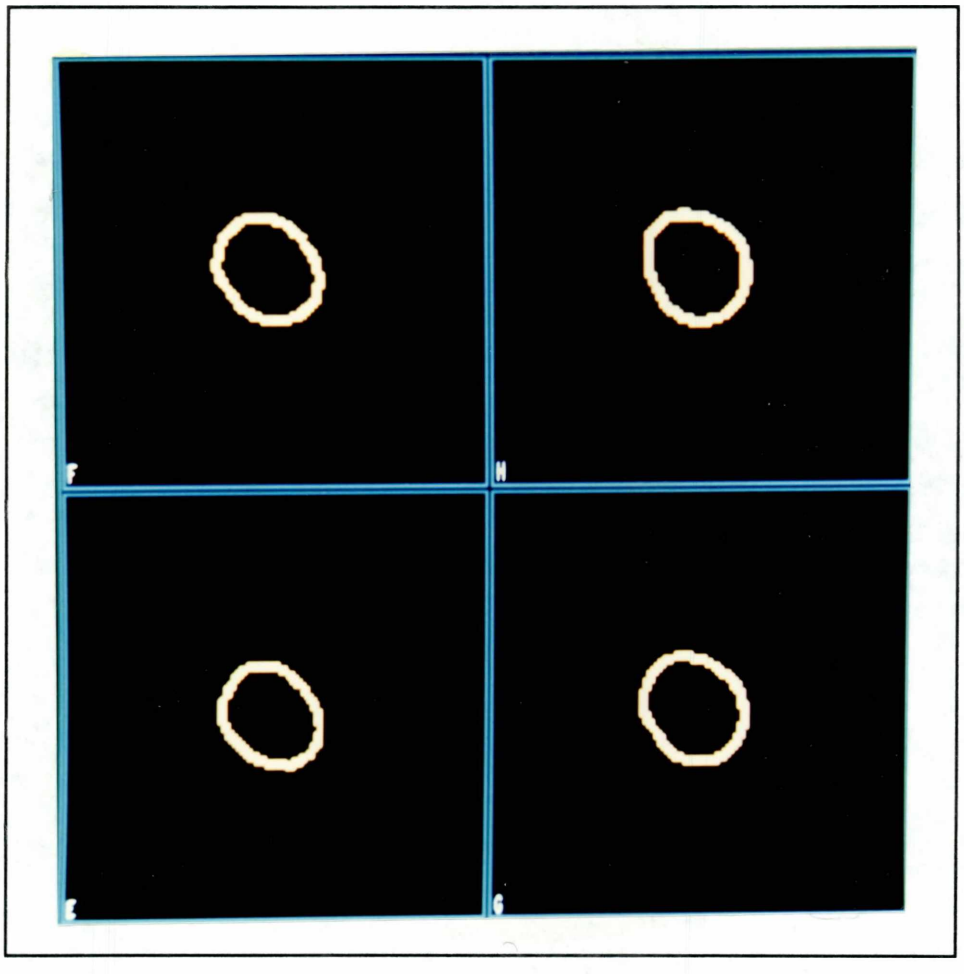


***Fig (5-21-b)*** *: The 2D reconstructed slices (E-H) of a diseased aortic tissue.*

***Fig (5-21-c)*** *: A 3D image of the aortic tissue reconstructed from the slices shown in Fig (5-21-a and b).*

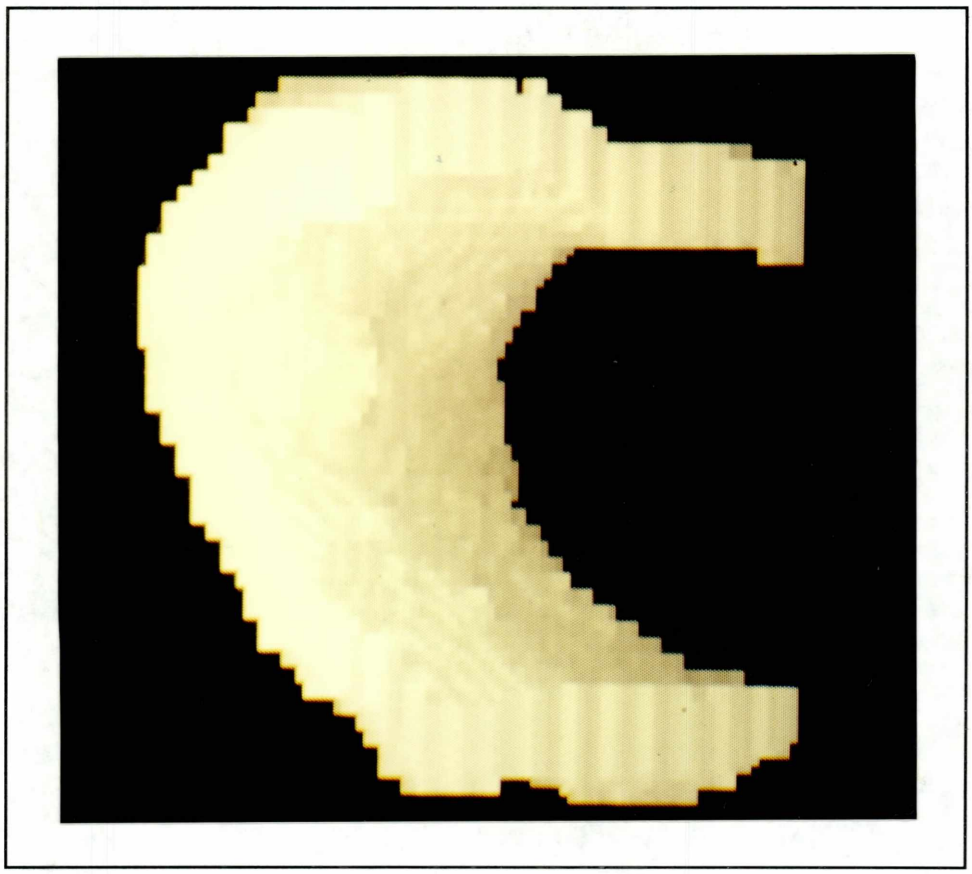

*Fig (5-22) : A planar cut of the reconstructed 3D image shown in Fig (5-21-c).*

**5-6 : SUMMARY :**

In summary, the 3D visualisation system which has been developed is capable of producing accurate 3D solid models of both normal and diseased arterial sections.

The results obtained from the perspex phantom showed the full capability of the *Miniature Ring Array Transducer*, *Hardware* and *Software* in reliable data acquisition and 3D image reconstruction. The experimenal work on the tissue specimens also achieved good results. However, more developements can be done on both the hardware and the software sides of the system which are discussed in chapter seven.

*Chapter six*

# *Transverse Doppler Flow Measurement*

## 6-1 INTRODUCTION :

Assessment of the capability of miniature ring array transducer (MRAT) in flow measurement is the subject of this chapter. It is believed that this device can be used as a diagnostic tool for blood flow measurement in a stenotic region of the blood vessels. First a brief theoretical discussion on Doppler flow measurement with emphesis on transverse Doppler is given. Then the experimental method of our study along with the acquired results by a single element transducer is presented. It should be mentioned that my aim in carrying out these experiments is to test the capability of the miniature ring array transducer in travsverse Doppler flow measurements. Enhancing the theory of transverse Doppler is beyond the scope of this thesis. Therefore, the interested researchers are referred to related references presented in our discussions in the rest of this chapter.

## 6-2 DOPPLER ECHO CARDIOGRAPHY :

On the basis of the Doppler equation when a wave with a nominal frequency of $f_i$ is emitted to a moving object, the reflected wave has a frequency of $f_r$ which is shifted by $\Delta f$ z. This shift or change in frequency depends on both the direction of the moving

object and its speed. Fig (6-1) illustrates the Doppler effect examination on the blood vessels and the associated waveforms. it can be seen that when the direction of blood cells is towards the transducer the reflected ultrasound wave is shifted to a higher frequency relative to the incident wave.

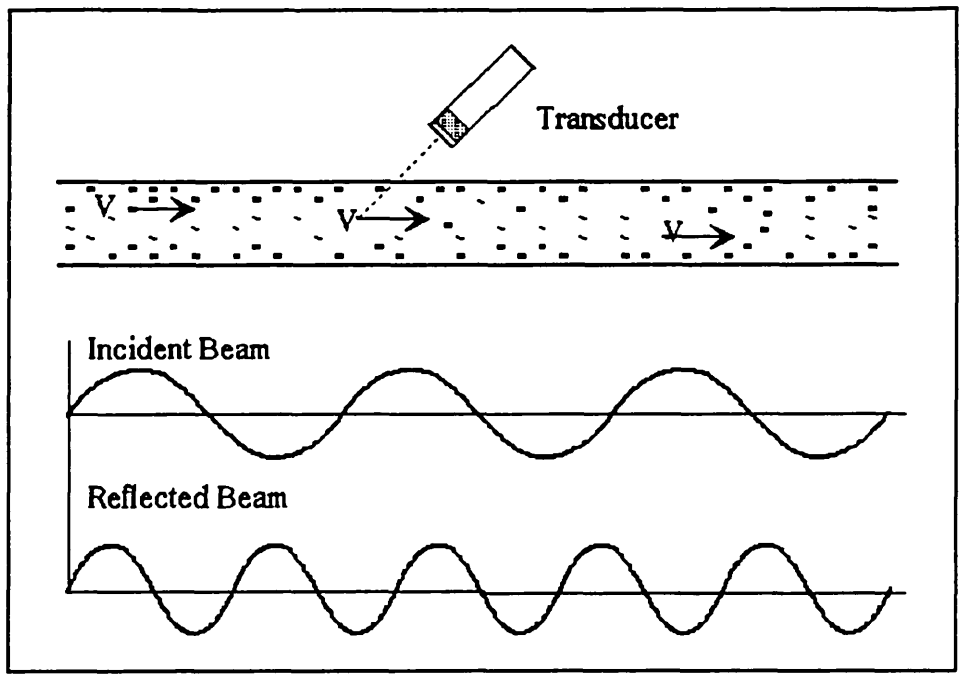


*Fig (6-1) : The Doppler effect. (a) Blood flow towards the transducer. (b) Incident and reflected waveforms.*

Now let us consider another situation in which the transducer is positioned against the bloodstream, as illustrated in Fig (6-2). In this case the bloodstream is directed away from the transducer and the frequency of the reflected ultrasound wave is shifted to a lower frequency. In either case the amount of frequency shift is directly proportional to the flow rate. On the other hand, it is possible to determine the direction of flow. This is done by assessment of the decrease or increase of the frequency in the reflected beam relative to the transmitted beam.

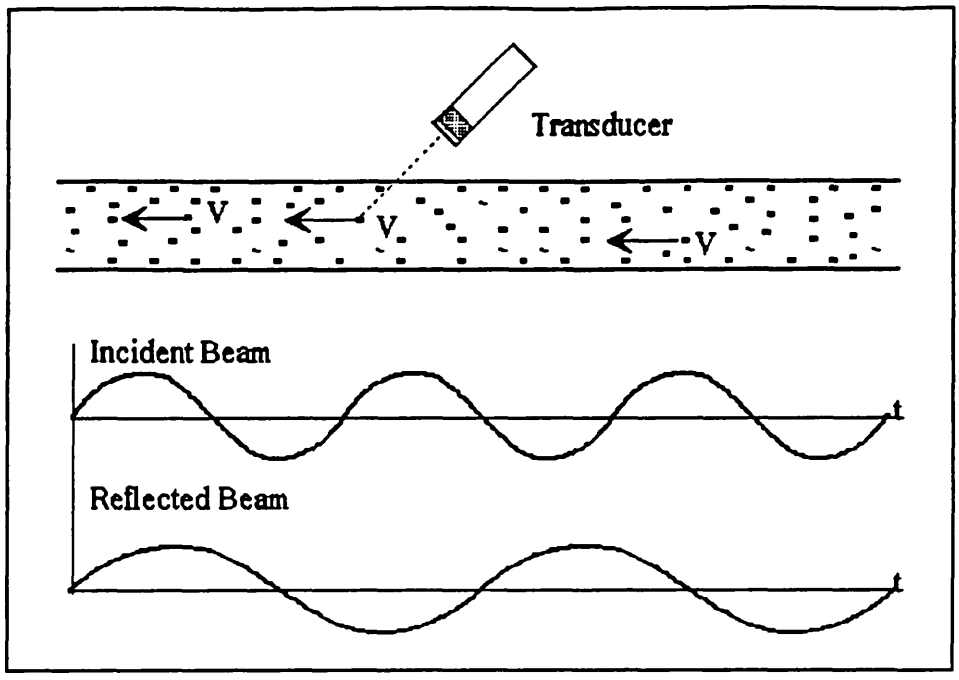


*Fig (6-2) : The Doppler effect. (a) Blood flow away from the transducer. (b) Incident and reflected ultrasound waves.*

In practice, this shift of frequency is measured by multiplication of the frequency of the transmitted and reflected ultrasound waves in a mixer circuit. Then to provide a time interval histogram, the output of the mixer is passed to a low pass filter to collect the Doppler shift frequency component. Fig (6-3) illustrates the block diagram of a continuous wave Doppler system which employs one transducer with two elements, one for transmitting and another for receiving of the ultrasound waves.

At the cost of more complicated electronic circuitry it is possible to use a single element transducer as both the transmitter and the receiver of the ultrasound waves.

In the pulsed Doppler technique a repetitive pulse with a duration of 1 $\mu$sec and a frequency of 5-10 KHz is employed for triggering the piezoelectric element of the ultrasound transducer.

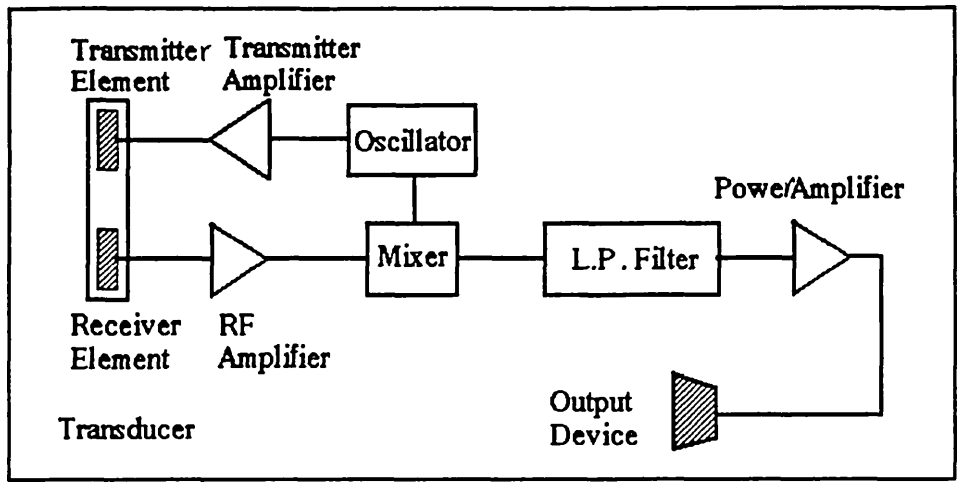


*Fig (6-3) : The block diagram of the Continuous Wave Doppler ultrasound system.*

In pulsed Doppler system a gating mechanism is responsible for selection of the echo signal from a desired point inside the patient's body. In other words the gating section counts the necessary time for the ultrasound wave to reach a target and return to the transducer. Therefore, the Doppler shift frequency is measured according to the signal reflected back by a particular target. The block diagram of a pulsed wave Doppler system is shown in Fig (6-4).

In biomedical applications of the Doppler effect the blood cells are acting as the moving targets and therefore, their velocity can be measured if we know the frequency shift in ultrasound waves emitted to the blood stream. In other words, measurement of the Doppler frequency shift of an ultrasound wave leads to the estimation of the direction and

velocity of blood flow in a vessel. As a consequence, the measurement of velocity permits an assessment of blood pressure which is of high importance in medical diagnosis.

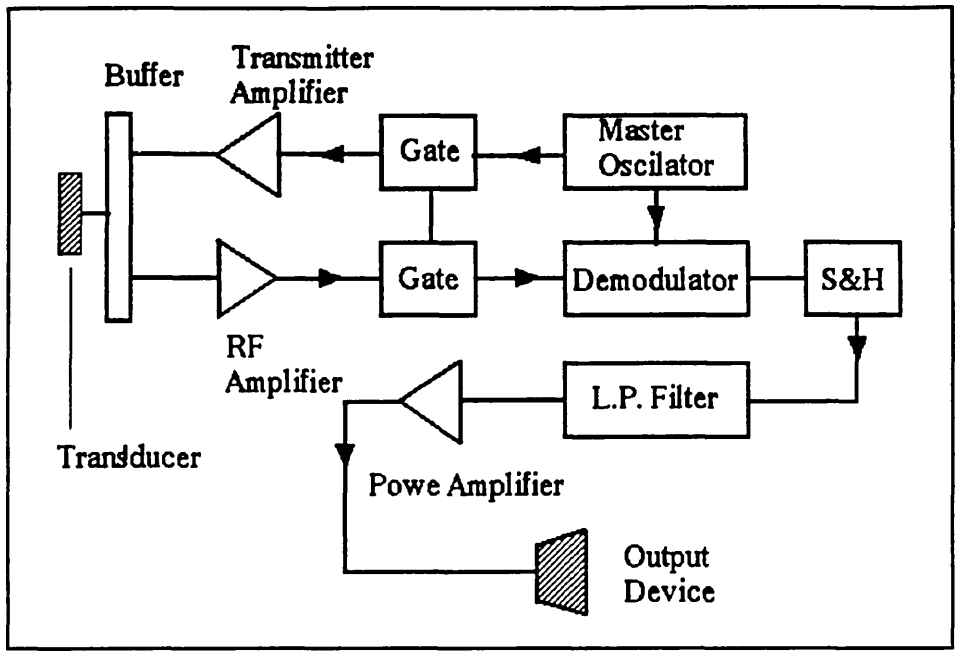


*Fig (6-4) : The block diagram of a Pulsed Doppler ultrasound system.*

The Doppler effect is expressed by the Doppler equation, Equ (6-1). This equation represents the relationship between maximum velocity, frequency shift, and the angle of the incident beam.

$$V_{max} = \frac{v \cdot \Delta f_{max}}{2.f.\cos\theta} \qquad (6\text{-}1)$$

where $V_{max}$ is the instantaneous maximum velocity of the blood stream (cm).

$v$ is the velocity of ultrasound waves in the tissue, (Approximately $1.54 \times 10^5$ cm/sec).

$f_{max}$ is the instantaneous maximum frequency shift, (Hz).

$f_i$ is the frequency of the incident ultrasonic beam, (Hz). and,

$\theta$ is the angle between the axis of the transmitted ultrasonic beam and the direction of the maximum velocity vector.

From Equ (6-1) it is understood that $\theta$ the angle of incident beam has an important role in the measurement of blood flow velocity. It is obvious that any unpredicted change in $\theta$, would lead to inaccurate results.

In medical diagnostic applications of the Doppler effect, it is mainly useful for assessment of the blood flow velocity across an obstruction in a blood vessel. This assessment can provide information about the pressure profile in the same area. Therefore, it is possible to evaluate the unusual obstruction of blood flow of the blood in a quantitative manner.

The relationship between the pressure and velocity of any fluid is described by the Bernoulli Equation. By neglecting the viscous friction in the stenotic region of a blood vessel, the simple form of the bernoulli equation can be written as,

$$\Delta P = 4V^2 \qquad (6\text{-}2)$$

where $\Delta P$ is the pressure gradient and $V$ is the instantaneous velocity of blood flow, Shah (1985)[147].

It should be noted that equation (6-2) is a good estimator for orifices with a diameter greater than 3.5 mm. Therefore, in most cases it is approximately a good estimator for blood pressure measurement.

## 6-3 : TRANSVERSE DOPPLER ESTIMATION :

So far we have considered a narrow ray of the ultrasound beam and its interaction with a single blood cell. However, in real examination of the Doppler effect it is necessary to consider other factors. One of the most important points is the curvature attitude of the ultrasound wave front. After the ultrasound wave is generated it spherically propagates away from the transducer. Therefore, different points of the front wave collide with the blood stream at different angles. Then it is necessary to consider the superposition principle in the study of the behaviour of the ultrasound wave at different angles of collision. The experimental work of Cineros (1985)[26] and theoretical work of Newhouse (1987)[119] revealed the possibility of providing reliable results from the Doppler Spectrum produced by an ultrasound beam perpendicular to the flow. It has been shown that the edge frequencies of the spectrum profile are proportional to the velocity of flow.

Equ (6-1) has been derived on the basis of a time harmonic (monochromatic) signal. If a pulse with a duration much longer than that of the wavelength of the incident (carrier) wave is used to trigger the transducer, then Equ (6-1) can be applied in pulsed Doppler measurements. In theory the Doppler effect disappears when the ultrasound beam is emitted perpendicular to the blood flow. However, in reality due to the approximately spherical wave front of the ultrasound wave, or equivalently, since transducer's aperture is finite, it is possible to achieve the Doppler spectra, even in the transverse mode,Censor(1988)[25].

Considering a single scatterer in a flow stream, the general description for the Amplitude spectrum is given by :

$$A(f) = A_o.\delta(f-f_c) * G_{par}(f) * G_{par}(f) * \delta(f-f_i) \qquad (6\text{-}3)$$

where $f_i$ is the frequency of the incident ultrasound beam, $A_o$ is the system gain, and $G$ represents the excitation frequency spectrum of the moving particle perpendicular to the ultrasound beam, Censor(1988)[25]. The term $\delta(f-f_c)$ in Equ (6-3) describes the classical Doppler shift, in which:

$$f_c = \frac{2f_i V_{per}}{v} \qquad (6\text{-}4)$$

where $V_{per}$ is the perpendicular component of the scatterer velocity relative to the transducer face and $v$ is the propagation velocity of the ultrasound wave.

Equation (6-3) shows that the Amplitude Spectrum of a single scatterer depends on both the vertical and the horizontal component of its speed.

The horizontal or parallel component dependency of the amplitude spectrum is expressed by the excitation frequency spectrum of the moving scatterer parallel to the transducer face. It is this part of Equ (6-3) which provides information related to the scatterer moving perpendicular to the ultrasound beam.

In Equ (6-3) it was assumed that there is only a single particle moving in front of the transducer. If we consider a group of particles with un-correlated positions, they produce un-correlated signals. The total effect of this incoherent process is obtained by adding the power spectra produced by all the individual un-correlated events.

In conclusion to this section it should be noted that the classical Doppler velocity

estimation is not accurate for angles approaching the transverse direction. This is exactly the case of our experimental work performed by *Miniature Ring Array Transducer.* Therefore, by consideration of both parallel and transverse mode Doppler effects, it can be possible to estimate the velocity component normal to the ultrasound beam as well as the one parallel to it.

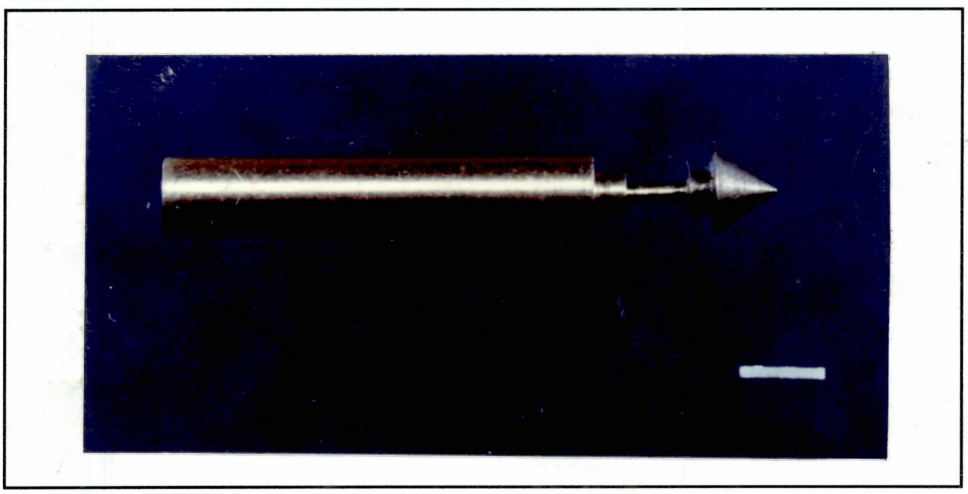

***Fig ((6-5)** : The body of transducer used in flow measurement examinations.*

## 6-4 : EXPERIMENTAL PREPARATION :

To assess the ability of the *MRAT* in flow measurement, it was decided to employ a single element transducer having a PZT element of the same size. The body of this transducer was machined from brass as shown in Fig (6-5). Then a single PZT element with the same size of the elements on the *MRAT* (0.35 x 2.7 mm) was mounted on the transducer body. After electrical connection to the single element of the transducer was completed, its whole body was dipped into wax. This was done to fill the air gap behind the PZT element with a low acoustic impedance material to have better sensitivity. Of

course this transducer had also the same nominal frequency of the *MRAT*, Operating at 6 MHz.

This transducer was placed inside a flow rig which was employed to produce a closed loop of water stream at a certain flow rate. Fig (6-6) shows the block diagram of the testing procedure. The flow rig is a circular perspex tube with an internal diameter of 3.5 cm and a thickness of 4 mm. The length of this rig is 3.2 meters, which is calculated to be sufficient to provide non turbulent flow. We decided to put the transducer at a distance of 1.1 meters from the tank outlet to the flow rig.

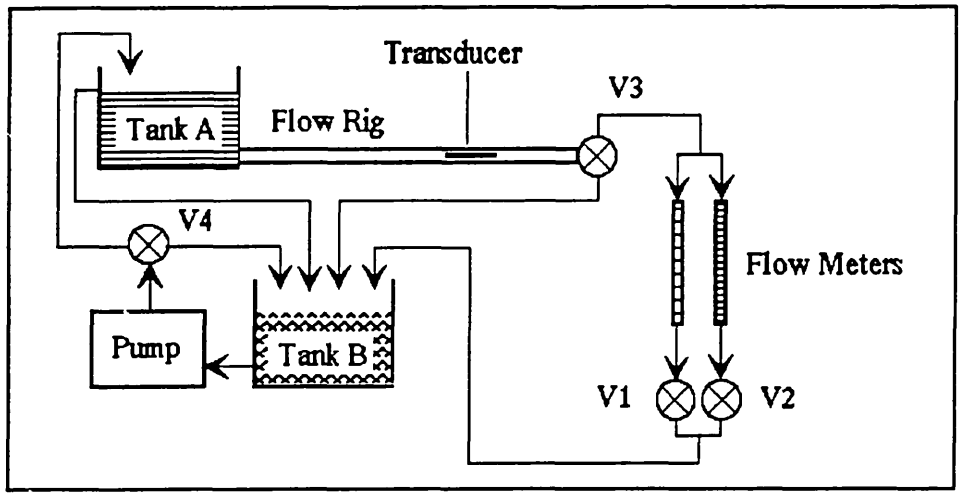


*Fig (6-6) : The block diagram of the flow rig system.*

As can be seen in Fig (6-6) the speed of water flow in the flow rig could be controlled by means of two valves $V_1$ and $V_2$ and obtain a desired flow rate. Also, other two valves $V_3$ and $V_4$ have control on the flow velocity as well as its direction through the water tank **A** or **B**.

In order to have a constant speed during the measurements it was necessary to keep the level of the water at a constant height in tank **A**. This was achieved by suitable adjustment of the control valves.

The transducer was connected to a Doppler measurement circuitry operating at 6 MHz. The output of this circuit was directed to an A/D card interfaced to a personal computer. It was expected to capture signals with frequency shifts of less than 250 Hz and therefore the sampling frequency of the A/D card was fixed at 500 Hz. To simulate blood cells in the water stream, the flow rig was seeded with purified talc powder to provide the moving scatterers.

The captured signals were analyzed with two different methods. In the first scheme the data signals were analyzed by averaging Fast Fourier Transforms. In the second approach the Auto-Regressive Moving Average (ARMA) method was utilised.

## 6-5 : EXPERIMENTAL RESULTS :

In this section the results of the experimental work on transverse Doppler flow measurement will be presented. We show that transverse Doppler effect can be used to determine the flow velocity. In fact, within the theory of the transverse Doppler effect phenomena, two different mechanisms can be defined which both relate a Doppler shift in frequency to the flow velocity.

The first mechanism is due to any angular misalignment between the transducer face and the major flow axes. Also, any disturbance in flow caused by an internally mounted transducer can add to this effect. This mechanism can produce a very small classical Doppler shift, which is nonetheless detectable. This may be estimated on a signal by computing the first moment of the signal spectrum, $f_{min}$.

The second mechanism uses the extent of the spectral broadening due to specifically the

parallel motion of the scatterers past the transducer face, Censor (1988)[25]. This may be estimated by determining the maximum frequency $f_{max}$, for which the signal power is above the noise floor. In both cases the Doppler shift is directly proportional to the flow velocity, but the constant of proportionality is different.

In this work, the major effort was concentrated on the mean frequency of the spectrum for a variety of the flow rate. To simulate different flow rates across the flow rig, the transducer was placed at the centre of the pipe and at a fixed distance of 4.5 mm from the transducer face. Then the flow of the water stream was controlled by means of the control valves to provide a non-turbulent flow at a constant velocity.

Due to difficulties in using equipement in a very noisy environment we first decided to concentrate on the first technique. Therefore it was necessary to study the frequency shift mostly caused by misal ignment of the transducer's element or turbulance created around the transducer tip.

Fig (6-7-a to e) illustrates the captured Doppler signals at the flow rates of 10 cm/sec, 12.5 cm/sec, 14 cm/sec, 18 cm/sec, and 26 cm/sec respectively.

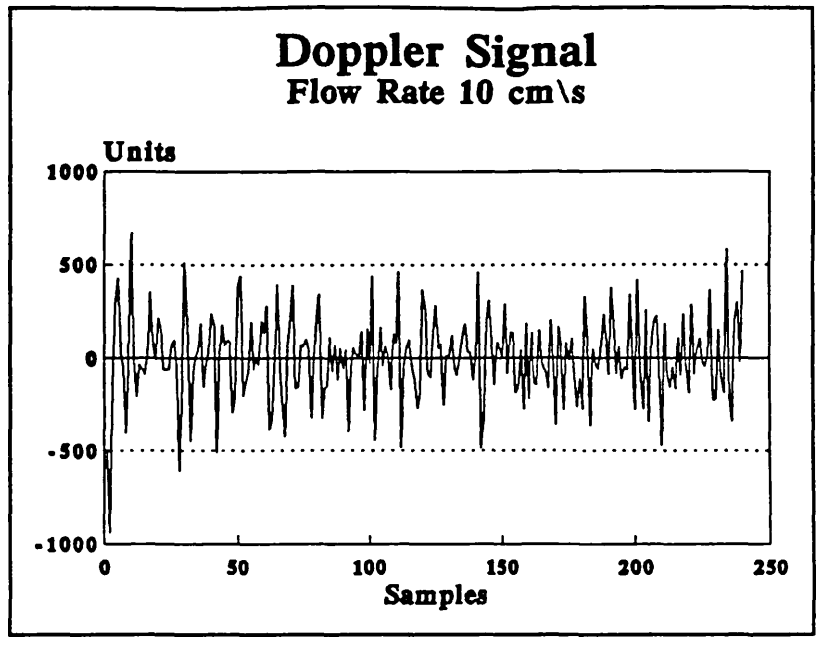


*Fig (6-7-a) : Unfiltered Doppler signal for flow rate of 10 cm/sec.*

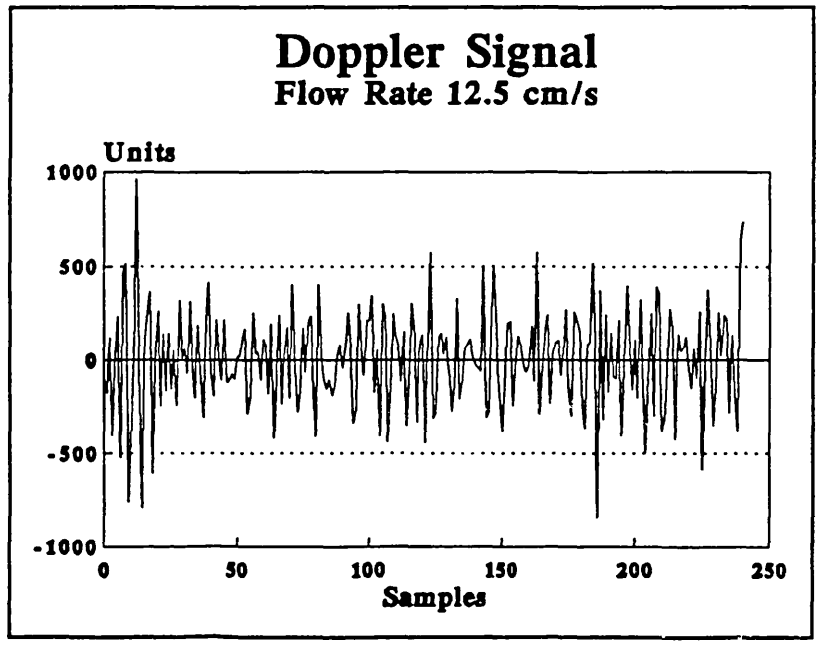


*Fig (6-7-b) : Unfiltered Doppler signal for flow rate of 12.5 cm/sec.*

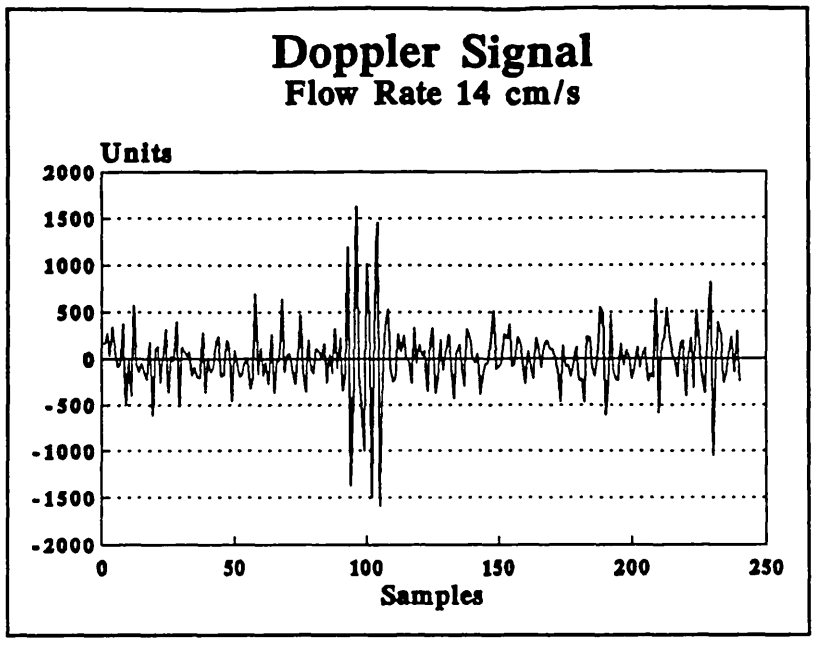


*Fig (6-7-c) : Unfiltered Doppler signal for flow rate of 14 cm/sec.*

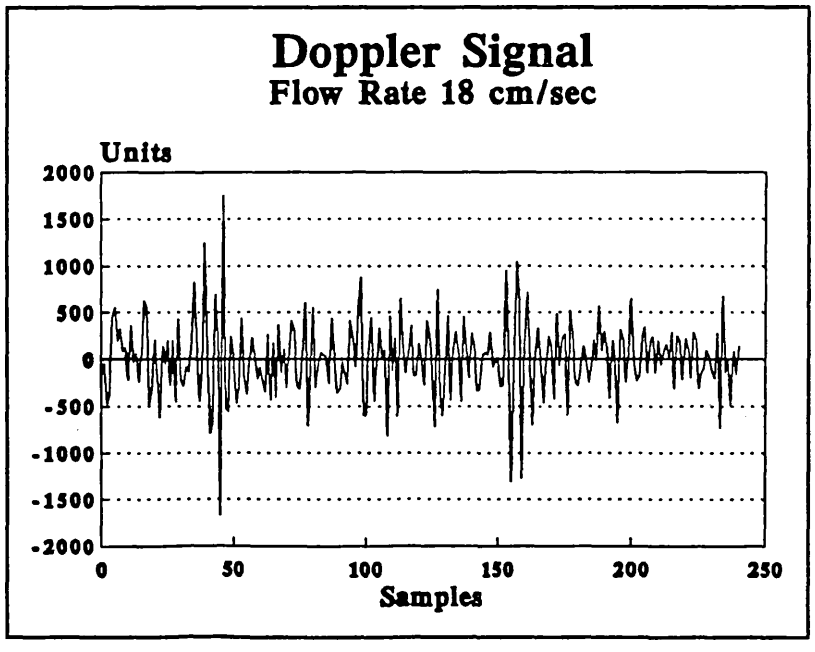


*Fig (6-7-d) : Unfiltered Doppler signal for flow rate of 18 cm/sec.*

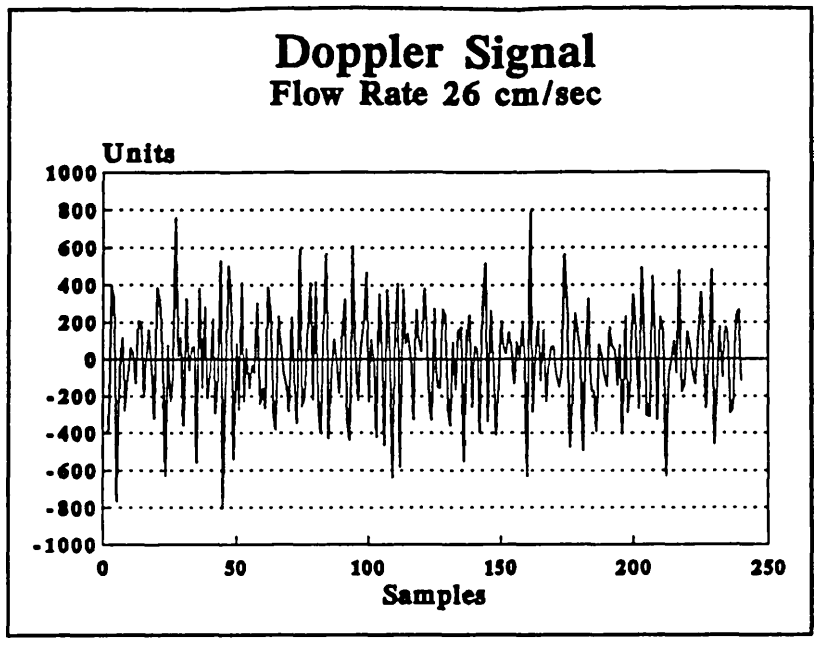


*Fig (6-7-e) : Unfiltered Doppler signal for flow rate of 26 cm/sec.*

In the first part of data analysis, by employing either Fast Fourier Transform or Auto Regressive Moving Average, the results did not correlate with the theory of Doppler shift effect. The relationship between frequency and flow velocity was completely unreliable. After more investigation it was found out that there is a powerful source of noise, probably generated by the machinery around the laboratory.

To find out the power and frequency of this noise a simple test was carried out. The transducer was placed inside the flow rig and the water stream was stopped. In other words, the only signal captured at the output of Doppler instrument was the noise caused by environmental or electrical factors.

This signal was analyzed and its FFT power spectral density is illustrated in Fig (6-8). As can be seen there is a powerful source of noise around 250 Hz. Also, there are other

considerable sources of noise particularly important at 50 Hz, 150 Hz.

This experiment was repeated several times and the obtained results convinced us of the necessity of pre-processing of the original Doppler signals by filtering them. To remove the high frequency noise the output of the Doppler instrument was first filtered through a 1 KHz low-pass filter. As will be explained later after the digitisation process the strange sharp harmonic noises were filtered through the necessary notch filters. These filters were designed in software to remove the noise signals at the frequencies of 50, and 240 Hz.

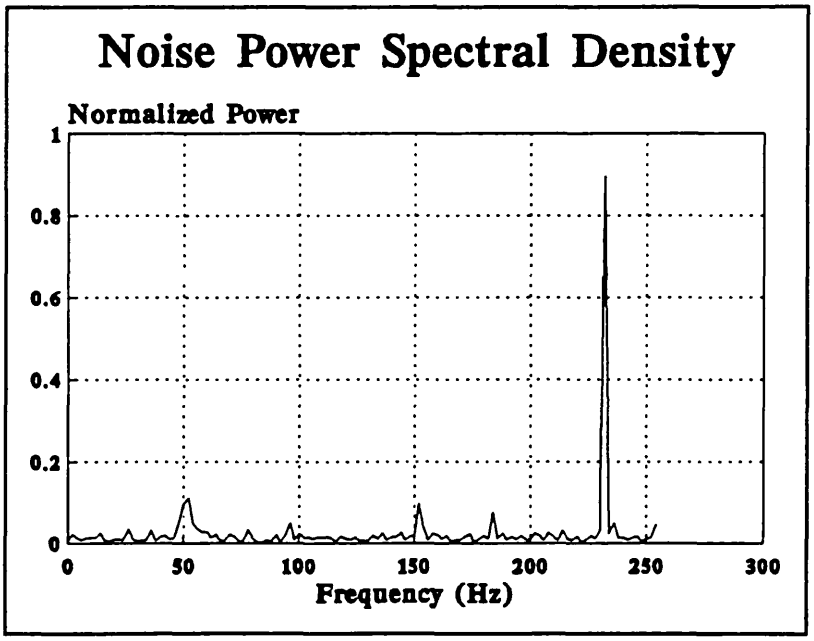


*Fig (6-8) : The FFT Spectral density of the noise.*

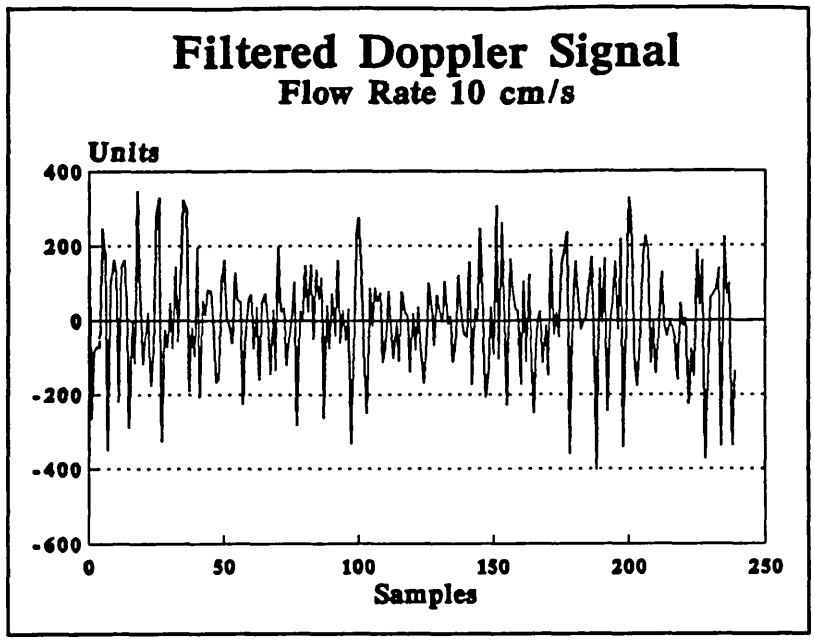


*Fig (6-9-a) : Filtered Doppler signal for flow rate of 10 cm/sec.*

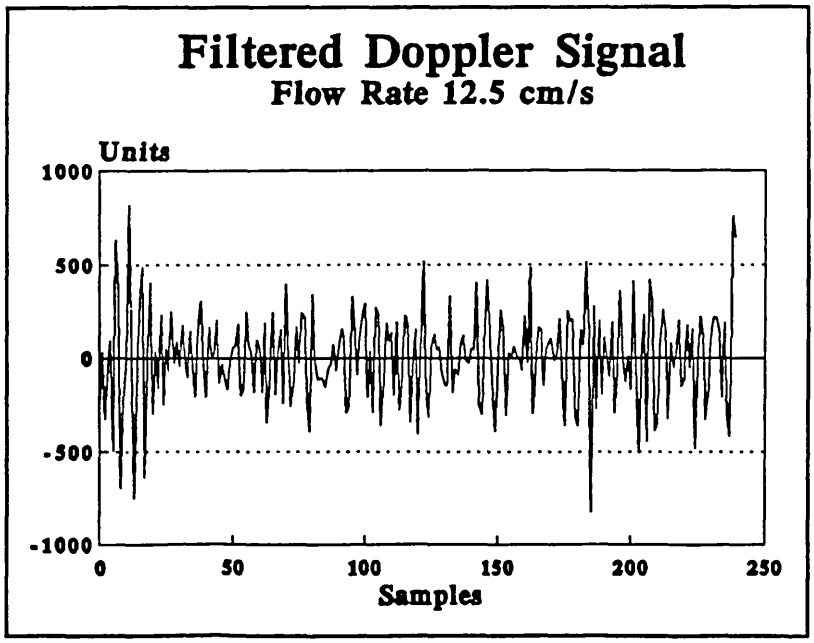


*Fig (6-9-b) : Filtered Doppler signal for flow rate of 12.5 cm/sec.*

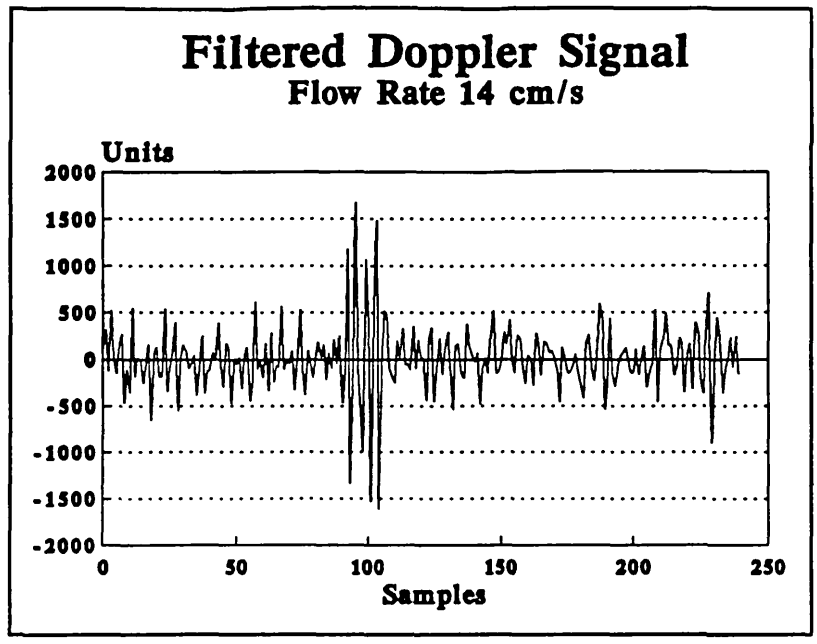


*Fig (6-9-c) : Filtered Doppler signal for flow rate of 14 cm/sec.*

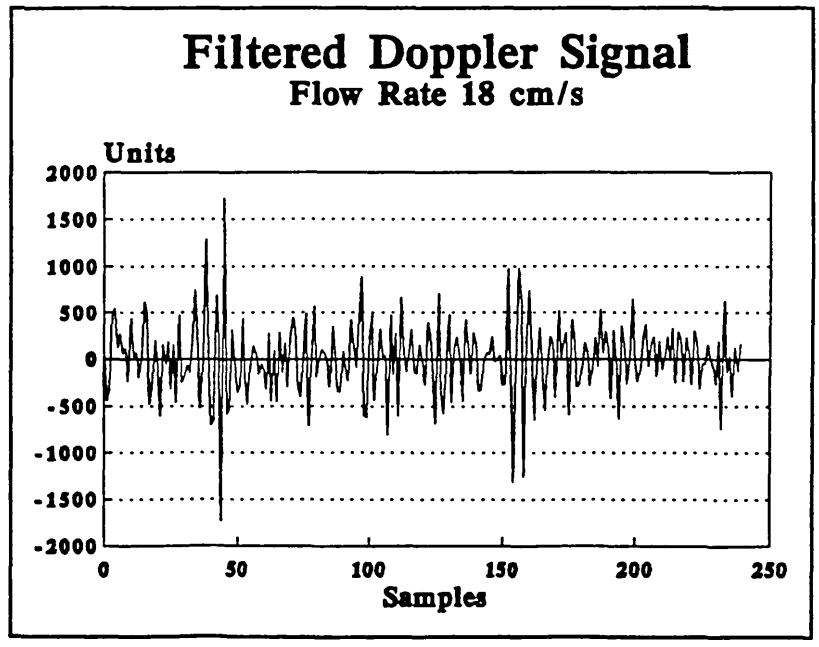


*Fig (6-9-d) : Filtered Doppler signal for flow rate of 18 cm/sec.*

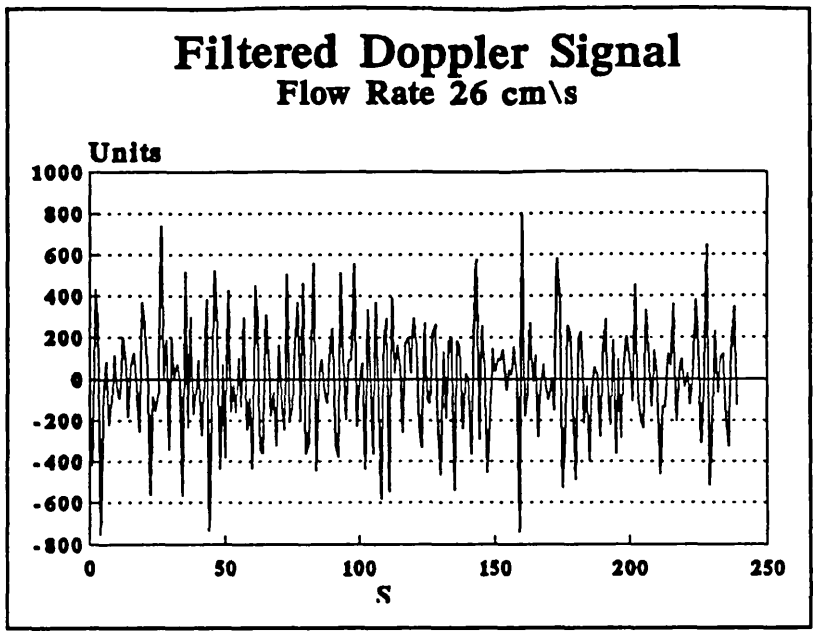


*Fig (6-9-e) : Filtered Doppler signal for flow rate of 26 cm/sec.*

In the first method it was decided to employ the FFT to process the Doppler signals. To obtain a better result the FFT was individually applied to 6 sets of data captured in a constant flow rate. Then the obtained power spectra were averaged. Therefore, the final result of this process is called Averaged FFT.

During this examination it was noted that if only one block of the Doppler signal is analyzed by using the FFT, it is difficult to observe a distinguishable shift in the mean frequency. However, after applying the FFT on six sets of individual Doppler signals, it was possible to see a more reliable shift of the mean frequency, $f_{mean}$. However, the frequency resolution of the FFT is not sufficient to distinguish the positions of peak frequencies.

To clarify the different stages of processing procedure, Fig (6-10) shows the flow chart of data acquisition and signal processing. It is seen that after the Doppler shift signal is generated, it is passed to a low-pass filter to cut off the unwanted frequencies above 1 KHz. Then the output of the filter is digitized and the data grabed by a personal computer. By means of a software DC remover filter the Doppler signal is cleared from the DC level shift. Then FFT algorithm is applied to provide the spectral power density of the Doppler signal. As it was mensioned before, there were some sources of strange periodic noises. Thus, the final stage of this process was to use the necessay notch filteres to remove the powerful noises.

The obtained results for Averaged FFT in different flow rates are presented in plates of Fig (6-11 a to e ).

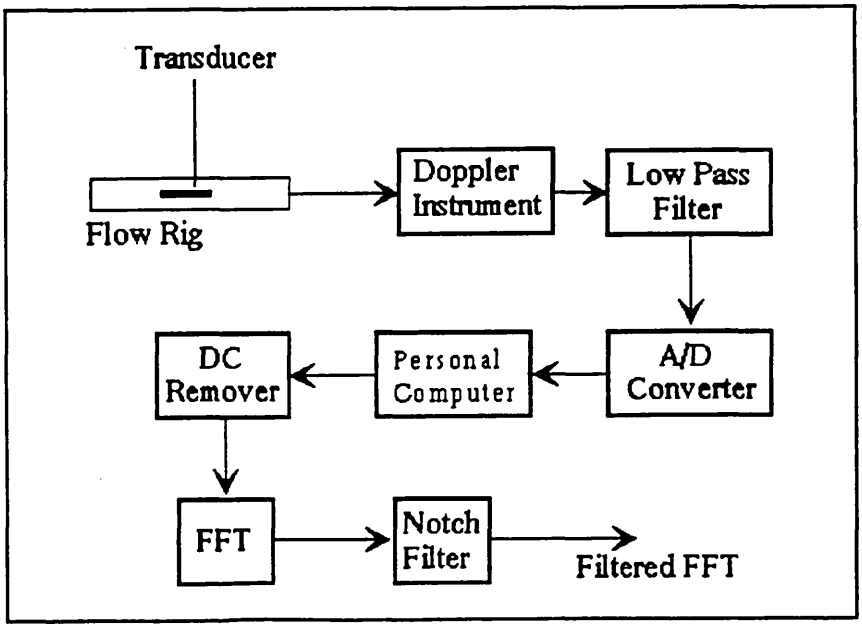


***Fig (6-10) : The flow chart of data acquisition and signal processing in Averaged FFT technique.***

The notch filter unit shown in Fig 6-10 contains three seperate stages of software notch filters operating at 50, 150, and 250 Hz. The nominal frequency of these stages were chosen on the basis of the obtained results shown in Fig (6-8). These filters are capable of smoothing the input signal spectrum to about five frequency bins around their nominal frequencies. It should be noted that the sampling frequency was fixed at 1 KHz and number of points per record is 256.

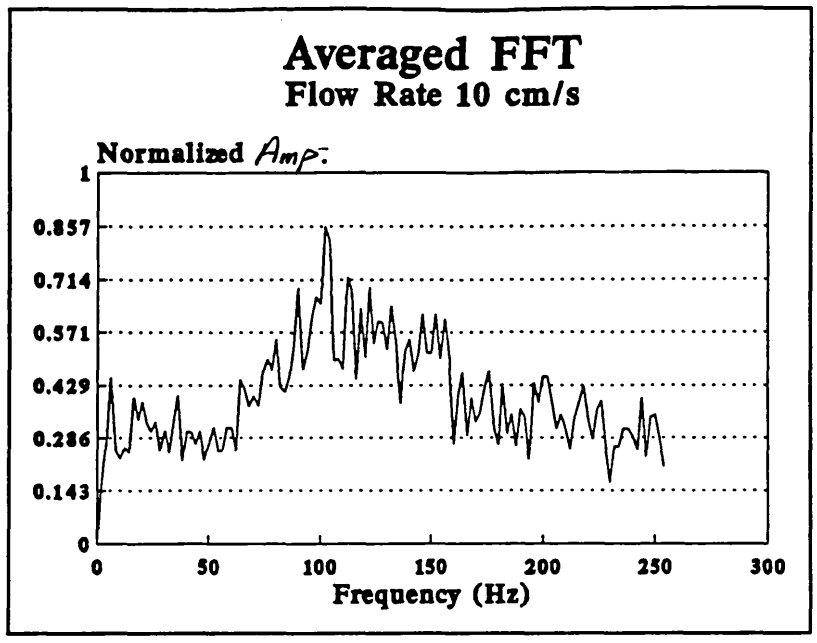


*Fig (6-11-a) : Averaged FFT spectrum for flow rate of 10 cm/sec.*

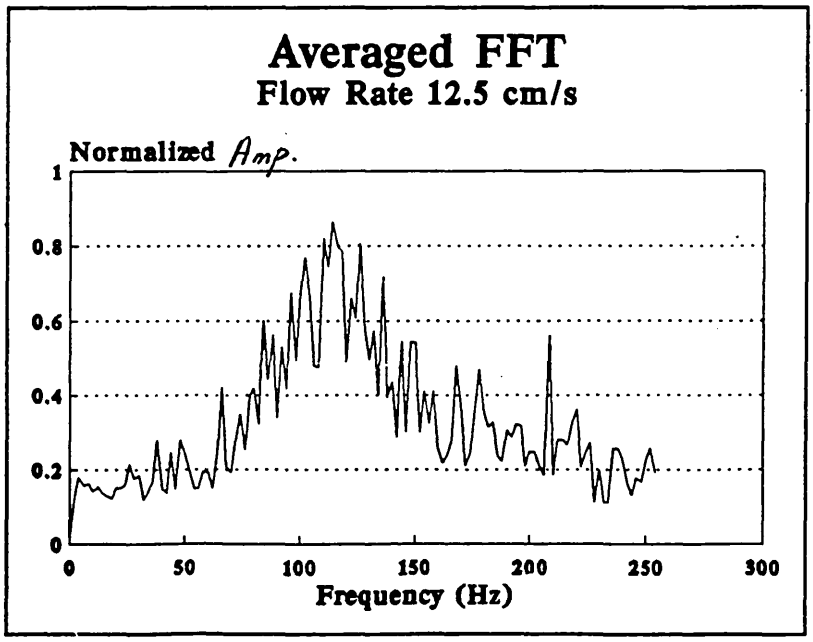


*Fig (6-11-b) : Averaged FFT spectrum for flow rate of 12.5 cm/sec.*

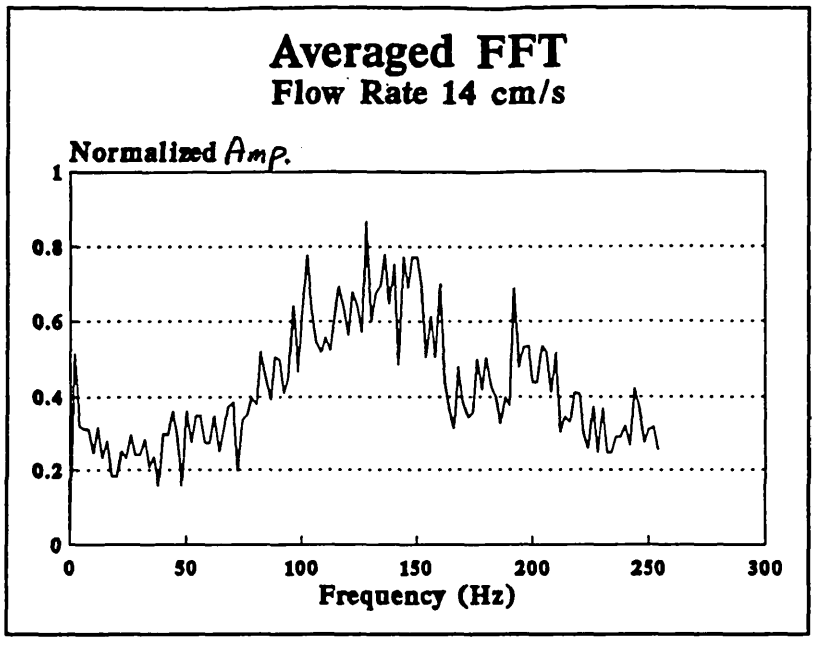


*Fig (6-11-c) : Averaged FFT spectrum for flow rate of 14 cm/sec.*

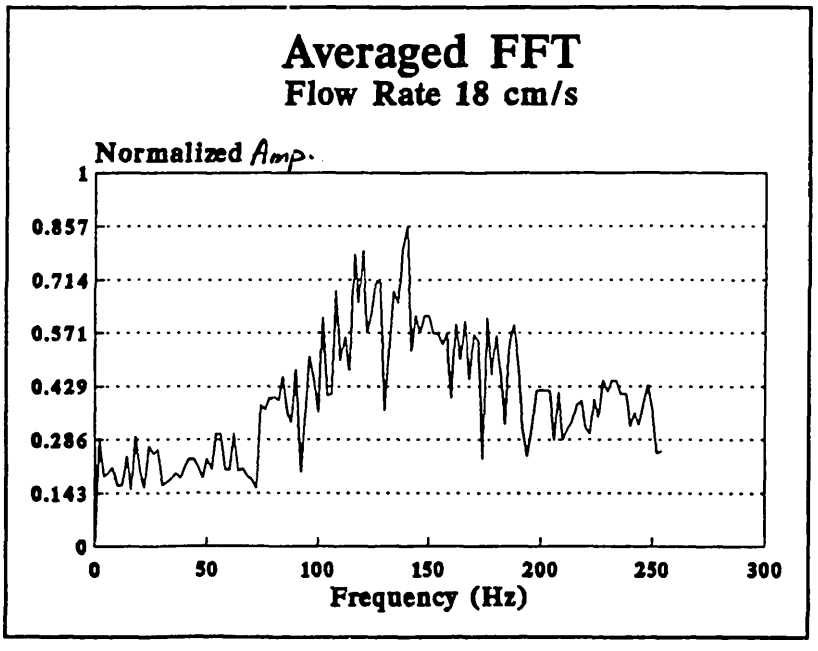


*Fig (6-11-d) : Averaged FFT spectrum for flow rate of 18 cm/sec.*

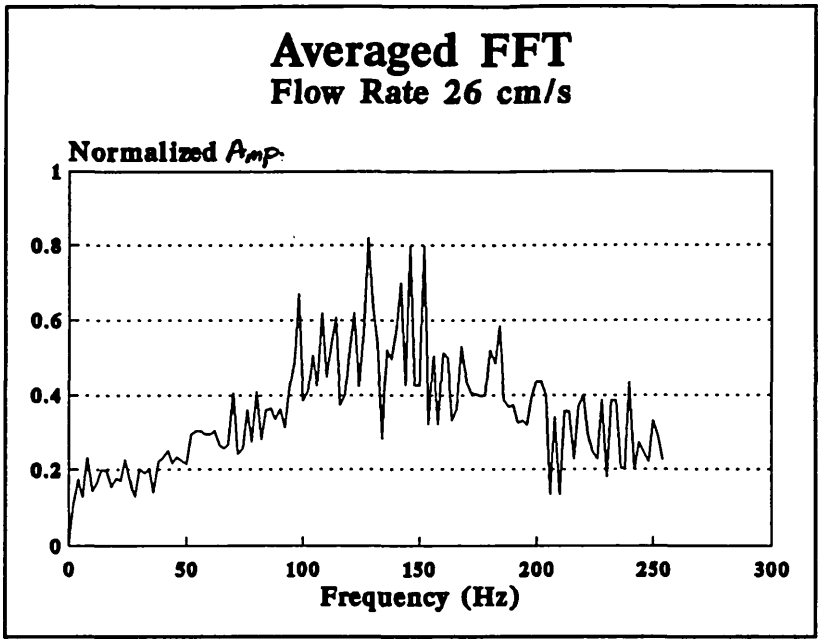


*Fig (6-11-e) : Averaged FFT spectrum for flow rate of 26 cm/sec.*

In the second part of our examination the Auto Regressive Moving Average (ARMA) algorithm was applied to the filtered Doppler signals. In the ARMA spectrum estimation it is assumed that the data can be produced in a random process described by :

$$x[n] = -\sum_{k=1}^{p} a[k]\, x[n-k] + \sum_{k=0}^{q} [b]\, u[n-k] \qquad (6\text{-}5)$$

where ***x[n]*** is the time series of the signal, and ***a[k]*** and ***b[k]*** are the associated time series to the model's system function. In other words these are the ***a[k]*** parameters form the autoregressive portion of the ARMA model and the ***b[k]*** parameters form the moving portion of the ARMA model, Marple (1987)[93].

In order to fit the ***a[k]*** and ***b[k]*** parameters to the Doppler signal, a Least Squares solution to the modified Yule-Walker equations can be used. The power spectrum can

be calculated from the $a[k]$, $(k = 1,p)$, and $b[k]$, $(k = 0, q)$. Therefore, the power spectrum can be defined as :

$$S(\omega) = \frac{|b[0] + b[1]e^{-j\omega T} + \ldots + b[q]e^{-j\omega T}|^2}{|1 + a[1]e^{-j\omega T} + a[2]e^{-2j\omega T} + \ldots + a[p]e^{-pj\omega T}|^2} \qquad (6\text{-}6)$$

where $p$ is the number of poles, $q$ is the number of zeroes associated with the model, and $T$ is the period of data sampeling, Papoulis (1984)[129].

In comparison to the FFT, it is possible to obtain higher resolution spectral estimates by employing the ARMA technique. Also, the results obtained show more reliable (lower variance) estimates. Fig (6-12) illustrates the flow chart of signal acquisition and signal processing.

In this method after FFT spectral estimation, the results were filtered by means of the necessary notch filters to remove the strange periodic noise. Then Inverse Fast Furrier Transform was applied to provide the original signal. To obtain the spectral power dencity, the ARMA technique was used to analyze the Doppler signals. It was noted that the ARMA technique provides very good results even with a lot of system noise. A noticeable fact was the capability of the ARMA technique in providing a high resolution effect in mean frequency shift. It was observed that without any need for averaging of the data or power spectra, it is possible to obtain good results from a single block of data signal.

Fig (6-13-a to e ) illustrates the results obtained by applying the Auto-Regressive Moving Average model on the Doppler's signals captured at the flow rates of 10 cm/sec, 12.5 cm/sec, 14 cm/sec, 18 cm/sec and 26 cm/sec, respectively.

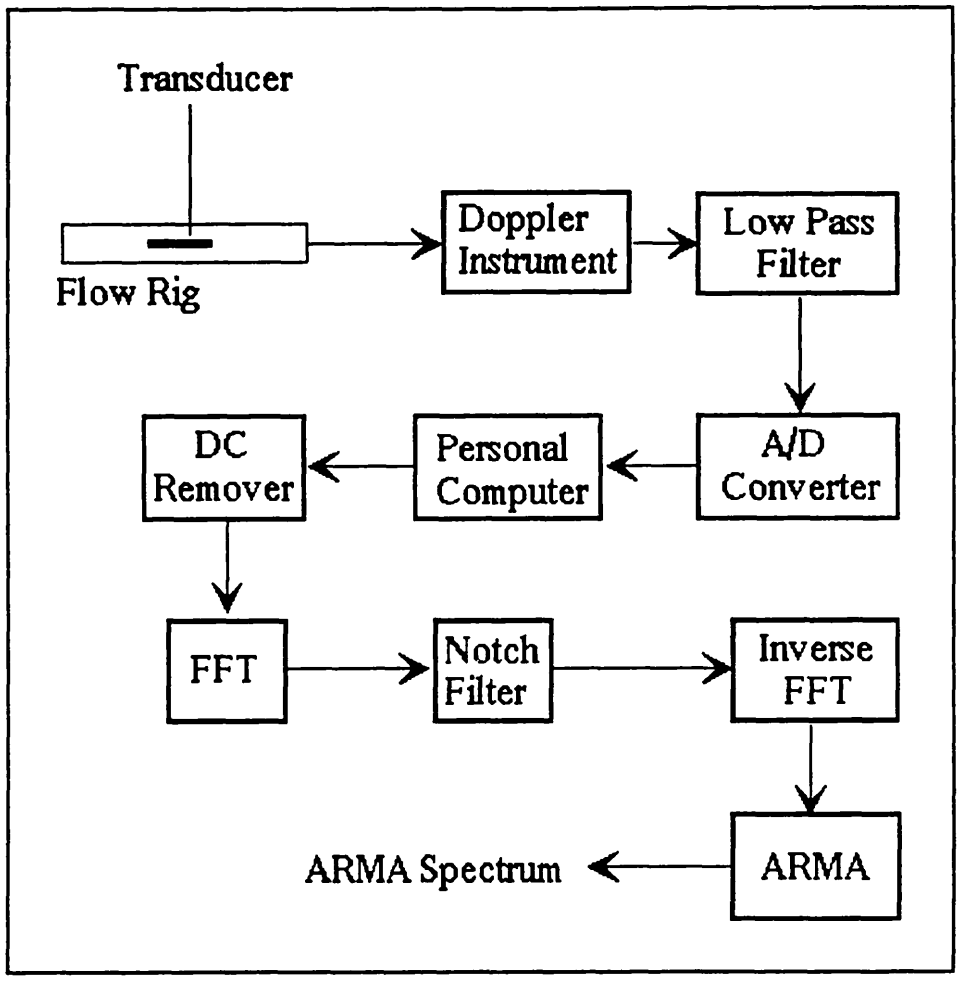


***Fig (6-12)** : The flow chart of data aquisition and signal processing for ARMA estimation model.*

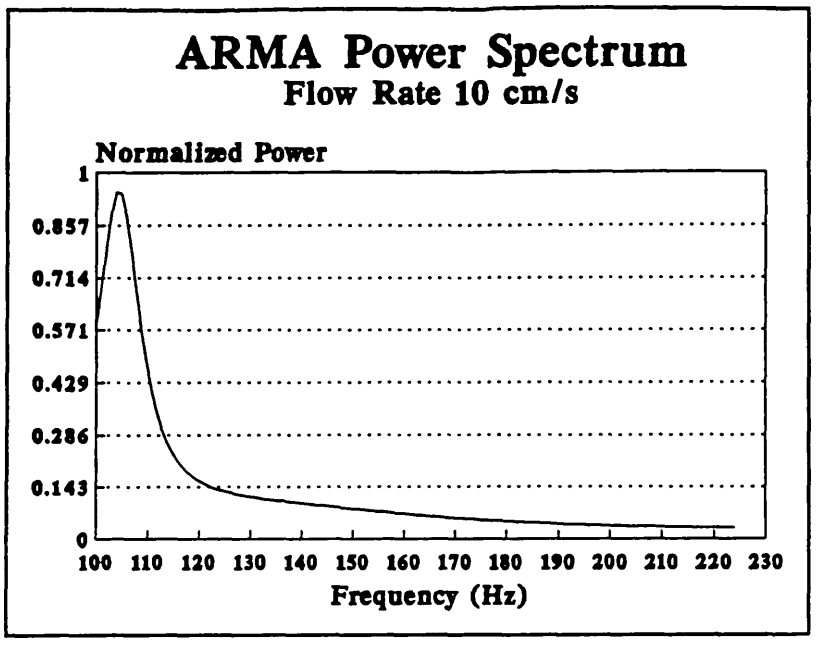


*Fig (6-13-a) : ARMA power spectrum for flow rate of 10 cm/sec.*

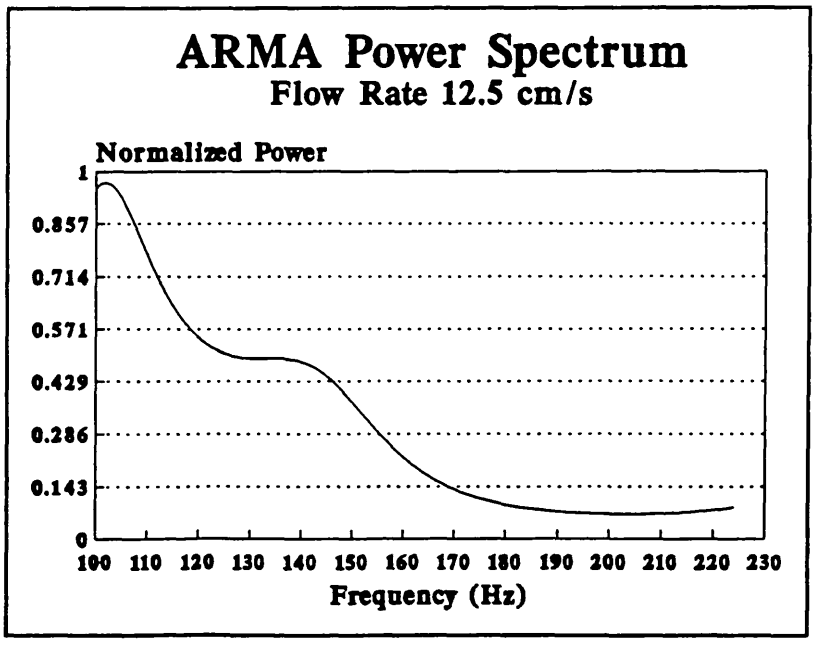


*Fig (6-13-b) : ARMA power spectrum for flow rate of 12.5 cm/sec.*

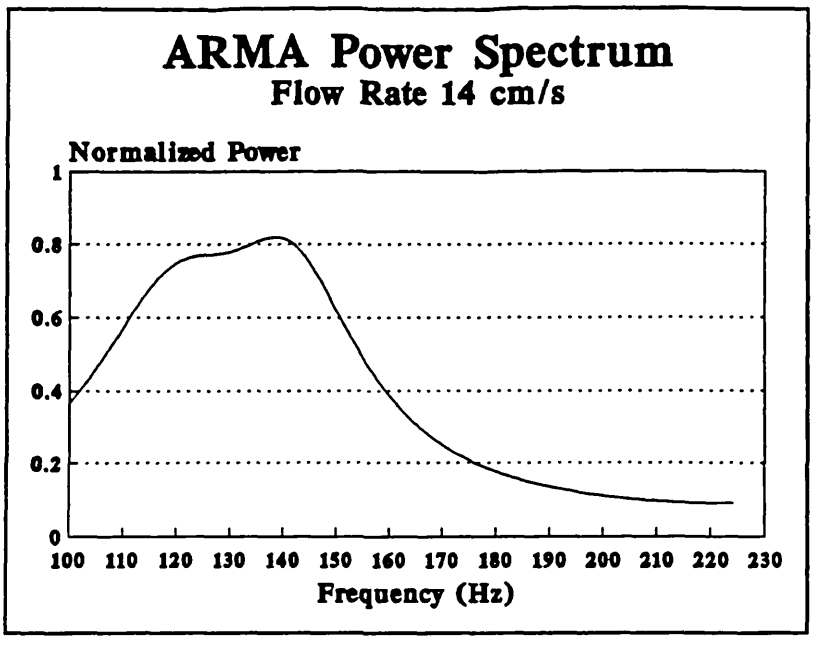


*Fig (6-13-c) : ARMA power spectrum for flow rate of 14 cm/sec.*

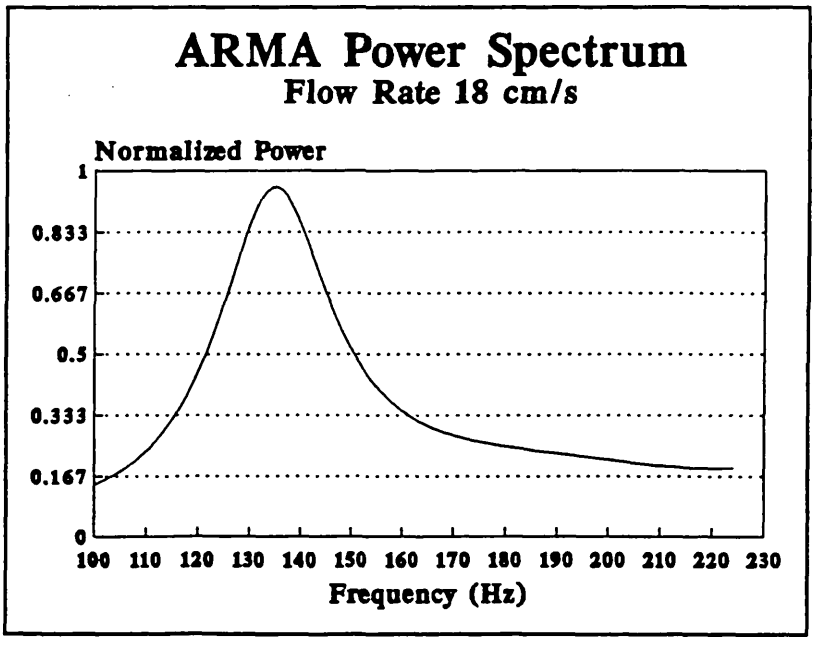


*Fig (6-13-d) : ARMA power spectrum for flow rate of 18 cm/sec.*

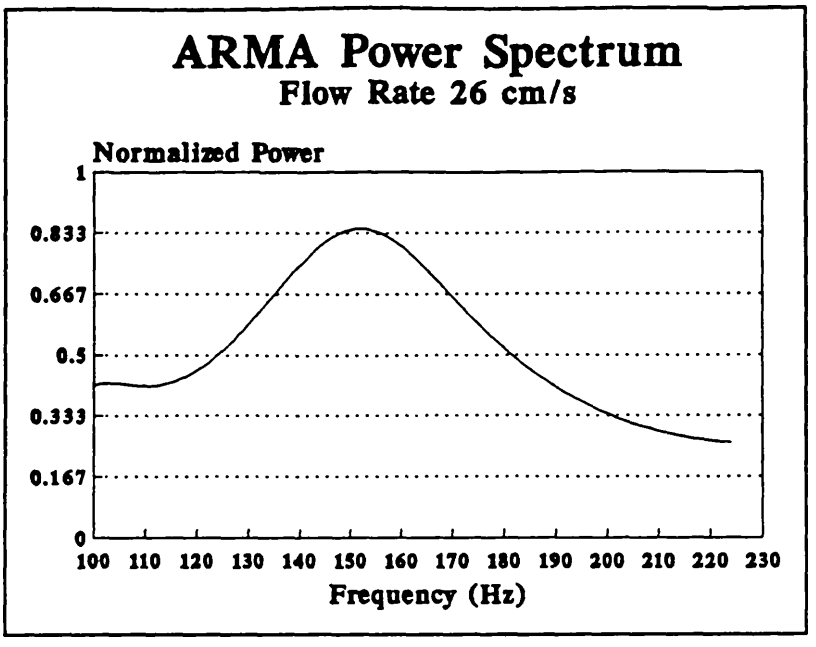


*Fig (6-13-e) : ARMA power spectrum for flow rate of 26 cm/sec.*

To investigate the accuracy of the experimental results, the first moment of the spectral density was calculated to obtain the mean frequency of each ARMA spectrum. Table (6-1) shows the mean frequency of each spectrum and its associated flow rate.

| Mean Frequency Estimates | |
|---|---|
| **Flow Rate** | **Mean Frequency** |
| 10.0 cm/sec | 128 Hz |
| 12.5 cm/sec | 135 Hz |
| 14.0 cm/sec | 143 Hz |
| 18.0 cm/sec | 153 Hz |
| 26.0 cm/sec | 159 Hz |

*Table (6-1)*

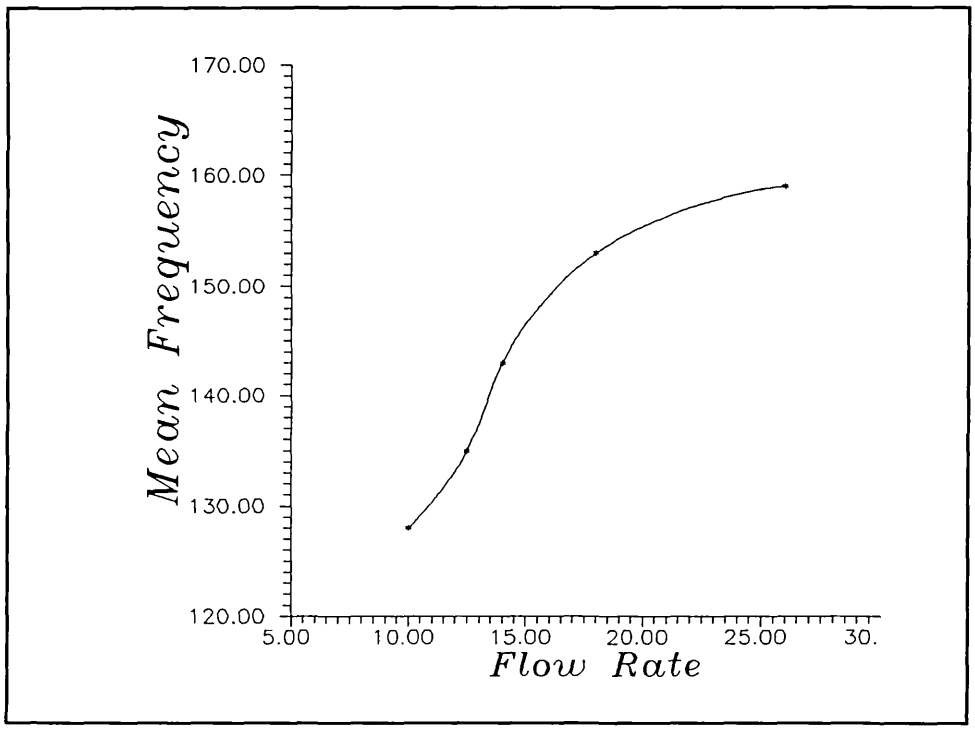


***Fig (6-14) :*** *The mean frequency versus flow rate.*

## 6-6 : CONCLUSION :

The experimental work of this chapter provides the capacity of Miniature Ring Array transducer in examination of transverse Doppler Effect. It was observed that the Auto Regressive Moving Average technique can be employed to produce high resolution power spectra for different flow rates. Also, it was shown that the computed mean frequencies show good agreement with theoretical aspects of the Doppler effect. In other words a clear increase in the mean frequency proportional to the increase in flow rate can be observed.

The work described so far, was considered a non-turbulent flow. Of course it is necessary to carry out more experimental work to examine the probable capacity of our catheter mounted transducer as a diagnostic tool in blood flow measurement.

If the signal to noise ratio could be improved, it should be possible to obtain an estimate of the absolute velocity in a similar fashion. To do this an estimate of the dominant flow angle is necessary which can be done on the basis of estimates for the maximum and the mean frequency.

*Chapter Seven*

# *Conclusions and Suggestions for Further Research*

## 7-1 : CONCLUSIONS :

In studying the preparation of the necessary material for transducer fabrication, electronic design and the work done by other people in the area of intravascular imaging, a great deal of knowledge has been gained which is of great importance. The most important aspects have been the discovery of the inherent capacity of man in solving problems, coping with problems with available tools and inventing novel techniques for easing the procedure of construction.

In a comprehensive review of the medical imaging systems, this work has further proven the fact that ultrasound imaging has established a new modality for medical diagnostic systems which has several priorities over other systems. In the first chapter of this thesis, where a review of the medical imaging systems was presented, it was seen that most

Medical imaging systems such as MRI, CT scanning, and X-ray are capable of providing images of good quality at the cost of very high investment on their foundation and maintenance. Looking into their constructions uncovered the fact that complicated structures of the systems need an advanced technology for their production which of course needs a great deal of expertise and financial investment.

Even for putting them into operation, especially trained personnel should be employed. In return for all the above mentioned drawbacks, they provide valuable images with high resolution. The capability and flexibility of these systems are highly dependent on the computer hardware and software. As computer hardware provides faster processing along with fast and cheap mass storage, it can be easier to improve the quality of the images captured by them.

On the other hand, these systems are highly software dependent. Nowadays much research is carried out to solve the problem of data storage, data comparison, and image enhancement on the output images produced by them. Another important fact is their physical source of radiation which makes them dangerous in long term operation. In particular this is true of X-ray and CT Scanning which utilize X-ray as their incident beam.

Considering all the above mentioned aspects of X-ray, Ct-scanning and MRI techniques, if we look at the portability, flexibility, and safety of ultrasound imaging systems we arrive at the key point of the wide spread and growing use of this technique. In particular, ultrasound imaging is the only technique which provides the facility for invasive diagnostic examination and even the imaging technique is cost effective in production, operation and maintenance. Adding to all these advantages, it is almost the

only portable system which provides a great deal of versatility for medical experts as well as general practitioners.

In Medical Ultrasound there has been no report of serious damage on human tissue caused by its application. This is another advantage of ultrasound which makes it the only safe technique for foetal examination during the pregnancy period. However, ultrasound has its own drawbacks. The resolution of images produced by ultrasound systems are usually poorer in comparison to those created by MRI and CT-scanning techniques. Since the spatial resolution is determined by the transducer geometry combined with the frequency and bandwidth of the ultrasound system, design and development of such a system requires careful attention to several delicate physical compromises. Thus, frequent improvements in one category will come at the expense of degradation in another. This is particularly true for sensitivity of the ultrasound transducer versus its perfect damping, and its special resolution versus depth of penetration.

At the same time different techniques employed in medical ultrasound systems have their own problems. Generation of two dimensional images is not possible with the A-mode technique. In B-mode and C-mode techniques it is possible to produce two dimensional grey level images, but each one has a fundamental problem which must be taken into account. In C-mode ultrasound despite the fact that it presents an image format similar to that obtained with X-ray fluoroscopy and is therefore more familiar to clinical radiologists, it has so far found no popularity in diagnostic medicine due to its relatively poor sensitivity and resolution.

B-mode ultrasound imaging is the most popular technique for the generation of 2D images. It has nevertheless some drawbacks which should be considered. For example

this technique suffers from an interference phenomenon which causes the mottled or speckled appearance of B-scan images. This phenomenon is caused by the interaction of the coherent waves produced by the transducer with the multiple scattering structure of tissue. On the basis of the first stage of this study, it is concluded that ultrasound is the most portable and safe technique in medical diagnostic applications, particularly for intravascular diagnostic examination and image reconstruction.

The second stage of this project was to acquire adequate knowledge about intravascular transducers with regards to their design and construction. These systems which are usually ultrasound transducers mounted on catheters have opened a new horizon in intravascular diagnostic examinations for more than a decade.The catheter mounted transducers are generally divided into two categories. First category contains a ring array of fixed elements of piezoelectric material mounted at the end of a catheter. The other class of catheter mounted transducers employs only one piezoelectric element which must be rotated to produce a complete closed slice 2 dimensional image of a slice of a vessel.

These two types of catheter mounted transducers have their own advantages and disadvantages some of which are common in both modalities. The first advantage of the fixed catheter mounted ring array transducers is their simple mechanical structures. It is much easier to fix elements on a stator transducer body than a rotator one. Of course this is at the expense of limited lateral resolution due to the limited number of piezoelectric elements.

On the other hand, although rotating catheter mounted transducers can provide very high lateral resolution due to their portable flexibility to capture data in any angle with an incremental step of 0.5°, they need a highly mechanical force transmission facilities.

Another problem of rotating type transducers is lack of accurate angle estimation in an actual examination. If it is decided to have the benefit of their capacity for rotation at any angle, then it is necessary to provide an accurate method of control and assessment of the angle of ultrasound beam generation.

There are prominent points common to both models. The catheter mounted ultrasound transducers are the only intravascular imaging transducers capable of not only viewing the internal surface of vessels, but also allowing visual inspection of almost the entire lumen of the vascular anatomy. The results obtained in this project and works done by other researchers have proved that images of diagnostic quality can be achieved. Catheter mounted transducers of either fixed ring array type or single rotating element can perform an important role in vascular angioplasty and surgery as an imaging and monitoring tool during the course of operations as well as recovery.

However, both types of catheter mounted transducers have some common problems which must be considered. The first problem relates to the small size of these transducer. It is obvious that to make them as small as possible it is necessary compromise on some issues. One of the fundamental elements in an ultrasound transducer is the piezoelectric element. To decrease the size of the transducer it is necessary to lower the thickness of the piezoelectric element which means having to use a high frequency piezoelectric material. Therefore, we are constrained to increase the bandwidth of the electronic circuitry and employ faster digitizers for analog to digital conversion. In addition, the fragile property of the piezoelectric element due to its tiny thickness makes the process of cutting and mounting of it on the body of the transducer a more difficult task.

Another problem which is of paramount importance concerns the connecting of the

electrical leads to the transducer's element(s) and coating them with suitable material. These factors are of more importance when it is decided to construct a rotating single element transducer. In this case, in addition to electrical consideration, it is necessary to pay careful attention to the mechanical requirements of the transducer. So far silver loaded epoxy resin and low temperature solders are the most common materials used in ultrasound transducer fabrications. However, considering the very tiny dimensions of the piezoelectric element on a catheter mounted transducer, and particularly in the case of fixed ring array transducers it is necessary to employ a specially built soldering tip and even cleaning flux.

The most important problem associated with catheter mounted transducers is the necessary methods for their localization. It is very important to ensure that the acquired block of data is decisively related to a complete slice of the vessel almost perpendicular to the transducer axis. It is obvious that any unpredictable movement of the transducer tip can provide false information which ends to misleading the system user.

On the basis of our survey on the catheter mounted transducers, the next stage of this project fulfilled the production of a Miniature Ring Array transducer with an overall diameter of 2mm .

During the different stages of prototype construction and necessary examination, it was discovered that working with tiny elements such as the transducer body, piezoelectric elements and micro-coaxial cables, requires precision tools and a great deal of care. During the mounting process and later in connecting the electrical leads to the piezoelectric element it was learnt that cleanliness of the joining objects has a particular importance. In addition it is necessary to place and hold these small pieces in their

locations during the mounting and connecting processes. Providing a small soldering joint also needs its own technique. It is possible to cut a very tiny piece of solder and place it at the point of soldering joint. This technique sometimes fails to work, this is due to the greasy surfaces and soldering irons tip. Therefore, having the joint surfaces and soldering irons tip cleaned can be a major key to simplifying the process of mounting the piezoelectric element.

One of the important lessons learnt in this stage was the necessary consideration of the catheter size, its flexibility and its construction. Each micro-coaxial cable has an overall diameter of 0.2 mm and considering the required number of them(12), it is necessary to make sure that enough space and necessary lumens for cable guide wires and some reserved lumens for load or drug transfusion are available.

Of course the internal construction of the catheter plays an important role in the flexibility and guidance of the mounted transducer at its end. In the course of this study it was learnt that it could be very helpful to have a special type of catheter containing the micro-coaxes inside its lumen wall. In this case due to the automatic placement of the cables they could be placed in parallel with some gaps which helps for having durable and more flexible transducer catheters.

We also discovered the need for a particular substance as the backing material. This should be a material with ease of shaping and manipulation. In the miniature transducers such as the one produced in this work the spatial gap behind the piezoelectric element is very small and particularly after the mounting process of these elements access to this space is very difficult. Therefore, there are two ways of fulfilling the act of putting the backing material behind the transducer element. It is either possible to put the backing

material before the elements are placed or inject it after the mounting process. In this work it was concluded that for having better coupling with a minimum air gap it is better to inject a high viscosity material such as wax which can be changed to a low acoustic impedance solid material at lower temperatures.

It was required to find a suitable material as an electrical insulator as well as a probable matching layer. Study of matching layers and their result on the pulsed ultrasound transducers was beyond the subject of this thesis, but encouraging reports were found in the literature about sensible improvements of even pulsed ultrasound transducers with matching layers. Therefore, it was decided to employ a special surgical spray mostly as an electrical insulator and possibly as a matching layer.

In the design of the hardware developed as one of the main component of this thesis the following observations were made. As the system developed was to be used in a clinical environment, special care was taken in making the size of the hardware relatively small. It was also important to keep the cost low hence implying the utilisation of commercially available components in the market.

In view of the effect of various active and passive components in analogue circuitry it was discovered the layout of these component in relation of each other made a great deal of difference to the performance of the circuit in terms of signal to noise ratio. We discovered the optimal positions of these components particularly the inductor and high frequency operational amplifiers. These optimal positions were arrived at partly based on the theory but mostly as a result of our own experimentation. This important fact should be born in mind by those wishing to design future similar circuitry.

In the study of phantoms using the MRAT excellent images were obtained of the volumes under investigation. Several phantoms were examined with the MRAT placed at the centre of each one. The MRAT showed itself capable of acquiring very accurate data on each occasion thus producing highly visual three dimensional images after reconstruction. The signal obtained was strongest when the MRAT was placed at the centre of the Phantom but this did not imply the lack of accuracy when the transducer was slightly out of position.

Stenosis in a blood vessel was simulated by placing blu-tac in one of the phantoms. Again good signals were obtained from the phantom which when reconstructed in 3D gave an excellent picture of the obstruction within the phantom. This was believed to be a very important result obtained as it proved the system capable of detecting irregularities in a cylindrical volume.

In exposing the MRAT to in-vitro measurements the results were promising for both healthy and diseased tissues. Even though in each case only eight slices of the artery were used in 3D reconstruction, the resulting pictures reveal a great deal of information about the anatomy of the specimen under investigation hence supporting our claim for its use as a diagnostic tool in a clinical environment. In the case of the diseased aortic tissue the picture clearly reveals a significant incursion by the plaque into the lumen.

We also experimented with the use of our one element transducer as a tool for blood flow measurement. We used the Fast Fourier Transform algorithm on the data obtained and can conclude that Classical Doppler has a greater effect when using this technique. When we switched to using the Auto Regressive Moving Average (ARMA) algorithm, it was evident that the transverse Doppler effect became much more apparent.

This was because the power spectra obtained in this case were much more clear and had a superior frequency resolution. On this basis we can conclude that there are significant advances to be made in devising better spectral analysis signal processing algorithms for blood flow measurements. These techniques could be used in furthering the use of intravascular ultrasound transducers for detecting blood flow irregularities and relating them to abnormal vascular structures.

## 7-2 : SUGGESTIONS FOR FURTHER RESEARCH :

Having spent some time in the research, design and development of the various components of the system, there are naturally many useful suggestions that the author would wish to recommend to anyone wishing to further this work. However, in this section a broad spectrum of points considered most vital in doing future investigations will be outlined. These can be put into four separate categories, Hardware, Software, Transducer design and further examinations.

In terms of furthering the hardware design, with the current availability of fast and powerful processors and the trend towards parallel processing, connection of a number of these processors together can create a very valuable real time visualisation system. This is a possibility today with the availability of processors such as transputers, signal processing chips, etc.

As axial resolution and tissue characterisation are of great importance in vascular imaging, increasing the operating frequency to 20MHz or more would facilitate these issues. Therefore, it is important to design such a system in any future research, having

a wider bandwidth, a faster A/D converter and faster memory chips. It is also considered necessary to study the reduction of the number of cables used in the catheter by means of a local multiplexer close to the transducer. This would enable the use of a thinner catheter and also greatly reduce the cost of production.

In terms of enhancements to the software, the development and study of tissue characterisation from ultrasound images poses a great challenge. In chapter five we were unable to represent normal and diseased tissues in different colours. Separation of these tissues by the appropriate algorithms would enable this, leading to clear understanding of diseased regions by the physician.

Another software enhancement would be to code many of the existing algorithms in assembler so that processing speeds can be improved, thus moving towards real time processing. If transputers are used for any future work, the use of a highly optimised language with mathematically proven performance such as OCCAM is recommended.

As it is important to have a degree of certainty about the data captured at a point, it is necessary to establish the localisation of the transducer very accurately. Not much work has been done in this area and it remains open for future investigation. At the same time in single element rotating transducers, control of the rotation and the direction of beam propagation needs further research.

As mentioned previously, increasing the operating frequency of the transducer would greatly aid tissue characterisation. It is recommended that further research is carried out in designing higher frequency transducers. This requires the study of other high frequency piezoelectric materials such as PVDF. If this material is suitable, further

development of suitable transceivers needs to be investigated in order to improve the poor electromechanical coupling factors of PVDF.

An important factor in making the catheter mounted transducer into a routinely used tool would be the investigation of the durability of the mechanical coupling and the safety factors involved in these joints. Great risks would be involved in using such devices without a scientific study of these joints.

In using the current MRAT we have noticed that the probe needs to be tested on phantoms that are thinner and longer. This would simulate a more realistic situation of a clinical examination. In case the system is developed further we will be in a position to carry out in-vivo measurements. This would require a higher signal to noise ratio, necessary for clinical applications and in accordance with medical standards of electronic devices. It would also be necessary to reduce the diameter of the catheter mounted transducer possibly to 1mm.This would prepare the use of the system for in-vivo measurements.

# *Refrences*


[1] **ALIAS P.**, "*Real-Time Acoustic Imaging with a 256x256 Matrix of Electronic Transducers*", Acoustic Holography, Vol. 5, New York, Plenume Press, pp. 671-684, **1974**.

[2] **ALLBON SAUNDERS Ltd.**, Pembroke Lane, Milton, Nr. Abingdon, Oxfordshire, OX14 4EA, ENGLAND.

[3] **ARDITI.M.**, **FOSTER.F.S.**, and **HUNT.J.W.**, " *Transient Fields of Concave Annular Arrays* ", Ultrasonic Imaging 3, pp. 37-61 , **1981**.

[4] **ASHFORD T.P.** and **FREIMAN D.G.**, "*Platelet Aggregation at Sites of Minimal Endothelial Injury*", American Journal of Pathology, Vol. 53, pp. 599, **1968**.

[5] **ASMUSSEN M.**, **LINDSTROM K.** and **ULMSTEN U.**, "*A Catheter-Manometer Calibrator - A New Clinical Instrument*", Biomedical Engineering, pp. 175-180, May **1975**.

[6] **BAINTON.K.F.**, and **SILK.M.G.**, " *Some factors which affect the performance of ultrasonic transducers* ", British Journal of NDT, pp. 15-20, January **1980**.

[7] **BARZILAI B.**, **SAFFITZ J.E.**, **MILLER J.G.**, and **SOBEL B.E.**, "*Quantitative Ultrasonic Characterization of the Nature of Atherosclerotic Plaques in Human Aorta*", Circulation Research, Vol. 60, No. 3, pp. 459-463, March **1987**.

[8] **BEAVER.W.L.**, " *A Method of Three Dimentional Electronic Focusing and Beam Steering Using Electronic delay Lines*" , IEEE Cat. 75 CHO 994-4SU, Ultrasonic Symposium Proceedings, pp. 88-90, **1975**.

[9] **BEAVER.W.L.**, " *Phase Error Effects in Phased Array Beam Steering* ", IEEE Cat. 77CH1264-1SU, Ultrasonic Symposium Proceedings, pp. 264-267, **1977**.

[10] **BERGMANN L.**, "*Der Ultraschall*", 6th edition, Hirzel, Stuttgart, **1954**.

[12] **BLITZ J.**, "*Fundamentals of Ultrasonics*", 2nd edition,, Butterworth, London, **1967**.

[13] **BIOCH F.**, "*Nuclear Induction*", Phys. Rev., Vol. 70, pp. 460, **1946**.

[14] **BLOOMFIELD P.E.**, "*Piezo and Piro electricity in polyvinylidene Flouride*", Naval Research Rev., Penntwalt Corp., 31.1, **1987**.

[15] **BODY D.P.**, and **PARKER D.L.**, "*Basic Prinsiples of Computed Tomography*", in Computed Tomography of the Body, Edited by Moss A.A., Gamsu G., and Genant H.K., WB Saunders, Philadelphia, **1983**.

[15] Bom N., **LANCEE C.T.** and **Van EGMOND F.C.**, "*An Ultrasonic Intracardiac Scanner*", Ultrasonics, pp. 72-76, March **1972**.

[17] **BOM N., SLAGER C.J., VAN EGMOND F.C., LANCEE C.T.** and **SERRUYS P.W.** "*Intra-Arterial Ultrasonic Imaging For Recanalization by Spark Erosion*", Proceedings of SPIE, Vol. 904 Microsensors and Catheter-Based Imaging Technology, pp. 107-109, January **1988**.

[18] **BRUNEEL C., DELANNOY B., TORGUET R., BRIDOUX E.** and **LASOTA H.**, "*Electrical Coupling Effects in an Ultrasonic Transducer Array*", Ultrasonics, Vol. 17, pp. 255-260, November **1979**.

[19] **BurCKHARDT C.B., GRANDCHAMP P.A.**, and **HOFFMANN H.**, "*Focussing Ultrasound Over a Large Depth with an Annular Transducer - An Alternative Methode*", IEEE Transactions on Sonics and Ultrasonics, Vol. SU-22, No. 1, pp. 11-15, January **1975**.

[19a] **BUDINGER T.F.**, "*Physical attributes of Single-Photon Tomography*", J. Nucl. Med. Vol. 21, pp. 579, **1980**.

[20] **BUDINGER T.F., DERENZO S.E.,** and **HUESMAN R.H.**, "*Instrumentation for Positron Emission Tomography*", Ann. Neurol., Vol. 15 (Suppl):S35, **1984**.

[21] **BUDINGER T.F., GULLBERG G.T.,** and **HUESMAN R.H.**, "*Emmission Computed Tomography*"' in Image Reconstruction from Projections: Implementation and Applications, Edited by Herman G.T. ,pp.147-246, Springer-Verlag, New York, **1979**.

[22] **BUI L., SHAW H.J.** and **ZITELLI L.T.**, "*Experimental Broadband Ultrasonic Transducers using PVF, Piezoelectric Film*", Electronic Letters, Vol-12, pp. 393-394, AUG **1976**.

[23] **CADY W.G.**, "*Piezoelectricity*", Mc Graw Hill, New York, **1949**.

[24] **CARLETON R.A., SESSIONS R.W.,** and **GRAETTINGER J.S.**, "*Diameter of Heart Measured by Intracavitary Ultrasound*", Medical Research Engineering, pp. 28-32, May-June **1969**.

[25] CENSOR D., **NEWHOUSE V.L., VONTZ T.,** and **ORTEGA H.V.**, "*Theory of Ultrasound Doppler-Spectra Velocimetry for Arbitrary Beam and Flow Configurations*", IEEE Transactions on Biomedical Engineering, Vol. 35, No. 9, pp. 740-751, Sept. 1988.

[26] **CISNEROS J.A.**, "*Medical Applications of Doppler Spectral AnalysisUsing a Normal Orientation of the Beam with Respect to the Direction of Flow*", Ph.D. Dissertation, Drexel University, Philadelphia, PA., 1985.

[27] **CHRISTENSEN D.A.**, "*Ultrasonic Bioinstrumentation*", John Wiley & Sons, New York, **1988**.

[28] **CHIVERS R.C.**, "*The scattering of ultrasound by human tissue - Some theoritical models*", Ultrasound Med. Biol., Vol. 3, pp. 1-13, **1977**.

[29] **COATES R.** and **MATHAMS R.F.**, "*Design of Matching Networks for Acousti Transducers*", Ultrasonics, Vol. 26, pp. 59-64, March **1988**.

[30] **COLE J.S. & HARTLEY C.J.**, "*The Pulsed Doppler Coronary Artery Catheter Preliminary Report of a New Technique for Measuring Rapid Changesin Coronery Artery Flow Velocity in Man*", Circulation, Vol. 56, No. 1, pp. 18-25, July **1977**.

[31] **COLLIN.R.E.**, "*Theory and Design of Wide-Band Multisection Quarter-Wave Transformers*", Proceedings of the I.R.E, pp. 179-185, February **1955**.

[32] **CORMACK A.M.**, "*Nobel Prize Acceptance Speech. Early Two-Dimenssional Reconstruction and Recent Topics Stemming from It*", Med. Phys. Vol. 7, pp. 277-283, **1980**.

[33] **CROOKS L.E.**, "*Overview of NMR imaging Techniques, in Nuclear Magnetic Resonance Imaging in Medicine*", edited by Kaufman L., Crooks L.E., and Margulis A.R., Igaku-Shoin, Tokyo, pp.30-52, **1981**.

[34] **DEHN J.T.**, " *Interference Patterns in the Near Field of a Circular Piston*", The Journal of the Acoustical Society of America, Vol. 32, No. 12, pp. 1692-1696,December **1960**.

[35] **DE JONG. N., SOUQUET.J., FABER.G.**, and **BOM.N.**, "*Vibration modes. Matching layers and grating lobes*", Ultrasonics, Vol. 23, pp. 176-182, July **1985**.

[36] **DEKKER.D.L., PIZIALI.R.L.** and, **DONG Jr. D.**, "*Effect of boundry conditions on the ultrasonic-beam charactristics of circular disks*", J.Acoust.Soc.Am., Vol.56, No.1, pp. 87-93, July **1974**.

[37] **Delpy D.T.**,"*A Cathter-Tip Capacitance Pressure Transducer*", Biomedical Engineering, pp. 16-20, January **1975**.

[38] **DESILET S.C, FRASE J.D** and **KINO G.S.** , "*The Design of Efficient Broad-Band Piezoelectric Transducers*" IEEE Transactions on Sonic and Ultrasonics , Vol. SU-25, No.3, pp. 115-125, May **1978**.

[39] **DETER R.L.** and **HOBBINS J.C.**, "*A Survay of Abdominal Ultrasound Scanners: The Clinician's Point of View*", Proceedings of the IEEE, Vol. 67, No. 4, pp. 664-671, April **1979**.

[40] **DIAS J.F.**, "*Construction and Performance of an Experimental Phased Array Acoustic Imaging Transducer*", Ultrasonic Imaging, Vol. 3, pp. 352-368, **1981**.

[41] **DIETZ.D.R., PARKS.S.I., LINZER.M.**, "*Expanding-aperture Annular Array*", Ultrasonic Imaging, Vol.1, No.1, pp. 56-75, **1979**.

[42] **DOBBS E.R.**, "*Electromagnetic Generation of Ultrasonic Waves*" In Physical Acoustic, edited by Mason W.P. and Thurston R.N., Vol. 10, pp. 127-191, Academic Press, New York, **1973**.

[43] **EGGLETON R.A., TOWNSEND C., KOSSOFF G., HERRICK J., HUNT R., TEMPLETON G.** and **MITCHELL J.H.**, "*Computerised Ultrasonic Visualisation of Dynamic Ventricular Configurations*", 8th ICMBE, Palmer House, Chicago, Illinois, July **1969**.

[44] **ELLIS R.A., CROWLEY R.J.** and **EYLLON M.M.**, "*Ultrasonic Imaging Catheter*", Proceedings of SPIE, Vol. 904 Microsensors and Catheter-Based Imaging Technology, pp. 127-130, January **1988**.

[45] **ERIKSON.K.R., FRY.F.J., JONES.J.P.**, "*Ultrasound in Medicine- A Review*", IEEE Trans. on Sonics and Ultrasonics, Su-21, pp. 144-170, July **1974**.

[46] **EVANS J.A.**, "*Physics The Nature of Ultrasound*", Practical Ultrasound, Ed. Lerski R.A., pp. 1-13, IRL Press, Oxford, **1988**.

[47] **EVANS R.D.**, "*The Atomic Nucleus*", New York, McGraw Hill, **1955**.

[48] FOLEY J.D., VAN DAM A., "Fundamentals of Computer Graphics. Addison Wesley, 1984.

[49] **FOSTER F.S.** and **HUNT J.W.**, "*The Design and Characterization of Short Pulse Ultrasound Transducers*", Ultrasonics, Vol. 16, pp. 116-122, May **1978**.

[50] **FREEMAN A.**, "*Sound Field of a Rectangular Piston*", The Journal of the Acoustical Society of America, Vol. 32, No. 2, pp.197-209, February **1960**.

[51] **FREESE M.** and **LYONS E.A.**, "*Ultrasonic Backscatter from Human Liver Tissue: Its Dependence on Frequency and Protein/Lipid Composition*", J. Clin. Ultrasound, Vol. 5, pp. 307-312, **1977**.

[52] **FROST H.M.**, "*Electromagnetic-Ultrasound Transducers: Principles, Practice, and Applications*", Physical Acoustics, Vol. XIV, Ed.Mason W.P. and Thurston R.N., pp. 179-275,

[53] **FRY D.L.**, "*Responce of the arterial wall to certain physical factors*", In Atherogenesis: Initiating Factors, Ciba Foundation Symposium 12 (new series), Edited by R. Porter and J. Knight, pp. 98, Elsevier, New York, **1973**.

[54] **FRY f.j.**, "*Biological Effects of Ultrasound - A Review*", Proceedings on the IEEE, Vol. 67, No. 4, pp. 604-620, April

[55] **GALLINO A.**, **HAEBERLI A.**, **BAUR H.R.**, and **STRAUB P.W.**,"*Fibrin Formation and Platelet Aggregation in Patients with Sever Coronary Artery Disease: Relationship with the Degree of Myocardial Ischemia*", Circulation, Vol. 72, No.1, pp. 27-30, July **1985**.

[56] **GICHARD.F.D., AUTH.D.C,** " *Development of a Mechanically Scanned Doppler Blood Flow Catheter*", IEEE Cat. 75 CHO 994-4SU Ultrasonic Symposium Proceedings, pp. 18-21, **1975.**

[57] **GOLDMAN D.E. AND HUETER T.F.,** "*Tabular Data of the Velocity and Absorption of High-Frequency Sound in Mammalian Tissues*", The Journal of Acoustical Society of America, Vol. 28, No.1, pp. 35-37, **1956.**

[58] **GOLL. G.H.** and **AULD.B.A.,** "*Multilayer Impedence Maching Schemes for Broadbanding of Water Loaded Piezoelectric Transducers and High Q Electric Resonators*", IEEE Trans. and Sonics and Ultrasonics, Vol. SU-22, pp. 52-53, January **1975.**

[59] **GOSS.S.A., JOHNSON.R.L.,** and **Dunn.F.,** "*Compilation of empirical ultrasonic properties of mammalian tissues. II*",The Journal of Acoustical Society of America, Vol. 68, No.1, pp. 93-108, July **1980.**

[60] **GOSS.S.A., JOHNSON.R.L.,** and **DUNN.F.,** "*Comprehensive Compilation of empirical ultrasonic properties of mammalian*"

[61] **GOSS S.A., FRIZZELL L.A.,** and **DUNN F.,** "*Ultrasonic Absorption and Attenuation in Mammalian Tissues*", Ultrasound Med. Biol., Vol. 5, pp. 181-186, **1979**.tissues", J. Acoust.Soc. Am., pp. 423-457, 64, Aug **1978.**

[62] **GRESHAM G.A.,** "*Early Events in atherogenesis*", Lancer, Vol. 1, pp. 614, **1975.**

[63] **GRIFFITH J., maciel m.** and **ZALESKY P.,** "*Factors Influencing Ultrasound Echoes from Arterial Walls*", Proceedings of SPIE, Vol. 904 Microsensors and Catheter-Based Imaging Technology, pp. 100-102, January **1988.**

[64] **HARTLEY C.J.** and **COLE J.S.,** "*An Ultrasonic Pulsed Doppler System for Measuring Blood Flow in Small Vessels*", Jour. Appl. Physio., Vol. 37, No. 4, pp. 626-629, October **1974.**

[65] **HARTLEY C.J.** and **MILLAR H.D.**, "*Ultrasonic Sensors for Measuring Coronary Blood Flow*", Proceedings of SPIE, Vol. 904 Microsensors and Catheter-Based Imaging Technology, pp. 17-22, January 1988.

[66] **HARTLEY C.R., SARTORI M.P.** and **HENRY P.D.**, "*Intravascular Imaging with Ultrasound*", Proceedings of SPIE, Vol. 904 Microsensors and Catheter-Based Imaging Technology, pp. 103-106, January 1988.

[67] **HAVLICE J.F.** and **TAENZER J.C.**, "*Medical Ultrasonic Imaging: An Overview of Principles and Instrumentation*", Proceedings of the IEEE, Vol. 67, No. 4, pp. 620-641, April 1979.

[68] **HAYMAN A.J.** and **WEIGHT J.P.**, "*Transmission and Reception of Ultrasonic Pulses by Circular and Square Transducers*", The Journal of the Acoustical Society of America", Vol. 66, No. 4, pp.197-209, October 1979.

[69] **HERMAN G.**(ed), "*Special Isue on Computerized Tomograpgy*", Proc. IEEE,Vol. 71, 1983.

[70] **HERMAN G.T.**, "*Image Reconstruction from Projections: The Fundamentals of Computerized Tomography*", Academic Press, NewYork, 1980.

[71] **HILL c.R.**, "*Calibration of ultrasonic beams for biomedical applications*", Phys. Med.Biol., Vol. 15, pp. 241-248, 1970.

[72] **HOUNSFIELD G.N.**, "*Nobel Prize Acceptance Speech. Computed Medical Imaging*", Med. Phys., Vol. 7, pp. 283. 1980.

[73] **HUNT J.W., ARDITI M.** and **FOSTER F.S.**, "*Ultrasound Transducers for Pulse-Echo Medical Imaging*", IEEE Transactions on Biomedical Engineering, Vol. BME-30, No. 8, pp. 453-481, August 1983.

[74] **HUETER T.F.**, and **BOLT R.H.**, "*Sonics*" John Wiley & Sons, New York, **1955**.

[75] **IRE COMMITTEE PERSONNEL**, "*IRE Standards on Piezoelectric Crystals:Measurements of Piezoelectric Ceramics, 1961*", Proceedings of the IRE, pp.1161-1169, July **1961**.

[76] **IRE COMMITTEE PERSONNEL**, "*IRE Standards on Piezoelectric Crystals: Determination of the Elastic, Piezoelectric, and Dielectric Constants - The Electromechanical Coupling Factor, 1958*", Proceedings of the IRE, pp. 764-778, April **1958**.

[77] **JOHNSON W.T.M.** and **HORWITZ O.**, "*Aterogenesis*", In Disease of Blood Vessels, Edited by Horwitz O., McCombs P., and Roberts B.,pp. 3-12, Lea & Febiger, Philadelphia, **1985**.

[78] **KADABA M.P.**, **BAGAT P.K.**, and **WU V.C.**, "*Attenuation and Backscattering of Ultrasound in Freshly Excised Animal Tissues*", IEE Trans. Biomed. Eng., Vol. 27, pp. 76-83, **1980**.

[79] **KINSLER L.E.** and **FREY A.R.**, "*Fundamentals of acoustics*", Wiley, New York, **1962**.

[80] **KIRK K.** and **MCGUIRE B.**, "*Development of Ultrasonically Marked Needle for Ultrasonically Guided Biopsy*", IEEE Ultrasonic Symposium 1989, pp. 119-120, **1989**.

[81] **KITNEY R.I.**, **MOURA L.**, and **STRAUGHAN K.**, "*3-D Visualization of Arterial Structures Using Ultrasound and Voxel Modelling*", International Journal of Cardiac Imaging, Vol. 4, pp. 135-143, **1989**.

[82] **KITNEY R.I.**, **MOURA L.**, and **STRAUGHAN K.**, **BURRELL C.**, **ROTHMAN M.T.**, and **McDONALD A.H.**, "*Ultrasound Imaging of Arterial Structures Using 3D Solid Modelling*", Proc. IEEE Conf. on Computers in Cardiology, Bethesda, pp. 3-6, Sept. **1987**.

[83] **KOJIMA T.**, "*Matrix Array Transducer and Flexible Matrix Array Transducer*" IEEE 1986 Ultrasonics Symposium Proceedings, pp. 649-654, **1986**.

[84] **KOSSOFF G.**, "*Balance Technique for the measurement of very low ultrasonic power outputs*",J. Acoust. Soc. Am., Vol. 38, pp. 880-881,**1965**.

[85] **KOSSOFF.G.** ,"*The Effects of Backing and Maching on the Performance of Piezoelectric Ceramic Transducers*" , IEEE Transactions on Sonic and Ultrasonics, Vol. SU-13, pp. 20-30, March **1966**.

[86] **KRAUTKRAMER J.** and **KRAUTKRAMER H.I.**, "*Ultrasonic Testing of Materials*", 2nd edition, pp. 587-595, Springer, Berlin, Heidelberg and New York,, **1977**.

[87] **KRINHOLTZ R., LEEDOM D.A., MATTHAEI G.L.**, "*New Equivalent Circuits for Elementary Piezoelectric Transducers*", Electronic Letters, Vol. 6, No. 13, pp. 398-399, June **1970**.

[88] **KWUN H., JOLLY W.D., LIGHT G.M.** and **Wheeler E.**, "*Effects of Variations in Design Parameters of Ultrasonic Transducers on Performance Characteristics*", Ultrasonics, Vol. 26, pp. 65-72, March **1988**.

[89] **LANCEE C.T., SOUQUET J., OHIGASHI H.** and **BOM N.**, "*Transducers in Medical Ultrasound: Part One Ferro-Electric Ceramics Versus Polymer Piezoelectric Materials*", Ultrasonics, Vol. 23, pp. 138-142, May **1985**.

[90] **LANCEE.C.T., DAIGLE.R., SAHN.D.J., THIJSSEN**, "*Transducer Applications in Echocardiology*", Ultrasonics, Vol.23, pp. 199-205, Ultrasonics September **1985**.

[91] **LAMBERT E.H.** and **WOODE.H.**, "*The Use of a Resistance Wire Strain Gauge Manumeterto Measure Intra-arterial Pressure*", Proceedings of the Society for Experimental Biology and Medicine, Vol. 64, pp. 186-190, **1947**.

[92] **LANZER P., BOTVINICK E.H., SCHILLER N.B., CROOKS L.E., ARAKAWA M., KAUFMAN L., DAVIS P.L., HERFKENS R., LIPTON M.J.,** and **HIGGINS C.B.,** "*Cardiac Imaging Using Gated Magnetic Resonance*", Radiology, Vol.150, pp. 469, **1984.**

[93] **LAURANCE S. & MARPLE S.L.,** "*Digital Spectral Analysis with Applications*", Prentice Hall, Naw Jersey, 1987.

[94] **LAUTERBUR P.C.,** "*Image Formation by Induced Local Interactions: Examples Employing Nuclear Magnetic Resonance*", Nature, Vol 242, pp. 190, **1973.**

[95] **LEWIN P.A.** and **Chivers R.C.,** "*Two Miniature Ceramic Ultrasonic Probes*", J. Phys. E. Sci. Instrum., Vol. 14, pp. 1420-1424, **1981.**

[96] **LEWIN P.A.** and **SCHAFER M.E.,** "*Wide-Band Piezoelectric Acoustic Sources*", IEEE Trans.Ultrason.Ferroelec.Freq.Contr., Vol. UFFC-35, pp. 174-184, March **1988.**

[97] **LILLY J.C., LEGALLIS V.,** and **CHERRY R.,** "*A Variable Capacitor for Measurement of Pressure and Displacements*", Journa of Applied Physics, Vol. 18, pp. 613-628, **1947.**

[98] **LIZZI F.L., LAVIOLA M.A.,** and **COLEMAN D.J.,**"*Tissue Signature Characterization Utilizing Frequency Domain Analysis*", Proceedings of IEEE Ultrasonic Symposium, pp. 714-719, September **1976.**

[99] **LOVINGER A.J.,** "*Poly(vinylidene flouride)*", chapter5, Develoments in Crystaline Polymers, Applied Science, ed. Bassett D.C., London, **1982.**

[100] **LOVINGER A.J.,** "*Poly(vinylidene fluoride)*", Chapter 5, Development in Crystalline Polymers, Edited by Basset D.C., Applied Science, London, **1982.**

[101] **MAGINNESS M.G.,** et. al, "*An Acoustic Image Sensor Using a Transmit-Receiver Array*", Acoustical Holography, Vol. 5, New York, Plenum Press, pp. 619-631, **1974.**

[102] **MAGINNESS M.G.**, "*Methodes and Terminology for Diagnostic Ultrasound Imaging Systems 4*", Proceedings of the IEEE, Vol. 67, No. 4. pp. 641-664, April **1979**.

[103] **MARINI J.** and **RIVENEZ J.**, "*Acoustical Fields From Rectangular Ultrasonic Transducers for Non-Destructive Testing and Medical Diagnosis*", Ultrasonics, Vol. 12, pp. 251-256, November **1974**.

[104] **MARTIN.R.W., POLLACK. G.H., PHILLIPS.j.**, " *An Ultrasonic Catheter Instrument for Measuring Volume Blood Flow* " Proc., **1975** IEEE Ultrasonic Symp., IEEE # 75CH0994-4SU, pp. 13-17, **1975**.

[105] **MARTIN R.W., SILVERSTEIN F., KIMMEY M., JIRANEK G.** and **Proctor A.**, " *B-Mode Imaging and Doppler Ultrasonic Cathters for Use with Optic Endoscopes*", Proceedings of SPIE, Vol. 904 Microsensors and Catheter-Based Imaging Technology, pp. 121-126, January **1988**.

[106] **MARTIN R.W., SILVERSTEIN R.E.** and **PROCTOR A.H.**, "*Back_face Only Electrical Connections of Thickness Mode Piezoelectric Transducers*", IEEE Transactions on Ultrasonics, Ferroelectrics, and Frequency Control, Vol. UFFC-33, No. 6, pp. 778-781, November **1986**.

[107] **MARTIN R.W.** and **WATKINS D.W.**, "*An Ultrasonic Catheter for Intravascular Measurement of Blood Flow: Technical Details*", IEEE Transactions on Sonic and Ultrasonics, Vol. SU-27, No. 6, pp. 277-286, November **1980**.

[108] **MARTINELLI M.A., ARETZ T.H., BUTTERLY J., SETZER S., THUNA P.** and **LITTLE A.D.**, "*Ultrasonic Imaging of Cronery Arterial Thickness & Ultrasonic Signature Typying of Internal Abnormalities*", Proceedings of SPIE, Vol. 904 Microsensors and Catheter-Based Imaging Technology, pp. 110-115, January **1988**.

[109] **MASON W.P.**, "*Electromecanical Transdures and Wave Filters*", Van Nostrand, Prinston, N.J., **1948**.

[110] **MATZUK.T., SKOLNICK.M.L.,** " *Novel Ultrasonic real-time scanner faeturing servo controlled transducers displaying a sector image*", Ultrasonics, pp. 171-178, July **1978.**

[111] **MCKEIGHEN.R.E., BUCHIN.M.P.,** " *New Techniques for Dynamically Variable Electronic Delays for Real Time Ultrasonic Imaging* ", IEEE Cat.77CH1264-1SU Ultrasonics Symposium Proceedings, pp. 250-254, **1977.**

[112] **METAL RESEARCH Ltd.,** Melbourn, Royston, Hertfordshire, ENGLAND.

[113] **MELTON H.E.** and **THURSTON F.L.,** "*Annular Array Design and Logarithmic Processing for Ultrasonic Imaging*", Ultrasound Med. Biol., Vol. 4, pp. 1-12, **1978.**

[114] **MEYER C.R., FITTING D.W., CHIANG E.H., WILLIAMS D.M.** and **BUDA A.J.,** "*High Resolution Intravascular Imaging via Ultrasonic Catheters: Proof of Concept*", Proceedings of the IEEE, Vol. 76, No.9, pp. 1074-1078, September **1988.**

[115] **MEYER C.R., FITTING D.W., CHIANG E.H., WILLIAMS D.M.** and **BUDA A.J.,** "*Development of an Intravascular Ultrasnic Catheter Imaging System*", Proceedings of SPIE, Vol. 904 Microsensors and Catheter-Based Imaging Technology, pp. 107-109, January **1988.**

[116] **MEYER C.R., FITTING D.W., CHIANG E.H., WILLIAMS D.M.** and **BUDA A.J.,** "*Feasibility and Diagnostic Value of Catheter-Based Ultrasonic Systems for Intravascular Imaging: In Vitro Comparisons with MRI*", IEEE 1988 Ultrasonic Symposium Proceedings, pp. 805-808, **1988.**

[117] **MILLER E.B.** and **THURSTONE F.L.,** " *Linear Ultrasonic Array Design for Echosonography*",J. Acoust. Soc. Am., Vol. 61, No. 6, pp. 1481-1491, June **1977.**

[118] **MOURA L.,** "********* ", Ph.D. dissertation, Imperial College, London, UK., **1988.**

[119] **MURAYAMA.N.,NAKAMURA.H., OBARA.H., SEGAWA.M.,** " *The Strong Piezoelectricity in Polyvinylidene Fluroide (PVDF)*" , Ultasonics, Vol. 14, pp. 15-23, January **1976.**

[120] **NEWHOUSE.V.L., CENSOR T., VONTZ J.A., CINEROS J.A.,** and **GOLDBERG B.,** "*Ultrasound Doppler Probing of Flows Transverse with Respect to Beam Axis*", IEEE Trans. Biomed. Eng., Vol. BME-34, pp. 779-789, **1987.**

[120a] **NEWHOUSE V.L., FURGASON E.S., JOHNSON G.F.,** and **WOLF D.A.,** "*The Dependence of Ultrasound Doppler Bandwidth on Beam Geometry*", IEEE Trans. Sonics Ultrason., Vol. SU-27, pp. 50-59, **1980.**

[121] **NEUMAN.M.R., LIU.C.,** " *Biomedical sensors in interventional Systems: Present problems and Future Strategies*", Proceedings of the IEEE, Vol.76.No.9, pp. 1218-1225, September **1988.**

[122] **NEWTON T.H.,** and **POTTS D.G.,** "*Radiology of the Skull and Brain*", Vol. V., Mechanical Aspects of computerized Tomography., St. Louis, C.V. Mosby, **1981.**

[123] **NICHOLAS D.,** "*Evaluation of backscattering coefficient for excised human Tissues: Results, Iterpretation and Associated Measurements*", Ultrasound Med. Biol., Vol. 8, pp. 17-28, **1982.**

[124] **ALIAS P.** and **FINK M.,** "*Frensel Zone Focusing of Linear Arrays Applied to B and C Echography*", Acoustical Holography, Vol. 7, New York, Plenum Press, **1977.**

[125] **NORTON S.J.** and **LINZER M.,** "*Ultrasonic Reflectivity Imaging in Three Dimensions. Exact Inverse Scattering Solutions for Plane, Cylindrical, and Spherical Apertures*", IEEE Transactions on Biomedical Engineering, Vol. BME-28, No. 2, February **1981.**

[126] **O'DONNEL, MIMBS J.W.,** and **MILLER J.G.,** "*Relationship between Collegen and Ultrasonic Backscatter in Myocardial Tissue*", J. Acoust. Soc. Am., Vol 62, pp. 580-588, **1981.**

[127] **Omoto R.**, "*Ultrasonic Tomography of the Heart: An Intracardiac Scan Method*", Ultrasonics, Vol. 5, No. 2, pp. 80-83, **1967.**

[128] **Papadakis E.P.** and **Fowler K.A.**, "*Broad-Band Transducers: Radiation Field and Selected Applications*", The Journal of acoustical Society of America, Vol. 50, No. 3, December **1969.**

[129] **PAPOULIS A.**, " *Probability, Random Variables, and Stochastic Processes* ", 2nd Ed., Mc Graw Hill, **1984.**

[130] **P. ENNWALT Corp.**, "*Kynar Piezo film Technical Manual*", Pennwalt Corp., **1987.**

[131] **PERSSON H.W.** and **HERTZ H.**, "*Acoustic Impedance Matching of Medical Ultrasound Transducers*", Ultrasonics, Vol. 23, pp. 83-89, March **1985.**

[132] **DEFRANOULD PH.** and **SOUQUET.J.**, " *Design of a two Dimentional Array for B and C Ultrasonic Imaging System* ", IEEE Cat. 77CH1264-1SU Ultrasonic Symposium Proceedings, pp. 259-263, **1977.**

[132a] **PARKS SI, LINZER M,SHAWKERTH**, " *Further development and clinical evaluation of the expanding aperture annular array system* " , Ultrasonic Imaging 1, 378-383, **1979.**

[133] **PICANO E.,LUIGI L., ALESSANDRO D., ANTONIO B., ROBERTA S.**, and **ANTONIO A.**,"*Fibrosis, Lipids, and Calcium in Human Atherosclerotic Plaque In Vitro Differentiation from Normal Aortic Walls by Ultrasonic Attenuation*", Circ. Res., Vol. 56, pp. 556-562, **1985.**

[134] **POHLHAMMER J.D., EDWARDS C.A.**, and **O'BRIEN W.D.**, "*Phase Intensive Ultrasonic Attenuation Coefficient Determination of Fresh Bovine Liver Over an Extended Frequency Range*", Med. Phys., Vol. 8, pp. 692-694, **1981.**

[135] **POORE E.R.** "*1 mm Catheter Tip Doppler Probe Using A Single Crystal and Bridge*", Ultrasonic Imaging, Vol. 1, No. 1, pp. 101-103, **1979.**

[136] **POSAKONY.G.J.**, "*Engineering Aspects of Ultrasonic Piezoelectric Transducer Design*", IEEE Cat. 75 CHO 994-4SU Ultrasonic Symposium Proceedings, pp. 1-5, **1975.**

[137] **PURECELL E.M., TORREY H.C.,** and **POUND R.V.**, "*Resonance Absorption by Nuclear Magnetic Moments in a Solid*", Phys. Rev., Vol. 69, pp. 37, **1946.**

[138] **RADON J.**, "*Uber die bestimmung von funktion durch ihre integralwerte langs gewisser mannigfaltigkeiten*", Saechsische Akad Wissens Leipzig, Berichte Verhandlungen, Vol. 62, pp. 262, **1917.**

[139] **REID J.M.**, "*Scattering of Sound by Tissues*", in Medical Physics of CT and Ultrasoun, Edited by Fullerton G.D., and Zagzebski J.A., American Institute of Physics, p. 388, **1980.**

[140] **RICHARDSON.P.D.**, "*Piezoelectric Polymers*", IEEE Eng. in Medicine and Biology Magazine, pp. 14-16,June **1989.**

[141] **ROBINSON D.E., LEES S.,** and **LEON BESS**, "*Near Field Transient Radiation Patterns for Circular Pistons*" IEEE Transactions on Acoustics, Speech, and Signal Processing, Vol. ASSP-22, No. 6, pp. 395-403, December **1974.**

[142] **ROONEY J.A.**, "*Determination of Acoustic Power Outouts in the microwatt-milliwatt range*", Ultrasound Med. Biol., Vol. 1, pp. 13-16, **1973.**

[143] **SACHAROFF A.C., CARO R.G., MULLER D.F.** and **BOLEZA E.J.**, "*Demonstration of Intraluminal Ultrasound Imaging*", Proceedings of SPIE, Vol. 904 Microsensors and Catheter-Based Imaging Technology, pp. 118-120, January **1988.**

[144] **SAYERS.C.M., TAIT.C.E,** *"Ultrasonic properties of transducer backings"*, Ultrasonics, Vol. 22, pp. 57-60, March **1984.**

[145] **SCHAEVITZ H.,** *"The Linear Variable Differential Transformer"*, Proceedings of the Society for Experimental Stress Analysis, Vol. 4, pp. 279-288, **1947.**

[146] **SEHGAL.C.M., GREENLEAF.J.F.,** *"Scattering of Ultrasound by Tissues"*, Ultrasonic Imaging, pp. 60-80, **1984.**

[147] **SHAH. P.M., VIJAYARAGHAVAN G.** and, **SINGHAM K.T.,** *"Doppler Echocardiography a Practical Manual"* , John Wiley, New York, **1985.**

[148] **SHIBATA S., KODA.T.,** and **YAMAGA J.,** *"C-mode Ultrasonic Imaging by an electronically scanned coaxial circular spherical receiving array"*, Ultrasonic, Vol. 16, pp. 65-68, March **1978.**

[149] **SHUNG K.K., SIGLEMANN R.A.,** and **REID J.M.,** *"The Scattering of Ultrasound by Red Blood Cells"*, in Ultrasonic Tissue Characterization, Edited by Linzer M., National Bureau of Standards Special Publication 453, pp. 207-212, U.S. Government Printing Office, Washington, DC, **1974.**

[159] **SIGELMANN.R.A.,** *"Design Method for Ultrasound Transducers Using Experimental Data and Computers"*, IEEE Cat. 77CH1264-1SU, Ultrasonics Symposium Proceedings, pp. 413-415, **1977.**

[151] **SMITH & NEPHEW Ltd.,** Welwyn Garden City, Hertfordshire, ENGLAND.

[152] **SOMER J.C.,** *"Electronic Sector Scanning for Ultrasonic Diagnosis"*, Ultrasonics, Vol. 6, pp. 153-159, July **1968.**

[153] **SOUQUET J., DEFRANOULD P.** and **DESBOIS J.,** *"Design of Low-Loss Wide-Band*

*Ultrasonic Transducers for Noninvasive Medical Application*", IEEE Transactions on Sonics and Ultrasonics, Vol. SU-26, No. 2, pp. 75-81, March **1979**.

[154] **STARK D.D., HIGGINS C.B., LANZER P., LIPTON M.J., SCHILLER N., CROOKS LE, BOTVINICK E.B.,** and **KAUFMAN L.**, "*Magnetic Resonance Imaging of the Pericardum: Normal and Pathologic Findings*", Radiology, Vol. 150, pp. 469, **1984**.

[155] **SUTTLE N.A.**, "*New Pizoelectric Polymers*", The GEC Journal of Reasearch, Vol. 5, No. 3, pp. 141-147, **1987**.

[156] **SZILARD J.**, "*Physical Principles of Ultrasonic Testing*", Ultrasonic Testing, Ed. Szilard J., pp1-24, John Wiley & Sons, London, **1982**.

[157] **TEXON M.**, "*Mechanical Factors Involved in Atherosclerosis*", In Atherosclerotic Vascular Disease: A Hahnemann Symposium, Edited by Brest A.N. and Moyer J.H., pp. 23, Appleton Century Crofts, **1967**.

[158] **THURSTON F.L.** and **Von RAMM O.T.**, "*New Ultrasonic Imaging Technique Employing Two-Dimensional Electronic Beam Steering*", In Acoustical Holography, Vol. 5, Editted by Green P., Plenum Press, New York, pp. 91-102, **1974**.

[159] **TRANOCZY T.**, "*Sound Focussing Lenses and Waveguides*", Ultrasonics, Vol. 3, pp. 115-127, September **1965**.

[160] **VERNITRON Ltd.**, Thornhill, Southampton, SO9 5QF, England.

[161] **VERNITRON Ltd.**, "*Five Modern Piezoelectric Ceramics*", Bulletin 66011/F, Vernitron Ltd., Southampton, England, **1969**.

[162] **VoGEL J., BOM N., RIDDER J.**, and **LANCEE C.**, "*Transducer Design Considerations in Dynamic Focusing*", Ultrasound Med. Biol., Vol. 5, pp. 187-193, **1979**.

[163] **Von RAMM O.T.** and **THURSTON F.L.**, "*CARDIAC IMAGING USING A PHASED ARRAY ULTRASOUND SYSTEM. 1: System Design*", Circulation, Vol. 53, pp. 258-262, **1976.**

[164] **Von RAMM O.T.** and **THURSTON F.L.**, "*Cardiovascular Diagnosis with Real Time Ultrasound Imaging*", In Acoustical Holography, Vol. 6, Editted by Booth N., Plenum Press, New York, pp. 91-102, **1975.**

[165] **WALKER.J.T., MEINDI.J.D,** " *A Digitally Controlled CCD Dynamically Focussed Phased Array* ", pp. 80-83 , IEEE Cat. 75 CHO 994-SU, Ultrasonic Symposium Proceedings, **1975.**

[166] **WEINS A.**, "*Radiation Field Calculations of Pulsed Ultrasonic Transducers. Part 1: Planar Circular, Square and Annular Transducers*", Ultrasonics, Vol. 18, pp. 183-188, July **1980.**

[167] **WEINS A.**, "*Radiation Field Calculations of Pulsed Ultrasonic Transducers Part 2: Spherical Disc -and Ring -Shaped Transducers*", Ultrasonics, Vol. 18, pp. 219-223, September **1980.**

[168] **WELLS.P.N.T, JONG.N.DE,** and **BOM.N.,SOMER.J.,** " *Transducers in medical ultrasound* " Ultrasonics, Vol. 24, pp. 230-232, July **1986**

[169] **WESBEY G., HIGGINS C.B., LANZER P., BOTVINICK E.,** and **LIPTON M.J.,** " *Imaging and Characterization of Acute Myocardial Infarction In-vivo by Gated Nuclear Magnetic Resonance*", Circulation Vol. 69, pp. 125, **1984.**

[170] **WILSON R.F., LAUGHLIN D.E., ACKELL P.H., CHILIAN W.M., HOLIDA M.D., HARTLEY C.J., ARMSTRONG M.L., MARCUS M.L.** and **WHITE C.W.**, "*Transluminal, Subselective Measurement of Coronary Artery |Blood Flow Velocity and Vasodilator Reserve in Man*", Circulation, Vol. 72, No. 1, pp. 82-92, **1985.**

[171] **ZEMANEK J.**, "*Beam Behaviour withinthe Near Field of a Vibrating Piston*", J. Acoust. Soc. Am., Vol. 49, pp. 181-191, **1971.**

[172] **RS Components Ltd.** PO Box 99, Corby, Northants, NN17 9RS

[173] **National Semiconductor (UK) Ltd** 301 Harpur Centre, Horne Lane, Betford, MK40 ITR.

[174] **TRW LSI Products Inc.**, Unit 28, Fredrick Sanger Road, Surrey Research Park, Gilford, Surrey, GU2 5YD.

[175] **Linear Technology Corp.** 1630 Mc Carthy Blv., Milpitas, CA. 95035

[176] **Advanced Micro Devices Inc.**,901 Thompson Place, PO Box 3453, Sunnyvale, CA., 94088-3453.

# *Appendix A : The 3-D Solid Modelling Software Package*

This appendix provides a brief overview of the function of the 3-D solid-modeling software used in this work. The interested readers are refeered to Moura (1988) for a complete description.

The special purpose software used in conjunction with the miniature ring array transducer for the creation of cross sectional contours works as follows. The transducer captures 12 blocks of data each of which represents the information associated with an individual echo back scattered from the object under examination. To find out the spatial position of the transducer the time interval of the echoes received from four elements situated with an angular interval of 90 degrees are calculated. Having calculated the transducer's spatial location, the positions of all other sampled points around the internal perimeter of the object are determined.

With these points available around the internal perimeter of the object, the software fits the best opproximation curve that passes through all these points. This is then a 2-dimensional matrix image with all the points representing the closed contour curve given the value 1 and all other points value 0. Similarly other contours are created for the data captured from the transducer positioned at various locations in the vertical axis of the object hence creating a series of these images.
As in practice there can only be a limited number of these images created by the transducer, the software linearly interpolates between two concecutive contours creating the missing plane. All these planes are then stacked up together generating a three dimensional volume of voxels having values 1 and 0.

With this three dimensional volume in hand the software then asks the user to define the angles of rotation about the x, y and z axes that the object should be rotated. Then each point of the object is transformed into a new point in the 3-d space depending on the angles of rotation. The next task that the software performs is to determine which of the rotated points are visible to the viewer's eye. It achieves this by shining imaginary rays into the screen and looks for the first point of the object that lies along its path. If the value of this point is a 1 this point is visible and its shaded value will appear in the final picture. If the value is a 0 travelling along this imaginary ray continues.

This process is repeated for all the (x,y) coordinates of the screen until all visible points of the object are determined. Then a shaded value for all the visible points is calculated which is

dependent on the number of imaginary lights present in the scene and the local gradient of the point in three dimensional space. These shaded values are the final picture which is presented to the user.

**Voxel Space Modelling**

In the Voxel Space approach the 3-D space is divided into Nv cubes called voxels arranged side by side. A voxel v can be defined by the co-ordinates of its centre (x, y, z), where x, y and z are assumed to be integers in the interval [1, $N_v$]. Hence, voxel space VS is defined by:

$$VS = \{ V/1 \leq x \leq N_v \Lambda 1 \leq y \leq N_v \Lambda \leq z \leq N_v \} \quad (1)$$

where the symbol {denotes The Set Of, / denotes so that, and Λ denotes the Boolean operator And.

An interesting feature of Voxel Space representation is that it always represents volumes, as opposed to surfaces. As a consequence Voxel Space models are always physically consistent.

A number V(v) associated with each voxel is called the 'voxel value' or 'voxel content' and can be used to determine whether a voxel is part of an object. In its simplest form a voxel v may be said to pertain to an object O if V(v) is non-zero ie

$$O = \{v/V(v) \neq 0 \Lambda \in VS \} \quad (2)$$

where the symbol ∈ stands for In.

The voxel, or volume element, can be considered as an extension to 3-D space of the digital image element or pixel (picture element). Indeed, the Voxel Space can be represented by a 3-D array in the same manner as the digital image is represented by a 2-D array. Any plane of the voxel space can be seen as a digital image. In particular, a plane defined by z = k - called a voxel plane - can be associated with a digital image D as follows.

$$D(x, y) = V(x, y, x) \quad (3)$$

$$1 \leq x \leq N_v \Lambda 1 \leq y \leq N_v \Lambda z = k \quad (4)$$

where D(x, y) is the pixel value at the pixel (x, y) on the image D and V(x, y, z) is the voxel

value at the Voxel Space co-ordinates (x, y, z). The analogy between voxels and pixels will not be discussed in any more detail here, it is sufficient under the present circumstances to view Voxel Space as an environment which resembles cubic images.

Voxel space representations tend to be extremely computer intensive because the number of voxels required to define complex, lifelike objects is large. In fact the number of voxels in Voxel Space - the voxel space resolution - determines the model complexity. Even though objects can be encoded in order to reduce the amount of memory required to store them, the processing time is ultimately dependent on the number of voxels in the Voxel Space.

**Voxel Modelling of Arterial Structures**

Let us assume that a 2-D image of an arterial cross-section is represented by M x M picture elements or pixels. This concept can be extended to the imaging of three dimensional objects. The depth, or z dimension, of the object can be constructed from a series of 2-D pixel planes by laying them one behind the other.

The 2-D picture elements (pixels) now become cubes. These cubes, which form the 3-D image, are called volume-elements or voxels. Hence a 3-D object can be modelled in M x M x N voxel space.
The software used for this work produces full voxel space images and allows the display and manipulation in both 2-D and 3-D, with the ability to easily transfer from one to the other. The design of the system also allows a wide range of operations to be performed on 3-D solid models. These include: rotation in all three dimensions; cross-sectional displays at any depth; shaded images using depth code; plane cuts so that any section of the model can be removed; and X-ray projection - where a 3-D structure can be made semi-transparent.

Using voxel models, a series of 2-D arterial slices can be used to produce a 3-D image. We have developed an alternative approach which is to acquire parallel 2-D slices from the artery under examination using a catheter-mounted ultrasonic probe. The 2-D morphological information obtained in this way is converted into a 3-D solid model of the section of artery under investigation. The time taken to acquire the data is small in comparison to the cardiac cycle, hence the slices can be aligned without significant movement error.

**Contour Definition**
If a single arterial slice is imaged in terms of N sets of polar co-ordinates, then each contour can

be described by:

$$R(i),\ \theta(i) \quad for \quad i = 1 \rightarrow n \tag{5}$$

where R(i) is the radius from the centre of the image plane and $\theta_i$, the corresponding angular direction.

On the basis of this information, for any given slice, a contour can be drawn which corresponds to a change in acoustic impedance. Multiple contours are similarly calculated. The information for a single slice is now contained in 2-D pixel space. This process is repeated N times to generate the slices which form the 3-D arterial volume. If the pixel space comprises M x M pixels, then the volume consists of M x M x N voxels. This information is then used to construct a solid model of the arterial section.

**3-D Interpolation**

One interpolation strategy is to assume that the radii vary linearly between the original slices. Consider the case where, for example, there are three slices separated in the digital scene in such a way that they correspond to the planes 10, 30 and 50. (The overall voxel space again being M x M x N.) It is necessary to calculate the contours for planes 11 to 29, and 31 to 49. In order to do this it is assumed that any given radius will vary linearly between any two original consecutive slices ie

$$R(m, j) = \frac{(m - m_0)}{(m_i\ m_0)\ .\ (\ R(m_1, j)\ -\ R(m_0, j)} + R(m_0, j) \quad for\ m = m_0 + 1,\ m_1 - 1 \tag{6}$$

where m is the $m^{th}$ slice to be calculated, $m_0$ is the position of the nearest 'below' original slice, and $m_i$ the nearest 'above' original slice. If equation (6) is now applied to the linear interpolation problem previously defined, then we have:

$$R(m, j) = \frac{(m - 30)}{(50\ 30)\ .\ (\ r(50, j)\ -\ R(30, j)} + R(30, j) \tag{7}$$